

Sheffield Hallam University

Reactions between refractories and steel melts under reduced pressure.

ALDRICH, Graham.

Available from the Sheffield Hallam University Research Archive (SHURA) at:

<http://shura.shu.ac.uk/19238/>

A Sheffield Hallam University thesis

This thesis is protected by copyright which belongs to the author.

The content must not be changed in any way or sold commercially in any format or medium without the formal permission of the author.

When referring to this work, full bibliographic details including the author, title, awarding institution and date of the thesis must be given.

Please visit <http://shura.shu.ac.uk/19238/> and <http://shura.shu.ac.uk/information.html> for further details about copyright and re-use permissions.

ProQuest Number: 10694118

All rights reserved

INFORMATION TO ALL USERS

The quality of this reproduction is dependent upon the quality of the copy submitted.

In the unlikely event that the author did not send a complete manuscript and there are missing pages, these will be noted. Also, if material had to be removed, a note will indicate the deletion.



ProQuest 10694118

Published by ProQuest LLC (2017). Copyright of the Dissertation is held by the Author.

All rights reserved.

This work is protected against unauthorized copying under Title 17, United States Code
Microform Edition © ProQuest LLC.

ProQuest LLC.
789 East Eisenhower Parkway
P.O. Box 1346
Ann Arbor, MI 48106 – 1346

SHEFFIELD COLLEGE OF TECHNOLOGY.

ENGLISH STEEL CORP. LTD.

REACTIONS BETWEEN REFRACTORIES AND STEEL MELTS UNDER
REDUCED PRESSURE.

Graham Aldrich.

A thesis submitted to the Council for National Academic Awards for the degree of Doctor of Philosophy on work carried out at English Steel Corporation Ltd., Sheffield, under the guidance of the Sheffield College of Technology.



<u>INTRODUCTION.</u>	(v)
<u>CHAPTER ONE - REVIEW OF THE LITERATURE.</u>	1.
<u>I EQUILIBRIA.</u>	1.
1. Thermodynamic equilibria between a melt and its vapour phase.	1.
1.1. General.	1.
1.2. The process of dissociation.	2.
1.2.1. Oxygen.	2.
1.2.2. Nitrogen.	2.
1.2.3. Hydrogen.	3.
1.3. Elimination of oxygen by a reduction process.	3.
1.3.1. The carbon/oxygen reaction.	4.
1.3.1.1. Effect of carbon dioxide.	6.
1.3.1.2. Thermodynamic data on carbon and oxygen in iron.	8.
2. Thermodynamic equilibria between melt and crucible.	12.
2.1. Dissociation of alumina.	12.
2.2. Dissociation of silica.	15.
2.3. Dissociation of magnesia.	18.
2.4. Complex oxides.	19.
2.4.1. Double oxide formation with silica.	19.
2.4.2. Double oxide formation with iron oxide.	21.
<u>II KINETICS.</u>	23.
1. Kinetic Theory.	23.
1.1. Homogeneous chemical reaction.	23.
1.2. Mass transfer in the gas phase.	24.

	<u>Page Number.</u>
1.3. Diffusion and convection in fluids.	25.
1.3.1. General theory.	25.
1.3.2. Boundary layer theory.	27.
1.3.3. Surface renewal theory.	30.
1.3.4. Convective flow model.	31.
1.3.4.1. Machlin's rigid flow model.	31.
1.3.4.2. Free convection model-Kraus.	32.
Application to induction furnace melts.	33.
1.3.5. Summary and comparison of mass transfer theories.	35.
1.4. Mass transport by bubbles.	36.
1.4.1. Nucleation of CO bubbles.	36.
1.4.2. Growth and motion of gas bubbles.	38.
2. Comparison of theory with experimental results.	40.
2.1. Kinetics of the C-O reaction.	40.
2.2. Kinetics of melt-crucible reactions.	44.
2.2.1. Kinetics of silica reduction.	44.
2.2.2. Kinetics of alumina reduction.	51.
2.2.3. Kinetics of magnesia reduction.	54.
2.2.4. Comparison of data on oxide decomposition.	59.
<u>III DEGASSING PROCESSES.</u>	63.
1. Hydrogen removal.	63.
2. Oxygen removal.	65.
<u>CHAPTER TWO - LABORATORY EXPERIMENTS.</u>	70.
<u>I 1. APPARATUS AND GENERAL PROCEDURE.</u>	70.
1.1. Heating.	70.
1.2. Vacuum vessel.	71.

1.3. Charging and melting.	72.
1.4. Pumping equipment and plumbing.	73.
1.5. Pressure measurement.	75.
1.6. Pressure control.	76.
1.7. Temperature measurement.	78.
1.8. Sampling from the melt.	79.
1.9. Gas analysis unit.	82.
<u>2. MATERIALS.</u>	87.
2.1. Iron base.	87.
2.2. Crucibles.	87.
2.3. Gas atmosphere.	88.
<u>II RESULTS AND DISCUSSION.</u>	89.
1. General.	89.
2. Routine calculations.	90.
2.1. Flow measurement plus gas analysis.	91.
2.2. Metal sampling.	93.
2.3. Comparison of methods of calculation.	94.
3. Donation by oxides other than silica.	95.
3.1. Donation of oxygen by water.	95.
3.2. Donation of oxygen by magnesia.	97.
3.3. Donation of oxygen by alumina.	99.
4. Decomposition of silica.	100.
4.1. General.	100.
4.2. Extent of the silica decomposition reaction.	101.
4.3. Kinetics of silica dissociation.	105.
4.3.1. General.	105.
4.3.2. Mass transfer models based on the boundary layer theory.	110.
4.3.2.1. Introduction.	110.

	<u>Page number.</u>
4.3.2.2. Model I.	114.
4.3.2.3. Model II.	119.
4.3.2.4. Model III.	121.
4.3.2.5. Model IV.	123.
4.3.2.6. Effect of the change in a SiO_2 with time.	125.
4.3.2.7. Summary of mass transfer models.	126.
5. Effect of oxide decomposition on the C/O relationship.	128.
<u>CHAPTER THREE - WORKS TRIALS.</u>	134.
1. Introduction.	134.
2. Equipment and experimental technique.	134.
2.1. Description of the vacuum treatment unit.	134.
2.2. Experimental heats.	136.
3. Experimental results and discussion.	137.
<u>CONCLUSIONS.</u>	148.
<u>FUTURE WORK.</u>	150.
<u>ACKNOWLEDGEMENTS.</u>	152.
<u>REFERENCES.</u>	153.
<u>APPENDIX I.</u>	162.

INTRODUCTION.

Although vacuum degassing was originally conceived and developed to solve the problem of hydrogen in large forging ingots, it was soon realised that the application of a vacuum could aid the manufacture of cleaner steel by reacting the soluble oxygen with carbon to form gaseous carbon monoxide. The processes which were soon developed received wide application in all branches of the world's steel industries and now vacuum degassing is utilised to produce a spectrum of steels which include vacuum decarburised, low carbon grades; vacuum decarburised stainless steels; and vacuum deoxidised alloy steels of many types.

Considerable research and development work has been undertaken where the objects have been the achievement of lower oxygen contents together with fewer and smaller non-metallic inclusions. This has included the vacuum treatment of steel in the 'open', semi-killed and fully-killed conditions, but, in spite of these studies, there does not yet seem to be any universal rule which can be applied for the production of clean steel. One thing is certain, however; the removal of oxygen by reaction with carbon has not taken place to the extent that was originally expected from thermodynamic considerations. Final oxygen levels have been equivalent at best to those in equilibrium with 70-100 torr of carbon monoxide even though the degassing pressures have often been less than 1 torr. This has been found for all processes and no one stands out as being superior.

The removal of oxygen is least efficient with the very high and the very low carbon levels and is at a maximum

where the carbon and oxygen contents are stoichiometric.

The fact that equilibrium is not reached is generally thought to be due to:-

- (i) the kinetics of the carbon-oxygen reaction where the diffusion of the minority species seems to be limiting,
- (ii) the presence of insoluble oxide inclusions, (either exogenous in nature from slag and refractory sources, or deoxidation products formed by reaction with trace amounts of aluminium), which do not permit absolute assessment by soluble oxygen.
- (iii) the pickup of oxygen from slag and refractories, the amount of which will vary with the slag composition, the type of oxides which are used to contain the steel, and the area to volume considerations.

The purpose of the work reported here was to examine, in the laboratory, the kinetics of oxygen transfer from those refractory oxides with which the steel normally comes into contact and to supplement this with information from steels degassed by the 30 ton Dortmund Horder (D.H.) unit at English Steel Corporation Ltd.

Chapter I reviews the published information on the thermodynamics and kinetics of the carbon-oxygen and oxide-metal reactions, and also includes a short section on results from large-scale degassing operations. Chapter II deals with laboratory melts and gives details of apparatus and experimental methods as well as presenting and discussing the results obtained. Chapter III presents the results obtained from the works trials and discusses their value with

respect to the carbon/oxygen reaction and the attainment of lower oxygen levels. The conclusions and suggestions for future work arrived at as a result of this work are given at the end of this dissertation.

I EQUILIBRIA.

1. Thermodynamic equilibria between a melt and its vapour phase.

1.1. General.

Removal of impurities may be effected in the following ways(1):-

In an ionic solution where the elements involved are gaseous (e.g. H_2 , N_2) or non-metals (e.g. C, O) removal can be by a dissociation process or by chemical reaction. Both are usually heterogeneous reactions occurring at interfaces involving the dissociation of the gas-metal compound, recombination to form a molecule and then desorption of the molecule into the gas phase.

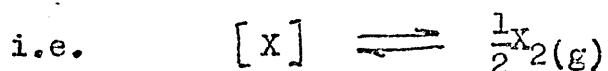
Metallic impurities may be removed by evaporation (Pb, Sn, Sb) but if the vapour pressures of the alloying elements are similar to that of the impurity then removal of these will also occur. Volatilisation of chemical compounds (e.g. metallic monoxides) may also be used to decontaminate the melt if their vapour pressures are sufficiently high.

The same possibilities exist if the impurities are not dissolved but float as a separate phase on the surface of the bath. They can be removed by a separate dissociation process, by chemical reaction at the phase boundaries or by evaporation from the surfaces exposed to the vacuum. If the impurities are dispersed in the melt, evaporation and gas evolution by dissociation or chemical reaction are hindered by the hydrostatic pressure. On the other hand, exchange processes via the equilibrium of the solute with

the melt are still possible.

1.2. The process of dissociation.

The equilibrium governing distribution of a diatomic gas between liquid and gas phases is described approximately by Sievert's law (2)



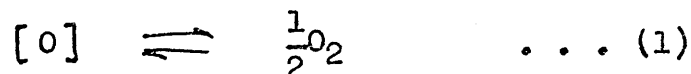
$$K = \frac{(p_{X_2})^{1/2}}{[a_X]} \quad \text{where } p_{X_2} = \text{partial pressure of X in gaseous phase.}$$

$$[a_X] = \text{activity of X dissolved in liquid iron.}$$

A short account follows commenting on its validity for oxygen, nitrogen and hydrogen in liquid steel.

1.2.1. Oxygen.

For oxygen dissolved in an iron melt



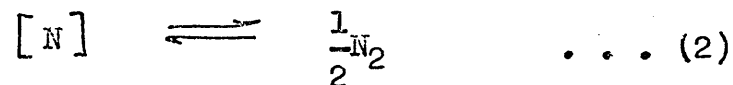
$$\Delta G^\circ = 28,000 + 0.69T$$

$$K_1 = \frac{p_{O_2}^{1/2}}{[a_O]} = 3.8 \times 10^{-4}$$

The effect of temperature on p_{O_2} can be found from Figures 1 and 2. Figure 3 shows curves for p_{O_2} against oxygen concentration for iron at 1540 and 1600° Centigrade(3). The linear relationship obtained is to be expected since the activity coefficient $f_O = a_O / \text{wt\% O}$ is constant over the whole solubility range (4,5). It will be seen from the dissociation pressure p_{O_2} values shown in Figures 1-3 that deoxidation by breakdown of gas-metal bonds in the iron-oxygen system requires such low pressures as to make the method impracticable.

1.2.2. Nitrogen.

For nitrogen dissolved in liquid iron(2)

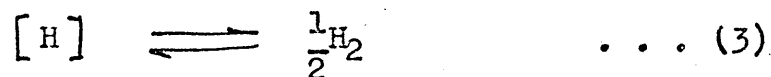


$$K_2 = \frac{p_{N_2}^{1/2}}{[a_N]} = 23.2$$

Assuming that this relationship is valid over a range of pressure (6), Figure 4 (1) shows the pressure dependence of nitrogen in liquid iron and illustrates that removal of nitrogen by the dissociation of the metal nitride is to be expected at industrial vacuum levels.

1.2.3. Hydrogen.

The behaviour of hydrogen is very similar to that of nitrogen. The breakdown of the gas-metal bond by reducing p_{H_2} does not present any difficulty. It is, in fact, much easier and more effective than reaction with oxygen, which in principle is also possible. Moreover equilibrium is reached much faster than with nitrogen because the diffusion rate of hydrogen is much faster than that of any other gas. Figure 4 shows the dependence of hydrogen in liquid iron upon the pressure, deduced from



$$K_3 = \frac{p_{H_2}^{1/2}}{[a_H]} = 370$$

1.3. Elimination of oxygen by a reduction process.

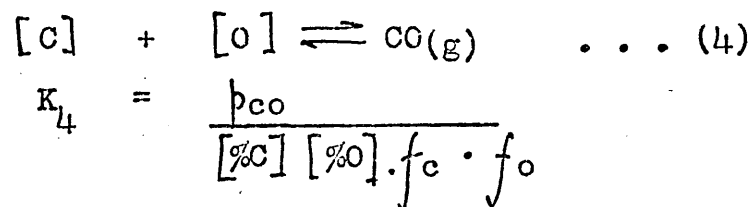
In Section 1.2.1. it is concluded that deoxidation by a dissociation process is impracticable and, therefore, chemical reaction involving a reducing agent must be employed whereupon the final oxygen content approaches an equilibrium limit determined by the concentration of the

reducing agent and the reaction product formed. Three reactions may be used; reduction with carbon, with hydrogen or with a metal having a higher affinity for oxygen.

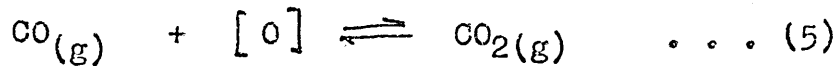
Deoxidation with metallic reducing agents is usually faster than with carbon or hydrogen since generally it is less dependent on nucleation and transport phenomena than reactions leading to bubble formation. Figure 5 (3) compares the deoxidising effects of carbon and other elements in liquid steel. However, complete removal of the insoluble deoxidation products is virtually impossible and therein lies the advantage of reduction by carbon or hydrogen where the products are gaseous. On the other hand, in cases where reduction by carbon or hydrogen does not attain an endpoint sufficiently quickly or completely, deoxidation by precipitation may be necessary. The main advantage of reduction by hydrogen is that, in the ultimate, the reducing agent can be removed from the bath by vacuum treatment providing temperature losses will allow this. Even so the efficiency of oxygen removal is low and consequently this technique is only used with the vacuum induction melting of elements which are easy to deoxidise, such as nickel. For other ferrous alloys reduction of oxygen by carbon is invariably adopted in practice since, whilst being much the cheaper it is also the more effective.

1.3.1. The carbon/oxygen reaction.

For the reaction between carbon and oxygen dissolved in liquid iron the equilibrium can be represented by



K_4 can be found by combining the data of reactions (5) and (6)

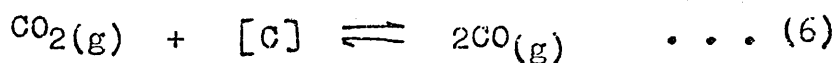


$$K_5 = \frac{p_{\text{CO}_2}}{p_{\text{CO}}[a_{\text{O}}]}$$

Figure 6⁽⁷⁾ summarises the evaluations of this reaction (8-12) and the following equations are considered the most useful (12)

$$\Delta G_5^{\circ} = -37,010 + 20.31T \text{ cal/mole}$$

$$\log K_5 = \frac{8,088}{T} - 4.438$$



$$K_6 = \frac{p_{\text{CO}}^2}{p_{\text{CO}_2} [a_{\text{C}}]}$$

Data (9, 10, 13, 14, 15) for this reaction are shown in Figure 7 (7) from which the most accurate equations are considered to be (14)

$$\Delta G_6^{\circ} = 33,300 - 30.40T \text{ cal/mole}$$

$$\log K_6 = \frac{-7,280}{T} + 6.65$$

since, in contrast to the others, these have been determined from actual experimental measurements of the CO/CO₂ ratios in equilibrium with liquid iron, K_4 can now be found by combining equations (5) and (6) to give

$$\Delta G_4^{\circ} = -3,710 - 10.09T \text{ cal/mole}$$

$$\log K_4 = \frac{811}{T} + 2.205$$

At 1600° Centigrade $K_4 = 434$.

The first quantitative studies of the C/O reaction began with Field (16) who, from studies on the rate of carbon elimination from BOH baths, deduced that an

equilibrium must be reached between carbon, oxygen and partial pressure of carbon monoxide above the metal surface. It was later shown by Herty (17) that for carbon contents of less than 0.20% $m = [\%C] [\%O] \approx 0.0022$. Laboratory studies were first started by Vacher and Hamilton (18) who showed that equilibrium could be approached from both sides. The early assumption that m was virtually independent of carbon content and temperature was proved invalid when Marshall and Chipman (19) equilibrated CO/CO₂ mixtures with liquid iron at pressures up to 20 atmospheres. The solubilities of both carbon and oxygen in liquid iron increase as the gas pressure is raised resulting in general improved accuracy of oxygen determinations except at high carbon contents. This is thought to be the reason why this study found an increase in m with an increase in carbon content. The experiments have since been repeated by Fuwa and Chipman (10) and as Figure 8 shows m is now thought to decrease as the carbon is raised. Two factors may account for this decrease. Firstly the gas in equilibrium with carbon dissolved in liquid iron is not pure carbon monoxide, but contains some CO₂, and secondly, the activities of dilute solutions of oxygen and carbon do not conform to Henry's law.

1.3.1.1. Effect of carbon dioxide.

From equation 5 and using the data of Fuwa and Chipman (10) the influence of the presence of carbon dioxide has been examined by Jackson and Hyams (20).

$$K_5 = \frac{p_{CO_2}}{p_{CO} [a_O]}$$

$$\text{therefore } \frac{p_{CO_2} + p_{CO}}{p_{CO}} = \dots (7)$$

If the gas in contact with the melt is composed solely of CO and CO₂ so that $p_{CO_2} + p_{CO} = p_T =$ system pressure,

$$p_{CO} = \frac{p_T}{1 + a_o \cdot K_5} \dots (8)$$

But from equation (4) (10) $p_{CO} = K_4 \cdot [\%C] [\%O] f_o \cdot f_c$

$$\text{and therefore } [\%C] [\%O] = \frac{p_T}{K_4 \cdot f_o \cdot f_c (1 + K_5 f_o [\%O])} \dots (9)$$

Equation (9) takes into account the formation of both CO and CO₂ and the results of the solution are shown in Figure 9 (20,21,22). The solid curves correspond to the true equilibria whereas the dotted lines correspond to the simple relationship $[\%C] [\%O] = \frac{p_T}{K_4}$. The temperatures chosen were 1600° Centigrade for the one atmosphere curve and 1550° Centigrade for the 100 mm, 10 mm and 1 mm pressure curves which correspond to the temperatures usually attained prior to tap and during vacuum treatment by the D.H. method. From Figure 9 it is evident that for equilibrium carbon and oxygen contents, the activities of carbon may generally be taken as equal to its weight % for all values between 0.005 and 0.20%C. Therefore, from equation (6)

$$\%C \cdot K_6 = \frac{p_{CO}^2}{p_{CO_2}} \dots (10)$$

This equation has been solved for $p_{CO} + p_{CO_2} = p_T$ for various values of p_T at a temperature of 1550° Centigrade. The resulting curves are plotted in Figure 10 from which it is evident that at all pressures less than 10 torr, CO - CO₂ mixtures in equilibrium with iron will contain negligibly small percentages of CO₂.

1.3.1.2. Thermodynamic data on carbon and oxygen in iron.

The solubility of pure FeO in high purity iron depends only on temperature but pure FeO is difficult to achieve due to contamination from the crucible and since the solubility of the pure oxide is greater than that of the impure oxide, a small correction must be applied. Assuming that the solubility is proportional to mole fraction, Figure 11 (23) shows corrected data of Chipman and Metters (24). Also shown is data of Taylor and Chipman (25) who obtained a direct measurement of the solubility of the pure oxide using a rotating induction furnace whereby the liquid oxide rested on top of the molten iron and out of contact with the crucible. Both sets of data are represented by the line whose equation is

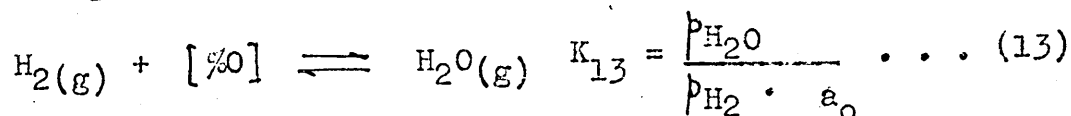
$$\log [\%O] = -\frac{6320}{T} + 2.734 \quad \dots (11)$$

Gokcen (12) gives the solubility of oxygen in liquid iron as

$$\log [\%O] = -\frac{5762}{T} + 2.439 \quad \dots (12)$$

Equations (11) and (12) agree closely at 1600° Centigrade as shown in Table I.

Floridis and Chipman (26) investigated the thermodynamics of oxygen in liquid iron making use of the H₂ - [O] - H₂O - Fe system. Similar work was undertaken by Gokcen (12) and Dastur and Chipman (27). The equilibrium can be expressed as



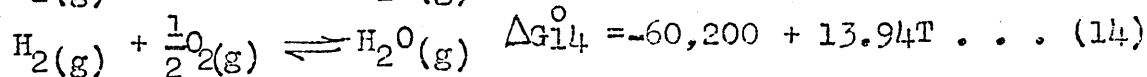
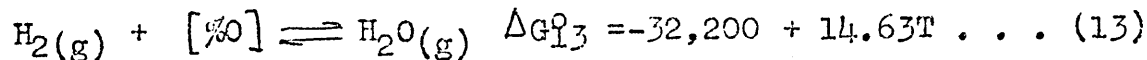
and the equations (12,26,27) have been summarised by Bodsworth (7), the best values being expressed by (26)

$$\Delta G_{13}^{\circ} = -32,200 + 14.63T \text{ cal/mole}$$

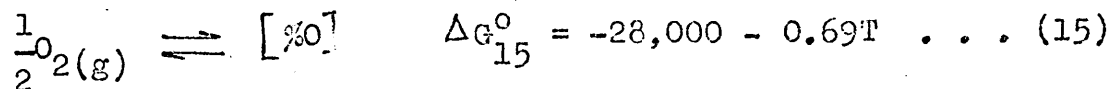
$$\log K_{13} = \frac{7050}{T} - 3.20$$

giving $K_{13} = 4.68$ @ 1550°C . and $K_{13} = 3.65$ @ 1600°C .

From this data the heat and free energy change accompanying the solution of gaseous oxygen in liquid iron may be obtained as follows:-



Combining equations (13) and (14) gives



The activity coefficient of oxygen was found (26) to decrease slightly with increasing concentration according to

$$\log f_o = -0.20 [\%O] \dots (16)$$

Figure 12 (7) shows the effect of other solutes on the activity coefficient of oxygen in iron at 1600° Centigrade.

The solubility of carbon in liquid iron is shown by the iron-carbon phase diagram where the relationship with temperature is linear in the range from the eutectic at 1153° Centigrade upwards to about 1900° Centigrade. The solubility is given by

$$[\%C] = 1.34 + 2.54 \times 10^{-3} t (^{\circ}\text{C}) \dots (17)$$

The variation, with temperature, of the activity of carbon in liquid iron has been determined for all concentrations up to saturation (13,14) and the combined data of these investigations are represented by the equation (14).

$$\log f_c = \frac{4350}{T} \left[1 + 4 \times 10^{-4} (T - 1770) \right] (1 - x_{\text{Fe}})^2 \dots (18)$$

The variation of activity with concentration is given in Figure 13 which shows that the activity varies markedly from Henry's law when the concentration of carbon exceeds 0.2^W/o. At 1540° Centigrade the data can be represented by (28)

$$\log f_c = 0.20 [\%C] - 0.008 [\%C]^2 \dots (19)$$

The activity changes only slowly as the temperature is raised and for concentrations up to 2^W/o C equation (19) represents the experimental data with sufficient accuracy over the temperature range of interest in steelmaking.

Within the composition range in which the activities conform to Henry's law the activity coefficient of carbon is given by

$$\log f_c = + 0.20 [\%C] \dots (20)$$

The effect of carbon on the activity coefficient of oxygen has been evaluated by the following procedure (8).

At any chosen temperature a plot of $\log K_4^* = \log \left(\frac{p_{CO}}{[\%C][\%O]} \right)$

versus %C intercepts the zero %C axis at the value of log K for that temperature. The slope of this plot is equal to $\log K_4^* - \log K_4 = \log f_o + \log f_c$ and for pure Fe - C - O melts is - 0.22 [%C] at 1600° Centigrade. Expanding the activity coefficients for oxygen and carbon and substituting this value gives the relation

$$\log f_o + \log f_o^c + \log f_c + \log f_c^o = -0.22 [\%C] \dots (21)$$

For all but very low carbon contents the values of $\log f_o$ and $\log f_c^o$ are very small and can be neglected and when the value for $\log f_c$ is substituted from equation (19) we obtain

$$\log f_o^c = - 0.42 [\%C] - 0.008 [\%C]^2 \dots (22)$$

In Figure 14 (7) the variation of this coefficient with carbon concentration (line I) is compared with other published

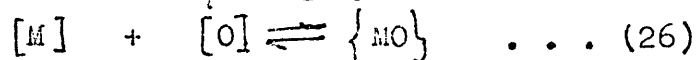
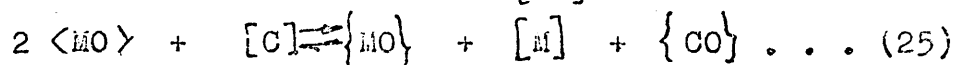
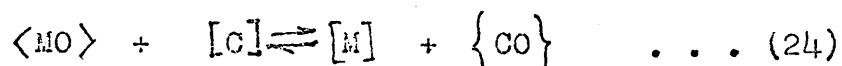
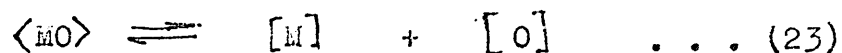
values (8-11, 15, 29, 30). Although line γ (10) differs from all the other equations the analytical techniques are probably the most accurate. In addition to this, chromium was added to the melts to increase the oxygen solubilities and improve the accuracy of the oxygen analyses. However, it must be remembered that the value of f_o^c is then dependent on the accuracy of the interaction coefficient for chromium with oxygen which is used to convert the data to the pure iron-carbon-oxygen system.

At one time the effect of carbon on the activity coefficient of oxygen was attributed to a small solubility of carbon monoxide in liquid iron (19, 31) which was thought to increase with carbon content. It is now recognised, however, that the effect is probably due to an interaction between the carbon and oxygen atoms (32, 33) which lowers the activity coefficients of both carbon and oxygen. Generally the concentration of carbon is very much greater than that of oxygen and the effect of oxygen on the activity of carbon is significant only at very low concentrations of carbon. Interaction effects of other solutes with carbon in liquid iron are shown in Figure 15.

and crucible.

In addition to the reaction between atmosphere and melt, there also exists in all melting processes in which oxide crucibles are used, a reaction between melt and crucible. This results in a constant supply of oxygen from the crucible during deoxidation of the melt by carbon or hydrogen and in a limitation of the oxygen level that depends on the chemical stability of the crucible material which cannot be improved upon.

Metal/oxide reactions can occur according to the following generalisations



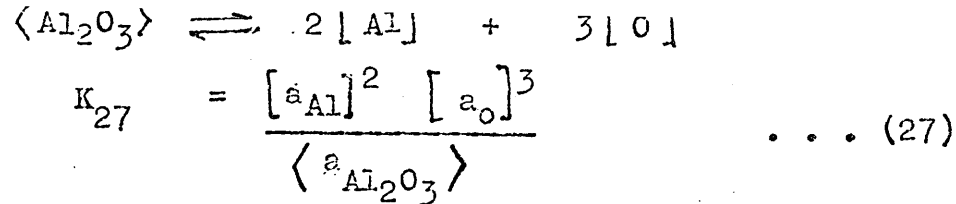
Reaction (23) would normally be followed by reaction of the oxygen with carbon at the gas/metal interface.

Equation (24) is the direct reaction between carbon and the oxide and occurs only at a three phase interface such as the surface of a melt or at a site where carbon monoxide bubbles are growing. Reactions (25) and (26) involve the formation of a gaseous sub-oxide phase and (25) like (24) can only occur at a three phase boundary

2.1. Dissociation of alumina.

Bodsworth (7) has compared work done on deoxidation by aluminium. The same equations can be modified to present the case for dissociation of the oxide.

For the dissociation reaction



This equilibrium constant can be calculated from the following data by combining



$$\Delta G_{28}^{\circ} = +196,000 - 47.44 T \text{ cal mol}^{-1}$$



$$\Delta G_{13}^{\circ} = +32,200 - 14.63 T \quad (26)$$

So for equation (27) $\Delta G_{27.1}^{\circ} = 292,600 - 91.33T$

$$\text{and } \log_{10} K_{27.1} = -\frac{63,960}{T} + 19.96$$

Figure 16 compares equation (27.1) with other determinations (23)(35,7)(34) and whilst there is some scatter (27.3) and (27.4) give the best agreement. These last two are revisions of (27.2) but with more recent activity data for aluminium in iron and hence are considered to be the most reliable. The data by Gokken and Chipman (34) has, therefore, been chosen to represent equation (27)

$$\Delta G_{27.4}^{\circ} = +290,500 - 93.7T \text{ cal mol}^{-1}$$

$$\log K_{27.4} = -\frac{63,500}{T} + 20.48$$

$$\text{At } 1600^{\circ} \text{ Centigrade } K_{27.4} = 3.78 \times 10^{-14}$$

The apparent equilibrium constant

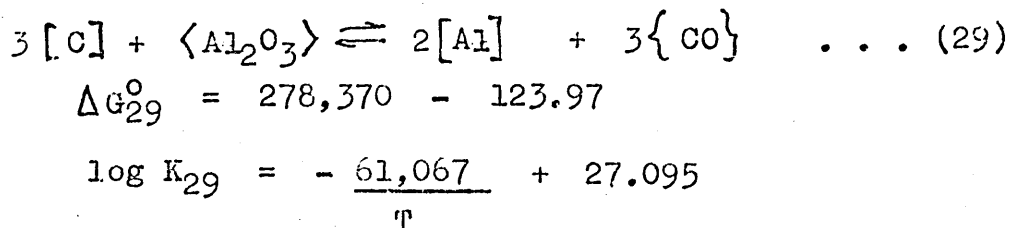
$$K_{27}^1 = \frac{[\% \text{Al}]^2 [\% \text{O}]^3}{\langle \text{a}_{\text{Al}_2\text{O}_3} \rangle}$$

has been determined by a number of investigators (36-39) for equilibrium with pure alumina and their values are also shown in Figure 16. It can be seen that as well as the wide scatter between these values they are all far removed from

the calculated values. This latter difference may be due to

- (i) strong negative deviation from ideality of aluminium in iron.
- (ii) interaction between aluminium and oxygen.
- (iii) sampling difficulties.
- (iv) persistence of small alumina particles.
- (v) inaccuracy of analysis at low levels of aluminium and oxygen.
- (vi) the formation of iron-alumina spinel at low aluminium levels resulting in a lowering of Al_2O_3 .

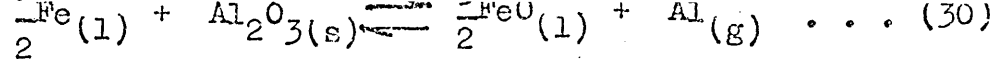
For the reaction between alumina and carbon according to (24) the data from equations (27.4) (34) and 4. (12,14) can be combined to give



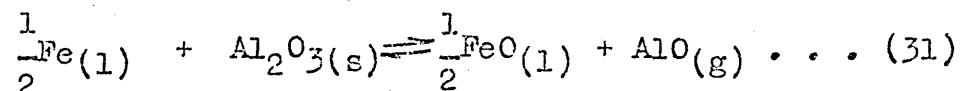
At 1600° Centigrade $K_{29} = 3.098 \times 10^{-6}$

A comparison of equations (27.4) and (29) shows the decreased stability of alumina at a three phase boundary where carbon monoxide can be continuously formed and pumped away. Reaction (27) would hardly be expected to occur under normal vacuum degassing conditions where the current lowest attainable oxygen levels are about 10 ppm. Reaction (29) is more likely as the activity of carbon increases and the chances of bubble formation improve.

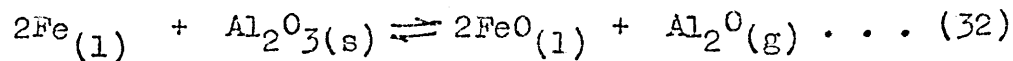
Reaction by vapour formation can also occur according to (40)



At 1600° Centigrade $K_{30} = 3.2 \times 10^{-9}$



At 1600° Centigrade $K_{31} = 4 \times 10^{-10}$



At 1600° Centigrade $K_{32} = 4 \times 10^{-14}$

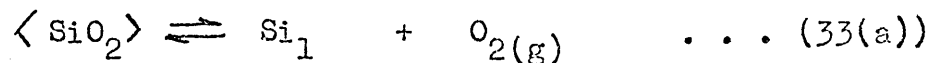
These values correspond to very low partial pressures of the vapour species and the reactions would not be expected to take place at industrial vacua.

2.2. Dissociation of silica.

The equilibrium constant for the reaction



can be found from



for which Ramstad and Richardson (41) have given

$$\Delta G_{33(a)}^0 = 222,800 - 47.62 T \text{ cal mol}^{-1}$$

The free energy of solution of oxygen gas in liquid iron according to (26,12,42)



has been estimated as $\Delta G_{15}^0 = -28,000 - 0.69 T$ (26)

and the free energy for the solution of silicon in iron has been found to be



$$\Delta G_{33(b)}^0 = -28,500 - 4.05 T \text{ cal/mol (7)}$$

from data for the reaction between silicon and oxygen in iron under a silica-saturated slag (43-45) and the heat of solution of silicon in liquid iron (38).

Hence the free energy change for reaction (33) is

found by combining the values for (33(a)) (15) and (33(b)) to give

$$\Delta G_{33.1}^0 = 138,300 - 53.00T$$

$$\log K_{33.1} = \log \left[\frac{[a_{Si}][a_o]^2}{\langle a_{SiO_2} \rangle} \right] = - \frac{30,240}{T} + 11.58$$

By a similar combination of free energy data the equilibrium constant has been evaluated by Gokcen (12) as

$$\Delta G_{33.2}^0 = 129,440 - 48.44T \text{ cal/mol;}$$

$$\log K_{33.2} = - \frac{28,300}{T} + 10.59$$

and by Chipman and Gokcen (43) as

$$\Delta G_{33.3}^0 = 133,340 - 50.37T \text{ cal/mol;}$$

$$\log K_{33.3} = - \frac{29,150}{T} + 11.01$$

The constant has also been evaluated by Chipman and Pillay (44) by measurement of H_2/H_2O ratios in equilibrium with silica and silicon dissolved in liquid iron to give

$$\Delta G_{33.4}^0 = 135,940 - 51.43T \text{ cal/mol;}$$

$$\log K_{33.4} = - \frac{29,700}{T} + 11.24$$

At 1600° Centigrade $K_{33.4} = 2.5 \times 10^{-5}$

The data agree reasonably well but since (33.4) has been obtained by a more direct method, it is thought to be the most accurate.

For pure iron-silicon-oxygen alloys it is found experimentally that the change in f_{Si} with the silicon and oxygen contents is almost exactly balanced by the corresponding change in f_o^2 for silicon concentrations up to 2.0^w%, i.e.

$$[f_{Si}] [f_o]^2 \approx 1 \text{ and } K_{33} \approx K_{33}^1 = \frac{\langle a_{SiO_2} \rangle}{[\%Si] [\%O]^2}$$

where K_{33}^1 is the apparent equilibrium constant.

Using equations 33.4 (44) and 14 (12,14) the free energy

change accompanying the three phase reaction between carbon and silicon can be evaluated.



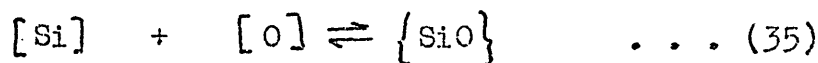
$$\Delta G_{34}^{\circ} = 128,520 - 71.61T \text{ cal/mol;}$$

$$\log K_{34} = \frac{-28,078}{T} + 15.65$$

$$\text{At } 1600^{\circ} \text{ Centigrade } K_{34} = \frac{f_{\text{Si}} [\% \text{Si}] p_{\text{CO}}^2}{\langle a_{\text{SiO}_2} \rangle [\% \text{C}]^2 f_c^2} = 4.56$$

For this reaction Kirkwood, Fuwa and Chipman (93) obtained $\Delta G^{\circ} = 131,400 - 73.4T$ ($K = 5.1$) by equilibrating silica with carbon dissolved in liquid iron.

The gaseous species SiO is fairly volatile

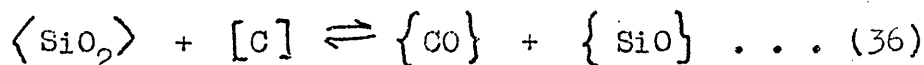


$$\Delta G_{35}^{\circ} = 20,900 - 4.92 T$$

$$\text{At } 1600^{\circ} \text{ Centigrade } K_{35} = \frac{p_{\text{SiO}}}{f_{\text{Si}} \cdot f_{\text{O}} [\% \text{Si}] [\% \text{O}]} = 4.9 \times 10^{-2}$$

At low silicon contents this reaction will be negligible but at 0.01% oxygen the equilibrium silicon concentration is 0.3% giving $p_{\text{SiO}} = 0.15$ torr. Thus if the pressure is lowered beyond this value, silicon and oxygen will be continuously removed from the melt and corrosion of the crucible will occur.

At a three phase boundary and in the presence of carbon the reaction becomes



and by combining equations (33), (35) and (4) the equilibrium constant can be found.

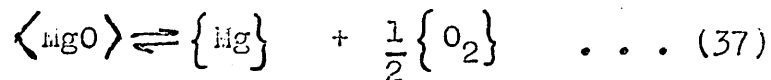
$$\text{At } 1600^{\circ} \text{ Centigrade } K_{36} = 5.32 \times 10^{-4}$$

Reaction (36) would, therefore, seem more likely to occur than reaction (35) but kinetics will be more favourable for the latter because of the greatly increased area for

From the foregoing reactions involving silica it is apparent that all four (33-36) are possible under normal vacuum degassing conditions. For instance by reaction (33) at 10 ppm oxygen and for pure silica the silicon content would have to increase to 25% before equilibrium could be attained. Similarly reactions (35) and (36) are likely to occur especially at the surface of the melt where there is contact with the crucible and with high carbon contents. However, since the limited data has so far shown a dependence of the rate upon the square of the crucible diameter, it is likely that most crucible corrosion occurs by reaction (33) followed by (4), i.e. dissociation of the silica to oxygen and silicon in solution, followed by reaction of the oxygen with carbon to form carbon monoxide.

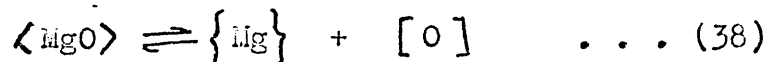
2.3. Dissociation of magnesia.

Chipman (23) gives free energy data for the reaction



$$\text{as } \Delta G_{37}^{\circ} = 174,750 - 49.09 T$$

Magnesium has only a limited solubility in iron and the stability of its oxide can be found by combining equation (37) with equation 15 (26) for the solution of oxygen in liquid iron to give



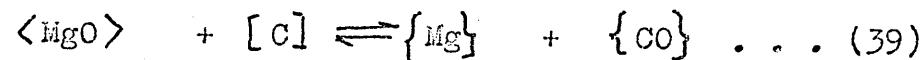
$$\Delta G_{38}^{\circ} = 146,750 - 49.78 T$$

$$\log K_{38} = \log \frac{P_{\text{Mg}} [\% \text{O}] \cdot f_{\text{O}}}{a_{\text{MgO}}} = \frac{-32,200}{T} + 10.90$$

from which it can be derived that at 1600^o Centigrade

$$\underline{K_{38} = 5.0 \times 10^{-7}}$$

Equations (4) and (38) can be combined to give the reaction



$$\Delta G_{39}^{\circ} = 143,040 - 59.87 T.$$

$$\log K_{39} = \log \frac{p_{\text{Mg}} \cdot p_{\text{CO}}}{\langle a_{\text{MgO}} \rangle [\% \text{C}] \cdot f_c} = \frac{-31,389}{T} + 13.105$$

which at 1600° Centigrade gives $K_{39} = 2.22 \times 10^{-4}$

According to equation (38) for an oxygen content of 10 ppm the reaction will only occur if the pressure falls below about 0.5 torr. For higher oxygen levels the dissociation process becomes increasingly less likely. For iron containing 1% C and assuming equal partial pressures of magnesium and carbon monoxide at the surface the pressure needs only to be lowered to about 20 torr for the reaction to commence. For a 0.1% C steel, the critical pressure is lowered to approximately 7 torr.

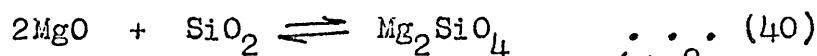
2.4. Complex oxides.

2.4.1. Double oxide formation with silica.

In practice, silica may be bonded with magnesia as forsterite (Mg_2SiO_4) and with alumina as mullite ($3\text{Al}_2\text{O}_3 \cdot 2\text{SiO}_2$)

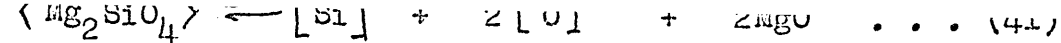
For forsterite ($2\text{MgO} \cdot \text{SiO}_2$)

The free energy change for the formation of forsterite has been given by Richardson and Jeffes (46) up to 1430° Centigrade and as a first approximation the relationship may also be applied up to 1600° Centigrade.



$$\Delta G_{40}^{\circ} = -15,120 - 0.0T \quad (46) \quad \left(\Delta S_{298}^{\circ} \text{ was found to be } -0.4 \pm 0.6 \text{ cal/}^{\circ} \right)$$

The free energy change for the dissociation of forsterite to silicon and oxygen in solution in iron can now be found by combining equations (40) and (33) resulting in

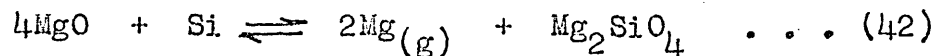


$$\Delta G_{41}^{\circ} = 151,060 - 51.45 T$$

$$\log K_{41} = \frac{-33,030}{T} + 11.25$$

$$\text{At } 1600^{\circ} \text{ Centigrade } K_{41} = 4.07 \times 10^{-7}$$

Pure forsterite, therefore, in contact with liquid iron containing 10 ppm oxygen would dissociate if the silicon concentration was below about 0.4% Schneider and Hesse (47) have measured the magnesium pressures in the equilibrium

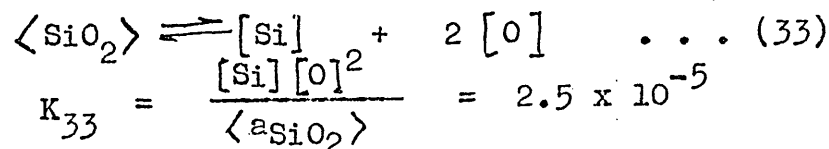


by an entrainment technique and have identified the forsterite by X-rays. Their results, however, lead to values for the free energy of formation of forsterite which are approximately double those recommended by Richardson (46), and it is considered that more reliance should be placed on the values given in equation (40) since these are determined by measuring the heat of solution of $\text{Mg}(\text{OH})_2$ and SiO_2 in 20% HF which is considered a more accurate technique.

For mullite ($3\text{Al}_2\text{O}_3 \cdot 2\text{SiO}_2$)

Free energy data is available for the formation of the aluminosilicates andalusite and kyanite ($\text{Al}_2\text{O}_3 \cdot \text{SiO}_2$) but not for mullite. However, it is known that for pure mullite the activity of silica is 0.42, (48) although when mullite and silica are present together in a crucible the activity of silica in the mullite is less than this at low silica levels and greater at high silica concentrations.

Hence for the reaction



where the silica is bonded as mullite

$$K^I = [\text{Si}][\text{O}]^2 = 2.5 \times 10^{-5} \times 0.42 = \underline{1.05 \times 10^{-5}} \dots (43)$$

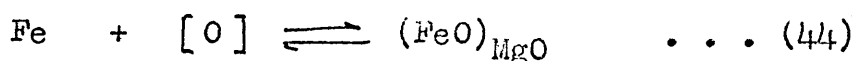
Mullite, therefore, is relatively unstable and would be expected to dissociate if the oxygen and silicon levels are sufficiently low.

2.4.2. Double oxide formation with iron oxide.

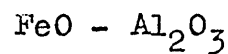
Oxygen arising from dissolution of the crucible may, at low carbon contents, react with the crucible to form a double oxide.



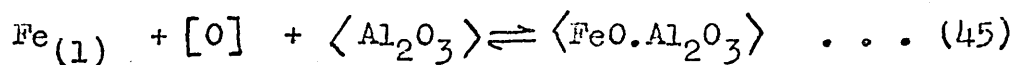
FeO is soluble in MgO, setting up the equilibrium (40)



The formation of FeO can thus act as a sink for oxygen and if a_{FeO} and $[\%O]$ are in equilibrium any increase in the oxygen concentration of the melt by further crucible decomposition will lead to a higher activity of iron oxide in the crucible.



Oxygen, arising from dissociation of the crucible can react with alumina only when its concentration is sufficiently high to form hercynite (40) by the reaction

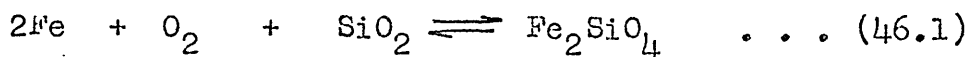


$$K_{45} = 12.67 \quad (40)$$

The oxygen potential $f_o \cdot [\%O]$ at this point is 0.079 which corresponds to an oxygen concentration of 0.082% using $\log f_o = -0.20 [\%O]$ (26).

Such high oxygen concentrations are met with in steelmaking at very low carbon levels and with $P_{\text{CO}} = 1$ atmosphere, and only under these conditions is the formation of hercynite at all likely.

For the reaction

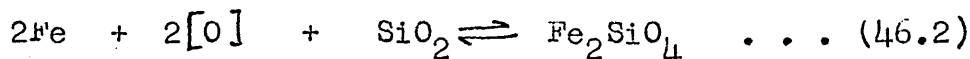


Richardson (46) determines the free energy change as

$$\Delta G_{46.1}^{\circ} = -135,300 + 34.4 T$$

(298-1478°K)

which, on the assumption that this value is still approximately valid at 1600° Centigrade and when combined with equation (15) for the free energy of solution of oxygen in liquid iron, gives

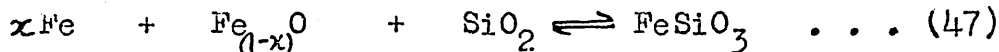


$$\Delta G_{46.2}^{\circ} = -79,300 + 35.78 T$$

$$\log K_{46.2} = \frac{17,340}{T} - 7.819$$

At 1600° Centigrade $K_{46.2} = 27.29$

Richardson and Jeffes (46) also give free energy data for the reaction



$$\Delta G_{47}^{\circ} = -28,000 \text{ cal}$$

(1873°K)

was calculated for the formation of liquid $FeSiO_3$ from liquid wüstite, liquid iron and liquid silica, from the activities of silica and wüstite corresponding to the composition $FeSiO_3$.

From this data $K_{47} = 1,854$ at 1600° Centigrade.—

The value for K_{47} shows that the formation of FeO - SiO₂ phases is likely for comparatively low oxygen levels.

In the practical application of vacuum processes the equilibrium between gas phase, crucible and melt, as already mentioned, often cannot be readily attained. Operation is usually carried out, therefore, in a region where the state of the melt is determined by the speed of reactions taking place.

1. Kinetic Theory.

1.1. Homogeneous Chemical Reaction.

The theory of absolute reaction rates developed by Eyring (49,50) and discussed in some detail by Darken and Gurry (51) provides the estimated rate for a chemical reaction. It is shown by Niwa and Shimoji (52) that if the rate for the carbon/oxygen reaction were controlled by a homogeneous process the rate of the reaction would be approximately

$$-\frac{dC}{dt} = \frac{RT}{Nh} \exp \frac{\Delta H^\ddagger}{RT} \frac{7}{1600} [C][O] \dots (48)$$

where [C] and [O] are w/o dissolved in liquid iron

- R = gas constant
- T = absolute temperature
- N = Avogadro's number
- h = Planck's constant
- ΔH^\ddagger = activation energy

This is derived from the general statement by Darken

(51) - Reaction rate

$$\frac{-dC}{dt} = \left(\frac{RT}{Nh} \right) \left(e^{-\Delta H^\ddagger / RT} \right) \left(e^{AS^\ddagger / R} \right) \left(\frac{\gamma_{R_1} \gamma_{R_2} \dots}{\gamma^\ddagger} \right) (C_{R_1} C_{R_2} \dots) \dots (49)$$

putting $T \approx 2000^\circ K$ and $\Delta H^\ddagger \approx 28 \text{ K cal}$ (53) the estimated change in the carbon-oxygen product $\frac{-dC}{dt} \cdot [C][O]$ is found to be 10^7 w/o per hour.

This result is much too large compared with observed

values of 0.12 - 0.18% C per hour for BoH practice (54). The same conclusion has been obtained by Darken (51) reaching a rate of $\frac{-dC}{dt} \cdot [C][O] = 4 \times 10^6$ w/o per hour or for $[O] = .04$ w/o, 10^4 % C per hour. This high rate suggests that the surface is rapidly depleted of the minority reactant (generally oxygen) and that the rate controlling step in the overall reaction is probably dependant on the rate of diffusion of the minority species (55).

It is to be noted that the rate of homogeneous reaction is not dependent on the bath size as shown in equation (48). However, in the case of the heterogeneous reaction, the bath size gives an inverse effect on the rate, an effect which is confirmed by practical observations.

1.2. Mass Transfer in the Gas Phase.

Due to the low pressures and high temperatures of the gas/metal interface during vacuum refining gaseous diffusion coefficients will be very large. Kinetic theory gives

$$D = \frac{1}{3} (\lambda \bar{c}) \quad \dots (50)$$

where λ = mean free path

\bar{c} = mean molecular speed of a molecule in the gas phase.

which for CO gives

$$D = 2 \times 10^{-8} \times \frac{T^{3/2}}{P}$$

so that if $P = 0.01$ atmos. and $T = 1500^\circ K$, $D = 0.1 \text{ cm}^2 \text{ sec}^{-1}$

This value is much greater than either carbon or oxygen in liquid iron (3) which are about $7 - 10 \times 10^{-5} \text{ cm}^2 \text{ sec}^{-1}$.

Convective turbulence will also be high in the gas phase under conditions where the gas is being continually removed and large temperature gradients exist. Consequently it is unlikely that the rate of the C/O reaction is limited by

1.3. Diffusion and Convection in Fluids. (56)1.3.1. General Theory.

Diffusion in liquids is essentially the same process as in solids and can be described by Fick's laws

$$J = -D \frac{\partial C}{\partial x} \quad \text{Fick's first law} \quad \dots (51)$$

and $\frac{dC}{dt} = D \frac{\partial^2 C}{\partial x^2} \quad \text{Fick's second law} \quad \dots (52)$

where J = flux of material (usually in moles/sec/sq.cm)
 C = concentration (moles/cc)
 x = length (cm)
 D = proportionality constant, diffusivity or diffusion coefficient (cm²/sec)

Strictly, the driving force for diffusion is not a difference in concentration (∂C), but a difference in chemical potential (57-59). Thus, if concentrations, and not activities are used to measure such differences, it is implied that D includes an activity coefficient term and it can be expected that D will be a function of concentration, an expectation confirmed by experiment (51).

In liquids convection is usually a more important transport process than diffusion and since they cannot sustain a shear force, bulk movements of large groups of molecules become possible, e.g.:- uniformity achieved by mechanical stirring, induction or gas bubbling.

When the flow of a fluid is streamline or viscous, molecular diffusion still accounts for mass transport in a direction perpendicular to the flow, but in the direction of flow there is the additional bulk movement of the fluid to aid transport. The total flux of material in a direction is then given by

$$J = -D \frac{\partial C}{\partial x} + v_x C \quad \dots (53)$$

where v_x is the component of fluid velocity in the x direction.

In turbulent flow, an additional mechanism of transport becomes operative, turbulent or eddy diffusion, which is a more rapid process than normal molecular diffusion. Though it is difficult to separate the various contributions to transport they are normally assumed to be additive and the total flux in the direction x is therefore:

$$J = -D \frac{\partial C}{\partial x} + v_x C - E \frac{\partial C}{\partial x} \dots (54)$$

where E = coefficient of eddy diffusion.

The simplest practical case is that of a fluid moving past a solid surface, such as the washing of liquid steel or slag against the refractory of ladles or furnaces. Since the liquid cannot sustain a shear, the frictional forces prevent any movement of the layer of liquid molecules right at the boundary. The velocity gradually increases with distance from the boundary until it reaches the bulk velocity (Figure 17). The value of δ_v is shown to increase as the distance along the flat surface (y) increases and as a consequence the diffusion rate in the x direction decreases.

For the solution of the solid in the liquid: if conditions in the fluid bulk are static then diffusion of the solute occurs away from the boundary, the concentration gradient gradually decreasing with time and slowing down the rate of solution. When the liquid is in streamline flow, dissolved material is continually swept away parallel to the surface so that the concentration gradient perpendicular to the surface (x direction) is markedly steepened and the rate of solution is increased. In turbulent flow, eddy diffusion further increases the rate of solution, since there is this additional mechanism for movement of solute away from the phase boundary. These latter two cases represent the conditions applying to an induction

stirred bath where no bubbles are formed, and a violently bubbling bath respectively.

1.3.2. Boundary Layer Theory.

For streamline flow, in forced convection, past a flat plate, Darken (56) has given the velocity boundary layer thickness δ_v as being

$$\frac{\delta_v}{y} = 4.64 \text{ Re}^{-\frac{1}{2}} \quad \dots (55)$$

where y = distance in the flow direction from the leading edge of the plate

Re = Reynold's number for the bulk flow.

A similar equation has also been used to give an approximate value for the boundary layer on the surface of CO bubbles (52)

$$\delta_v \approx \frac{r}{\sqrt{\text{Re}}} \quad \dots (56)$$

where $\text{Re} = \frac{\rho v r}{\eta}$
 ρ = density of liquid iron
 r = radius of bubble.
 η = viscosity coefficient of liquid iron.
 v = velocity of bubble and bulk liquid.

Putting in values of $v > 1$ cm/sec, $r \approx 1$ cm, $\text{Re} \approx 10^3$, $\rho = 7$ gm/cc and $\eta = 10^{-2}$ poise, the thickness of the surface layer of a gas sphere can be calculated as being 0.03 cm which is a value ten times that given by Darken (54).

If the plate is soluble in the fluid a concentration gradient will be set up. The concentration or diffusion boundary layer thickness δ_c , does not necessarily have the same value as that of the velocity boundary layer.

The calculated thickness is given by the equation

$$\frac{\delta_c}{y} = 4.64 \text{ Re}^{-\frac{1}{2}} \cdot S_c^{-\frac{1}{3}} \quad \dots (57)$$

where $S_c = \text{Schmidt number} = \frac{\nu}{D}$ with D the diffusion coefficient of the solute in the fluid.

The diffusion boundary layer thickness δ_c therefore, depends on the flow conditions specified by Reynold's number and is smaller for high velocities and low viscosities; it also decreases with decreasing values of D.

In the case of a flat plate δ_c increases with distance from the leading edge. In the case of steel in contact with refractory δ_c will vary from point to point over the phase boundary, so that some average value has to be specified.

For mass transfer calculations the actual boundary layer thickness is not so useful as its effective value. This is that value which would result in the same flux if only molecular diffusion were operative. Figure 18 shows schematically the concentration changes which occur when fluid flows past a solid in a streamline manner.

The effective boundary layer thickness δ is defined as

$$\delta = \frac{C_b - C_s}{\left[\frac{\partial C}{\partial x} \right]_{x=0}} \dots (58)$$

where C_s and C_b are the phase boundary and bulk concentrations respectively.

The rate of solution can be calculated from equation (53), but $\bar{v}_x = 0$ at $x = 0$. Thus

$$J = -D \left[\frac{\partial C}{\partial x} \right]_{x=0} \dots (59)$$

This result also applies to turbulent flow conditions, since the flow must become streamline very close to the boundary and there is, therefore, no eddy diffusion in this region.

Combining the last two equations we have

$$J = \frac{D (C_s - C_b)}{\delta} \dots (60)$$

this is the most useful expression for mass transport to and from a fluid-solid boundary.

For the case of the flat plate $\delta = \frac{D}{3\delta_c}$ and so from equation (57)

$$\frac{\delta}{y} = 3.09 R_e^{-1/2} S_c^{-1/3} \dots (61)$$

The dependence of δ on R_e and S_c will not be the same for turbulent flow and generally somewhat larger values for R_e may be expected.

Using $R_e = 10^4$, $v = 10$ cm/sec and $D = 1 \times 10^{-4}$ cm²/sec and applying equation (61)

$$\delta = .002 \text{ cm}$$

This value is in accordance with experimental evidence and those derived by other techniques (52,60). Riddiford (61) has shown that $\frac{D}{\delta}$ has an exponential dependence upon temperature.

$$\frac{D}{\delta} = A \left(\frac{D}{\delta}\right) \exp \frac{E(D/\delta)}{RT} \dots (62)$$

where $E\left(\frac{D}{\delta}\right) = \frac{4E_D + E_V}{6}$ for laminar flow

and $E\left(\frac{D}{\delta}\right) = \frac{2E_D + E_V}{3}$ for turbulent flow

E_D = activation energy for diffusion of rate controlling component in the melt.

E_V = activation energy for viscous flow in molten metal.

Sharma and Ward (62) used this theory to explain the temperature dependence of the rate constant in the reduction of silica in Fe - C melts.

A disadvantage of the theory is the difficulty associated with the calculation of δ . In most cases of practical interest it can only be estimated. King (55) points out that δ is a function of the diffusion coefficient

and the degree of convective stirring being larger for larger values of D and smaller the higher the flow velocity of convective currents past the boundary.

1.3.3. Surface Renewal Theory. (63)

In this model the idea of a static boundary layer is rejected and turbulence is considered to exist to the surface. Volumes of the liquid are continually being brought into and out of contact with this surface and transport occurs by a process of unsteady state diffusion. A parameter 'S' "the surface renewal factor" is introduced and, in so far as it a function of the convective turbulence, takes over the role of δ in the boundary layer theory.

If there is no resistance to transfer at the surface i.e. instantaneous equilibrium between surface concentrations and gas, then the theory predicts that the rate of mass transfer from melt to gas is given by

$$\text{Rate} = A_{gm} \cdot (DS)^{\frac{1}{2}} (C_b - C_e) \quad \dots (63)$$

where C_b is the bulk concentration of the solute in the liquid and C_e is the equilibrium concentration at the gas/metal interface and S is the surface renewal factor, equal to the fractional rate of renewal at the surface. Danckwerts (63) extended the theory to the case where there is resistance to transfer at the surface and a local equilibrium does not exist and concluded that the rate of transfer in this case is given by

$$\text{Rate} = \frac{A (C_b - C_e)}{\left(\frac{1}{k} - \frac{1}{(DS)^{\frac{1}{2}}} \right)} \quad \dots (64)$$

where k is a constant.

1.3.4. Convective Flow Model.

This theory deviates from Danckwert's statistical approach only in that expressions are determined for S. But basically they are the same models of surface renewal rejecting the principle of a static boundary layer. Instead a flow layer is envisaged within which flow velocity is invariant with depth and is parallel to the surface. Carbon and oxygen are introduced to the layer by convection. Transport to the surface then takes place by diffusion only.

1.3.4.1. Machlin's Rigid flow model (64)

Machlin's model is restricted to an inductively stirred cylindrical bath. It is assumed that under these conditions the rigid flow model (Figure 19) (65) can be applied.

In this model the liquid within the surface layer moves in streamline flow with no velocity gradient perpendicular to the surface and in a direction radially outwards from the centre. Thus an element appears at the centre, discharges its contents by diffusion as it flows across the surface and is then mixed into the bulk at the boundary. The 'dwell time' is the time taken by the element to flow from the centre to the edge of the melt surface.

On this basis Machlin derived the equation

$$\frac{dC_b}{dt} = 2 (C_b - C_s) \left[\frac{2Dv}{\pi r h^2} \right]^{\frac{1}{2}} \dots (65)$$

where v = velocity of surface layer.
r = radius of crucible or surface layer.
h = height of metal bath.
D = diffusion coefficient of solute.

which is equivalent to

$$\frac{dn}{dt} = \beta A_{gm} (C_b - C_s) \dots (66)$$

where the mass transfer coefficient

$$\beta = \left(\frac{2Dv}{\pi r} \right)^{\frac{1}{2}}$$

and $A_{gm} =$ area of gas/metal interface.

1.3.4.2. Free Convection Model - Kraus (60)

This model considers natural convection caused by mass and heat losses from the gas/metal interface. Otherwise the transfer mechanism is the same as in the 'rigid flow model' (Figure 19).

The boundary conditions for solution of the diffusion equation are as given previously. As the element's residence time on the surface increases so does the depth of the diffusion zone within the element.

This depth, is given at any instant by

$$\delta_t = 2(Dt)^{\frac{1}{2}} \quad \dots (67)$$

where $t = \frac{y}{v}$

and at any instant the rate of diffusion according to Fick's first law is given by

$$\frac{dn}{dt} / A_{gm} \approx \frac{D}{\delta_t} (C_b - C_e) \quad \dots (68)$$

If the distance travelled on the surface by an element is y , then from (67) and (68) the rate of diffusion from an element of area $dA = zdy$, is:-

$$d\left(\frac{dn}{dt}\right) \approx \frac{1}{2} \left(\frac{Dv}{y}\right)^{\frac{1}{2}} \cdot (C_b - C_e) \cdot zdy \quad \dots (69)$$

then the number of particles which are exchanged through the area $z\lambda$ in unit time is obtained by integration of the above equation from $0 - \lambda$ (λ is the distance between stagnation points on the surface). This gives

$$\frac{dn}{dt} = z\lambda \left(\frac{Dv}{\lambda}\right)^{\frac{1}{2}} \cdot (C_b - C_e) \quad \dots (70)$$

and the rate of evolution from unit area is $\left(\frac{Dv}{\lambda}\right)^{\frac{1}{2}} \cdot (C_b - C_e)$

for the total area A_{gm} , therefore, the rate is

$$\frac{dn}{dt} = A_{gm} \beta (C_b - C_s), \quad \dots (71)$$

where $\beta = \left(\frac{v}{\lambda} \right)$

Assuming that the flow at the surface is friction free, Kraus (60) derived an expression for the dwell time of a liquid element:

$$t^{\frac{1}{2}} = \frac{\lambda}{\bar{v}} = \left[\frac{\rho C_p \eta}{g \chi q} \right]^{\frac{1}{2}} \dots (72)$$

where η = kinematic viscosity (cm²/sec)
 and χ = expansion coefficient (°C⁻¹)
 C_p = specific heat (cal.g.°C)
 q = heat flow

Evaluation gives $\frac{\lambda}{\bar{v}} = 0.1$ sec.

Kraus (60) interpreted this as indicating that λ was small - approximately 0.1 mm.

With the above value for $t = \frac{\lambda}{\bar{v}}$, the mass transfer coefficient is given by:-

$$\beta = D^{\frac{1}{2}} \left[\frac{g \chi q}{\eta \rho C_p} \right]^{\frac{1}{4}} \dots (73)$$

and evaluation gives $\beta = 0.025$ cm sec⁻¹.

For flow with friction at the surface Kraus shows that β is reduced by a factor of $\left(\frac{D}{\eta} \right)^{\frac{1}{3}} \approx \frac{1}{5}$ for molten steel using $D = 6.0 \times 10^{-5}$ cm²/sec (66,67) and $\eta = 7 \times 10^{-3}$ cm²/sec (68).

Application to induction furnace melts.

Figure 20 (93) shows diagrammatically the flow pattern in the induction furnace. The magnetic field forces the liquid metal up in the centre of the furnace, the height of which increases with power input. From the dome of the bath thus formed the melt flows down again to the sides.

The distance between the stagnation points λ in equation (70) is determined by the radius r of the crucible. The average

velocity \bar{V} at the phase contact areas has been deduced
 " by Knuppel (93) as follows:-

The pressure on the melt causing the bath dome is calculated from

$$P_s = 31.6 \sqrt{\frac{\mu}{\sigma f}} \cdot \frac{N_i}{A} \quad \text{kg/cm}^2 \quad \dots (74)$$

where μ = relative permeability
 σ = specific resistance of melt $\left[\frac{\Omega \text{ mm}^2}{\text{M}} = \Omega \text{ cm} \cdot 10^{-4} \right]$
 f = frequency (c/s)
 N_i = induced power (kW)
 A = cylindrical surface area of melt (cm^2)

The pressure p_s is held in equilibrium by the gravitational pressure ρh

where ρ = S.G of melt, h = rise of bath.

$$\therefore P_s = \rho h = 31.6 \sqrt{\frac{\mu}{\sigma f}} \cdot \frac{N_i}{A} \quad \dots (75)$$

$$\text{Hence } h = 31.6 \sqrt{\frac{\mu}{\sigma f}} \cdot \frac{N_i}{A} \cdot \frac{1}{\rho} \quad \dots (76)$$

" For liquid iron Knuppel and Oeters (93) obtain

$$h = 1.78 \text{ cm @ } 1600^\circ \text{ Centigrade}$$

$$h = 2.02 \text{ cm @ } 1700^\circ \text{ Centigrade}$$

The average velocity \bar{V} is calculated approximately by assuming flow along an inclined plane (Figure 21)

$$\text{where } \bar{V} = \frac{1}{2} \sqrt{2gh}$$

Hence inserting the above values for h

$$\bar{V} = 29 \text{ cm/sec @ } 1600^\circ \text{ Centigrade}$$

$$\bar{V} = 32 \text{ cm/sec @ } 1700^\circ \text{ Centigrade}$$

Experimental determination measuring the speed of removal of a piece of coal to the outer edge gave $\bar{V} = 20 \text{ cm/sec}$, in reasonable agreement with the calculations.

" Knuppel and Oeters (93) used equation (71) for consideration of nitrogen removal under vacuum and obtained good agreement with their experimental results:-

	$\bar{v} \times 10^3$ (cm/sec) from equ. (71)	$\bar{v} \times 10^3$ (cm/sec) (experimental)
1600°C.	20.6	14.5
1700°C.	23.8	17.3

They concluded that in their case streamline parallel flow had taken place, but that in accordance with Kraus's calculations where the rate of flow tends to zero i.e. at the surface, the thickness of the boundary layer is given by

$$\delta = 2.9 \times 10^{-3} \times 4.4 \approx 13 \times 10^{-3} \text{ cm}$$

and correspondingly the mass transfer coefficient would be smaller by a factor of 4.4.

Kraus obtained $\delta \approx 12 \times 10^{-3}$ in melts on iron melts in which film formation on floating slag particles could be recognised.

1.3.5. Summary and comparison of mass transfer theories.

The foregoing theories of the kinetics of degassing from quiescent melts start off with the basic assumption that the rate controlling step is the transfer of components from the bulk of the melt to the gas/metal interface. The mechanism of transport is then analysed and the transport coefficient evaluated in attempts to deduce the factors which influence the rate.

All four theories yield expressions for the rate of the same form

$$\frac{dn}{dt} = \beta A_{gm} (C_b - C_e)$$

where $\beta = \text{constant}$.

Kinsman (65) has summarised them in Figure (19). The first two theories are the most general; they are applicable under all hydrodynamic and geometrical conditions. They differ in their concept of the process, but for practical purposes are much the same, since they both contain an

adjustable parameter (β or β') which is a function of the convective stirring.

Machlin and Kraus obtain β in terms of fundamental parameters such as kinematic viscosity which can be directly measured and consequently they are more amenable to experimental testing than the others.

1.4. Mass transport by bubbles.

1.4.1. Nucleation of CO bubbles.

The importance of bubble nucleation was first realised by Korber and Oelsen (69) who discovered that under certain conditions an iron melt supersaturated in carbon and oxygen could be prevented from forming CO gas. This was especially true of glazed crucibles.

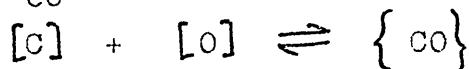
Using the Volmer - Becker - Doring theory (70, 71) Niwa (52) derives the critical radius r^* which must be achieved prior to growth of a stable bubble as

$$r^* = \left[- \left(\frac{2RT}{N_0 \Delta G_{co}} \right) - \frac{4}{3} \right] \frac{\sigma}{P} \dots (77)$$

where σ = surface tension of liquid iron

P = total pressure on bubble
excluding surface tension
i.e. atmosphere + ferrostatic

ΔG_{co} is the free energy change for the reaction



and N_0 = Avagadro's number

From this equation it is shown that

$$r^* = \left[\frac{2}{\ln(O_b/O_e)} - \frac{4}{3} \right] \frac{\sigma}{P} \dots (78)$$

where O_e is the equilibrium oxygen content

and O_b is the actual oxygen content of the melt.

The free energy change of the critically sized gas bubble is given by

$$\left[\left[\frac{4\sigma}{r^*} + 3P \right] \right]$$

the probability of forming the critical size being

$$f^* = e^{\frac{-N_0 \Delta G^*}{RT}} \dots (80)$$

Inserting $r^* = 10^{-3}$ cm

and $\sigma = 1500$ dynes/cm

f^* is found to be extremely small.

Similarly Bogdandy (72) gives the nucleation frequency of gas bubbles as

$$J = F \cdot e^{\frac{-W}{RT}} \text{ nuclei/cm}^3/\text{sec} \dots (81)$$

where the work of nucleus formation is $W = \frac{1}{3} \sigma 4\pi r^{*2}$

He gives the radius of the nucleus as

$$r^* = \frac{2 \sigma M}{\rho RT \ln \frac{C_b}{C_s}} \dots (82)$$

where the supersaturation under steel making conditions is defined by

$$\frac{C_b}{C_s} = \frac{p_{CO}}{p^s_{CO}} = \frac{[\%C][\%O]}{2.5 \times 10^{-3}}$$

Equation (81) applies originally to the formation of vapour bubbles under reduced pressure. According to Bogdandy (72) it can be used as an estimate for the nucleation of bubbles in supersaturated melts, although the frequency factor F cannot be determined with accuracy (73,74,75).

Figure 22 (72) shows that the frequency of nuclei formation is extremely low and the calculation (73,75) shows that the formation of CO nuclei within the melt is practically impossible. Hence a CO boil must rely on heterogeneous nucleation and it is, therefore, necessary for the vessel wall to contain many crevices in which gas may be trapped. Growth

and release of bubbles will then occur from these sites. That this conclusion is valid is demonstrated by the experiments of Korber and Oelsen (69) and by the investigations of Brower and Larsen (76). The fact that the CO boil is generally controllable is evidence that nucleation of bubbles is not rate determining. However, it is worthy of note that recent attempts to achieve vacuum-killed low carbon steel (77) and low carbon stainless steel has resulted in a lack of the C/O reaction when the starting carbon content is less than about 0.04%. Initiation of the reaction has been achieved by small additions of carbon or metal seeds (78).

1.4.2. Growth and motion of gas bubbles.

It is only in recent years that it has been established (79) that the bubbles observed in steelmaking processes, which are usually greater than 1 cm in diameter have the spherical-cap shape shown in Figure 23. Niwa (52) shows that the Stokes-Navier equation is inadequate to describe bubble movement.

The frictional force on a sphere having a radius r and velocity V is

$$F_{RS} = 6\pi\eta rV \quad \text{according to Stoke's law} \quad \dots (83)$$

Balancing this against the buoyancy of the gas bubble

$$V = \left(\frac{2}{9} \frac{g}{\eta} \right) \rho r^2 \quad \dots (84)$$

Substituting $\rho = 7$, $\eta = 2 \times 10^{-2}$ poise the velocity comes to 700 m/sec, an exceptionally fast rate leading to a Reynold's number R_e of 10^5 . Hence this equation cannot possibly describe the conditions appertaining in practice.

Using Newton's equations

$$\text{the velocity } v = \left(\frac{4}{3} r g \right)^{\frac{1}{2}} \dots (86)$$

which is in agreement with Haberman and Morton (80).

Work of Davies and Taylor (81) on spherical cap bubbles gives

$$v = \frac{2}{3} \sqrt{g R_c} \dots (87)$$

where R_c = radius of curvature of spherical cap.

which in terms of an equivalent spherical radius is similar to equation (86).

Figure 24 shows the good agreement obtained by Bradshaw (82) in experiments with a variety of media.

It is, therefore, apparent from this work that the rate of rise is unaffected by the properties of the fluid such as the density of the liquid and the surface tension at the gas/liquid interface. It is dependent only on the size of the bubble except for liquids with viscosities greater than about 100 cp., where there is a decrease in rate of about 10-15% due to a slight change in bubble shape.

Studying the transfer of CO_2 between water and gas bubbles Baird and Davidson (83) give the following equation for the mass transfer coefficient (cm/sec) from consideration of laminar flow about the spherical cap.

$$\beta = 0.975 d_e^{-\frac{1}{4}} \cdot D^{\frac{1}{2}} \cdot g^{\frac{1}{4}} \dots (88)$$

where d_e = radius of a spherical bubble of equivalent volume.

The small inverse relationship between β and d_e shown in the above equation is not supported by Richardson (79) who suggests that β is virtually independent of bubble size although bubble shape, being altered by viscosity has a small influence on β . For spherical cap bubbles it appears

than across the cap and is about 20% of the total.

2. Comparison of Theory with Experimental Results.

2.1. Kinetics of the C-O reaction.

It has been shown that at the low pressures encountered in vacuum degassing, it is unlikely that transport in the gas phase determines the rate. It is possible that either heterogeneous chemical reaction or mass transport in the liquid is the rate-controlling step. The experimental evidence indicates that in the quiescent stage of the C/O reaction the rate of evolution of carbon monoxide is

$$\frac{dn}{dt} = \beta A_{gm} (C_b - C_s)$$

Because the rate controlling step is proportional to the surface area and because of the argument outlined in Section 1.1., homogeneous chemical reaction can be ruled out as rate determining.

A summary of experimentally determined values for the mass transfer coefficient is given in Table 2.

The boundary layer theory gives $\beta = \frac{D}{\delta}$ from which Larsen (89) estimates δ as 0.0022 cm. On the other hand the basic hydrodynamic theory under 1.3.1. gives $\beta = 0.03$ cm (52) for the surface layer of bubbles which is in rough agreement with the work of Schvartsman (87). Darken (56) agrees with Larsen (89) and also gives 0.003 cm.

Using this value and the diffusion coefficient of oxygen $D_o = 7.8 \times 10^{-5} \text{ cm}^2 \text{ s}^{-1}$ (7), Kinsman (65) gives

$$\beta = \frac{D}{\delta} = 0.026 \text{ cm sec}^{-1}.$$

Knuppel and Oeters (93) use the Kraus model to study the mass transfer mechanisms of hydrogen and nitrogen from their calculations of β for nitrogen removal and using

$$\beta = \frac{D}{\delta}$$

assuming a value of $D = 6.0 \times 10^{-5} \text{ cm}^2 \text{ sec}^{-1}$ (66,67) they deduce that $\delta = 2.9 \times 10^{-3} \text{ cm}$ for friction-free flow and $13 \times 10^{-3} \text{ cm}$ for flow with friction.

Using the boundary layer approach and applying it to four limiting cases, since it is shown that the surface concentrations of carbon and oxygen change with those of the bulk of the melt, Knüppel determines the effective mass transfer coefficient as .047 cm/sec for oxygen contents of between 0.010 - 0.020 (C% .06 - .14%). With increasing oxygen and decreasing carbon, β reaches the value 0.014 cm/sec at .053% O (.031% C). The fact that β becomes smaller with decreasing carbon (down to stoichiometric C/O ratio) indicates that $\beta_c/\beta_o \neq 1$. Knüppel (93) determines this value as 0.14.

Machlin's (64) rigid flow model is applicable to induction stirred melts and gives

$$\beta = 2 \left(\frac{2DV}{r\pi} \right)^{\frac{1}{2}}$$

(where the surface area is related to r by $A_{gm} = \pi r^2$).

Unfortunately it is not possible to compare theory with experiment owing to the uncertainty of the value for the velocity v . Machlin assumes 10 cm sec^{-1} , but a better value of $20\text{-}30 \text{ cm/sec}^{-1}$, by a comparison of theory with experiment, (Section 1.3.4.2.) is given by Knüppel and Oeters (93).

Taking the value for the diffusion coefficient of oxygen as $1 \times 10^{-4} \text{ cm}^2/\text{sec}^{-1}$ this gives β as

$$\beta = 2 \left(\frac{1 \times 10^{-4} \times 20}{r_c \pi} \right)^{\frac{1}{2}}$$

$$\beta = \frac{0.05}{r_c^{\frac{1}{2}}}$$

The theory developed by Kraus (60) gives β as a function of fundamental constants, i.e.

$$\beta = D^{\frac{1}{2}} \left[\frac{g \chi q}{\eta \rho C_p} \right]^{\frac{1}{4}}$$

giving $\beta = .025 \text{ cm sec}^{-1}$

where $\chi = 2.0 \times 10^{-4} \text{ deg C}^{-1}$

at 1600°C

$$\eta = 7 \times 10^{-3} \text{ cm}^2/\text{sec.}$$

$$\rho = 7.0 \text{ g/cc.}$$

$$C_p = 0.2 \text{ cal.g.deg.C.}$$

giving good agreement with experimental results.

The transfer coefficients determined by Parlee (85) are considerably smaller than the theoretically derived values of the boundary layer and Kraus models and the other experimentally determined values shown in Table 2. Kinsman (65) states that a possible explanation for this is that the conditions for Parlee's experiments were not friction free, contamination possibly having occurred from a thin surface layer of alumina. Hence the derivation of Kraus for friction at the surface, the normal value of approximately 0.04 cm sec^{-1} would be expected to be reduced by a factor of $\frac{1}{5}$ i.e. 0.008 . This is now in line with the results quoted by Parlee of $0.0015 - 0.0126 \text{ cm sec}^{-1}$. Similarly Kraus (60) found that when a visible oxide film had formed β was only $0.005 \text{ cm sec}^{-1}$.

No data is available for the frequency of bubble nucleation as a function of pressure and concentration and hence the rate of degassing during the boil cannot yet be theoretically investigated. However, Kraus (60) did succeed

in deriving an approximate expression for the rate in the presence of excess bubble nuclei i.e. when boiling is so vigorous that the melt effectively becomes a foam.

The gas flow which leaves the liquid passing through a cross-sectional area A is, therefore:

$$\frac{dN}{dt} = \psi \frac{A v p}{RT} \dots (89)$$

where v = velocity of rising bubbles.
 p = pressure in bubbles
 ψ = ratio of gas volume
 liq.vol.+ gas volume.

this approximates to

$$\frac{dN}{dt} \approx 2 (DgC_e/C_b)^{\frac{1}{3}} \psi A c_b \dots (90)$$

$$\text{and } \beta = 2 (DgC_e/C_b)^{\frac{1}{3}} \psi \dots (91)$$

For CO formation in steel melts of between 0.05 - 0.5% C

and for $\psi = \frac{1}{2}$

$$\beta = 0.1 - 0.3 \text{ cm/sec.}$$

which represents a rate 10 x that in the absence of bubbles.

This large degassing rate has been found experimentally only in large industrial installations and the data given in the literature is scanty. However, the values given in Table 3 give good agreement with the determination of Kraus. This evidence on foaming melts is contrary to the calculation of Richardson (79) who used equation (88) for the removal of CO as bubbles in the open hearth process. He obtained a value of 0.04 cm/sec⁻¹ (Table 2), a value very close to that for normal diffusion-controlled calculations.

From the foregoing, it seems almost certain that transport in the melt is the rate determining step for quiescent melts. Richardson suggests that there is also good reason to believe that the growth of CO bubbles is also

controlled by the same mechanism. (Surface activation is thought to play little part since the surface of the bubble is renewed at a rapid rate, unlike the gas/metal boundary in a static melt.) The experiments of Sharma and Ward (62) on the reduction of silica by an iron-carbon melt provide additional confirmation of this. The predicted temperature dependence derived from the model based on slow diffusion of oxygen in the melt, agreed closely with the experimental results.

In view of these thoughts the conclusions of Kraus on foaming melts need further explanation.

2.2. Kinetics of melt-crucible reactions.

2.2.1. Kinetics of silica reduction.

Turkdogan et al (94) studied the rate of reduction of silica from silicate slags by graphite-saturated iron in the presence of carbon monoxide and at 1600° Centigrade. In order to minimise changes in slag composition during the experiment the bulk ratio of slag to metal was maintained at a high level of about 33 to 1, i.e. 200g slag to 6g metal. The rate curves shown in Figure 25 were found to be linear with time for the first 5 to 10 hours of reaction time after which there was a gradual decrease in the slopes of the curves. Because of this Turkdogan suggested that the rate-determining process in the breakdown of silica was due to an interfacial chemical reaction rather than mass transport of the reacting species in either of the bulk phases.

For the adsorption of silicate ions at the slag-metal interface,



where \square and $\square \text{SiO}_2$ are vacant and occupied sites at the

Turkdogan derived the rate equation

$$\%Si = \frac{445.8}{l} \times \frac{k_1 \cdot K_a \cdot a_{SiO_2}}{1 + K_a \cdot a_{SiO_2}} t + I \dots (92)$$

where I = integration constant determined from the initial silicon content of metal.
 l = depth of cylindrical melt.
 k_1 = rate of forward reaction.
 K_a = equilibrium constant for adsorption reaction.

The rate of the reverse reaction, k_2 , is assumed to be negligible at this stage.

The rate constant R, for a given temp. and silica activity is given by;

$$R = \frac{k_1 \cdot K_a \cdot a_{SiO_2}}{1 + K_a \cdot a_{SiO_2}} \quad , \dot{n}_{Si}/sq.cm./hr. \dots (93)$$

which, on rearrangement, gives the following expression;

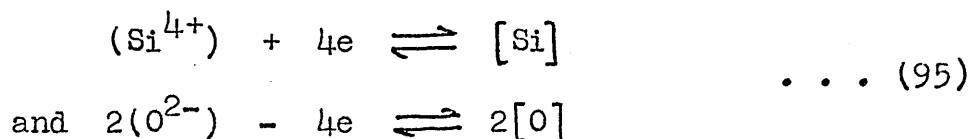
$$\frac{R}{a_{SiO_2}} = k_1 K_a - K_a R \dots (94)$$

which should result in a straight line with a negative slope for a plot of $\frac{R}{a_{SiO_2}}$ against R. Figure 26 shows the plot of Turkdogan's results and because of the agreement he concludes that the foregoing rate theory is applicable to the reduction of silica from a silicate melt by graphite-saturated Fe-Si alloys. For prolonged reduction times (10 hours) where the rate of reaction decreases with time, Turkdogan found continued agreement with this theory providing the reverse rate of the reaction was taken into account.

In the absence of CO bubbles at the slag/metal interface the rate of reduction was found to be reduced and the results suggested that under these conditions the rate controlling process was the diffusion of oxygen to the

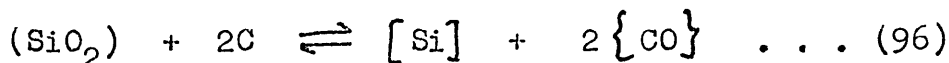
graphite walls of the crucible near the slag-metal-graphite 3-phase boundary. The interdiffusivity of silicon in graphite-saturated iron was also obtained from this work and found to be $(5.4 \pm 0.4) \times 10^{-5}$ sq.cm/sec, in agreement with other data (95).

Grimble and Ward (96) have examined the possibility that the reduction of silicon from silica-saturated slags by carbon-saturated iron in graphite crucibles may occur by both chemical and electrochemical means. In the dissociation of silica the simultaneous reactions

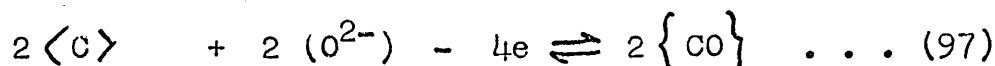


will probably occur at adjacent sites so that electrons will be transferred directly between them and the overall reaction will be chemical rather than electrochemical in nature.

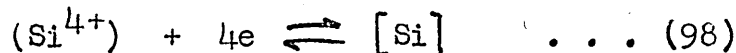
The three-phase reaction between silica and carbon



can also occur by an electrochemical mechanism consisting of separated anodic and cathodic reactions. In a graphite crucible these are the anodic reactions,



occurring at the slag/graphite interface and a cathodic reaction



at the slag-metal interface.

Ward (96) conducted experiments using electrochemical cells with separated anodic and cathodic areas and showed that the electrochemical reduction of silica by carbon does occur. Although the fractional contribution by electrochemistry to the overall reduction of silica in graphite

crucibles cannot be assessed in this way, the comparison of the rate of silica reduction in simple graphite cells with that of sleeved crucibles shown in Figure 27, strongly suggests that the contributions of electrochemistry and chemistry are of similar magnitude. In view of this work it would seem that the electrochemical reduction of silica plays an important part when graphite crucibles are used. This applies to the work of Turkdogan et al (94) and suggests that his data should not be used when considering simply the chemical dissociation of silica which occurs with refractory crucibles.

Sharma and Ward (97) have investigated the kinetics of the chemical process operating in the absence of any electrochemical reaction. They suggest that the reduction of silica by carbon is unlikely to occur as a single stage process since this would involve a three-phase reaction which could only occur along a line. Instead the overall reaction must consist of a number of steps and the following partial reactions are proposed;

- (i) dissociation of silica at the oxide-metal interface, $\langle \text{SiO}_2 \rangle \rightleftharpoons [\text{Si}] + 2 [\text{O}] \dots (33)$
- (ii) diffusion of (a) oxygen and (b) silicon through the boundary layer at the silica-metal interface.
- (iii) transport of oxygen, silicon and carbon in the bulk metal.
- (iv) diffusion of (a) oxygen and (b) carbon through the boundary layer at the metal-gas interface.
- (v) reaction of carbon and oxygen at the metal-gas interface to form carbon monoxide,

Ward suggests that the chemical reaction rates (i) and (v) are not controlling since the rate curves he obtained in his experiments were not linear. Of the remaining mass transport steps, (iii) was considered to be rapid in an induction-stirred system and (ii)b and (iv)b were thought to be rapid because of high concentrations of carbon and silicon in the melt. The diffusion of oxygen in the metal boundary layers were thus concluded to be the rate-determining steps. The chemical reaction steps (i) and (v) were considered to be sufficiently rapid to maintain the equilibrium oxygen level in the metal at the oxide-metal and metal-gas interfaces, and the oxygen gradients in the system were represented schematically as in Figure 28.

A model was accordingly derived by Ward using the boundary layer theory, making the assumptions that $\delta_R = \delta_g$, the concentration of oxygen in the surface layers of the metal were zero and that the product of the activity coefficients for oxygen and silicon were equal to unity

($f_o \times f_{Si} = 1$). The final rate equation took the form;

$$\frac{d \%Si}{dt} = \frac{M_{Si}}{2M_o} \cdot \frac{A}{V} \cdot K_{33}^{\frac{1}{2}} \frac{Dx(1-x)}{\delta} [\%Si]^{-\frac{1}{2}} \dots (99)$$

where x = fraction of metal surface in contact with silica.

and $1 - x$ = fraction of metal surface in contact with gas.

Reasonable agreement was found between theoretical and experimental determinations of the final silicon content.

The experiments were carried out at temperatures between 1370 and 1600° Centigrade which allowed calculation of the rate constant

$$k = \frac{d [\%Si]}{dt} \cdot \frac{2M_o}{M_{Si}} \cdot \frac{V}{A} \cdot [\%Si]^{\frac{1}{2}} \dots (100)$$

and using $k = A \exp\left(\frac{-E}{RT}\right)$ the activation energy for the reaction was determined.

Figures 29 and 30 show plots of $\log k$ against $\frac{1}{T}$.

Table 4 shows the good agreement obtained between the theoretical and experimental values for the activation energy in the high temperature range (1425 - 1600° C) which suggests that under the conditions used by Ward the model of rate control due to the slow rate of oxygen diffusion in the metal may well be correct. A line drawn through the low temperature points (< 1425° C) for the unsaturated melts shown in Figure 30 gives an apparent activation energy of 120 k cal/g.mole, a value which is too high to be explained by the diffusion model and Ward suggests chemical rate control associated with the breaking of Si - O bonds (98) in solid silica. The curved form of Figure 30 could, therefore, represent a transition from predominantly chemical control at low temperatures to predominantly diffusion rate control at high temperatures.

Graham and Argent (99) have studied the crucible reactions in the vacuum melting of a 0.2% C steel using aluminosilicate crucibles containing 95 - 42% alumina. Using arguments similar to those used by Sharma and Ward (97), Argent makes the basic assumption that the rate-determining step is the transport of silicon and oxygen across the boundary layer of the crucible-metal interface. Machlin's rigid flow model (64) was used to calculate the rate of reaction with the lining, on the assumption that the crucible wall could be represented by areas of alumina and silica proportional to their volume fractions in the refractory and that alumina could be considered inert by comparison with silica. Figure 31 shows that the carbon loss and silicon

reaction;



The final oxygen levels achieved were about 0.001 w/o irrespective of crucible composition.

The initial rates of silicon pickup for melts in 95,60 and 42% alumina crucibles were predicted to be 0.035%/hour, 0.12%/hour and 0.196%/hour which are in excellent agreement with the observed rates of 0.04%/hour, 0.12%/hour and 0.20%/hour. The total pickup over 85 minutes was calculated to be 0.04, 0.14 and 0.22% as compared with the experimental values of 0.05, 0.10 and 0.16%; whereas final oxygen contents were estimated to be 0.002, 0.0065 and 0.007% and are thus much higher than the experimental value of 0.001%. Graham and Argent concluded that the agreement between predicted and observed silicon contents was good and that the discrepancies between the theoretical and observed oxygen and silicon contents might be explained by the fact that no account was taken of either the leaching-out of the silica-rich component of the refractory or the surface activity of oxygen in iron melts. This aspect of refractory-metal interface reactions is dealt with in the present work (see Section 3.2).

Tiberg (88) has investigated the dissolution of oxides in carbon steel melts under vacuum. Material studied included silica, aluminosilicates, alumina, magnesia and lime at an initial carbon content of 0.8% and at pressures between 1 - 600 torr. The rate of solution was determined by measuring the reduction in diameter of the bars after a given time of immersion in the melt, but although this technique is useful for comparing the performance of the

to allow a quantitative assessment to be made.

2.2.2. Kinetics of alumina reduction.

The rate of deoxidation from melts in alumina crucibles (99.7% Al_2O_3) under quiescent conditions, was studied by Parlee, Seagle and Schuhmann (85) who studied the evolution and adsorption of carbon monoxide at pressures between 650 and 1000 torr. The experimental procedure involved equilibrating a melt with a known pressure of carbon monoxide and then rapidly altering the pressure to the required value for degassing. The pressure was kept constant at this value by altering the volume of the system and a record of volume against time was made. Their results are summarised in Figure 32 (65). In low carbon runs the rate initially varied and then became constant (processing time 40-50 mins) and sometimes equal to zero. High carbon runs, however, gave a constant rate throughout. The straight line portions of the volume against time graphs were interpreted as being the steady state rate when the oxygen concentrations were such that the rate of oxygen supply had become equal to the rate of deoxidation. In some graphs the final slope was negative indicating a reversal of the crucible reaction and a precipitation of alumina. In the case of the high carbon runs, corrosion of the crucible was found to be very severe and the high rate of gas evolution was considered to be due entirely to reaction with the crucible. A decrease of pressure resulted in an increased rate of carbon monoxide evolution. They interpreted their results on the basis of transport in the melt being rate controlling and using the boundary layer theory they derived the expression;

$$\ln \frac{(V_0 - y)_{t=0}}{(V_0 - y)} = \beta \frac{(A_{cm} + A_{gm})}{V_m} t \dots (101)$$

where $y = V - vt$
 $v =$ volume of system
 $\beta = \frac{D_0}{\delta_0}$

and $r =$ steady state rate of evolution of CO

The parameter y may be regarded as the value of V in the absence of a crucible reaction ($y_0 =$ final volume and $y =$ volume at any time t). The experimental data was found to follow an equation of the form of (101) and the constant β was found to range from 1.5×10^{-3} to 12.6×10^{-3} cm/sec depending on the carbon content. As shown in Figure 33, a large increase in β occurs with carbon contents of less than 0.2 w/o

The thickness of the stagnant boundary layer is not necessarily the same as the effective thickness of the concentration gradient zone and Machlin (64) attempted to avoid this concept in his rigid flow model. He considered that the surface layer moves in streamline flow with no velocity gradient perpendicular to the surface. Mass transfer occurs by diffusion during the movement of the surface from the centre to the outside of the bath. He derived the general rate equation;

$$\frac{dC_b}{dt} = 2(C_b - C_s) \left[\frac{2Dv}{\pi r h^2} \right]^{\frac{1}{2}} \dots (65)$$

which can be used to consider the deoxidation at the melt-gas interface.

For the melt-crucible interface, a given element of metal comes into contact with a length $(h + \frac{r}{2})$ in a single sweep and so equation (65) becomes;

$$-\frac{dC}{dt} = 2(C_p - C_s) \left[\frac{1}{\pi} \left(\frac{h}{r^2 h} + \frac{h}{r h^2} \right) \right] \dots (102)$$

A similar modification can be made for a double loop mixing pattern where the mixing lengths are $\frac{h}{2}$, $\frac{h}{2}$ and $\frac{r}{2}$.

Machlin applied this model to the case of $\frac{d\%O}{dt} = 0$ for iron-carbon melts in alumina crucibles, assuming that equilibrium is maintained at the two surfaces, and obtained reasonable agreement with the experimental work of Fischer and Hoffman (100) as shown in Table 5.

In a similar way, Machlin attempted to apply his model to the work of Parlee et al (85) and, although several large assumptions were made, he obtained fair agreement with the experimental data.

Birks and Booth (101) have studied the mechanism of the reduction of oxide inclusions by carbon in liquid iron during vacuum fusion analysis. The rate of reaction was measured by the volume of carbon monoxide evolved during the quiescent stage and the two were shown to be related by

$$1 - \frac{V}{V^+} = 1 - \left(\frac{t}{t^+} \right)^3 \dots (103)$$

where $V =$ volume of CO evolved at any time t

$V^+ =$ total amount of CO evolved during the reaction time t^+ . assuming that all the particles are equally sized spheres.

Figure 34 shows a plot of $\log \left(1 - \frac{V}{V^+} \right)$ against $\log \left(1 - \frac{t}{t^+} \right)$ and compares experimental data on casts killed with aluminium and silicon + manganese with a straight line through the origin of slope three, according to equation (103). The good agreement between theory and experiment is thought to confirm that the dissolution of alumina is the rate controlling process, although the final stages proceed more

end is thought to be due to errors in determining the true end-point of the reaction plus the fact that, in the final stages, a large number of the more evenly sized particles may have disappeared leaving only a few larger ones to be reduced during this period.

2.2.3. Kinetics of magnesia reduction.

There is some variation in the results given in the literature on the resistance of magnesium oxide to liquid iron. Fast (102), in investigations on the suitability of different crucible materials, obtained highest purity with magnesia crucibles.

"Kothemann, Treppschuh and Fischer (103) produced a crucible by electrically fusing magnesia of different grain sizes and in this, no reactions could be observed between crucible and melt. The same authors also found (104) that no reaction could be established when fused magnesia was introduced in powder form on to the iron melt and was allowed to act for thirty minutes at 10^{-4} torr. Earlier work by Weber, Fischer and Engelbrecht (105) contradicts the above results, stating that satisfactorily pure iron could not be obtained by melting in magnesium oxide crucibles; the lowest oxygen content obtained was 0.012%.

Machlin (64) has shown that if transport in the liquid phase is the rate-controlling factor in both deoxidation and melt-magnesia reactions, then from the rate equations it can be predicted that a minimum oxygen level will occur, which persists until the carbon concentration becomes very low (1, 86, 106). Earlier work of J.H. Moore (106) had investigated the kinetics of oxygen transfer from magnesium oxide crucibles containing iron. In this work an oxygen

The oxygen content then rose very rapidly and after a further thirty minutes had reached a value of 0.050%. Brotzmann (107) repeated this experiment and obtained ostensibly the same results, the carbon and oxygen contents falling rapidly when the pressure was lowered from 600 to 10 torr and the oxygen level rising rapidly at low carbon contents. From the final analyses 12g of oxygen was found to have been absorbed by the 25 kg melt within an hour.

Winkler (1) has given an account of work carried out by Kraus (86) whose experimental results are shown in Figures 35-37. A constant pressure of 10^{-3} torr was used and the rate was measured by removal and collection of the carbon monoxide evolved. From this and a final analysis of the melt, the manner in which the carbon and oxygen concentrations changed during degassing could be estimated (Figure 35). Figure 36 shows a plot of $\frac{dN}{dt}$ against the gas content of the melt where the curved portion of the graph represents the changing rate at the end of the boil period. Then for the first 25 minutes of the quiescent period $\frac{dN}{dt}$ is proportional to the gas content of the melt and the oxygen content falls as shown in Figure 35. A period is then reached when $\frac{dN}{dt}$ tends to zero and the oxygen concentration tends to increase; i.e. an approach to thermodynamic equilibrium with MgO is made. The graphs show that under Kraus' experimental conditions a carbon-bearing melt of 27 g (approx. 4 cc) with an initial carbon level of 600 ppm and an initial oxygen level of 60 ppm contained in an electrically heated magnesia crucible, a minimum oxygen level of 0.0012^w/o was attained. This began to increase after about 55 minutes when the carbon

Bennett, Protheroe and Ward (108) carried out investigations on vacuum deoxidation from magnesia crucibles, in which they examined the influence of agitation and argon purging on the degree of deoxidation achieved. They found that the degree of deoxidation achieved in melts subject to agitation by continuous sampling ($0.0007^W/o[O]$) was greater than in static melts ($0.001^W/o[O]$) and argon lancing brought about a further improvement ($0.0005^W/o[O]$). (Figures in brackets are the final oxygen figures attained by each technique). The fact that Bennett (108) achieved lower final oxygen levels than Kraus (86) is due not only to the fact that Kraus' melts were not subjected to agitation, but also because the $\frac{A_{gm}}{V_m}$ ratio was greater in Bennett's case and his final carbon levels were higher.

Brotzmann (107) has also investigated the reactions between magnesia and iron melts under reduced pressure. With preliminary experimental melts of 2kg and 25kg he found that the effect of moisture content, the proportion of silica and the pretreatment of the crucible had to be taken into account. This he did using gas analysis to record the quantities of carbon monoxide and hydrogen formed and by analysis of samples taken from the melt for carbon, silicon and oxygen. Oxygen donation from magnesia was then calculated by an oxygen balance. With low carbon melts, quantities of iron oxide were formed and absorbed by the crucible which led to inaccuracies in an oxygen balance and, therefore, for studies with magnesium oxide only melts containing carbon were used.

The main experiments were concerned with the behaviour

of the crucible on melting iron containing carbon as a function of temperature, pressure and carbon content and to minimise interference by water and silica charge weights of 25 kg were used.

In the theoretical interpretation of the results the assumption was made that the MgO was reduced by iron and that the oxygen, then formed, was removed by carbon as carbon monoxide. It was felt that, rather than the products of reaction being transferred across the metal-gas interface, an easier and more likely route would be through the pores of the crucible. This was demonstrated by allowing the surface of the melt to freeze over while the bulk of the metal remained just above the liquidus. Only a slight decrease in the rate of gas evolution was noticed and Brotzmann, therefore, concluded that most of the magnesium and carbon monoxide products, formed by reaction at the melt-crucible interface, were transported through the crucible wall and did not contaminate the melt.

Actual gas flows measured for various carbon contents and pressures are shown in Figure 38. Calculations based on the Hagen-Poiseuille equation result in the amount of gas produced by the reaction being described by

$$\frac{\dot{M}}{2} = K(T) \left\{ \frac{4.4 \times 10^{-4}}{\frac{1}{2} \sqrt{90\dot{M} + P^2}} - 2.9 \times 10^{-6} \times \frac{1}{[C]} \times \frac{1}{2} \sqrt{90 + P^2} \right\} \dots (104)$$

for large gas flows or pressures < 10 torr.

$$\text{and } \frac{\dot{M}}{2} = K(T) \left\{ \frac{4.4 \times 10^{-4}}{MP} - 2.9 \times 10^{-6} \frac{1}{[C]} \sqrt{\frac{90\dot{M}}{2} + P^2} \right\} \dots (105)$$

for small gas flows or pressures > 10 torr.

where \dot{M} = amount of gas drawn through the refractory.

and P = system pressure.

Figures 39 and 40 show the values derived from these

equations plotted as a function of carbon content and pressure for a temperature of 1610° Centigrade. In the range between 0.1 and 0.2 litres (NTP) per minute CO the values were calculated by both methods and, as can be seen from the figures, there is a transition from one equation to the other. A comparison of Figures 39 and 40 with Figure 38 shows reasonable agreement notwithstanding the large assumptions made. At lower temperatures (1530°C) larger deviations were found.

Fujii and Araki (109) conducted experiments in which electrolytic iron was melted in a pure magnesia crucible under a flow of 100% argon. After adding 0-0.8% carbon to the molten iron, the concentration of oxygen in the argon was controlled constantly at 0, 2, 5, 6, 8, 10, 13, 16 and 20% and the temperature was controlled at 1600° Centigrade. The authors found that by using this technique, which was principally to allow understanding of the kinetics of the C-O reaction in the oxygen converter, decarburisation was linear with time down to 0.15% C independent of the carbon concentration in the molten metal. This constant rate of decarburisation was increased with an increase in the oxygen concentration of the atmosphere according to Figure 41.

The rate of supply of oxygen from the magnesia crucible was assessed using an atmosphere of pure argon. Here, in spite of the fact that the reaction rate was expected to be zero, the rate of decarburisation was, in fact, 0.275 (g/min $\times 10^{-4}$) at 0.6% C to 0.268 (g/min $\times 10^{-4}$) at 0.2% C for a bath weight of 1.4 kg. This was considered to be due to reaction with magnesia and was deducted from the total decarburisation rate on subsequent heats to assess the true

rate of reaction between carbon in the melt and gaseous oxygen. The oxygen concentrations in the molten metal were found to be below the theoretical values in equilibrium with carbon.

Decarburisation rate was studied at temperatures of 1550, 1600 and 1650° Centigrade, and was found to increase linearly with temperature. From this, the activation energy for the carbon-oxygen reaction was found to be 34.6 k cal/mole, a value higher than those of other workers thought to be due to the fact that in these cases the pollution reaction rate was not subtracted from the total decarburisation rate.

The effect of varying the metal depth from 5.1 - 7.3 cm was found to have no effect on the rate of carbon loss which is not surprising since the C-O reaction did not rely on bubble formation and the $\frac{A_m/c}{V_m}$ ratio was roughly constant.

The effect of the gas-metal surface area was studied by placing a series of magnesia rings on the surface of the metal. Again, the decarburisation rate was constant with time but, as expected, there was a decrease as the inner diameter of the ring was reduced. The decarburisation rate by gaseous oxygen was calculated by subtracting the decarburisation rate of the reactions for both the crucible and the ring from the total rate. A plot of this rate against the free surface area is shown in Figure 42 and is suggested by the authors as being approximately linear.

2.2.4. Comparison of data on oxide decomposition.

Wherever possible the rate of oxygen supply from the various oxide materials tested and reported in the literature has been calculated in terms of the number of moles of oxygen transferred/unit area/unit time and these values have been

two cases the only dimension of the crucible given was the diameter and it was necessary to calculate the length of the crucible/metal interface using the charge weight. In another case only the charge weight was given and the assumption was made that $h = 2D$ where h = height of crucible and D = diameter of crucible.

Conditions varied immensely from melt to melt, but even though the experiments are not truly comparable they do serve to indicate the range of transfer rates which might be expected for the various oxides.

The data of Fujii and Araki (109) and those of Brotzmann (107) are in apparent agreement, contrary perhaps to expectations since Brotzmann's work was carried out under vacuum and, therefore, the oxygen levels should be lower and the transfer rates higher than in the experiments of Fujii whose work was done at one atmosphere pressure. Two reasons may account for the high rate observed by Fujii. Firstly he took no account of the interfering effect of silica and water contents of the magnesia (Brotzmann corrected his data) and secondly, he notes that the oxygen values in his experiments are below the equilibrium values. The first of these reasons is likely to be the more important. In accordance with theoretical considerations, Brotzmann observes a decrease in the transfer rate with a decrease in the driving force for the reaction as controlled by the pressure and the carbon content. Kraus (86) obtains a lower value than either Brotzmann or Fujii, but his experiments were carried out at low carbon levels, i.e. about 100 ppm carbon and this is to be expected. From thermodynamic considerations alumina has been shown to be more stable than

expected. The work of Parlee et al (85) and Fischer and Hoffmann (100) has confirmed these predictions showing the transfer rate from alumina to be 10-20 times slower than from magnesia. The influence of a vacuum above the melt surface in speeding up the reactions is demonstrated by the results of Fischer (100) where the rate is seen to increase by a factor of three in comparison with the high carbon melt of Parlee.

The results of Sharma and Ward (97) on the dissociation of silica are consistent within themselves, but are an order lower than those reported by Turkdogan (97) and Graham and Argent (99). Ward points out that the difference in the two sets of results may be due to the presence of an electrochemical reaction as demonstrated by the experiments of Grimble and Ward (96), although this would hardly explain the discrepancies between the results of Ward and those of Argent. Turkdogan has indicated that lower rates are possible when the process is diffusion-controlled, but even so the transfer rates measured by Ward cannot be fully explained on this basis. It is possible, however, that both the smoothness of the translucent silica crucible and its geometry (tall with a small diameter) are responsible since these factors will influence the rate of removal of oxygen from the crucible interface. The results of Graham and Argent, as might be expected with lower silica activities, are in general agreement with, though a little lower than, those reported by Turkdogan. One feature of the oxygen transfer rates presented in Table 6 needing further explanation is the high rate of decomposition of magnesia

probably be discounted since there is no evidence that corrections were made for the donation of oxygen from other sources such as silica and water. Brotzmann (107), however, claimed to have accounted for these contaminants and it is difficult to find errors, either in his work or the method of calculation, large enough to grossly alter his results. Presumably the explanation lies in the fact that this work was carried out under vacuum, thus greatly favouring the dissociation of magnesia since both products of reaction are gaseous. On the other hand, unless silicon monoxide is formed, only one product of the silica-carbon reaction, carbon monoxide, is gaseous and the application of a vacuum would not be expected to increase the rate of the silica reaction to the same extent as that of magnesia.

III DEGASSING PROCESSES.

The purpose of including a short section on industrial degassing is to indicate the levels of gas removal which are being obtained by the various techniques and also to attempt to illustrate the complexities of obtaining steels with low oxygen contents and thereby low residual contents of non-metallic inclusions. Several reviews of the various vacuum degassing processes have been given. Mund (110) and Edstrom (111) both gave summaries in 1962 and more recently Flux (112) has reviewed degassing plants and Eketorp (113) has dealt with the more difficult problem of critically comparing processes and their achievements.

Figure 43, from Flux (112), shows schematically the degassing methods which are currently in operation and although no further elaboration of process details is required here, some comparison of degassing efficiency is needed to highlight the factors controlling the removal of oxygen.

1. Hydrogen removal.

The ability of a process to remove hydrogen is, to some extent, a guide also to its ability to remove oxygen by the carbon-oxygen reaction since such factors as the area of steel surface exposed are important. For this reason data on hydrogen removal by the various techniques has been compiled (114-123) and is shown in Figure 44 and Table 7. A true comparison can only be done, of course, if sampling and analytical techniques are consistent. However, this is not the case and samples have been taken from the ladle, teeming stream, ingot head and machined from the ingot.

From Figure 44 and Table 7, it can be seen that stream degassing (114, 115) is the most efficient and gives the lowest hydrogen levels, many below 1 ppm. The dilution (116, 117) and circulatory processes (121), the DH and RH respectively, come next and static ladle degassing (118, 119) is poorest, but can be brought up to the same level as the RH by agitating the steel with bubbles of argon injected through a porous plug in the base of the ladle (118). Results from Domnarvet (119), however, where a similar process is in use fit on the same curve as those from Beardmore Ltd., which do not have argon injected. The conclusion might be drawn that the method and / or quantities of gas introduced at Domnarvet are inadequate and further improvement could be made.

Wahlster (121) and McMillan (118), though with different processes (RH and static ladle respectively), both report that gas agitation serves to maintain a consistently low hydrogen level which is shown up by the lack of correlation between initial and final hydrogen levels.

The effect of surface area exposed to vacuum is not only illustrated by the difference between the individual processes but also by the results on open, semi-killed and fully killed steels (114, 122), the former having a higher efficiency of hydrogen removal for a given hydrogen level. The effect of the $\frac{A}{V}$ ratio can also be seen from the results of McMillan (118) with different sized ladles. The 20 ton non-agitated heats are almost comparable with the 80 ton argon-agitated heats. In spite of these considerations, a considerable amount of hydrogen removal is obtained by means of diffusion to the free surface rather than by entrainment in bubbles

killed steels.

Although there are differences between processes, most techniques seem to be capable of obtaining less than 3 ppm of hydrogen after treatment but, whilst this may be sufficient for many applications, there are still grave doubts about the ability of most processes to treat steel satisfactorily for the production of large forging ingots. Vacuum casting alone is proven in this respect and to give freedom from hairline cracking, especially in low sulphur and heavily worked steels, final hydrogen levels of 1.5 ppm seem to be essential.

2. Oxygen removal.

Variations in steelmaking technique, deoxidation practice and steel composition prohibit a general comparison of oxygen removal by vacuum degassing. Difficulties are increased by variations and inaccuracies in sampling and analytical techniques, particularly at low oxygen levels.

As pointed out by Eketorp (113), besides the effect of promoting a reaction between carbon and oxygen, vacuum degassing improves the rate of elimination of oxide inclusions due to the turbulence created. The two effects can be isolated such that deoxidation is carried out only by means of the carbon-oxygen reaction (124) or by means of the addition of aluminium (123) in which case the treatment is limited to the removal of oxides to free surfaces. All the intermediaries between these two forms are possible and much work is at present being done to find the procedure best suited to individual requirements. Wahlster (121) has shown (Figure 45) that the final oxygen content after treatment depends partly on the initial oxygen level and partly on

deoxidation, the lowest values being achieved when the steel is in the 'open' condition. Similarly Perry (124) describes a carbon deoxidation practice employed at Republic Steel Co., on 90 ton heats using the induction-stirred ladle technique shown in Figure 43b. Here the carbon-oxygen reaction starts at 600-500 torr and reaches its maximum at 30-10 torr. After reaching a base pressure of 0.1 torr, a short period is allowed before alloys, deoxidants and possibly carbon are added. Table 8 shows that 0.1 - 1.0% C steels produced by this procedure have lower oxygen and nitrogen contents than by conventional two slag practice.

Even so, with steels deoxidised with the less active elements such as silicon or manganese, the oxygen content can usually be reduced. For example, Leach and Sorby (116) have found that, providing the carbon content is high, oxygen levels of 40-60 ppm in the furnace (double slag practice) can be lowered by 50%.

Innumerable combinations of carbon deoxidation and alloy deoxidation can be contemplated. Wahlster in communication to Eketorp (113) has reported results from 100 ton basic open hearth heats containing .18% C, .35% Si, 1.4% Mn, .03% Al, which were tapped with an oxygen content of about 500 ppm, the required manganese being added to the ladle. With the first method all the silicon was added to the ladle and an aluminium addition of 0.6 kg/ton was made 5-7 minutes before the end of vacuum treatment. The second technique was to fully deoxidise the steel with an aluminium addition to the ladle prior to degassing. The results, which are given in Figure 46 and which are the average values of a large number of heats, show that the lowest final oxygen contents are

achieved in the case of the fully deoxidised steels and, therefore, it cannot be taken for granted that a combination of carbon deoxidation plus precipitation deoxidation yields better results than the latter alone. Knaggs and Broxham (125) have published data concerning different deoxidation techniques used with the ladle to ladle stream degassing of 110 ton plain carbon and low-alloy steel heats, where 20-30 heats were treated according to each technique. The final oxygen contents achieved by each technique are shown as frequency curves in Figure 47, from which it can be seen that methods C and D, which involve the vacuum treatment of ordinary double slag steels and of silicon killed single slag steels yielded much better results than normal practice. The lowest oxygen contents of about 17 ppm were obtained when the preliminary deoxidation was just powerful enough to give sufficient dispersion of the stream during degassing (E and F). Kato et al (126) have shown that it is possible to control carbon deoxidation to such an extent that semi-killed steel can be produced by means of DH vacuum treatment. They first established the relationship between the momentary oxygen content of the steel and the pressure change in the system. By means of this control of the oxygen content they were able to make the aluminium addition required to give the desired ingot structure.

Aluminium can become a high-grade deoxidant provided the deoxidation products can be removed. Flockinger (127) and Torsell (128) have both demonstrated the importance of collisions and turbulence in the separation of deoxidation products, particularly those of aluminium. More detail is, therefore, needed on the extent of turbulence (129) required

be designed with this in mind (113, 130). Particularly with aluminium deoxidised steel care must be taken to avoid air oxidation by teeming in an inert or reducing atmosphere. In this connection Leach and Watson (115) have demonstrated that ladle to mould stream degassing yields a cleaner steel and attribute this to the lack of oxidation on teeming.

Everything points to the fact that aluminium will find wider use as a deoxidant than ever before; and vacuum degassing, despite earlier optimism with carbon deoxidation, will be able to provide assistance in this respect since by this means additions can be made with much more precision. In reality no higher aluminium contents than about 0.02% are required to ensure an oxygen level as low as that obtainable in practice with carbon in spite of the fact that, theoretically, carbon under vacuum should be a more potent deoxidant than aluminium as Figure 48 (3) shows. In practice equilibrium is far from obtained, even under the best conditions as represented by vacuum induction melting, and values lower than those corresponding to an equilibrium pressure of carbon monoxide of 75-100 torr are rarely obtained with carbon. Figure 49 illustrates a collection of data on the carbon and oxygen values achieved with three of the major processes where addition of deoxidants has not been made. Information from papers by Sickbert (131) and Samarin (132) has supplemented works data on the DH process operated by the English Steel Corporation, Sheffield. This diagram shows that, in general, all the well-tried degassing methods achieve similar oxygen levels. None are as good as vacuum induction melting in terms of oxygen levels attained and yet,

in terms of attainment of equilibrium, they are superior. The lowest carbon x oxygen products are achieved near to the stoichiometric line where both carbon and oxygen are present in sufficient amounts since, as has been shown earlier, the rate at which the minority species diffuses to gas-metal interfaces can control the kinetics of the C-O reaction. The rate that this reaction proceeds in the various degassing processes has been studied only in slight detail and mention will be made of these studies in the discussion. The influence of the dissociation of oxides present in the slag and refractories and the presence of non-metallic inclusions both on the final oxygen levels attained and on the shape of the curves in Figure 49, is, as yet, unknown. With this in mind the aim of the work reported in this dissertation was to provide new information on the mechanisms of oxide-metal reactions and the sources and kinetics of oxygen donation during the degassing of steel by the DH process.

I 1. APPARATUS AND GENERAL PROCEDURE.

The apparatus for this study had to be designed and built at the commencement of the project. Help was required from electronic engineers in the assembly of parts of the gas analyser but otherwise the equipment was built and maintained under the direction of the author. Over a year was spent in planning, making and assembling the various pieces of equipment and a further six months were needed to develop the best experimental techniques commensurate with obtaining a high degree of accuracy. Photographs of the furnace and ancillary equipment are shown in Figures 50 and 51 and a schematic diagram of the arrangement is shown in Figure 52. It is comprised of a 5lb vacuum induction furnace assembly to which has been made suitable attachments for metal and gas sampling, pressure control and flow measurement. By the side of the furnace and generator was constructed an apparatus for the analysis of the gaseous atmosphere in the furnace chamber.

1.1. Heating.

A Radyne C.90, 450 Kc/s generator having an output of 12 kW and having water cooling at the rate of 10 litres per minute was used to induction heat the metal load. The working coil was constructed of 1" x $\frac{1}{8}$ " copper strip with a $\frac{1}{4}$ " diameter copper tube brazed to it to carry the power and cooling water from the generator. It was made up of five turns, according to the manufacturers' recommendation, (the height being 6 $\frac{1}{2}$ " to fully cover the material to be melted) and placed outside the vacuum vessel to avoid

CORONA DISCHARGES AND SIMPLIFY CONSTRUCTION. THIS positioning also provided more room inside the vacuum vessel and less seals were required, thus reducing the chances of leakage.

Preliminary air melts with this equipment were unsuccessful, the 5lb charge not quite reaching the melting point of iron. On the manufacturers' recommendation a Radyne Mica-Stack, oil cooled, loading condenser of 0.06 m³ capacity, with separate water cooling at a rate of 3 litres per minute, was sited as near as possible to the work coil.

Magnetic fields outside the coil, found to cause heating of the steel framework were reduced by replacing the mild steel with aluminium wherever possible and by breaking up any surrounding construction with an insulating material such as Sindanyo. Using this equipment it has been possible to melt down a 5lb charge in less than an hour on 6-7 kW full load. Usually, however, a preheating time of 1½ - 4 hours has been used so that the crucible might be gradually heated in order to avoid cracking, premature breakouts due to hot spots and excessive thermal gradients.

1.2. Vacuum vessel.

The vacuum vessel had to be impermeable, resilient, electrically insulating, able to withstand thermal gradients and shocks and stable at the pressures and temperatures involved. The choice for cheapness and good dimensional tolerance was a translucent vitreous sil material, the dimensions of which were decided by the size of the crucible and the minimum cross-sectional area which would accept a

bubbling tube together with their O-ring seals. With these things in mind the vessel finally chosen was a tube $24'' \pm \frac{1}{32}''$ long, the ends being ground flat to the axis and machined to $5'' \pm 0.010''$ for $1\frac{1}{2}'' \pm \frac{1}{32}''$ lengths with a $4\frac{1}{2}''$ minimum to $4\frac{11}{16}''$ maximum bore, 6-7 mm wall and glazed inside and outside. The ends of the tube were sealed by VIT O-rings compressed by machined aluminium caps.

1.3. Charging and melting.

The vessel was designed to be charged from the bottom, the crucible and its support resting on the aluminium bottom cap which was bolted into position after charging. The crucible assembly, shown in Figure 53, consists of a cylindrical mullite sleeve into which was fitted a crucible of the material under investigation, the gap between the two being tightly packed with fused alumina powder (200 mesh) and topped with a packed ring of asbestos wool. The assembly was then cemented onto an alumino-silicate seat and support tube using alumina cement. Oxidation reactions from crucibles covering a range of alumino-silicate materials, from nearly pure silica to nearly pure alumina, and crucibles consisting of 90% magnesia were examined.

In the preliminary melts the initial charge was 3lb of mild steel rods, $\frac{3}{4}''$ diameter x 5" long, which were melted down and then 2lb of $\frac{1}{4}''$ diameter mild steel rods was fed into the melt through the vacuum lock. The $\frac{1}{4}''$ diameter rod was in 2ft. lengths, tapped and cut at each end to a 2 B.A. thread. Difficulties soon arose, however, which made this method of charging impracticable. Bridging of the initial charge occurred on melting causing hot spots and breakouts of metal and ramming the bridge

by the feeder rod only succeeded in further cracking of the crucible. Another difficulty was that the feeder rod had to be free from rust and oil, with a polished surface, which presented storage problems and demanded time-consuming labour.

The second (and present method) of charging was to suspend a 5lb block of iron away from the crucible sides and then lower it into the crucible when the temperature of the iron was about 1,000^o centigrade. In this manner the critical expansion difficulties between crucible and charge were avoided and subsequently there were very few breakouts.

The charge consisted of pure iron machined to a cylinder 2 $\frac{1}{2}$ " diameter x 3 $\frac{1}{2}$ " with a 2 B.A. x $\frac{1}{2}$ " thread tapped into the centre of one face. After degreasing and shotblasting the block was suspended, with the 2 B.A. tapping, by a $\frac{1}{4}$ " diameter rod through the vacuum lock.

The carbon content of the melt was controlled by placing the required amount of graphite on top of the iron. This produced localised melting at those areas with which it was in contact, but the liquid metal remained on top of the charge and melting was mainly from the bottom of the charge upwards. By this technique a yield of about 100% was achieved in the 0.10% C. range, but a slight loss occurred in the 1.0% C. range. In a few melts a ridge of metal was formed around the crucible perimeter which subsequently gave difficulties with thermocouple insertion.

1.4. Pumping equipment and plumbing.

It was visualised that at pressures greater than 1 torr, the rate of gas evolution from the melt would be within the capacity of a rotary pump but that below 1 torr, an oil diffusion pump would be necessary.

oil-sealed rotary pump I SC 50B (Figures 52 and 54) which the manufacturers claimed to have an ultimate vacuum of 0.005 torr without ballast and 0.5 torr with ballast (48 litres per minute displacement). With the empty vessel sealed off at the ball valve, thermocouple, gas and pressure lines, a final pressure of less than 0.005 torr could be reached, but with all the lines open and the charged crucible in position, the ultimate pressure varied from 0.01 to 0.03 torr, and 0.50 torr with ballast. The leak rate from 0.030 torr and with all lines open was 0.10 torr per hour. The system was checked before each melt after pumping down and if the pressure reached was less than 0.05 torr then it was regarded as operational. Pumping down with gas ballast for at least 12 hours was necessary to remove water vapour given off from the crucible and thermocouple constructions.

The pump line was fabricated from 1" i.d. copper tubing and connected to the bottom aluminium plate via a flexible connection. An isolation valve and P_2O_5 moisture trap were fitted to the pump and a pressure controller was fitted as near as possible to the vacuum vessel. A second rotary pump P_2 , Edwards ES35, with an isolation valve and moisture trap, was used to pump down the vacuum lock during sampling, it being controlled by an electromagnetic valve EMV.1. It had an ultimate pressure of 0.01 torr. This pump could be utilised to give faster pumping down of the whole system when required. Plumbing lines, $\frac{5}{16}$ " o.d., were connected from P_2 by EMV.1. to the manometer and by EMV.2. to the McLeod gauge and to the vacuum vessel at the guide tube by EMV.3. Carbon monoxide, hydrogen and argon lines were

by needle valves plus Fischer and Porter flowmeters (0.5 litres per minute). Trial melts had previously been carried out using vacuum taps as a means of control, but these were fragile when unsupported in the plumbing line and great care was required in operation to prevent breakage or leakage. Replacement by electromagnetic valves allowed a much more robust and compact plumbing line with the valves, their rectifiers and on-off switches easily accessible. After a few melts the electromagnetic valves and needle valves had to be cleaned free from copper filings, turnings and dust from the plumbing line to prevent leaks across the valves and the valves then functioned without further trouble. The correct operation of the electromagnetic valves and needle valves in conjunction with the ball valve gave the required pressure and atmosphere in the vacuum lock and/or vacuum vessel.

1.5. Pressure measurement.

Pressures from 0.005 to 800 torr had to be accurately measured, the lower ranges being required for leak rates and detection. For accurate work at the higher pressure ranges the pressure gauge had to read all gases and condensable vapours. Two gauges were used for the present work.

The simple mercury manometer, used to measure pressures from 800 to 1 torr, was accurate to within ± 2 torr giving a continuous reading and measuring all gases. To allow rapid reliable reading and avoid measuring a difference in heights, a movable scale ($0.5 \text{ mm} \equiv 1 \text{ torr}$) was used to adjust for variations in atmospheric pressure. The pipe line from

one manometer led through EMV.2. to measure the vacuum lock or through EMV.3. to the guide tube which was approximately 7" above the melt.

The Genevac Measurvac T.D. 1. Mk.III McLeod gauge was used to cover a pressure range of 150 - 0.001 torr, the compression of the gas being operated by a spring-loaded plunger against a mercury reservoir. The operation was simple and rapid and accurate readings, especially in the range 1 - 0.01 torr, were obtainable but it had the disadvantage of not measuring total pressure. The gauge was connected directly to the vacuum lock and to the vacuum vessel by way of the ball valve or by EMV.2. and 3 and the guide tube.

1.6. Pressure Control.

For investigations into the kinetics of gas reactions with molten iron two approaches are possible. Firstly the volume of the system can be kept constant and the pressure rise measured, or secondly, the pressure can be kept constant and the increase in volume measured. In the first case, however, the pressure increase results in a change of equilibrium conditions and a decrease in the rate of the carbon-oxygen reaction. In experiments such as these, involving large quantities of reacting silica, the pressure rise necessary to achieve equilibrium would be extremely large and the data would be virtually meaningless. For these reasons it was decided that the reactions undergoing investigation should be controlled at constant pressure, the change in volume being measured, at intervals of 10 minutes), by means of a Parkinson-Cowan flowmeter in the exhaust line of P_1 to an accuracy of ± 0.002 litres. Corrections for N.T.P. were then applied.

possible to the vacuum vessel, the requirements being that pressure variations should be corrected rapidly and smoothly without the need for the introduction of other gases to maintain a positive leak. The Edwards VPCI controller was rejected for this last reason plus the fact that it had a limiting vacuum of 150 torr. Some considerable time was also spent designing and making an automatic pressure controller which would give a permanent record of the flow rate. This consisted of a motorised fine needle valve (Edwards LB2A), geared to a potentiometer and sending electrical signals to a Rikadenki mV recorder. The motor received signals from a main controller which in turn was activated by a pressure transducer. Preliminary trials, however, showed an undesirable time lag between signals received from the transducer and the movement of the valve which gave rise to pressure fluctuations of 10 torr. This equipment was, therefore, rejected in favour of the Edward's Cartesian manostat which depended upon the movement of a cartesian diver for its action. The diver was a tube with a closed top, floating upright in a mercury seal with both the inside and the outside of the tube communicating with the system to be controlled. Gas, at the required control pressure, was trapped inside the diver and cut off from the system by an on-off valve. The diver lifted to close the exhaust orifice through which the system was being evacuated. If the pressure in the system rose the diver was depressed, opening the exhaust orifice so that evacuation could resume, when the system pressure fell below the control pressure the diver was lifted against the exhaust orifice so that

evacuation ceased. The distance between the driver and the exhaust orifice could be changed by a fine control to provide an accurate adjustment to the control pressure.

Using this technique, large amounts of gas, such as that given off during melt down and upon melting, caused rapid fluctuations of about 4 mm around the set pressure, but virtually no variation was observed under steady conditions at 760 and 76 torr. The manufacturers claimed a flow rate of 4 litres per minute at 400 torr and 0.5 litres per minute at 50 torr across the 1.0 mm orifice with a sensitivity of ± 2 torr at 400 torr and 0.4 torr at 100 torr. For melts at 3 torr, the flow rates with the manostat in circuit were insufficient to quickly obtain the desired pressure and for these melts a 1" diameter pipe section replaced the manostat, the pressure being controlled manually by 1" and $\frac{1}{4}$ " diaphragm valves.

1.7. Temperature measurement.

The reactions undergoing investigation were very sensitive to temperature changes and, therefore, good control of the bath temperature at 1600° Centigrade $\pm 10^\circ$ Centigrade was essential. Dip thermocouple readings were not considered to be sufficiently accurate, trials with inserted couples had shown that there were severe temperature gradients through the crucible wall and so a continuous immersion technique was sought. It was soon found that standard Pt - Pt/13% Rh couples were prone to failure at 1600° Centigrade and 20% Rh/80% Pt - 5% Rh/95% Pt, 0.5 mm diameter, wires were found to be the most reliable. The e.m.f. generated at the thermocouple junction was fed to a Rikadenki, fast response, mV recorder and the compensating

alumina from Thermal Syndicate (3 mm bore x 12" long) was chosen as sheath material since it was considered to be relatively inert at the pressures used and since the area of sheath exposed to the melt was very small compared with the surface area of the crucible. The design of the thermocouple, however, proved to be difficult and it was some time before a completely reliable thermocouple, with a life of over 6 hours at 1600° Centigrade was found. The design finally chosen is shown in Figure 55. The 12" alumina sheath was first broken and recemented at a position about 3" from the tip. This allowed thermal expansion to take place without further cracking and the danger of metal penetration was substantially reduced. The thermocouple wire was run through a 2.5 mm o.d., twin bore alumina tube and a bead formed at the tip, a fresh length of wire being used for each experiment. The sheath was then cemented onto this tube, the remainder of the wire being protected by a 4 mm diameter twin bore silica. The design was completed by an aluminium cap with suitable O-ring seals to prevent leaks and explosions in the case of a thermocouple failure, the holes in the twin bore silica being filled with molten black wax. It was decided that the thermocouple should be immersed $1\frac{1}{2}$ " - 2" in the melt and consequently the total length of the thermocouple was chosen at $21\frac{1}{2}$ ", leaving $3\frac{3}{4}$ " protruding above the top cap of the furnace chamber. A second couple was always in position in the furnace in case of a premature failure with the first one.

1.8. Sampling from the melt.

The accuracy of the results is very dependent upon

The analysis for oxygen, particularly, is fraught with difficulties in the event of piped or porous samples and several techniques were examined before a reliable one was found. A major difficulty was that the furnace design prohibited the storing of samples in the chamber and each one, after being taken from the melt, had to be withdrawn through the vacuum lock and guide tube. This tube was only 1" diameter which further restricted the size and shape of the sample and its holder attachments. Silica suction techniques, evacuated pyrex pintubes and silica spoons were rejected at the outset because of the likelihood of contamination. A variety of metal cans and spoons were tried but it was difficult to obtain the correct thickness to prevent melting on the one hand, and temperature changes on the other. These were eventually rejected because of the difficulties and cost of manufacture and also because their design did not allow them to be withdrawn smoothly from the melt.

Finally, the design shown in Figure 56 was found which has since given satisfactory results, but even so satisfactory samples of 1% C. irons have been difficult and sometimes impossible to take at pressures of about 3 torr due to the initiation of a boil on immersion of the sampler. This device consisted of a mild steel tube, $\frac{5}{8}$ " o.d. 16 gauge, which was sealed at one end by a welded mild steel cap; at a position $1\frac{1}{8}$ " above the sealed end of the tube was an intake orifice, made by milling away half the diameter of a 1" section. The position of this sampling tube could be adjusted to one of five positions in order to allow sampling to continue if the metal level in the

crucibles began to drop due to changes in crucible geometry as the reaction proceeded. Samples 1" long x $\frac{1}{2}$ " diameter were obtained by turning off the tube shell on a lathe. Further turning gave samples for carbon and silicon determination and the specimen core was used for analysis of oxygen. Extreme care was taken to avoid greasy and burnt chippings and in a similar way all sampling tubes were degreased and shotblasted prior to use. In order to fully deoxidise the metal and provide sound samples for oxygen analysis 0.1 wt/o of coiled 0.5 mm diameter aluminium wire was placed in each sampling tube before immersion. Preliminary trials showed that, to avoid temperature fluctuation with the small mass of metal used, the optimum frequency of sampling was at 30 minute intervals. It was felt that control of temperature was more important than obtaining large numbers of samples which, in addition to temperature variations, also results in a lowering of the charge in the crucible.

Automatic sampling of the melt was achieved by fitting the sample tube in its holder onto a 43" stroke, pneumatically powered steel rod which travelled, through O ring seals, in the guide tube. This technique ensured that the residence time of the sampling tube in the melt was no more than one second, thus avoiding contamination of the melt by the tube and keeping temperature losses to a minimum. High carbon samples were annealed immediately after being taken to facilitate machining.

An important feature of design which enabled a satisfactory sampling procedure to be established was the building of the vacuum lock (Figure 57) to isolate the

sampler from the vacuum vessel and provide the required pressure and atmosphere when the sampler was in the furnace chamber. This lock was a cylindrical chamber consisting of 1" diameter copper tubing attached to the vacuum vessel by a 1" ball valve and a 1" diameter copper guide tube. The ball valve opened the vacuum lock to the vessel when sampling was in progress and sealed it off when the lock was required to be open to atmosphere. On the top of the vacuum lock chamber was a detachable brass fitting, sealing the chamber from the outside atmosphere and also retaining a vacuum tight seal for the pneumatic sampling rod. Attached to the chamber were lines for evacuation, gas entry, pressure measurement and air admittance. The evacuation line from P₂ passed through EMV.1. to pump out air, from the vacuum lock, before sampling and the furnace atmosphere, from the lock, after sampling. Air was admitted to the lock to prevent explosion from occurring on taking out the hot sample.

The pneumatic sampler ($\frac{1}{4}$ " diameter rod)(Figure 57) was operated at a pressure of 100 lbs per sq.ins. Reducing valves adjusted the speed of the sampler such that the sampling tube entered the melt slowly, with a minimum of splashing and was withdrawn as quickly as possible. It is worth noting that previously, the sampling had been undertaken manually, pushing a sampling rod through the vacuum lock. However, although speed control was good the control of alignment was difficult and the sampler sometimes broke the thermocouple.

1.9. Gas analysis unit.

Previous work (107) has shown that contamination of the melt can take place from the water contained in the

removes the bulk of this moisture, some always remains and its effect can be very important particularly at low carbon levels, where the evolution of carbon monoxide is slower, and with magnesia crucibles. In addition to this, at low carbon levels and high pressures the formation of carbon dioxide can be important. It was, therefore, thought that analysis of the gas phase above the melt was necessary, firstly in order that an accurate oxygen balance could be done and secondly since the gas composition above the melt affected the carbon-oxygen equilibrium.

The apparatus was constructed, according to the diagram shown in Figure 58, out of 10 mm diameter pyrex glass tubing and was arranged horizontally on a bench top as shown in Figures 59 and 60. It relied upon the successive measurement of the gas pressure in a standard volume as each of its components was removed. For this measurement, a pressure transducer was used which generated an e.m.f. if there was a pressure difference across its two metal diaphragms. Hence if the pressure on one side of the transducer was made equal to zero then the reading obtained was that of the pressure on the other side of the transducer. The measuring head itself was comprised of two transformers, whose magnetic circuits consisted of two symmetrical fixed parts and a common movable core. Movement of this core varied, in opposite senses, the reluctances of the two magnet circuits by altering the air gap. The inductance of the primary windings and the coefficients of primary to secondary mutual inductances varied with the displacement of the core, in one sense for one transformer, and in the opposite sense for the other

the circuit inductance was constant and, when energised by an alternating voltage of constant amplitude, the alternating current in the primary circuit was also of constant amplitude. The difference between the secondary voltages was proportional to the primary current, to its frequency and to the difference between the two coefficients of mutual inductance, that is to say, the movement of the core. The range of the transducer used on the gas analyser was ± 50 mb, and the alternating voltage was provided by a 3000 c.p.s., 24v oscillator. From the transducer, the output was originally fed straight into a rectifying circuit and then measured by a Rikadenki mV recorder which had a series of mV ranges and worked on the principle of null balancing the system potentiometer. This set up was satisfactory whilst the high frequency furnace was not in action but great difficulty was experienced in obtaining a constant signal whilst melting was in operation and so to combat this 'pick-up' effect the transducer was screened with a double layer of copper gauze at earth potential. This improved matters but did not, by any means, make the trace satisfactory and, as a result, three types of rejection filter were tried but, again, all were unsuccessful. Finally, the problem was solved by using an acceptance filter finely tuned to the frequency of the oscillator, i.e. about 3 Kc/s and a good analysis trace was obtained throughout the whole of the melting period.

Calibration of the pressure transducer was carried out by means of an accurate Toepler gauge and the procedure and results of this calibration are given in Appendix I. By this, it was found that the relationship between pressure and the output from the transducer (mV) was exactly linear

up to 10 torr (Figure 57) so that the mV reading could be used directly in the analysis calculations, thereby avoiding tedious reference to the calibration curve.

The circuit had two Leybold Q20 mercury diffusion pumps (10^{-3} - 10^{-8} torr) one of which (D_1) was used to evacuate the space at the back of the transducer. This pump was backed by an Edwards mechanical rotary pump 2SC20A which had an ultimate vacuum of 0.001 torr without gas ballast and a displacement of 22 l. per minute. The second diffusion pump (D_2) backed by an Edwards ES35 rotary pump having an ultimate vacuum of 0.01 torr without gas ballast and a displacement of 35 l. per minute, was used to evacuate the whole system when required. All the valves marked V1-V10 shown in Figure 58 were electromagnetic and were controlled from a central panel. Both the mV recorder and the transducer had separate zero adjustments and checks were made before each run to ensure that the system was leak-free.

The procedure subsequently adopted for analysis of the gaseous atmosphere above the melt was as follows:-

After completely evacuating the system all the valves were closed and a small amount of gas (of pressure less than .5 torr) was pumped from the furnace by way of electromagnetic valves, V_1 and V_2 , the gas being compressed into the transducer chamber on the high pressure side of the diffusion pump D_1 . When a pressure of 3 - 4 torr (6-8 mV) was obtained in the chamber, valve V_1 was first closed, followed by V_2 when the pressure became constant. The gas was circulated over phosphorus pentoxide to remove water vapour by opening V_3 , V_7 and V_{10} . After approximately

2 minutes V_3 was closed and the gas pumped back into the chamber. When the pressure again became constant V_{10} and V_7 were closed and the pressure noted. The gas was next analysed for carbon dioxide by opening valves V_3 , V_8 and V_9 to remove this component by passing it through a liquid nitrogen freezing trap. Again after a few minutes when all CO_2 had been removed, V_3 was closed and the gas pumped back into the chamber and when the pressure had become constant V_9 and V_8 were closed and the pressure reading taken. Similar procedures were undertaken to analyse for hydrogen and carbon monoxide. For hydrogen removal, the gas passed through a copper oxide furnace controlled at 650° Centigrade which oxidised CO to CO_2 as well as H_2 to H_2O . By opening V_3 , V_5 , V_6 and V_7 the water vapour was removed by absorption onto P_2O_5 , leaving the carbon dioxide (originally CO) to be frozen out by liquid nitrogen on the next analysis cycle. A typical analysis chart from such a sequence is shown in Figure 62 from which it can be seen that the volume fractions of the gaseous components in the furnace chamber are found by dividing the initial total gas pressure (or mV) into the pressure (or mV) differences between each analytical cycle. Analysis of samples taken from the furnace was carried out as often as possible during the course of the melt. The slow step in the analysis cycle, however, was the collection of gas from the copper oxide furnace after the removal of hydrogen which generally resulted in a turn-round time of 15 - 20 minutes. All other steps in the procedure were rapid and if time had allowed the technique could have been speeded up by re-designing this part of the circuitry.

2.1. Iron base.

Swedish iron was used as a melting base in all experimental melts and, although two suppliers had to be used for this material, there are no differences in composition likely to affect the results. (See Table 9.)

2.2. Crucibles.

For the majority of these experiments the crucibles were obtained from Refractory Mouldings and Castings Ltd., Kegworth, Nr. Derby. For one or two heats recrystallised magnesia crucibles from Degussit were used. The composition of the crucibles used for the bulk of the work are shown in Table 10. A check was kept on composition throughout the work. Table 11 gives details of the preparation and of the phases present in these crucibles after firing. The optical and x-ray crystallographic analysis necessary for this is discussed in more detail in the section on results. 2 - 3% colloidal silica was added as a bond on M and P grade crucibles and up to 8% on MAG and HS grades. During calcination of the powder, a glass forms at approximately 1680° Centigrade with the molochite powder and at approximately 1600° Centigrade with the silliminite powder so that the M and P crucibles finally consist of mullite grains, silica glass and a small amount of α or β quartz. The glass remains undetected by x-ray crystallographic analysis whereas the colloidal silica, having been fired at relatively low temperatures is detected as quartz. The silica bond added to the magnesia to form MAG crucibles appears to have reacted to form forsterite. Physical tests were also performed on sections

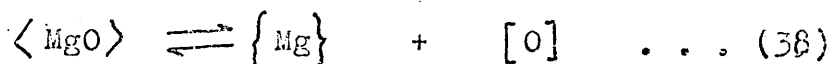
2.3. Gas atmosphere.

Carbon monoxide was used as the furnace atmosphere on all heats. After pumping down to high vacuum the system was backfilled with carbon monoxide and the procedure repeated. The gas was used straight from a high pressure bottle and was supplied by Air Products Ltd., to the following composition, CO-99.5%, hydrocarbons -- 40 ppm, air - balance.

0.5?

1. GENERAL.

Previous work on oxide-melt reactions has indicated that the extent of the oxidation reaction is primarily controlled by the soluble oxygen content of the melt according to the equations,

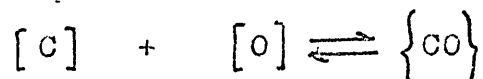


The rates of these reactions are also generally thought to be governed by the oxygen content of the bulk liquid and by the interfacial area of contact;

$$\frac{dn_o}{dt} = \beta A_R (O_R - O_M)$$

- where
- β = mass transfer coefficient $\frac{D}{\delta}$
 - D = diffusion coefficient (cm^2/s)
 - δ = boundary layer thickness (cm)
 - O_R = oxygen content in equilibrium with oxide.
 - O_M = oxygen content of the bulk liquid.

where carbon is present the dissociation reaction will be followed by the carbon-oxygen reaction at a gas-metal interface according to,



The direct reaction between carbon and the oxide is not thought to be controlling since this occurs only at a three phase interface.

Hitherto most of the work reported in the literature has been carried out either under high vacuum or with carbon-saturated melts and under such conditions the soluble oxygen

content is at a minimum and the dissociation reaction proceeds at its fastest rate. These conditions rarely apply with works practice where, in the absence of other deoxidants, the oxygen content is controlled by the carbon content and may vary from 10 up to 1000 ppm. Reactions involving the ladle refractories and, to some extent, the refractories used to line vacuum vessels, will proceed at rates defined by these conditions.

Because of these considerations it was decided that a knowledge of the effect of oxygen level upon the rates and extents of these reactions would be useful and it was hoped that this information would allow a suitable rate model to be formulated. The oxygen content of the metal was controlled by varying the carbon content of the melt and the working pressure of carbon monoxide in the furnace. Wherever possible six sets of experimental conditions were used for each crucible composition such that all the crucibles listed in Table 10 were investigated at initial carbon contents of 0.1 and 1.0^W/o and pressures of 760, 76 and 3 torr. The changes in composition of the melts were followed by analysis of metal samples for carbon, silicon and oxygen and/or by a combination of flow measurement and gas analysis. These results are shown in Table 13. For ease of reference, the data from each melt, including calculations and graphs, were prepared in book form.

2. Routine Calculations.

It was found necessary, at an early stage, to carry out an oxygen balance on each melt in order to assess the quantities of oxygen coming from the various sources. To check the reproducibility of the experimental technique this

from the melt and the measured volume of the analysed furnace gases. The results for each melt are given in Table 14.

2.1. Flow measurement plus gas analysis.

On the assumption that the gas samples taken from the melt chamber accurately represent the bulk composition of the gaseous phase then, in order to calculate the true rate of carbon monoxide evolution, allowance must be made for the dilution of the gas evolved from the surface by the furnace atmosphere. This is particularly important at high pressures and low carbon contents where the rate of evolution of carbon monoxide is small compared with the total volume of the furnace chamber plus ducting.

The furnace chamber is of volume V (7.0 litres at 760 torr and room temperature) and contains gas of composition $\%CO_{(1)}$ at time t_1 . If the melt then evolves gas of composition, $\%CO_{(M)}$ in time $t_2 - t_1$, then, assuming that as ΔV_T of $\%CO_{(M)}$ enters the system ΔV_T of $\%CO_{(1)}$ leaves, maintaining a constant pressure, the percentage of carbon monoxide now remaining in the chamber and analysed at time t_2

$$= \%CO_{(2)} = \%CO_{(1)} - \frac{\Delta V_T}{V} (\%CO_{(1)} - \%CO_{(M)}) \dots (106)$$

?
Hence $\%CO_{(M)} = \frac{V}{\Delta V_T} (\%CO_{(2)} - \%CO_{(1)}) + \%CO_{(1)} \dots (107)$

and the volume of carbon monoxide evolved during time $t_2 - t_1 =$

$$\Delta V_T \%CO_{(M)} = V(\%CO_{(2)} - \%CO_{(1)}) + \Delta V_T \%CO_{(1)} \dots (108)$$

In order to approximate V to N.T.P. the average gas temperature in the chamber was measured to be 400° Centigrade giving values for V at 760, 76 and 3 torr of 2.84, 0.284 and 0.01 litres respectively.

Gas analysis has indicated that, during the melt, the only gases present in the system are hydrogen and carbon monoxide. On occasion, with very low carbon contents, carbon dioxide has been detected but only in small amounts. It can, therefore, be assumed that the total gas volume measured by the flowmeter is made up of hydrogen and carbon monoxide only.

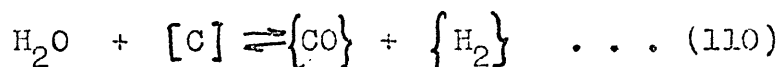
$$\text{Hence } \Delta V_T - \Delta V_{T\%CO(M)} = \Delta V_H \quad \dots (109)$$

where ΔV_T is total gas volume evolved during time Δt , as measured by flowmeter and corrected to N.T.P.

ΔV_H is volume of hydrogen evolved from the melt in time Δt .

$\Delta V_{T\%CO(M)}$ is volume of carbon monoxide evolved from the melt in time Δt .

As will be shown later, it seems that the production of hydrogen is due to the reaction,

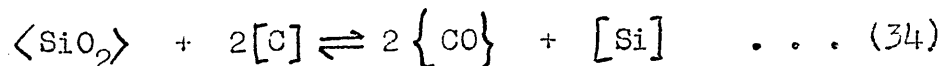


and so, where the only reactions producing carbon monoxide are those involving silica and water, and since, from equation (110), 1 vol. $H_2 \equiv$ 1 vol. CO

$$\Delta V_{T\%CO(M)} - \Delta V_H = \Delta V_{CO_{SiO_2}} \quad \dots (111)$$

where $\Delta V_{CO_{SiO_2}}$ = volume of carbon monoxide produced by reaction with silica.

Also according to the overall reaction



1 litre of carbon monoxide is equivalent to $\frac{28}{2 \times 22.4} =$

0.625 gm. silicon.

$$\text{and therefore } \Delta\%Si = \frac{\Delta V_{CO_{SiO_2}} \times 0.625 \times 100}{M} \quad \dots (112)$$

where M = mass of melt in gms. during time interval Δt .

A series of such equations were programmed into an Olivetti desk computer and by feeding in the measured values for V , ΔV_T , $\%CO_{(1)}$, $\%CO_{(2)}$ and M , values for $\Delta\%Si$, $\Delta\%C$, $\Delta\%O_{SiO_2}$, $\Delta\%O_C$, ΔV_H and $\Delta\%O_{H_2O}$, were calculated, with time, for each melt.

where $\Delta\%O_C =$ Wt % oxygen removed by carbon in Δt .
 $\Delta\%O_{SiO_2} =$ Wt % oxygen donated by silica in Δt .
 and $\Delta\%O_{H_2O} =$ Wt % oxygen donated by water in Δt .

2.2. Metal sampling.

Metal samples were taken at regular intervals, usually every 30 minutes, and the times t_1 , t_2 etc., and their respective masses tabulated. The volume of carbon monoxide evolved between samples was calculated from,

$$\Delta V_T \%CO_{(M)} = \frac{22.4}{12} \times \frac{\Delta\%C}{100} \times M \quad \dots (113)$$

where $\Delta\%C =$ Wt percentage carbon removed between t_1 and t_2 . and the volume of hydrogen produced in the same time period was then calculated from

$$\Delta V_H = \Delta V_T - \Delta V_T \%CO_{(M)} \quad \dots (109)$$

The partial pressures of hydrogen and carbon monoxide above the melt were then simply the proportion of each gas multiplied by the total system pressure.

The amounts of oxygen donated by water and silica and removed by reaction with carbon were then calculated from,

$$\Delta\%O_{H_2O} = \frac{\Delta V_H}{M} \times \frac{16}{22.4} \times 100 \quad \dots (114)$$

$$\Delta\%O_{SiO_2} = \Delta\%Si \times \frac{32}{28} \quad \dots (115)$$

where $\Delta\%Si$ was measured from the plot of wt %Si against time.

$$\Delta \%C = \Delta \%O \times \frac{16}{12} \dots (116)$$

where $\Delta \%C$ was measured from the plot of wt %C against time.

An oxygen balance was now possible where

$$\Delta \%O_C = \Delta \%O_{SiO_2} + \Delta \%O_{H_2O} + \Delta \%O_{Sol} + \Delta \%O_x \dots (117)$$

where $\%O_{Sol} = \%O_{initial} - \%O_{analysed \text{ at } t}$.

and $\Delta \%O_x =$ amount of oxygen donated from other oxides such as MgO or Al_2O_3 during Δt .

Usually the soluble oxygen content had reached a constant level by zero time and when oxygen donation from other oxides was absent, as in the majority of melts, the oxygen balance may be represented simply as

$$\Delta \%O_C = \Delta \%O_{SiO_2} + \Delta \%O_{H_2O} \dots (118)$$

Cases occurred where the measured volume V_T was less than the volume of carbon monoxide calculated according to equation (113) and this is discussed under 3.

2.3. Comparison of methods of calculation.

The two methods of calculating an oxygen balance, as outlined in 2.1 and 2.2., are compared in Table 15 where the oxygen contributions from silica and water and that removed by carbon are listed for most of the melts in this series. The agreement between the two sets of data must be considered quite good which indicates that the experimental technique has been satisfactory. The gas analysis falls down of course on those heats where the carbon monoxide has come from more than one source, i.e. oxygen has been contributed by MgO or Al_2O_3 in addition to silica and water. It will be seen from Table 15 that for 1% C melts in magnesia crucibles the $\Delta \%O_{SiO_2}$ calculated by gas analysis plus flow measurement is higher

than that from metal sampling. This is because this term really contains ΔO_{MgO} in addition to ΔO_{SiO_2} as indicated by equation (117). It will also be noticed that on these same melts, and those with 1% $93Al_2O_3$ crucibles, the calculated oxygen removed by carbon is less by gas analysis than metal samples indicating that carbon monoxide is being lost from the melt, but not measured by the flowmeter (see 3.2.)

From this comparison it can be concluded that gas analysis plus flow measurement can be used in place of metal sampling, but only where silica and water are the sole contributors. When other oxides such as MgO or Al_2O_3 are also donating oxygen, the progress of the melt must be followed by metal sampling plus flow measurement.

3. Donation by oxides other than silica.

3.1. Donation of oxygen by water.

Hydrogen was evolved from all the melts and analysis of the gaseous atmosphere above the melt indicated amounts varying from near zero to 50%. This appeared to depend solely on the rate of evolution of carbon monoxide since the total amounts of oxygen contributed by the water were reasonably constant at about 0.03^W% in 210 minutes (Figures 63 and 64). Several experiments were conducted to determine the source of the hydrogen.

- (i) A degassed carbon block was suspended in an alumina crucible and heated to 1600° Centigrade at a constant pressure of 76 torr and initially in an atmosphere of carbon monoxide. The gas in the chamber was analysed throughout the experiment and found to change from 100% CO to 50% CO - 50% H₂.
- (ii) Experiment (i) was repeated using an argon

contents of the gaseous atmosphere increased together and the ratio $\frac{\%CO}{\%H_2}$ was always unity.

(iii) Experiment (ii) was concluded by pumping down the system to 2 torr and closing all valves. Carbon monoxide was evolved at a greater rate than hydrogen at the lower pressures, but as the pressure increased to 76 torr the gas composition approached 50% CO - 50% H₂ showing that the two rates were equalising. After holding at 76 torr a gas composition of 50% H₂/50% CO was achieved.

(iv) Experiments were conducted with alumina crucibles which had been prefired at 1550° Centigrade under high vacuum. Hydrogen and carbon monoxide were still evolved when the crucible was reheated to 1600° Centigrade by a carbon block under argon and the gas flow rates remained unaltered whether or not the rest of the refractory assembly was present.

(v) Analysis of the gaseous atmosphere prior to the melting of the charge on experimental runs showed that initially water vapour and carbon dioxide were present in the system. No hydrogen was present at this stage. With the melting of the charge and the onset of the carbon-oxygen reaction, both carbon monoxide and hydrogen were evolved and the water vapour and carbon dioxide contents diminished to zero.

These experiments indicated that water vapour, initially present in the crucible as combined water, reacted during the melt with carbon to form carbon monoxide and hydrogen,

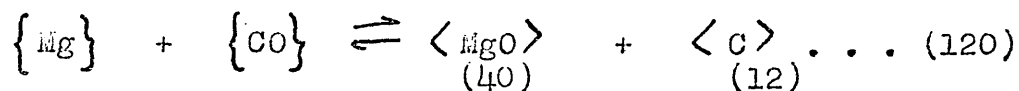


Figures 63-65 indicate the relative importance of this oxygen source. Figure 65 shows a cumulative plot of the weight percent oxygen contributed by water and silica together with that removed by carbon as the melt progresses. Under such circumstances where the dissociation rate of silica is low, water plays a significant part in decarburisation and must be accounted for. Attributing all the loss of carbon to reaction with silica would lead to a calculated silicon pickup of more than 25% greater than that actually analysed. Figures 63 and 64 show the contribution of oxygen in 210 minutes from water and silica to melts in magnesia and aluminosilicate crucibles respectively, plotted against the static oxygen content of the melt. Although there are slight changes with crucible type and oxygen content the amount of oxygen contributed by water changes only slightly from about 0.03^W%. Hence at high reaction rates, typified by high silica activities, high carbon contents and low pressures, the contribution of oxygen by water becomes insignificant and the composition of the gaseous atmosphere rarely drops below 95% CO. At the other end of the scale, however, where the oxygen content of the melt is above the equilibrium value for the silica activity, water is the only contributor of oxygen (melt 19) and the lowering of the carbon content can only be attributed to this source.

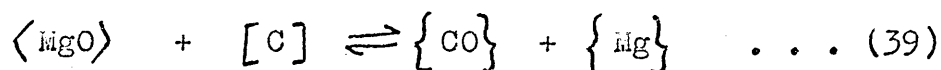
3.2. Donation of oxygen by magnesia.

With 1% C melts in magnesia crucibles it was noticed that the volume of gas measured by the flowmeter was less than the volume of carbon monoxide calculated from loss of carbon. At the same time, a rubbery-textured material was

found on the top of each crucible which had not been seen on other heats. Subsequent analyses of this material are shown in Table 16, which show it to be composed mainly of iron, magnesia and carbon. The proportion of magnesia to carbon was, in general, about 4 to 1 which would be expected from the oxidation of magnesium by carbon monoxide according to,



Thus each mole of carbon monoxide produced by the reaction



was lost to the system by the recombination of the two gases at lower temperatures. Hence carbon may have been removed from the melt by reaction with magnesia, but may not have been measured as carbon monoxide by the flowmeter.

The dissociation rate of magnesia was calculated from

$$\Delta V_{CO_{MgO}} = \Delta V_{T\%CO(M)} - (\Delta V_{CO_{SiO_2}} + \Delta V_{CO_{H_2O}}) \dots (121)$$

where $\Delta V_{CO_{MgO}}$ = volume of CO evolved by reaction with MgO in Δt .

$\Delta V_{T\%CO(M)}$ = total volume of CO evolved, calculated from carbon loss by equation (113)

$\Delta V_{CO_{SiO_2}}$ = volume of CO evolved by reaction with SiO_2 in Δt .

$\Delta V_{CO_{H_2O}}$ = volume of CO evolved by reaction with H_2O in Δt . In most of these melts this quantity is very small compared with the total CO evolved and may be ignored.

Table 17 shows values of $V_{CO_{MgO}}$ for fine melts of high carbon content in magnesia crucibles from which the dissociation rates of magnesia were calculated. The specific rates of oxygen transfer were found to vary from 0.48×10^{-7} (1.0% C, 760 torr) to 1.87×10^{-7} (1.0% C, 76 torr) moles of oxygen/

sq.cm/sec, which are in good agreement with the work of Brotzmann (107) who obtained $0.67(0.1\%C, 20 \text{ torr}) - 3.1 \times 10^{-7}$ (1.0%C, 1 torr) moles of oxygen/sq.cm/sec.

Table 18 and Figure 63 show the various contributions of oxygen from all oxides present in magnesia crucibles which are compared at the various levels of the melt oxygen content. These show that, with initial carbon contents of 0.1%, only silica and water have contributed oxygen ($[O_M] = 0.0122 - 0.003\%$) but that with initial carbon contents of 1.0% and oxygen contents of 0.0014 - 0.0022% the decomposition of magnesia becomes important and must be taken into account.

3.3. Donation of oxygen by alumina.

Analysis of the solidified ingots showed that aluminium had been picked up by 1%C melts at 76 and 3 torr in both $Al_2O_3 - 7SiO_2$ and $Al_2O_3 - 37SiO_2$ crucibles. No pickup ($<.002\% Al$) had occurred with high carbon, 760 torr melts or any of the melts having initial carbon contents of 0.1%. Table 19 gives a list of heats where aluminium pickup occurred and shows an increase in the final aluminium content with decrease of pressure and oxygen content and with increase in the alumina content of the crucible. Figure 64 and Table 20 also show that the contribution of oxygen from silica and water is insufficient to account for all the carbon lost by the melts, marginally with 61% Al_2O_3 crucibles, but to a much larger extent with 93% Al_2O_3 crucibles.

In contrast to the dissociation of magnesia where both products are gaseous, it is to be expected that aluminium, formed by decomposition of alumina, will go into solution in the liquid iron-carbon melt. With 93% Al_2O_3 crucibles (1.0%C, 3 and 76 torr) the volume of gas calculated from the carbon

drop was greater than that measured by the flowmeter. By comparison with magnesia melts this indicated that aluminium was being oxidised by carbon monoxide. However, since condensed species were rarely present and since the volatilisation of such low concentrations of aluminium would not be expected it is thought that oxidation of the aluminium must have occurred on the surface of the melt. There is some support for this in that on many of these melts a scum was seen to form on the edges of the melt surface. On cooling down, however, this scum was only visible as an extremely thin layer of surface oxide, the analysis of which was impossible. In view of these considerations, these determinations must remain somewhat inconclusive, but even so, as an indication, the specific rate of oxygen transfer has been calculated (Table 19) based, firstly on the quantity of aluminium picked up by the melt and secondly on the carbon removed in excess of that necessary for reaction with silica. The results of these last calculations give a specific rate of $5-7 \times 10^{-8}$ moles of oxygen/sq.cm/sec transferred from alumina to the melt. These are above the values of $0.015 - 1.3 \times 10^{-8} \dot{n}_O$ /sq.cm/sec given by Parlee(85) (Table 6) and $3.8 \times 10^{-8} \dot{n}_O$ /sq.cm/sec given by Fischer and Hoffman. Values from the amount of aluminium picked up throughout the melt, based on the average mass of the charge (1950-2050 gm) vary from $0.96-4.8 \times 10^{-8}$ for $61Al_2O_3-SiO_2$ crucibles and $2.4-4.8 \times 10^{-8} \dot{n}_O$ /sq.cm/sec for $93Al_2O_3-SiO_2$ crucibles which seem to be in better agreement with the other published values.

4. Decomposition of silica.

4.1. General.

... of the metal silicon content against time for all crucibles investigated. Also given below the graphs is the average oxygen content and the rate of silicon transfer $\frac{d^w/oSi}{dt}$ at three values of the time t.

In all melts, but those where the carbon content fell to a low value, the oxygen content was kept at a constant level[†] by reaction with carbon and followed a pattern similar to Figure 28. It can be seen that an increase in the carbon content and a decrease in the pressure results in lowering of the static oxygen content and a higher concentration of silicon in the melt at any time.

4.2. Extent of the silica decomposition reaction.

The rate of dissociation of silica from aluminosilicate and magnesia refractories, as measured by the amount of silicon picked up by the metal, decreased with time and in many cases approached zero (Figures 66-70). This may be due to,

- (i) elimination of carbon, restricting the rate of the C-O reaction and resulting in an increase in the soluble oxygen content. The reaction slows down and eventually ceases when the oxygen level rises above that in equilibrium with the activity of silica and the silicon content of the metal.
- (ii) complete removal of silica due to its leaching out by the dissociation reaction and resulting in its complete replacement by the remaining alumina.
- (iii) the approaching of an equilibrium state

[†]Footnote: Hereafter referred to as the static oxygen content.

between the activity of silica at the interface and the silicon and oxygen contents of the bulk metal.

With melts MAG 37, 90; M 89, 44, 41; P 67, 68, 87; HS 84, 88; this zero rate was approached though never actually achieved, but in melts MAG 82, 19, 18, 76; M 86, 45, 49; P 57, 61, 79; HS 63, 64, 66, 71; an equilibrium state appeared to be established as indicated by the slopes of the curves in Figures 66-70.

For further investigation of this phenomenon a sample of the refractory layer in immediate contact with the metal was scraped off the crucible after each melt. Great pains were taken to remove as little of the surface as possible. Chemical analyses of these samples shown in Table 21 illustrate the large losses of silica which occurred at the surface during the melt. X-ray diffraction studies were also carried out on transverse sections of several crucibles, mounted in araldite under vacuum. After analysis of the surface layer, the specimen was surface ground and re-examined in steps of 20 thousandths of an inch. Although the silica glass, known to be present, could not be detected by this technique, Table 22 does show that, in many cases, mullite (and therefore silica) has been consumed at the surface. Melt 57, on the other hand, having a high oxygen content of 0.020^w% shows only very slight attack at the surface as might be expected. The original phases of the crucible become apparent as the depth below the surface increases. From these results, the crucible would generally appear to be attacked to a depth of 20-40 thou. (0.05-0.1 cm) at low oxygen contents (< .0025%) and virtually not at all at

The activity of silica finally in contact with the melt has been calculated from the final silicon and oxygen contents according to,

$$\langle \text{SiO}_2 \rangle \rightleftharpoons [\text{Si}] + 2[\text{O}] \quad \dots (33)$$

where $K_{33} = 2.5 \times 10^{-5} = \frac{[\text{Si}][\text{O}]^2}{\langle \text{SiO}_2 \rangle}$

$f_o^2 \times f_{\text{Si}}$ is assumed to equal unity and concentrations have been used instead of activities.

The activity of silica thus calculated is shown in Table 23 together with the analysed silica content of the crucible surface layer. Figure 71 shows a plot of the calculated final a_{SiO_2} against the silica content of scraped samples. This shows that the relationship from the present experiments is not the one that might be expected, the activity having reached high values at only moderately low silica contents. This is to be expected where the melt oxygen and silicon contents are below the equilibrium values for mullite ($a_{\text{SiO}_2} = 0.42$) where $K_{33} = 1.01 \times 10^{-5}$. Here, with $O_M = 0.02$ only 0.025% silicon is required in the melt to establish equilibrium and, under such conditions mullite can be considered more or less inert and would not be expected to dissociate. At 1600^o Centigrade grade P crucibles consist of approximately 20% silica glass and 80% mullite and grade M crucibles consist of about 50/50 mullite/silica glass. Figure 71 indicates that only the silicate matrix of these crucibles would be expected to dissociate at high oxygen contents and, if time allows, the silicon content will continue to increase until equilibrium is established with the silica. In some cases the equilibrium silicon content is

too high for this to happen and most of the silica and mullite are leached away before equilibrium is reached. Melts which fall between these two extremes reach equilibrium with mullite + alumina. It is worth noting that with the HS crucible the colloidal silica bond would be expected to transform to mullite at 1600° Centigrade. Figure 71 shows that an a_{SiO_2} value of 0.42 is approached at 7% SiO_2 , the content of this crucible. The mole fraction of silica present should not really be used in place of the activity in all cases since it seems that the amount of phase present does not always determine the final equilibrium.

For kinetic considerations also it may be better to assess the amount of each phase present and, knowing the true activity of silica in that phase, calculate the separate rates of transfer.

Figure 72 shows a plot of the final silica content of the crucible surface layer against the oxygen content of the melt. It can be seen that the depletion of silica from the interface is dependent upon the soluble oxygen level and as this rises above 0.02% the silica approaches its initial value.

Figure 73 shows the same data plotted in terms of % silica depletion against oxygen content. Here all points lie approximately on the same curve in spite of the different crucible types.

Figures 74 and 75 show the extent of the reaction, measured by the final silicon content, as affected by the static oxygen content of the melt and crucible composition. As would be expected from equation (33) the amount of silicon, and therefore oxygen, transferred to the melt has increased

with increasing silica content of the crucible and with decreasing oxygen content. The differences between the crucibles have become more apparent at low oxygen levels where the amount of silicon necessary to achieve equilibrium is drastically increased. Thus, whether or not equilibrium is achieved depends both on the activity of silica and the time available. Melts in low silica crucibles ($8\text{SiO}_2\text{-MgO}$, $7\text{SiO}_2\text{-Al}_2\text{O}_3$) appeared to achieve equilibrium in all cases as did the low carbon melts with the higher silica crucibles ($56\text{SiO}_2\text{-Al}_2\text{O}_3$, $37\text{SiO}_2\text{-Al}_2\text{O}_3$). With the high carbon melts in high silica crucibles, however, the reaction was still proceeding even after five hours as indicated by the plots of silicon against time in Figures 66-70. This suggests that the termination of reaction has not been due to physical factors such as the surface tension between liquid iron and refractory which might possibly be thought to cause cessation of the reaction when the liquid interface lost contact with the silica-bearing refractory due to the holes and pores created by the leaching out of these components. Instead it would seem that the reaction has continued to proceed until equilibrium has been reached with the silica remaining (at its average activity) and the bulk silicon and oxygen contents. Even so, as has already been mentioned, where the bulk oxygen concentration was high, i.e. at low carbon contents and high P_{CO} values, the mullite phase did not dissociate and equilibrium was reached with the silicate matrix of the crucible.

4.3. Kinetics of silica dissociation.

4.3.1. General.

Although the total silicon pickup is an indication of

the overall stability of the crucible it gives little information with respect to the local conditions which vary over the surface of the crucible.

Sections of the MAG, HS, P and M crucibles were held at 1600° Centigrade for four hours, under vacuum, and water quenched. After vacuum mounting in Araldite the specimens were lightly etched in a 5% HF solution, examined and photographed. Specimens in the as-supplied condition were also examined for comparison and the phases present are given in Table 11. It is thought that the heat-treated structures shown in Figures 76-79 adequately represent the crucible surface at 1600° Centigrade prior to the onset of reaction. As indicated from the $\text{SiO}_2\text{-Al}_2\text{O}_3$ equilibrium diagram shown in Figure 80, the X-ray diffraction studies given earlier and microscopic examination, the M crucibles (56^W/_o SiO_2 - Al_2O_3) at 1600° Centigrade consist of 55^W/_o SiO_2 matrix and 45^W/_o mullite needles; the P crucibles (37^W/_o $\text{SiO}_2\text{-Al}_2\text{O}_3$) at 1600° Centigrade consist of 23^W/_o SiO_2 matrix and 77^W/_o mullite needles; and the HS grade (7^W/_o SiO_2 - Al_2O_3) consists of 67^W/_o corundum grains with 33^W/_o mullite at grain boundaries. During the melt the silicate matrix dissolves FeO and may form an iron silicate liquid at the surface.

The rate of dissolution of silica will, therefore, vary with the phase and this is illustrated in Figure 81 (Table 24). Here the total silicon transfer, plotted against the static bulk oxygen content, is calculated in terms of moles of silicon per unit area of silica, by dividing the silicon content achieved at the end of the melt ($t = 18,000$ s) by the mole fraction of silica initially present in the crucible. This assumes that the crucible can be represented by areas

of silica and alumina as illustrated schematically in Figure 82, and that the reaction proceeds evenly over the whole surface. As Figure 81 shows, those crucibles which can achieve equilibrium at low oxygen levels either due to their low activity of silica (MAG, HS) or to their rapid reaction rates ($92\text{SiO}_2\text{-Al}_2\text{O}_3$) generally achieve a higher specific silicon transfer for a given oxygen content. Those crucibles which have mullite present ($57\text{SiO}_2\text{-Al}_2\text{O}_3$ and $46\text{SiO}_2\text{-Al}_2\text{O}_3$) cannot achieve their equilibrium silicon values for low oxygen contents in the time available and consequently show a lower specific silicon transfer.

Following on from this approach it is of interest to calculate the depth of erosion of the silicate phase using the relationship,

$$A_{\text{SiO}_2} \times W \times \rho_{\text{SiO}_2} = \text{wt of SiO}_2 \text{ transferred to metal} \quad \dots (122)$$

where A_{SiO_2} = area of contact between silica and metal assuming the conditions in Figure 82 to apply where A_{SiO_2} remains constant with time and is equal to $N_{\text{SiO}_2} \times A_R$.

W = depth of erosion of silica

ρ = density of silica = 2.2 gm/cc.

The weight of silica transferred to the melt (gms)

$$= \text{wt\% Si} \left(1 + \frac{2M_O}{M_{\text{Si}}} \right) \times \frac{\text{mass of melt}}{100}$$

$$\text{and Hence } W = \frac{\text{wt\%Si} \left(1 + \frac{2M_O}{M_{\text{Si}}} \right) M}{N_{\text{SiO}_2} \times A_R \times \rho_{\text{SiO}_2} \times 100} \quad \dots (123)$$

where M = 2,000 gms.

and A_R = 200 cm².

The relationship between W and oxygen content is shown in Figure 83 for three aluminosilicate crucibles where it can

be seen that this quantity, like the specific silicon transfer, is sensitive to changes in oxygen content at the lower levels and increases as the initial silica content of the crucible decreases. It will also be noticed that the agreement between these calculations and the X-ray diffraction work reported earlier is good, giving the depth of reaction at low oxygen contents of 0.05-0.1 cm.

These differences in the behaviour of crucibles shown in Figures 81 and 83 are not necessarily due to equilibrium and time considerations, i.e. the rate of decomposition of the silica bearing phases will vary both with their composition and position and the concentrations of silicon and oxygen in the melt.

Figure 84 (Table 25) shows the specific rate of silicon transfer (moles/cm² silica/sec) plotted against the melt oxygen content at t = 600s. The former has been calculated from a knowledge of the initial silica concentration and the rate of silicon pick-up at t = 600s.

It can be seen that, at oxygen levels below 0.005^{w/o}, the specific rate of silicon transfer is much higher for the 7%SiO₂-Al₂O₃ and 8%SiO₂-MgO crucibles than for the 46%SiO₂-Al₂O₃ and 57%SiO₂-Al₂O₃ crucibles. This could, in principle, be due to three reasons.

- (i) The silica in the HS(7 %SiO₂-Al₂O₃) crucibles is present only as a bonding material, initially as α or β quartz and, as with the 95%SiO₂ material, has a local silica activity of unity. Thus those crucibles having silica in the uncombined form exhibit a higher specific rate of silicon transfer than those where part

or the whole of the silica is combined as mullite, even though in these cases the total silica content of the crucible is higher.

(ii) The silica in the HS and MAG grades represents the total silica content of these crucibles and, being the bond, is present at grain boundaries only. Because of the high energies associated with these regions, rates of dissociation and diffusion will be faster than at the centre of a large grain.

(iii) When considering the reaction on a micro-scale the true activity of the phases must be used. These phases, having their own equilibrium concentrations of silicon and oxygen dissolved in the adjacent liquid metal, set up a diffusion gradient across the boundary layer which is steeper the lower the bulk silicon and oxygen concentrations. The oxygen level in the bulk liquid is generally maintained constant by the carbon-oxygen reaction, whereas the silicon content increases until equilibrium is established. Hence at any time the silicon content of a melt in a high silica crucible is higher than that of a low silica crucible as shown in Figures 66-70, 74 and 75, with the result that diffusion gradients are less steep, particularly if the reacting phase is mullite and not pure silica. Hence with respect to a unit area of silica the diffusion gradient is steeper for HS and MAG grades than for M, P and silica crucibles and, therefore,

both the specific rate of silicon transfer and the total specific silicon transfer are higher.

This latter explanation of the local rates of transfer is probably the most correct since, as will be shown later, when the silicon content of the metal is taken into account, the low silica crucibles obey the same rate laws as the high silica grades.

4.3.2. Mass transfer models based on the boundary layer theory.

4.3.2.1. Introduction.

Mass transfer by diffusion obeys the modification of Fick's first law,

$$\frac{dn}{dt} = \beta A (C_B - C_S) \quad \dots (71)$$

where C_B = concentration of solute in bulk medium.

C_S = surface concentration of solute, usually assumed to be in equilibrium with the second phase.

In equation (71) β is the mass transfer coefficient and, whilst it can be interpreted in many ways, it is generally expressed as the ratio of the diffusion coefficient to the thickness of the boundary layer, i.e. $\frac{D}{\delta}$. There are many difficulties associated with the interpretation of equations such as (71). The values of the diffusion coefficient of many elements in liquid iron are not known with absolute certainty. Whilst D for carbon has been fairly accurately established as $7-8 \times 10^{-5}$ (3,55,66) cm^2/sec at 1600° Centigrade, the best values for oxygen and silicon are not so well known. It is thought, however, that the best value for both these elements is 1×10^{-4} cm^2/sec (56,133). Generally the value for δ increases with the diffusion coefficient but factors affecting the flow at the diffusion

induction stirring also exert a large influence.

The concentration (or activity if used) of the solute at the second phase interface may also not be accurately known. This will depend on, and will vary with, such factors as the activity of the second phase and the activities of any other solutes involved. When silica dissociates, silicon and oxygen atoms are released to the melt at the refractory-metal interface. The activities of the silica and solutes are taken to be in equilibrium at this position, but their values are not known. They may be estimated, however, firstly by assuming that the activity of silicon at the interface Si_R is equal to the bulk concentration Si_M and then, by applying the law of mass action to equation (33)

$$K^* = \frac{[Si_M] [O_R]^2}{\langle a_{SiO_2} \rangle} = 2.5 \times 10^{-5}$$

Here $f_o^2 \cdot f_{Si}$ is assumed to be unity.

Secondly, as shown later, the diffusion equations themselves can be used to eliminate the surface activities of the solutes according to,

$$K_{33} \langle a_{SiO_2} \rangle = \left[\left(\frac{dSi}{dt} \frac{\delta Si \cdot V}{D_{Si} A} \right) + Si_M \right] \left[\left(\frac{dO}{dt} \frac{\delta O \cdot V \cdot M_{Si}}{D_O A 2M_O} \right) + O_M \right]^2 \dots (124)$$

The determination of O_R is still hampered, however, by a lack of knowledge of the value for the activity of silica. The activities of silica and other oxides in many slag systems are not known and, therefore, for mass transfer from slags the value for a_{SiO_2} can usually be chosen with some accuracy. Also when working with pure oxides the activity is known to be unity and both experimental work and calculations may be greatly simplified. In these investigations, however, the

change continually during each experiment as the silica is leached away from the surface. The situation is made more complex since the crucibles are not made up of chunks of silica and alumina (or magnesia) but separate phases such as mullite and forsterite and, therefore, the activity of silica in the combined form should really be used. Even so, the silicate glass and mullite, which are the phases present for compositions between 5 and 70^W% alumina will dissociate at different rates once the oxygen content has been lowered below the corresponding equilibrium values and their activities will again be unknown.

Figure 85 shows values for the bulk silicon content Si_M calculated for various values of D_O , D_{Si} , δ , $\frac{A}{V}$, a_{SiO_2} and $\frac{d\%Si}{dt}$ from equation (124). It shows how sensitive to variation some of these parameters are, especially at high rates of transfer. Slight inaccuracies in any one of them is sufficient to put the calculation out by a large amount. What now follows is an attempt to examine several approaches to this problem, all of which are based on the boundary layer theory. The accuracy by which the rate of silicon transfer can be predicted from a knowledge of bath and crucible conditions increases progressively from model I to model IV. The first, by Ward (97), employs several assumptions which make it difficult to apply in all cases. One parameter, the gas-metal interfacial area (A_g) is virtually unknown and at best can only be approximated. The use of the measured stagnant surface area together with the assumption that the boundary layer thickness at the gas-metal and crucible-metal interfaces are equal leads to such gross errors that the

application of this model becomes severely limited.

Models II to IV avoid the value of A_g by using the analysed value of the metal oxygen content and considering, therefore, only one transfer process, that at the crucible-metal interface. By this means the uncertainties in the gas-metal surface activities of carbon and oxygen are also avoided.

The assumption that the activity of silicon at the crucible-metal interface can be represented by the bulk silicon concentration (1st and 2nd models) is avoided in Models III and IV and the final model also makes no assumptions with regard to the average activity of silica in the crucible, the separate rates of transfer from silica and mullite being added to give the total rate.

Progression from Model I to Model IV results in an increase in the correlation coefficient (given on the relevant figures) from 0.017 to 0.76, suggesting a definite improvement in accuracy. The dotted lines on the figures for each model represent the best line through each population as given by a regression analysis of the results.

The boundary layer for the transfer of oxygen at the crucible-melt interface was found to have a thickness of 0.018 cm after preliminary calculations following the work of Knuppel and Oeters (93). These workers showed that for flow with friction the value of $\delta = .003$ cm, postulated for the gas-metal interface, was increased by a factor of 4.25 to 0.013 cm. Using values less than this would have led to predicted transfer rates which were higher than those measured experimentally. As it was, the agreement obtained using a value of 0.018 cm in models II to IV was good and it is

thought that this helps to confirm the findings of these workers.

4.3.2.2. Model I

This model has been used by Sharma and Ward (97) in their investigations into the dissociation of silica in carbon-saturated iron where the main assumptions made were that,

- (i) the boundary layer thicknesses at the crucible-metal and gas-metal interfaces are equal, $\delta_R = \delta_g$.
- (ii) the equilibrium silicon concentration at the metal-refractory interface Si_R can be represented by the bulk concentration Si_M .
- (iii) the oxygen concentration at the gas-metal interface is very small compared with that at the refractory-metal interface and can be neglected.

The oxygen gradients in the system were assumed to follow the pattern shown in Figure 28 and since O_M is kept constant the oxygen fluxes across the boundary layers may be written,

$$\dot{n}_O = A_R \frac{D_O}{\delta_R} (O_R - O_M) = A_g \frac{D_O}{\delta_g} (O_M - O_g) \dots (125)$$

Ward assumes that the stirring conditions at the metal-silica and metal-gas interfaces are identical and $\delta_R = \delta_g$ and, therefore, equation (125) gives

$$O_M = \left(\frac{A_R}{A_g + A_R} \right) O_R + \left(\frac{A_g}{A_g + A_R} \right) O_g \dots (126)$$

where $\left(\frac{A_R}{A_g + A_R} \right)$, $\left(\frac{A_g}{A_g + A_R} \right)$ are the fractions of the metal surface in contact with silica, gas and putting these as

metal as,

$$O_M = x O_R + (1 - x) O_g \quad \dots (127)$$

and substituting these in equation (125),

$$\dot{n}_O = A_R \frac{D_O}{\delta} (1 - x) (O_R - O_g) \text{ and since } A_R = xA, \text{ then}$$

$$\dot{n}_O = A \frac{D_O}{\delta} x (1 - x) (O_R - O_g) \quad \dots (128)$$

O_R is then assumed to exceed O_g by an order of magnitude making $f(O_g)$ negligible. (This is true only for high carbon contents and/or low p_{CO} values).

Also since two oxygen atoms are transferred for every silicon atom the silicon flux is,

$$\dot{n}_{Si} = \frac{\dot{n}_O}{2} = \frac{A D_O}{2\delta} x (1 - x) O_R \quad \dots (129)$$

$$\text{Using } K_{33} = \frac{[h_{Si}][h_O]^2}{\langle a_{SiO_2} \rangle}, \text{ assuming } f_O^2 \cdot f_{Si} = 1,$$

and converting to wt. percentages gives

$$\frac{d\%Si}{dt} = \frac{M_{Si}}{2M_O} \frac{A}{V} \frac{K_{33}^{\frac{1}{2}} D_O x (1 - x) \langle a_{SiO_2} \rangle^{\frac{1}{2}}}{\delta [\%Si]^{\frac{1}{2}}} \quad \dots (130)$$

Equation (130) has been applied to the present results

allowing the rate of silicon transfer, $\frac{d\%Si}{dt}$, to be calculated at $t = 600s$ where,

$$\begin{aligned} K_{33} &= 2.5 \times 10^{-5} \\ A &= \text{total area} = 235 \text{ cm}^2 \\ V &= 300 \text{ cm}^3 \\ M_{Si} &= 28 \\ M_O &= 16 \\ D_O &= 1 \times 10^{-4} \text{ cm}^2/\text{s}, \\ x(1-x) &= 0.139 \\ \delta = \delta_{O_R} = \delta_{O_g} &= .018 \text{ cm}. \end{aligned}$$

The calculated rates are shown in Table 26 and are plotted

in Figure 86a against the experimentally determined values at $t = 600s$. As Figure 86a shows, the calculated results are very scattered and can be either higher or lower than the measured value. They are higher than the ideal at low rates mainly because no account has been taken of O_g . This can be important at low carbon contents and high p_{CO} values and will have the effect of decreasing the calculated rate. Better models (models II - IV) take this into account by removing O_g and considering only the mass transfer at the crucible-melt boundary along the concentration gradient O_R to O_M . Here no assumptions are made with regard to the values for δ_R and δ_g since only δ_R is required in the calculation.

In model I, by Ward, δ_g is assumed to equal δ_R , and it may be that this assumption is invalid since it has been shown that for flow with friction δ is about four times larger (93)

7.?

$$\text{i.e. } \frac{\delta_{\text{friction}}}{\delta_{\text{free flow}}} = \frac{.013}{.003} = 4.25$$

Such conditions apply at the melt-crucible interface, but not at the melt-gas interface and consequently it is thought that δ_R could be about four times larger than δ_g .

If this situation does in fact apply then the value for O_M calculated from equation (127) in model I will be too high and will result in a calculated silicon transfer rate which is too low.

When the true, measured value of O_M is inserted into equation (127) together with values for O_R , A_g and A_R the value for δ_R can be approximated, applying the better known value of 0.003 cm for δ_g . This procedure, however, results in values for δ_R which are much larger than expected and which are very variable and this suggests that some other factor in the equation is incorrect. The only other

parameter known to be subject to uncontrolled variation is A_g , the gas-metal interfacial area. The value taken in the calculations for model I was 35 cm^2 measured from the crucible geometry, but this must be subject to large variations, since on many heats, especially those at low pressures and high carbon contents, a carbon-oxygen boil of varying intensity could be observed. The boil subsided as the refractory-metal reaction slowed down, but by this time calculations based on equation (126) are difficult because the true activity of silica at the crucible-melt boundary is no longer known.

The variation in the gas-metal surface area, A_g , can be found for $t = 10$ minutes, taking the thickness of the boundary layer adjacent to the crucible, δ_R , as 0.018 cm and that of the gas-metal boundary, δ_g , as 0.003 cm . Under these conditions equation (125) gives,

$$O_M = \frac{\left(A_R \frac{D_o}{\delta_R} O_R \right) + \left(A_g \frac{D_o}{\delta_g} O_g \right)}{\left(A_g \frac{D_o}{\delta_g} + A_R \frac{D_o}{\delta_R} \right)} \dots (131)$$

$$\left(\frac{A_g}{\delta_g} + \frac{A_R}{\delta_R} \right) = \frac{O_R}{O_M} \left(\frac{A_R}{\delta_R} \right) + \frac{O_g}{O_M} \left(\frac{A_g}{\delta_g} \right)$$

$$\frac{A_g}{\delta_g} \left(1 - \frac{O_g}{O_M} \right) = \frac{A_R}{\delta_R} \left(\frac{O_R}{O_M} - 1 \right)$$

$$\text{Hence } A_g = \frac{\delta_g}{\delta_R} A_R \left[\frac{\left(\frac{O_R}{O_M} - 1 \right)}{\left(1 - \frac{O_g}{O_M} \right)} \right] \dots (132)$$

where $A_R =$ surface area of crucible - metal interface = 200 cm^2

$O_M =$ soluble oxygen content of metal at $t = 600\text{s}$.

$O_g =$ gas-metal surface concentration of oxygen found

$$\text{from } K_4 = \frac{P_{CO}}{[C][O]} = 454$$

calculated from an equation of the type,

$$\frac{d\%Si}{dt} = \frac{MSi}{2M_0} \frac{A_R}{V} (O_R - O_M)$$

Figures 87, 88 and Table 27 show the values of A_g calculated for most of the melts in this series and plotted firstly against the oxygen content at $t = 600s$ (Figure 87) and secondly against the total rate of silicon transfer at $t = 600s$ (Figure 88). These values are subject to errors because of the uncertainty in the values for O_R , δ_g , and δ_R but nevertheless they serve to indicate the general trend and give an approximate guide to the amount of turbulence in the melt either by boiling or otherwise, shortly after the zero time. It will be seen that only in melts with high oxygen contents (i.e. high pressures, low carbon contents) and low reaction rates does the value for A_g approach that calculated from the crucible geometry (35 cm^2). At low oxygen contents and high reaction rates the curves rise more steeply, but it will be seen that A_g for the less reactive crucibles ($7SiO_2-Al_2O_3$, $8SiO_2-MgO$) is always lower than that calculated for the high silica crucibles. It would, therefore, appear that in all high carbon melts, irrespective of pressure, the gas-metal interfacial area is much greater than one would be led to believe from crucible geometry. The same applies to most of the low carbon melts at pressures less than one atmosphere. This is only to be expected in those heats where boiling was observed, however slight, but where boiling was not seen it can only be assumed that the bubbles were too small or too infrequent to be properly noticed or that diffusion of gas took place through the crucible wall. In any event it is plain that it is this increase in area,

plus the increased value for O_R which is mainly responsible for the low soluble oxygen contents (O_M) measured here.

It is, therefore, concluded that the model for oxygen transfer proposed by Ward cannot be applied satisfactorily if there are uncertainties in the value of A_g or if O_g is significantly high as it will be at high p_{CO} values and low carbon contents.

The value chosen for δ_o for Model I was 0.018 cm since this will subsequently be shown to be the most appropriate value. From Figures 87 and 88 it can be seen that, at low oxygen contents, the degassing surface area has been increased by a factor of about 20.

Modifying the value for A_g in equation (126) gives $(1-x)$ as being increased by a factor of 5 over the previous calculation which gave $(1-x) = 0.15$.

Substitution of this increased value in equation (127) then leads to values for the rate of silicon transfer which are more in line with those found experimentally. This generalisation has been tested by correcting the values of A , x and $(1-x)$ used in equation (127) using the calculated value of A_g given in Table 27. The new predicted rates (model I(b)) are given in Table 26 and are plotted in Figure 86(b) from which it can be seen that there is now better agreement with the actual measured rates.

4.3.2.3. Model II

In this and the following models only the mass transfer at the crucible-melt boundary is considered and so the inaccuracies involved in A_g , O_g , and δ_g are removed. Model II is simplified, however, by assuming that the silicon content at the crucible-metal interface Si_R is equal to the

concentration of silicon in the bulk liquid Si_M .

The oxygen flux at this boundary can be described by,

$$\dot{n}_O = A_R \frac{D_O}{\delta_{O_R}} (O_R - O_M) \dots (125)$$

or expressing the silicon transfer in wt. percentages as already outlined in model I,

$$\frac{d\%Si}{dt} = \frac{A_R \cdot M_{Si}}{V \cdot 2M_O} \frac{D_O}{\delta_{O_R}} \left[\left(\frac{K_{33}^{\frac{1}{2}} \cdot (a_{SiO_2})^{\frac{1}{2}}}{Si_M^{\frac{1}{2}}} \right) - O_M \right] \dots (135)$$

where $\delta_{O_R} = 0.018 \text{ cm}$

$D_O = 1 \times 10^{-4} \text{ cm}^2/\text{sec}$

$A_R = 200 \text{ cm}^2$

and $V = 300 \text{ cm}^3$

This equation has been solved for the present melts at $t = 600\text{s}$. The measured oxygen content at this time is equal to O_M and the activity of silica is taken as the mole fraction of silica present in the original crucible as shown below,

<u>Approximate composition of crucible.</u>	<u>Mole fraction silica</u>
8%SiO ₂ - 92%MgO	0.055
7%SiO ₂ - 93%Al ₂ O ₃	0.12
37%SiO ₂ - 63%Al ₂ O ₃	0.50
56%SiO ₂ - 44%Al ₂ O ₃	0.69
95%SiO ₂ - 5%Al ₂ O ₃	approx 1.0

The values calculated for $\frac{d\%Si}{dt}$ by this approach are listed in Table 26 and are shown in Figure 89 plotted against the measured rates for comparison. From this diagram it can be seen that the calculated values are much closer to the measured values than those derived from Model I(a). There is also less scatter and there is an obvious trend. However, most of the calculated values are higher than those measured

experimentally and whilst it is thought that leaching of silica from the surface may be responsible for this on one or two melts, on the whole it is thought that the rates measured from the silicon/time curves of Figures 66-70 are reasonably accurate and are not responsible for this disagreement.

4.3.2.4. Model III.

The assumption that $Si_R = Si_M$, used in model II, has been eliminated in model III as follows:-

The rate of silicon transfer to the melt

$$\frac{d\%Si}{dt} = \frac{D_{Si}}{\delta_{Si}} \times \frac{A_R}{V} (Si_R - Si_M)$$

and also

$$\frac{d\%Si}{dt} = \frac{D_O}{\delta_O} \times \frac{A_R}{V} \times \frac{M_{Si}}{2M_O} (O_R - O_M)$$

$$\text{Hence } Si_R = \left(\frac{d\%Si}{dt} \times \frac{\delta_{Si}}{D_{Si}} \times \frac{V}{A_R} \right) + Si_M \dots (134)$$

$$\text{and } O_R = \left(\frac{d\%Si}{dt} \times \frac{\delta_O}{D_O} \times \frac{2M_O}{M_{Si}} \times \frac{V}{A_R} \right) + O_M \dots (135)$$

Equations (134) and (135) can now be related by the equilibrium equation

$$K_{33} = 2.5 \times 10^{-5} = \frac{[Si_R][O_R]^2}{\langle a_{SiO_2} \rangle}$$

$$\text{giving } K_{33} \times \langle a_{SiO_2} \rangle = \left[\left(\frac{d\%Si}{dt} \times \frac{\delta_{Si}}{D_{Si}} \times \frac{V}{A_R} \right) + Si_M \right] \left[\left(\frac{d\%Si}{dt} \times \frac{\delta_O}{D_O} \times \frac{2M_O}{M_{Si}} \times \frac{V}{A_R} \right) + O_M \right]^2 \dots (124)$$

Simplifying, results in the cubic equation

$$ZY^2B^3 + 2YB^2ZC + ZBC^2 + AY^2B^2 + 2YABC + AC^2 = K \dots (136)$$

$$\text{where } Z = \left(\frac{\delta_{Si}}{D_{Si}} \times \frac{V}{A_R} \right)$$

$$Y = \left(\frac{\delta_O}{D_O} \times \frac{2M_O}{M_{Si}} \times \frac{V}{A_R} \right)$$

$$B = \frac{d\%Si}{dt}$$

$$C = O_M$$

$$A = Si_M$$

$$K = K_{33} \langle a_{SiO_2} \rangle$$

$$\text{Letting } ZY^2 = L$$

$$2YZC + AY^2 = M$$

$$ZC^2 + 2YAC = N$$

$$\text{and } K - AC^2 = P$$

results in the simplified equation

$$LB^3 + MB^2 + NB = P \quad \dots (137)$$

Using Newton's approximation

$$B_{(N+1)} = B - \left(\frac{LB^3 + MB^2 + NB - P}{3LB^2 + 2MB + N} \right) \dots (138)$$

Equation (138) has been programmed into an I.C.T. 1500

computer from which the rate of silicon transfer, $B = \frac{d\%Si}{dt}$

can be found. Newton's approximation is cycled until B and

$B_{(N+1)}$ are within 5% of each other. This programme has been

used for models III and IV with slight variations.

For model III the following values were chosen.

$$D_O = 1 \times 10^{-4} \text{ cm}^2/\text{s.}$$

$$D_{Si} = 1 \times 10^{-4} \text{ cm}^2/\text{s.}$$

$$\delta_o = 0.018 \text{ cm.}$$

$$\delta_{Si} = 0.018 \text{ cm.}$$

$$\frac{V}{A_R} = \frac{300}{200} = 1.5$$

$$M_O = 16.$$

$$M_{Si} = 28.$$

O_M and Si_M were the bulk oxygen and silicon contents at $t = 600\text{s.}$

The values calculated for $\frac{d\%Si}{dt}$ by equation (138) are given in Table 26 and are shown in Figure 90 plotted against the measured rate of silicon transfer at $t = 600\text{s.}$ The pattern of points for model III is very similar to model II

because of the replacement of Si_M by Si_R . It would, therefore, seem that equations (124) and (138) used for model III very nearly describe the mass transfer at the crucible-melt interface.

4.3.2.5. Model IV

It has already been shown that a pseudo-equilibrium is often reached with a higher silica activity than is indicated from the analysis of crucible scrapings. This demonstrates, as might be expected, that there are conditions, determined by the initial silicon and oxygen values, whereby only the silica glass is unstable and the mullite can be considered inert.

Using average values for the activity of silica, as defined by the mole fraction of silica in the refractory, and considering mass transfer to take place over the total surface area must therefore lead to errors in the rate calculation which make it desirable that the separate activities and areas of the phases involved should be used to give a more accurate assessment.

The phase diagram for the $Al_2O_3 - SiO_2$ binary is shown in Figure 80 (134) where the high silica eutectic occurs at 3.85 mol.% Al_2O_3 and 1595° Centigrade. The phases according to this diagram are,

- M crucible - 55 m/o SiO_2 , 45 m/o mullite
- P crucible - 23 m/o SiO_2 , 77 m/o mullite
- HS crucible - 33 m/o mullite, 67 m/o corundum.

Hence the area of phases for a total surface area of 200 sq.cm. is,

M	110 cm ² SiO_2	90 cm ² mullite.
P	46 cm ² SiO_2	154 cm ² mullite

15 65 cm mullite 154 cm corundum.

Equations (124) and (137) were applied, using model III and the A_R values tabulated above, $\langle a_{\text{SiO}_2} \rangle = 1$ for silica and $\langle a_{\text{SiO}_2} \rangle = 0.42$ for mullite, together with the experimental values for O_M and Si_M at $t = 600s$. The results are shown in Figure 91 and Table 26 from which it seems that this is the most accurate approach so far used. Comparison of Figures 90 and 91 show that the rapid reaction rates of the high silica melts appear to have been unaffected, presumably since both the mullite and silica are dissociating and thus both methods give identical results. With melt 49 (0.02% oxygen) model IV has predicted almost the measured rate whereas all the other models gave a calculated rate of zero. This is because previously a_{SiO_2} has been assumed to equal 0.69 which is in equilibrium with $Si_M = .04\%$ at $O_M = .020\%$ and since .04% Si has already been achieved at $t = 600s$, the predicted rate is zero. In point of fact, however, 55% of the crucible surface has a silica activity of unity which is in equilibrium with .06% Si at $O_M = .020\%$ and, therefore, there is a measurable reaction which can only be predicted by Model IV. Similar considerations apply to HS melts where a large surface area has been assumed to have a low activity of silica, whereas in reality, only 53% of the area has a value of 0.42. This adjustment has brought the predicted rates more into line with the measured values.

Table 28 and Figure 92 show the separate rates of oxygen transfer from the silicate and mullite phases. It can be seen that, for the same oxygen content, the rates of transfer are the same irrespective of the overall crucible composition. The total transfer, measured by adding the

as shown in Figure 93, and thus the separate calculated dissociation rates can be taken to be reasonably accurate. These values are higher than those measured by Ward (97), but are in good agreement with the work of Graham and Argent (99) and Turkdogan et al (94) (see Table 6).

4.3.2.6. Effect of the change in a_{SiO_2} with time.

As mentioned earlier, none of these models can be applied accurately when silica has been leached from the surface since the value for a_{SiO_2} is then unknown. This is shown in Figure 94 and Table 29 where two methods of calculation have been used to illustrate the problem. In method A the driving force for oxygen transfer has been determined directly from the oxygen rate equation (125) where

$$(O_R - O_M) = \frac{d\%Si}{dt} \left(\frac{\delta_O}{D_O} \cdot \frac{V}{A_R} \cdot \frac{2M_O}{M_{Si}} \right) \dots (139)$$

As the reaction proceeds, of course, the points still lie on the straight line whose slope is $\left(\frac{D_O}{\delta_O} \cdot \frac{A_R}{V} \cdot \frac{M_{Si}}{2M_O} \right)$ but they gradually move downwards towards zero rate and zero driving force.

With method B the value of O_R is actually calculated from K_{33} and Si_R by first applying equation (134)

$$Si_R = \left(\frac{d\%Si}{dt} \times \frac{\delta_{Si}}{D_{Si}} \times \frac{V}{A_R} \right) + Si_M$$

and then substituting Si_R into equation (133)

$$\left[\left(\frac{K_{33}^{\frac{1}{2}} \langle a_{\text{SiO}_2} \rangle^{\frac{1}{2}}}{Si_R^{\frac{1}{2}}} \right) - O_M \right] = \frac{d\%Si}{dt} \times \frac{V}{A_R} \times \frac{2M_O}{M_{Si}} \times \frac{\delta_O}{D_O} \dots (140)$$

where $\delta_{Si} = 0.018 \text{ cm.}$

$\delta_O = 0.018 \text{ cm.}$

$D_O = D_{Si} = 1 \times 10^{-4} \text{ cm}^2/\text{sec}$

$\frac{V}{A_R} = 1.5$

$(O_R - O_M)$ is, therefore, dependent on $\langle a_{SiO_2} \rangle$ for its correct value. The fact that the points do not always fall on the expected line is due to the fact that the initial activity of silica (mole fraction) is used in the equation to calculate O_R and the result, as the graphs in Figure 94 show, is that with an increase in time the values for the predicted driving force do not decrease as quickly as the rate. The fact that they decrease at all is due to the pick up of silicon. There is no way that the model can be applied correctly in these cases since the only way to find a_{SiO_2} , once the reaction has started, is either to use the same model to predict it, or to stop the melt and examine the crucible. Some attempt has been made in this latter respect by using in equation (140) the final analysed silica content of the crucible surface for those melts where the reaction had not ceased when the melt was stopped. Although there are only a few results and they do not cover a wide range of rates Figure 94 C does show that the $(O_R - O_M)$ values have been brought more into line with the expected values.

4.3.2.7. Summary of mass transfer models.

In view of the good agreement that models II-IV give with the experimentally measured rates it would seem that the results of this work lend support to those who claim that the dissociation of silica is a diffusion and not chemically controlled process at 1600° Centigrade. This is further confirmed by the increase in rate which is brought about by the lowering of O_M . At low silicon contents a change in Si_M has a large influence on O_R thus affecting the driving force, but at higher silicon levels such a change will not affect O_R or alter the driving force. The differences in

reaction rates for one crucible type at different pressures and carbon contents must, therefore, be due to the differences in O_M as a result of the carbon-oxygen reaction. Where O_M is hardly altered by a change in p_{CO} due to the kinetics of the C-O reaction then the rates of oxygen and silicon transfer from the interface will be similar.

The fact that $\delta_o = .018$ cm has been found to apply to flow with resistance at a refractory interface gives good agreement with the work of Kraus and Knuppel and Oeters who gave $\delta = .013$ cm.

One noticeable feature of all the plots for these models is that the regression line for each population does not exactly agree with the ideal relationship. Predicted values for aluminosilicate crucibles are slightly higher at low rates and slightly lower at high rates, whilst those for high rate melts in pure silica crucibles are much too low. It is noticeable also that the deviation from ideality at these high transfer rates increases with increasing silica content of the crucible.

Observation of the melts showed that there was an increased tendency (with 1% C melts) for the initiation of a carbon-oxygen boil as the proportion of the dissociating phase increased, so that with pure silica crucibles a considerable quantity of metal was ejected from the crucible, so violent the reaction. The rate of carbon loss on these melts was extremely high and 1% carbon could be removed from the melt in 80 minutes. The flow conditions on these melts would be turbulent and the thickness (δ) of the boundary layer would consequently be progressively reduced as the intensity of the boil increased. Hence it is to be expected

that the value of δ will become progressively smaller as the pressure is lowered and the carbon content of the melt and silica content of the crucible are increased. One single value of δ cannot then truly be used for all melts and separate values should be determined as the conditions alter. For example, with low pressure melts in silica crucibles a value of $\delta = .002$ cm is required to give agreement with the measured rates. This value is in good agreement with the accepted value of 0.002 - .003 cm postulated for boiling melts (56,89).

Even so, as can be seen from Figures 86, 89, 90 and 91 where the boiling action is only slight it is not too inaccurate to assume the same value of δ (i.e. 0.018 cm) irrespective of crucible type, pressure or carbon content.

Equations (124) and (138) have been used to produce models for oxygen transfer which are shown in Figures 95(a) and 95(b) using the method outlined under model III. These show the effect that the bulk oxygen and silicon contents and the activity of silica have on the rate of donation of oxygen from refractories. It can be seen that the transfer rate becomes more sensitive to changes in the silicon content as the oxygen value increases. For medium-high carbon steels having oxygen contents less than 50 ppm the transfer rates are very similar and eventually appear to merge so that the variation of silicon levels met with in practice has little effect. This is because at low oxygen contents the lowering of O_M increases the oxygen concentration difference across the melt/crucible boundary layer by only a small amount with little change in the driving force for mass transfer.

5. Effect of oxide decomposition on the C/O relationship.

The oxygen content of all the melts remained static until the carbon fell to a low level at which point it began to rise. Table 30 shows the (equilibrium) quotient for the C-O reaction at three values of t which has been calculated from

$$K_4^t = \frac{p_{CO}}{[\%C_M][\%O_M]}$$

where p_{CO} is the partial pressure of carbon monoxide above the melt as measured by analysis of the gaseous phase. The general trend is for K_4^t to increase with time, the higher values ($K_4 = 434$ from equation (4)) being obtained at high pressures and low carbon contents. Consequently on those melts where K_4^t eventually approaches the equilibrium value it is not as a result of a decrease in oxygen, but because of the lowering of the carbon content by reaction with the oxygen transferred from the crucible.

With melts made in $56SiO_2 - Al_2O_3$ crucibles the relatively high oxygen contents in equilibrium with low carbon steels can be reached at pressures of both 760 (melt 49) and 76 torr (melt 45). With the $37SiO_2 - Al_2O_3$ crucibles, however, the rate at which oxygen enters the melt is lower and this results in less carbon loss (melt 61) and a lower value of K_4^t . The static oxygen level (100 ppm) of the 76 torr melts does not appear to have been altered by lowering the silica content of the crucible.

With similar melts in lower silica crucibles $7SiO_2 - Al_2O_3$ (melt 66) and $8SiO_2 - MgO$ (melt 18) the C-O equilibrium is eventually achieved by a reduction in the carbon contents but this time at a much lower oxygen level, (29 and 25 ppm respectively). It appears that the C-O reaction has been able to keep the oxygen at a lower static level as a result

of the reduced rate of oxygen transfer and as a consequence the true equilibrium value of K_4 is approached more slowly than in the case of the high silica crucibles.

Lower oxygen levels (7-10 ppm) are attained at pressures of 3 torr for 0.1% C heats and for 1.0% C melts at both 3 and 76 torr despite the fact that these systems are further from equilibrium. Inspection of Table 30 shows that a reduction in pressure from 76 to 3 torr for the 1% C melts appears to have had little effect either on the oxygen level achieved or the rate of crucible breakdown. This is to be expected if, according to reaction (33), the soluble oxygen content controls the extent and rate of decomposition. Hence although the rate of crucible dissociation can influence the oxygen level achieved, as instanced by the effect of crucible silica content on the 76 torr, 0.1% C melts, this in turn can be controlled by other factors affecting the kinetics of the C-O reaction. Such a factor is likely to be the ferrostatic head of metal in the crucible and its influence on bubble formation.

The value of p_{CO} directly above the metal determines the relationship between the concentration of carbon and oxygen in the surface layer of the metal only. In the process of interaction in the molten metal the p_{CO_x} value is controlled by the relationship,

$$p_{CO_x} = p_1 + \rho h + \frac{2\sigma}{r} \dots (141)$$

- where p_1 = barometric pressure above the metal.
 ρ = molten metal density.
 h = depth of metal at the level of bubble formation.
 σ = surface tension of molten metal

the effect of vacuum upon the deoxidising power of carbon is determined by the ratio of the values of P_1 and $(ph + \frac{2\sigma}{r})$. Where $(ph + \frac{2\sigma}{r}) \gg P_1$ further reduction of pressure above the metal cannot change the value of p_{CO_x} and, therefore, is of no effect in increasing the deoxidising power of carbon.

p_{CO_x} has been calculated for the conditions of the melts in this series and for barometric pressures of 760, 76 and 3 torr. Values of $\rho_{Fe} = 7$ gm/cc, $h = 70$ mm and $\sigma = 1000$ dynes/cm have been used for these calculations. If the pressure is expressed in torr then equation (141) becomes,

$$p_{CO_x} = P_1 + 0.515 h + \frac{1.47}{r} \dots (142)$$

Figure 96 shows p_{CO_x} plotted against r for the various values of P_1 where only a slight change occurs in p_{CO_x} with bubble radii greater than 0.01 mm. Hence for bubbles of radius greater than 0.01 mm the value of $(ph + \frac{2\sigma}{r})$ lies between 37 and 50 torr and lowering the pressure (P_1) below these levels will have only a small effect on deoxidation i.e. at pressures less than 37-50 torr only similar numbers of bubbles will be allowed to grow and hence oxygen contents will be only marginally less.

A more rigorous examination of the kinetics of the C-O reaction cannot be carried out since in all melts oxygen was transferred from the crucible. Hence the true change in rate of the reaction cannot be assessed since this is generally a function of the rate of oxide decomposition. However, it is of interest here to re-examine the previous calculations of the gas-metal surface area A_g under section 4.3.2.2., the results of which were listed in Table 27 and plotted in Figures 87 and 88. Because of the uncertainties in some of

the constants these values were
taken to be approximately correct. In any case the important
feature of interest is the effective mass transfer coefficient
 $K_{\text{eff.}} = \frac{D}{\delta} \frac{A_g}{V}$ and, since D , δ and V are more or less constant,
the value derived for A_g is indicative of the effectiveness
of the carbon-oxygen reaction. It will be seen from Table 27
that for the low silica crucibles ($8\text{SiO}_2\text{-MgO}$ and $7\text{SiO}_2\text{-Al}_2\text{O}_3$)
 A_g is roughly the same for all melts ($100\text{-}180\text{ cm}^2$) and is
much higher than the 35 cm^2 calculated from the crucible
diameter. The high silica ($56\text{SiO}_2\text{-Al}_2\text{O}_3$, $37\text{SiO}_2\text{-Al}_2\text{O}_3$)
crucibles with 1% C have much higher values for the surface
area which indicates that a carbon-oxygen boil has taken
place.

Since the measured surface area of the crucible is
 200 cm^2 , in good agreement with the A_g values for MAG and
HS melts, it would appear that the removal of oxygen in these
crucibles takes place by diffusion through the walls as well
as at the gas/metal interface, whereas with low carbon melts
in high silica crucibles, having a much lower value of A_g ,
transfer appears to take place only at the stagnant gas-metal
interface. These points are in keeping with usual observations
of the melts, the boiling action being sometimes prolonged
in the high carbon heats, but no metal movement being seen
on any of the low carbon or low silica melts. The reasons
for this probably lie in the make up of the crucibles them-
selves. Although Table 12 shows the crucibles to have similar
permeabilities at room temperature, the M and P crucibles
have large amounts of silicate matrix which, if not entirely
liquid, will be highly vitreous at 1600° Centigrade. This
may have the effect of preventing diffusion of gas through

the crucible-metal interface. The differences in oxygen content of the melts probably also can be explained on this basis. A fact which was surprising at first was that high carbon melts in low silica crucibles (HS, MAG) had slightly higher oxygen contents than those in high silica crucibles (M and P). This effect may be due to the difficulty of initiating a metal-crucible reaction boil in crucibles which are porous to the gas with the result that the rate of removal is limited and the oxygen content of the metal is higher. With non-porous crucibles a boil is initiated and exposes a much larger surface area for degassing giving lower oxygen levels.

With low carbon heats, however, the carbon content is too low to initiate a crucible-metal reaction boil in all cases. Those crucibles which are porous, however, allow the products of reaction to be removed from a large surface area so that the oxygen content of the metal is kept at a lower value.

With the M and P crucibles the rate of crucible decomposition is faster and coupled with the lower value for A_g the result is a higher value of the bath oxygen content.

1. Introduction.

The laboratory experiments have demonstrated that dissociation of silica can occur over a wide range of metal oxygen and silicon levels and that magnesia and alumina can also donate oxygen to the melt if the conditions are suitable. A decrease in the silica content of aluminosilicate refractories results in a lowering of the amount and rate at which oxygen is transferred. Transfer still occurs, however, and can only be prevented by increasing the silicon content of the melt to a level above that in equilibrium with the bulk oxygen content and the activity of silica in the refractory.

In the course of vacuum treatment the steel may be out of equilibrium with several oxygen sources, the ladle and degassing vessel refractories and the slag being the main ones. What has not yet been clearly established are the rates and extents of oxygen transfer from such sources and whether or not they affect the reaction between carbon and oxygen. By studying this problem in relation to the Dortmund-["]Horder vacuum treatment process it was hoped that the factors affecting the achievement of low oxygen contents could ultimately be made known so that improvements could subsequently be made.

2. Equipment and experimental technique.

2.1. Description of the vacuum treatment unit.

A 30 ton D.H. (91,117,123,135-139) unit, sited at the Openshaw works of English Steel Corporation Ltd., was used for these investigations. A photograph of the arrangement is

vessel is given in Figure 98. In order to degas a steel melt the filled 40 ton ladle after tapping is placed on a carriage and brought under the electrically-heated vacuum chamber. The nozzle, having a conical metal slag-breaker in position over its open end, is immersed in the liquid steel and the chamber evacuated. Next, by the raising and lowering of the ladle by hydraulic rams, about 5 tons of steel are taken into the chamber and passed back to the ladle, where it mixes at the bottom of the ladle with the steel that has not yet been degassed (91, 135). The ladle moves upwards by about twelve inches and the duration of the lift or cycle can be varied, but in these tests was between 18 and 22 seconds. About 32 - 40 part treatments or cycles follow each other so that, if in each lift 5 tons of steel are drawn in by vacuum, this corresponds to a total steel quantity passed through the chamber of 160-200 tons. As the ladle contents amount to 30 tons this is, therefore, circulated five or six times.

For the control of degassing the following parameters are measured and continuously recorded in this installation.

- (a) the steel quantity drawn in at each lift (tons)
- (b) the pressure in the vacuum chamber (torr)
- (c) the composition of the gas drawn off by suction.
- (d) the platform lift.
- (e) the temperature prevailing in the chamber.
- (f) the temperature of the melt in the ladle (measured before and after treatment).

The change in the oxygen content of the steel in the ladle depending on the number of part treatments is theoretically obtained from a so called recursion formula. In this the mean concentration in the ladle (α_{n+1}) is

evaluated from the data of the previous relevant cycle. It is then presupposed that the amount (M) and the mean concentration of the quantity of steel found in the ladle prior to the $(n + 1)$ lift, the quantity of steel drawn in by suction (m) and its ingoing (α_n) and outgoing (β_{n+1}) concentrations are known.

$$\alpha_{n+1} = \alpha_n - \frac{m}{M} (\alpha_n - \beta_{n+1}) \dots (143)$$

This formula is valid if the concentration of oxygen of the steel in the ladle is kept homogeneous by the mixing action of the cyclic process.

2.2. Experimental heats (140)

Many of the heats investigated were made by a conventional single slag process and were blocked in the furnace by a prior-to-tap addition of silicomanganese and ferrosilicon. Whenever possible, no further additions of deoxidants were made until late in the degassing process. Several heats were special experiments on low carbon steels to which no additions of silicon were made and in some cases the ladle was coated with a magnesia or alumina-chromic oxide slurry. It is conventional practice to remove most of the slag in the furnace so that a maximum of two inches remains on the steel after tapping. 2 cwts. of a firebrick-coke breeze mixture are then added to this slag before the ladle is taken to the DH unit. On one or two heats, however, the bath was slagged as cleanly as possible and powdered magnesia thrown onto the steel after tap in place of the usual mixture.

It was considered appropriate not only to consider the final oxygen contents of the treated steel but to measure the complete course of the oxygen removal in the ladle by sampling and to compare this with the theoretical course. To do this,

samples were taken as frequently as possible from the ladle using the argon suction technique. After about one third of the experiments had been completed this apparatus was redesigned according to Figure 99 so that they could be taken by one operator instead of the two or three men usually required. In so doing, the number of acceptable samples was sharply increased. Each volume of steel sucked into the 5 mm i.d. silica tubes was killed with aluminium distributed as a coil evenly throughout the length of the tube.

Subsequently each specimen was analysed for carbon, silicon and oxygen, two corresponding determinations being required for the latter. All the previously mentioned records of the degassing treatment were also retained for examination.

3. Experimental results and discussion.

At the outset it was hoped that the contribution of oxygen from the ladle lining could be followed by tracing the quantity of silicon picked up by the melt. Unfortunately the steel-making technique employed for these 30 tons arc furnace casts often meant either a blocking addition of ferrosilicon and silicomanganese prior to tap or a small addition of silicon to the ladle. Consequently in most cases at the commencement of degassing the silicon content was greater than 0.01% (in many cases, much higher) which both limited the accuracy of chemical analysis and sometimes, in the case of high oxygen melts, was sufficient to bring the Si-O-SiO₂ system to a state of equilibrium. Hence only on one cast was the silicon pickup accurately measured and so the data of Oeters and Vardag (135) was used to supplement this.

Table 31 shows that good agreement was obtained between the experimentally measured rates of oxygen transfer from silica and those predicted by model III when the boundary

layer thickness was put equal to 0.0075 cm. This reduced value of δ over the 5lb induction melts is to be expected in view of the increased turbulence in the ladle caused by the ejection of large quantities of metal from the vacuum chamber after each cycle.

It serves to show that the rate model described by equation (124) can be accurately used to describe the transfer of oxygen from the ladle lining into a steel melt. It also shows that in the practical cases so far examined additional sources of silica have contributed little or no oxygen. This is principally due to the fact that the reacting area of slag is small compared with that of the ladle lining. In addition to this, slag is absent from many of the 80 ton heats in accordance with the Hoesch practice of degassing the first ladle to be tapped from an open hearth furnace and the activity of silica is low in slags rich in lime as in the 30 ton Openshaw heats.

Figures 100 to 116 show the changes in oxygen, carbon and silicon contents of the present melts and in addition the theoretical oxygen path had equilibrium been reached between carbon and oxygen in the vessel.

Table 32 shows the relationship that pertains, prior to degassing, between silicon, oxygen and carbon on some of the heats.

The theoretical oxygen contents in equilibrium with the analysed carbon (equation (4), $p_{CO} = 1at.$) and silicon (equation (33), $a_{SiO_2} = 1$) contents can be compared with the actual oxygen concentration of the steel in the ladle. It can be seen that the silicon and carbon contents can be considered to be in equilibrium with the same oxygen content

in the case of numbers 1, 2, 3, 5, 8 and 10. ferrosilicon and silicomanganese was added as a blocking addition on heat numbers 3, 4, 6, 7, 9 and 11, but no addition of silicon was made prior to degassing on any of the other heats in Table 32). Irrespective of whether or not silicon has been added to the furnace, equilibrium between carbon, silicon and oxygen has been approached in the majority of cases, the exceptions being the casts with a high carbon content where both the actual oxygen content and that theoretically in equilibrium with carbon is lower than that in equilibrium with silicon. More silicon is required to bring these casts to equilibrium, but the rate of addition, by way of decomposition of silica is not sufficient to make a noticeable effect at this high level (nos. 6, 7, 11). A similar situation also applies on those casts where no silicon was added yet as much as 0.015% has been picked up from some source (Nos. 1, 2, 5, 8 and 10).

Perhaps surprising is the fact that equilibrium between carbon and silicon is still approached even on those low carbon casts where silicon was added. This cannot be coincidence since, although roughly the same amount has been added, the yield is variable and increases with increasing carbon content (Table 33).

It would seem that where the carbon content is high it controls the oxygen in preference to silicon and, therefore, little silicon is used up by oxidation. With lower carbon steels the addition of silicon is likely to be followed by a decrease in oxygen to a level below that in equilibrium with carbon. Some slight reoxidation will occur in the remaining short period in the furnace, but the major oxygen

pickup will occur on tapping. Further oxidation of silicon may then occur and a point reached where the deoxidising power of carbon and silicon are equal. From this time carbon and silicon will be removed together (Nos. 3, 4, 9) as oxygen is introduced and all three will be in equilibrium.

By this mechanism, therefore, the steel will arrive at the degassing unit with the oxygen, silicon and carbon contents in equilibrium, providing that in all cases where silicon pickup is necessary only a small amount is required. If the equilibrium silicon content is high such as on high carbon steels then there will be insufficient time for this silicon content to be reached and equilibrium will not be attained (Nos. 6, 7 and 11).

In order to assess the amount of oxygen donated during vacuum treatment it was necessary to assess the lowering of the soluble oxygen content of the melt and compare it with the amount of oxygen which had been actually removed by carbon as carbon monoxide. The low carbon casts can be assessed using the as-analysed carbon and oxygen changes during degassing, but this approach cannot be used with carbon contents greater than 0.1% where the limits of chemical analysis becomes important. To get around this problem the removal of carbon was calculated from the pressure changes in the vessel and a knowledge of the flow characteristics of the Openshaw unit. The pressure in the vessel is continually reduced during the degassing period, but in a cyclic manner as the steel enters and leaves the vessel as shown in Figure 117. The flow rate of gases out of the vessel depends on the pressure of the gas in the chamber and the characteristics of the steam ejector set which can be

measured by preparing a calibration curve as shown in Figure 118. For the present evaluation the quantities of carbon monoxide removed from the metal were determined for those cycles where the pressure was less than 10 torr and prior to the addition of deoxidants. This generally meant that measurements were not made prior to the 6th cycle or after the 24th. It has already been shown (116) that much of the hydrogen is removed during the first few cycles since the change follows an asymptotic curve similar to that of the average pressure. In any case the volume of hydrogen evolved is small compared with carbon monoxide and so the gas coming off the steel in the vessel was assumed to be pure carbon monoxide. The area under each pressure curve was first found using a planimeter and by dividing this by the cycle time the average pressure rise resulting from gas evolution was found. Two flow rates were then measured using Figure 118; that due to the total pressure in the vessel halfway through the cycle and that which would have prevailed had there been no gas evolution. The two rates were then subtracted to give the number of pounds of carbon monoxide per minute evolved at that time. This approach avoided the assumption of a linear relationship between pressure and pumping rate and, therefore, should be more accurate. The pressure is measured at room temperature in the water cooled section of the pumping line and since the calibration curve was also prepared at room temperature, no corrections for temperature were needed. From these calculations, the loss of carbon from the ladle contents has been found and compared with that measured analytically on the low carbon casts. From Table 34 the agreement can be seen to be satisfactory and justifies the

use of this approach for the assessment of high carbon casts.

Table 35 shows the oxygen balances and rate measurements for all the present casts. Data from the 80 ton Hoesch heats is also given for comparison. The melts appear to fall into three ranges - those where the removal of carbon and oxygen has been stoichiometric, (e.g. LM 3775, LM 3598, LM 3426); those where only donation of oxygen from silica has occurred (e.g. VB III, VB XVIII); and those where the transfer rate of oxygen was too high to be accounted for by silica dissociation alone (most of remainder). The total amount of oxygen donated to the melt was calculated from,

$$\Delta O_D = \Delta O_C - \Delta O \quad \dots (144)$$

where ΔO_D = % oxygen donated in time Δt .

ΔO_C = % oxygen removed by carbon as CO, calculated from the carbon analysis on low carbon steels and pressure measurement on high carbon steels.

and ΔO = % soluble oxygen analysis removed from melt-as analysed.

For the present experimental melts the rate of oxygen transfer from the silica lining of the ladle was then calculated from model III using $\delta_R = 0.0075$ cm and knowing the average silicon and oxygen contents. The rate of oxygen transfer from sources other than silica was then found from,

$$\Delta O_x = \Delta O_D - \Delta O_{SiO_2} \quad \dots (145)$$

When present, this extra rate of oxygen donation can be many times greater than that from silica and is, therefore, more important.

It can be seen from Table 35 that, of the melts at Openshaw, cast Nos. LM 3598, LM 3426, LM 3355 and LM 3722 had silicon and oxygen contents which were above those in

equilibrium with a $\text{SiO}_2 = 1$ and hence the fact that the carbon-oxygen reaction was stoichiometric on two of these casts was to be expected. It should, however, be noted that one of these casts (LM 3398) had a wash of magnesia on the ladle surface and both had magnesia powder added to the ladle slag. The extra oxygen source of oxygen was absent in both casts. It will also be seen that the low theoretical rate of oxygen transfer from silica in LM 3775 cannot be measured and the carbon-oxygen reaction has been recorded as being stoichiometric.

All other casts in the present series have shown the presence of a third oxygen source which has contributed more than 200 ppm of oxygen in the worst cases. Figure 119 shows the relationship that has been obtained between the rate of oxygen transfer from this other source and the average carbon content during the degassing period. 80 ton heats of Hoesch are included for comparison. The points fall into two main groups; those which show a positive increase in rate with increase in carbon content and those low carbon melts which have higher and more variable rates of oxygen donation. Considering first those which can be related to the carbon content of the melt. When the carbon level falls below 0.1% the rate of extra oxygen transfer tends to zero indicating a stoichiometric carbon-oxygen relationship. Table 36 shows the assembled data on all slag samples taken and it can be seen that these casts have, in general, total slag iron contents of less than 3% which tend to decrease with time. The double slag casts have slag iron contents of less than 1% and Figure 119 shows that the extra oxygen transfer rate is lower on these casts. An increase in the rate of donation is to be

expected on account of the lower soluble oxygen contents at higher carbon levels, thus increasing the driving force for diffusion across the slag-metal layer. A contribution of oxygen from the magnesia lining of the degassing unit is very unlikely at these relatively high oxygen contents, the laboratory work indicating the absence of such a dissociation reaction at oxygen levels greater than 20 ppm. Even if the oxygen content of the steel in the unit is lowered by reaction with carbon beyond this value calculations show that the rate could only be of the order of 4×10^{-7} w/o/sec although it must be admitted that the flow conditions in the unit are unknown and a much smaller value of δ could increase the rate to 3×10^{-6} w/o/sec. Even so, the rates of extra oxygen donation have been measured to be as high as 8×10^{-5} w/o/sec and so this source of oxygen can be ruled out.

In fact, this extra oxygen source can be positively identified as iron oxide in the slag. Figure 119 shows that the single slag heats where the rate of extra oxygen supply decreased with decreasing carbon content all received a blocking addition of ferrosilicon and silicomanganese to the furnace prior to tap which resulted in a lowering of the slag iron content from 8 - 11% to 1 - 3%. Similarly all the low carbon casts exhibiting high and variable donation rates did not receive such an addition and consequently the slag was in a high state of oxidation (8-20% FeO)(Table 36) on arrival at the DH unit. It is interesting to note that the 80 ton Hoesch heats follow a similar pattern to the 30 ton Openshaw heats, but here a larger proportion of the low carbon heats exhibit stoichiometry presumably because there is little, if any slag, on most of these heats. The fact that the rate of

as the Openshaw casts is in good agreement with the ratio of ladle dimensions for the two plants (Table 37)

$$\begin{aligned} \text{i.e. } \frac{\text{Area slag - Hoesch.}}{\text{Area slag - Openshaw}} &= \frac{1.5}{1} \\ \text{and } \frac{\text{Area ladle - Hoesch}}{\text{Area ladle - Openshaw}} &= \frac{2.0}{1} \end{aligned}$$

The surface area of reactive slag unfortunately cannot be calculated since, in addition to that which floats on the steel surface, some is taken into the vessel during immersion of the snorkel and some is bound to react with the ladle lining at tap or be left over as a ladle glaze from the previous heat. The main source, however, is thought to be that which floats on top of the ladle (20) and it is obvious (from Figure 119) that this can be largely eliminated by the application of the correct deoxidation procedure prior to tapping. Oxygen donation can probably also be eliminated on medium and high carbon steels in a similar way. Slag deoxidation by carbon or powdered ferrosilicon should enable an almost stoichiometric carbon/oxygen to be attained on all steels. The low rate of oxygen transfer from the ladle appears to be hardly significant with carbon contents up to 0.5%, especially with double slag steels where the silicon content is generally made up to 0.2 - 0.4% prior to degassing. Of course, on high carbon grades the soluble oxygen content may be as low as 20 ppm and extra care with slag deoxidation will have to be taken and donation from the ladle lining may even be important and have to be eliminated by a ladle wash.

Figure 120 shows how the donation of oxygen during degassing affects the efficiency of the carbon-oxygen reaction. It can be seen that the efficiency of oxygen removal is

highest where the external oxygen supply is at a minimum and where the carbon content is low. The effect of decreasing carbon content in low carbon steels cannot be seen from this diagram but, in general as Table 35 shows, the efficiency decreases with decreasing carbon content for initial levels less than 0.05%. At low carbon levels (.05%) the donation of oxygen can reduce the degassing efficiency by more than 50%, and at very low levels the effect is drastic, hardly any removal of oxygen taking place. Similar conclusions may be reached with respect to high carbon steels where the rate of oxygen transfer to the gas-metal interface is rate-determining.

One striking feature of all casts, noticeable from Figures 100 to 116 is the rapid effect of alloy deoxidation compared with the carbon-oxygen reaction, whereupon the traditional acceptance of the benefits of the latter is almost reduced to a myth. In fact the removal of oxygen by reaction with carbon is generally very poor, rarely attaining an efficiency of greater than 60%. Figure 120 shows that it is possible to attain this figure all the time by eliminating the supplies of oxygen from the various sources, but even so, as Figure 100 to 116 show the carbon-oxygen reaction would still not attain equilibrium and here the kinetics of this process would seem to require further investigation. It has already been shown that the formation of gas bubbles (93,135) is very important in achieving rapid gas removal and more work on the fluid mechanics of the various processes is needed as does the influence of inert and reactive gas bubbling. Work has been done in this respect in theory and laboratory (79-83) but little has been carried out on the

plants themselves.

It is the author's opinion, however, that the advantages of alloy decoxidation are already established and further exploitation of these elimination processes would appear to provide the quickest answer to the quest for cleaner steel.

- (i) Laboratory experiments show that silica donates oxygen to an iron melt at a high rate resulting in a static oxygen content for as long as the carbon and silica lasts.
- (ii) The rate and total amounts of oxygen and silicon transferred to the melt decreases as the alumina content of the crucible increases and as the soluble oxygen content increases. The carbon-oxygen equilibrium is not reached at reduced pressures, but the oxygen contents achieved are lower. A limiting oxygen content of 10 ppm is reached which is thought to be due, not only to the continuous supply of oxygen from the crucible, but also to the influence of ferrostatic pressure or crucible porosity on bubble formation.
- (iii) The dissociation reaction can reach chemical equilibrium at high soluble oxygen levels where the equilibrium silicon content is low. More usually, however, it only stops when the silica has been leached completely from the surface and has been replaced by a porous layer of alumina (or alumina + mullite) in the case of the lower reaction rates.
- (iv) The dissociation rates of magnesia and alumina have been measured and are in good agreement with previous determinations.
- (v) A rate model has been programmed into an I.C.T. 1500 computer to determine the theoretical transfer rates for oxygen and silicon. Good agreement has been found with experimental results which is thought

diffusion-controlled process. Agreement has also been found with works experimental results on 30 ton and 80 ton scales, indicating that within the range of steels studied, the ladle lining is the only source of silica likely to contribute oxygen.

(vi) In addition to the soluble oxygen content of the steel and the oxygen supplied by silica, there is also a third major source which has been shown to be iron oxide present in the slag. Correct attention to the deoxidation of slag prior to tapping has been shown to be a simple way of largely removing this source.

(vii) The influence of the rate of oxygen donation on the efficiency of oxygen removal by the DH process has been examined. It is shown that, as the transfer rate increases, the efficiency is lowered both on high and low carbon steels. The efficiency also drops as the carbon content is raised. The elimination of oxygen donation should make it possible to maintain the efficiency of the carbon-oxygen reaction at 50-70%.

(viii) Further improvements can only be brought about by either improving the kinetics of the carbon-oxygen reaction itself or by forming insoluble, removable oxide products by alloy deoxidation. In this respect attention to the sequence and amounts of deoxidant addition are of paramount importance and, added during degassing, the increased turbulence can be used to increase the rate of elimination of the products to free surfaces.

The following areas, associated with the subject matter of this thesis, are suggested as being worthy of further investigation.

1. The present work is in good agreement with the determinations of Brotzmann of the rates of magnesia dissociation. However, whilst Brotzmann reported measurable rates up to high oxygen levels ($.020^W/o$), the author has found no evidence of such a reaction at oxygen levels greater than about $0.002^W/o$. This critical oxygen level, associated with a critical pressure, requires further examination.
2. It is evident from the works of Ward and Turkdogan that the conditions where chemical control takes over from diffusion control as the rate-determining step in silica dissociation are not fully known.
3. More work is required on the effect of oxide decomposition on the removal of oxygen by the various degassing processes. With some techniques the metal is not in contact with slag during the vacuum treatment and it would be expected that this would aid the removal of oxygen from the melt. Equally important, however, are the kinetics of the C-O reaction during degassing of these different techniques and there is plenty of scope here for further studies.
4. The present work has shown the iron oxide content of the slag to be a large source of oxygen capable of being transferred to the metal. Techniques for slag deoxidation without metal deoxidation should, therefore,

be sought, i.e. use of aluminium pellets, powdered FeSi or carbon. Deoxidation of the metal should be avoided since this will tend to maintain a high driving force for oxygen diffusion.

5. It has not been possible to investigate the contribution of oxygen from the silica of the ladle lining at very low oxygen levels. This should be examined and the possible use of suitable ladle washes borne in mind.

6. Much work requires to be done on the effective use of deoxidants as a means to obtaining clean steel. Here the degassing vessel could be a very useful tool in controlling the sequence and amounts of the additions and in providing the turbulence necessary to aid the removal of the insoluble products.

I particularly wish to thank Mr. P. Letcher for his painstaking assistance on laboratory melts and data collection and Mr. D. Damms for the help he has given with the construction of apparatus and calculations.

I am also indebted to Messrs. J.C.C. Leach and T.J.J. Smith for the useful discussions we have had.

Finally my thanks are also due to English Steel Corporation Ltd., in particular to Dr. A.H. Sully, for continued financial support and to those departments of E.S.C., who provided the many services needed for the completion of this work.

REFERENCES.

1. Winkler, O. "Theory and practice of vacuum melting". Met Review 1960, V5, No.17.
2. Chipman, J. and J.F. Elliott. "Electric furnace steelmaking". V2, 95-175, 1963, Interscience.
3. Bradshaw, A.V. and F.D. Richardson. "Vacuum degassing of steel". I.S.I. Sp.Rep.92. P24-44.
4. Wriedt, H.A. and J. Chipman. Trans AIMME, 1956, 206, 1195.
5. Wriedt, H.A. and J. Chipman. Trans AIMME, 1955, 203, 477.
6. Moore, J.H. Metal Progress 1953, 64, (3), 103.
7. Bodsworth, C. "Phys.Chem. of iron and steel manufacture". 1963 - Longmans.
8. Elliott, J.F. "Phys.Chem. of steelmaking" New York, John Wiley, 1958, P.37.
9. Chipman, J. J.I.S.I., 1955, v180, P.97.
10. Fuwa, T. and J. Chipman. Trans AIMME 1960, v218, p887.
11. Schenck, H. and G.H. Gerdorf. Arch.Eisenhütten. 1959, v79, p451.
12. Gokcen, N.A. Trans AIMME 1956, v206, p1558.
13. Richardson, F.D. and W.E. Dennis. Trans Far.Soc. 1953, v49, p171.
14. Rist, A. and J. Chipman. "Physical chemistry of steelmaking" John Wiley & Sons Inc. New York. 1958, p3.
15. Turkdogan, E.T., L.S. Davis,, L.E. Leake and G.C. Stevens, J.I.S.I. 1955, vol 181, p123.
16. Field, A.L. Trans AIME (ISD) 1928, p114. Cargegie Inst.Tech.Coop.
17. Herty, G.H. Jnr, C.F. Christopher, H. Freeman and J.F. Sanderson. Bull. No.68, 1934.

- E.H. Hamilton.
19. Marshall, S. and J. Chipman. Trans. Am.Soc.Metals. 1942, v30, p695.
 20. Jackson, F.L. and W. M. Hyams. Pittsburgh Regional Tech.Meeting Oct. 1963, A.I.S.I.
 21. Electric furnace steelmaking AIME Vol.II.(1963), p128.
 22. Ohtani, M. and N. A. Gokcen. Trans AIME, v128 (1960) p533.
 23. B.O.H. Steelmaking, S. W.Mudd series, AIME 1964, 3rd Ed. P650.
 24. Chipman, J. and K.L.Fettars. Trans.Am.Soc.Metals. 1941, v29, p953.
 25. Taylor, C.R. and J. Chipman. Trans AIME, 1943, v154, p228.
 26. Floridis T.P. and J. Chipman. Trans Met.Soc. AIME 1958, v212, p.549.
 27. Dastur, N. and J. Chipman. Trans AIMME 1949, v185, p313.
 28. Bennett, G.H.J., H.T.Protheroe, and R.G. Ward. J.I.S.I. 1960, v195, p174.
 29. Chipman, J. J.I.S.I. 1955, v180, p97.
 30. Matoba, S. and S. Ban-ya. Tech.reps. Tohoku Univ. 1955, v20, p131: Tetsu-to-Hagane 1958. v44, p643.
 31. Sims, C.E. Trans AIMME, 1947, v172, p176.
 32. Chipman, J. Metal progress 1949, v56, p211.
 33. Richardson, F.D. Disc. Far. Soc. 1948, No.4. p114.
 34. Gokcen, N.A. and J. Chipman. Trans AIMME 1953, v197, p173.
 35. Sawamura, H. Suiyokwai Shi, 1956, v13, p142.
 36. Wentrup, H. and J. Hieber. Tech.Mitt.Krupp. 1939, v1, p47.
 37. Geller, W. and K. Dicke. Arch. Eisenh. 1943, v16, p431.

- W. Crafts.
39. Yagihashi, T. and Z. Shibata. Sci.Reps.Res.Inst.Tohoku Univ. Series A, 1954, v191, p111.
 40. Meadowcroft, T.R. and J.F.Elliott. Trans vac.Met.Conf. 1963, ed. Bunshah.
 41. Ramstad, H.F. and F.D.Richardson. Trans AIMME. 1961, vol.221.p1021.
 42. Chipman, J, J.C.Fulton, N.A.Gokcen and G.R.Caskey. Acta. Met. 1954, v2., p439.
 43. Chipman, J. and N.A.Gokcen. Trans AIMME 1952, v194, p131, 1953, v197, p1017.
 44. Chipman, J. and T.C.M.Pillay. Trans AIMME 1961, v221, p1277.
 45. Fischer, W.A. and H.Engelbrecht. Stahl und Eisen, Dusseldorf, 1955, v75, p70.
 46. Richardson, F.D. and J.H.E.Jeffes. J.I.S.I. 1950, 166, 213-234
 47. Schneider, A. and E. Hesse. Zeitschrifte für Elektrochemie, 1940, vol 46, p279.
 48. Bell, H.B. J. West of Scot. I.S.I. v71, 1963-64, No.6.
 49. Glasstone, S. K.J.Laidler and H. Eyring. "Theory of rate processes". McGraw Hill, New York 1941.
 50. Eyring H. J.Chem.Phys 3. 107, (1934)
 51. Darken, L.S. and R.W.Gurry. "Physical Chemistry of Metals" McGraw Hill, London 1953.
 52. Niwa, K, M. Shimoji, T.Kishida and Y. Itoh. Tetsu-to-Hagane, Sept.1961. Vol.1. 18-22.
 53. Fornander, S. Discussions Far.Soc.No.4.296(1948)
 54. Darken, L.S. "Physical Chemistry of steelmaking" ed.J.F.Elliott. p101, 1958.

55. King, T.B. "Vacuum metallurgy" ed. Bunshah. p35, London (Chapman and Hall).
56. Darken, L.S. "B.O.H. Steelmaking" S.W. Mudd Series AIME 1964, 3rd Ed. Chap 15. p586.
57. Einstein, A. Ann. Phys. 17 (4), 549 (1905)
58. Hartley G.S. Trans. Far. Soc. 27, 10 (1931)
59. Harned and Nuttall. J. Am. Chem. Soc. 69, 736, (1947)
60. Kraus, T. Trans Vac. Met. Conf. 1963, Bunshah ed.
61. Riddiford, A.C. J. Phys. Chem. 56, 1952, 746.
62. Sharma, S.K. and R.G. Ward. J.I.S.I., 205, 1967, 196.
63. Danckwerts, P.V. Ind. Eng. Chem. 43, 1951, 1460.
64. Machlin, E.S. Trans. Met. Soc AIME. 1960, 218, 314-326.
65. Kinsman, G.J.M. B.I.S.R.A. report C/75/67.
66. Morgan, D.W. and J.A. Kitchener. Trans. Far. Soc. 1954, 50, 51-60.
67. Dahlke, O. and O. Knacke. Archiv. Eisenh. 1955, 26, 373-378.
68. Barfield, R.N. and J.A. Kitchener. J.I.S.I. 1955, 180, 324-329.
69. "Korber, F. and W. Qölsen. Mitt. Kaiser-Wilhelm-Inst. Eisenforsch. Dusseldorf, 17, 39, (1935)
70. Becker, "R. and W. Doring. Ann. Physik. 24, 732 (1935)
71. Garmer, W.E. "Chemistry of the solid state" Butterworths 1955, Ch.6.
72. Von Bogdandy, L. Chipman Conference M.I.T. press. June 1962, p156.
73. Von Bogdandy, L. Archiv. Eisenhüttenwesen 32, No.5. May 1961. 275.
74. Von Bogdandy, L. W. Dick and I.N. Stranski. Arch. Eisenh. 29, 329, (1958)

75. von Boguandy, L. "Z. Elektrochem. 63, 150 (1959)
R. Schmolke, and
I.N. Stranski.
76. Brower, T.E. and "Proc. Nat. Open Hearth Comm."
B.M. Larsen. AIME 29, 162 (1946)
77. Internal report of English Steel Corp. Ltd. Sheffield.
78. "Improvements in the vacuum degassing of metal melts"
Patent No. 1,037,369. July 27. 1966.
79. Richardson, F.D. "The climate of extractive
metallurgy in the 1960's". 1964
Howe memorial lecture. Iron &
Steel Div.
80. Haberman, W.L. and "The David Taylor Model Basin".
R.K. Morton. Rep. No. 802, NS. 715-102. 1953.
81. Davies, P.M. and Proc. R. Soc. 1950, A. 200, 375.
G. Taylor.
82. Bradshaw, A.V. and "Symposium on Chemical Engineering
F.D. Richardson. in the Iron & Steel Industry".
Swansea, March 1968.
83. Baird, M.H.I. and Chem. Eng. Sci. 1962, v17, p87.
J.F. Davidson.
84. Larsen, B.M. AIME New York, No. 1. 1956.
85. Parlee, N.A., Trans. Met. Soc. AIME, 212, 1958, 132.
S.R. Seagle and
R. Schuhmann Jnr.
86. Kraus, T. "The results from high vacuum
technology and the physics of
thin layers". Published by
M. Auwärter. 1957, Stuttgart;
p184-194.
87. Schvartsman, L.A., J. Phys. Chem. (U.S.S.R.) 21, 1027,
A.M. Samarin, and (1947)
M.I. Temkin.
88. Tiberg, L. Jernkont Ann. 144, 1960, 757.

89. Larsen, B.M. "B.O.H.Steelmaking". AIME, New York, 1951, 867.
90. Sokolov et al. Izvestija VUZ, Chem.Met. (1959)
91. Harders, F. et al. Stahl u. Eisen, 76, 1721-1728(1956)
92. Harders, F. et al. Stahl u. Eisen. 79, 267-272 (1959)
93. Knüppel, H. and " F. Oeters. Archiv.Eisenhüttenw 1962, 33 (11) 729-743.
94. Turkdogan, E.T., P.Grievesson and J.F.Beisler. Trans.Met.Soc.AIME. vol.227. Dec.1963, p1258-1274.
95. Saito, T, Y. Kawai, K. Maruya and M. Makai. Physical Chemistry of Process Metallurgy, Part I, pp 523-33, Met.Soc.Conf.vol 7. Inter Science public New York 1961.
96. Grimble, M, R.G.Ward and D.G.Williams. J.I.S.I. March 1965, p264-267.
97. Sharma, S.K. and R.G.Ward. J.I.S.I. Feb.1967. p196-202.
98. Ward, R.G. "Physical Chemistry of iron and steelmaking", 173, 1962, London, Arnold.
99. Graham, S.W. and B.B.Argent. J.I.S.I. Oct.1967. p1066-1068.
100. Fischer, W. and A.Hoffmann. Arch.Eisenhütten June 1958, p339.
101. Birks, N. and D. Booth. J.I.S.I. April 1966, p340-343.
102. Fast, J.D. Stahl u Eisen. 1953, 73, 1484-1496.
103. " Kothemann, H. Treppschuh and W.A.Fischer. Arch.Eisenhütten 1956, 27, 563-566.
104. Fischer, W.A, H.Treppschuh and K.H.Kothemann. Arch. Eisenhütt. 1956, 27, 567-572.
105. Weber, F, W.A.Fischer and H. Engelbrecht. Stahl u Eisen. 1954, 74, 1515-1521.

106. Moore, J.H. Met.Progress. 64, 1955, 105.
107. Brotzmann, C. Arch Eisenhütten. 1960, 31,
(2) 67-81.
108. Bennett, G.H.J.,
H.T.Protheroe and
R.G.Ward. J.I.S.I., 195, 1960, 174.
109. Fujii, T. and
T. Araki. Tetsu-to-Hagane, Overseas Vol.5.
No.4. Dec.1965. p290.
110. Mund, A. J.I.S.I. 1962, 200, 804-819.
111. Edstrom, J.O. Jernkont. Ann. 1962, 146, 549-679.
112. Flux, J.H. "Vacuum degassing of Steel".
I.S.I. Special report No.92.
p.1. 1965.
113. Eketorp, S. Jernkont. Ann. 1966, 150, (9)
p585-685.
114. Sickbert, A. "Vacuum degassing of Steel". I.S.I.
Sp.Report 92, 1965, p95.
115. Leach, J.C.C. and
E.H.Watson. ibid p80.
116. Leach, J.C.C. and
W.Sorby. "Steelmaking in the basic arc
furnace". I.S.I.Special Report
87. 1964.
117. MacLean, I.K. and
J.M.Lupton. "Vac.deg.of steel". I.S.I. Sp.
Report 92, 1965, p176.
118. McMillan, A.G.
J.Wylie and
P.W.Clark. ibid p63.
119. Lindskog, L. Contribution to discussion of a
paper on "the possibilities of
vacuum treatment" by Sven Eketorp
Jernkont.Ann. 1966,150,(9),
585-685.
120. Hoyle, G. and
M.A.Ramsbottom. "Vacuum degassing of steel".I.S.I.
Sp.Report 92, 1965, p135.

- A. Dammer, and
H.H.Reichel.
122. Hirase, M. ibid. p154.
123. Leach, J.C.C. and ibid. p170.
 W.Sorby.
124. Perry, T.E. ibid. p105.
125. Knaggs, K. and ibid. p170.
 P.H.Broxham.
126. Kato, T,
 K.Matsuda and
 M.Harada. ibid. p164.
127. " Plockinger, E. "Clean Steel". I.S.I. Sp.Rep. 77
 1962, p51-56.
128. Torsell, K. Jernkont. Ann. 151 (1967) (12)
 p890-949.
129. Forster, K. 2nd International D.H.Conference,
 Puerto Rio, 1964.
130. Brotzmann, K. "Vac.degassing of Steel".I.S.I.
 Sp.Rep.92, 1965, p148-153.
131. Sickbert, A. ibid. p95.
132. Samarin, A.M. "Vacuum metallurgy". ed.
 Sunshah. 1957. p255.
133. Elliot, J.F. and "Thermochemistry for steelmaking"
 M.Gleiser. Pergammon press 1960.
134. "Phase diagrams for Ceramists Fig.314, p123.
135. " Knuppel, H, An extract from the Dr.Ing.
 F.Oeters and dissertation of Vardag. Read at
 S.G.K.Vardag the Session of committee for
 Metallurgical Foundations at
 the V.D.E h on July 15th 1964.
136. Harders, F. J.I.S.I. Nov.1958, p306-311.
137. Finlay, W. G.M. of A.I.S.I. May 1961,
 (New York).Blast furnace and
 steelplant Sept.1961.

April 1967.

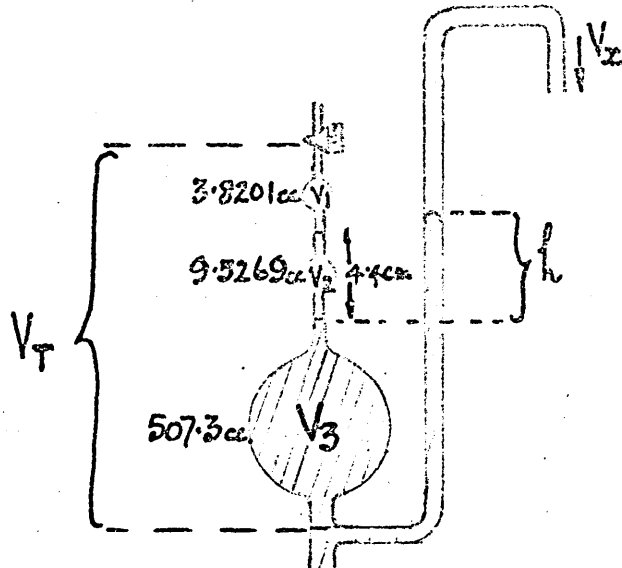
139. International D.H. conferences Nos. 1-4. proceedings private.

140. Aldrich, G. Internal paper presented at the 4th International D.H. conference Switzerland 1968.

APPENDIX I. Calibration of pressure transducer by the use of a Toepler gauge.

The Toepler gauge itself required investigation before the transducer could be calibrated.

1. Calibration of volumes of Toepler gauge.



Volume V_1 and V_2 were determined by the weight of mercury required to fill them. The largest volume V_3 was measured by weighing the amount of water required to fill it. Each weighing was repeated until consistent results were obtained. The volumes determined are shown in the above sketch.

2. To calculate pressure in system (P_0)

With reference to the above diagram.

For Volume V_1

$$V_1 P_0 = V_1 (h_1 + P_0)$$

Hence $P_0 (V_T - V_1) = h_1 V_1$

and $P_0 = \frac{h_1 V_1}{V_T - V_1} = \frac{h_1 V_1}{V_2 + V_3}$

Therefore the conversion factor for height (h_1) to pressure

$$(P_0) = \int P_1 = \frac{V_1}{V_2 + V_3} = \frac{3.8201}{9.5269 + 507.3} = 0.007391$$

If h_1 is measured in cms. then $f_{P_1} = 0.0739$ to give P_0 in torr.

For Volumes ($V_1 + V_2$)

$$V_T P_0 = (V_1 + V_2)(h_{12} + P_0)$$

Hence $P_0(V_T - V_1 - V_2) = h_{12}(V_1 + V_2)$

and $P_0 = \frac{h_{12}(V_1 + V_2)}{V_3}$

So $f_{P_{12}} = \frac{(V_1 + V_2)}{V_3} = \frac{3.8201 + 9.5269}{507.3} = 0.02631$

If h_{12} is measured in cms. then $f_{P_{12}} = 0.263$ to give P_0 in torr.

3. Calibration of backing volume V_x

The procedure for this was as follows:-

- (i) h_1 and h_{12} were measured in the two appropriate volumes.
- (ii) The gas collected in the measuring volume was pumped out through the top tap.
- (iii) The mercury was allowed to fall and the gas in the rest of the backing system was allowed to fill all the backing volume.
- (iv) h_1 and h_{12} were again measured in the same two volumes.

Now $P_0 = f_{P_1} h_1 = f_{P_{12}} h_{12}$

where f_{P_1} and $f_{P_{12}}$ are the pressure factors appropriate for each volume, calculated from the volume calibration of the McLeod gauge (section 2).

Therefore, referring to the above procedure, in the first

measurement $P_a = f_{P_1} h_{1a} = f_{P_{12}} h_{12a}$

and after rejecting this gas from the McLeod gauge

$$P_b = f_{P_1} h_{1b} = f_{P_{12}} h_{12b}$$

all the system at pressure P_b and therefore

$$\begin{aligned} V_x P_a &= P_b (V_T + V_x) \\ V_x (P_a - P_b) &= V_T P_b \\ \therefore V_x &= \frac{V_T P_b}{(P_a - P_b)} \end{aligned}$$

Hence $V = \left(\frac{f_1^{h_{1b}}}{f_1^{h_{1a}} - f_1^{h_{1b}}} \right) V_T$

or in general terms $V_x = V_T \left(\frac{h_b}{h_a - h_b} \right)$

N.B. It is better to use pressures since the correspondence of pressure measured in two different volume is a good test that condensibles are absent and that the zero mark for each bulb is correct.

The results obtained by this procedure are shown in Table 38 h_{1a} is corrected for the difference in heights of the zero marks V_1 and V_2 i.e. - 4.4 cm.

Taking the average for the values obtained on the small bulb (V_1) the backing volume was found to be

$$V_x = 87.9 \text{ mls.}$$

4. Volume factors.

Total volume of system $V = V_T + V_x = 608.5$ mls.

To determine the volume of gas collected in the various bulbs, converted to N.T.P.

for volume V_1 , $f_{V_1} = f_{P_1} \times \frac{V}{760} = .0739 \times \frac{608.5}{760} = .0592$

$$f_{V_1} = .0592$$

for volumes $V_1 + V_2$, $f_{V_{12}} = f_{P_{12}} \times \frac{V}{760} = .263 \times \frac{608.5}{760} = 0.2106$

$$f_{V_1} = 0.2106$$

These factors are to convert h , measured in cms, to the volume of gas in mls.

A small amount of gas was taken from the furnace by opening valves V_1 and V_2 and pumped, by the diffusion pump (D_1) through V_3 and V_4 into the Toepler gauge. (N.B. D_2 was not operative). When all the gas had been pumped to the high pressure side the millivoltage output from the transducer was measured by the mV recorder and the pressure in the system was measured by running the mercury into the now accurately calibrated Toepler gauge. The results obtained are shown in Table 39.

The graph of mV/torr from these results is shown in Figure from which it can be seen that the relationship is linear up to 4.5 torr or 8 mV. This range is quite sufficient for accurate gas analysis and well within the safe working limits for the backing pressure of the diffusion pump D_1 . Because of this linear relationship the need for reference to a calibration curve was unnecessary and the millivoltage output has been used directly for the calculation of gas composition by volume.

TABLE 1. Comparison of data for the solubility of oxygen in liquid iron.

Temp. °C		1550	1600	1650	1700
Equation 11. (24, 25)	[wt.%O]	0.185	0.229	0.281	0.340
Equation 12 (12)	[^w /o O]	0.190	0.230	0.277	0.330

TABLE 2. Experimentally determined values of the mass transfer coefficient for the carbon-oxygen reaction.

Mass transfer coefficient β (cm/sec)	Investigator.
0.02	Larsen, B.M. (84)
0.04	Bogdandy, L.V. (73)
0.03	Tiberg, L. (88)
0.0015 - 0.0126	Parlee, N.A. et al (85)
0.03	King, T.B. (55)
0.014 - 0.047	Knuppel, H and F. Oeters (93)
0.038	Kraus, T. (86)
0.040	Richardson, F.D. (79)

TABLE 3. Mass transfer coefficients on foaming melts in vacuo

β_{c-o} cm/sec	Investigator.
0.1 - 0.3	Kraus (86) calculation from equation (91)
0.1 - 0.2	Sokolov et al (90) (ladle)
0.2 - 0.4	Harders et al (91) (D.H.)
0.1 - 0.2	Harders et al (92) (crucible)

values of apparent activation energy (97)

	$(Q \pm \sigma)$ k cal/g.mole.
Theoretical value (97)	77 - 84
Saturated, graphite on surface.	74.8 \pm 3.1
Saturated, graphite submerged.	74.3 \pm 2.8
Unsaturated with carbon.	85.1 \pm 5.1

TABLE 5. Dissociation of alumina in contact with
Fe - C melts.

	Machlin model(64)	Experimental results of Fischer et al (100)
%O _b	4.4-6.4x10 ⁻⁴	1 x 10 ⁻³
%Al _b	1.1-1.9x10 ⁻²	3 x 10 ⁻³
%O _{C/M}	6.3-9.3x10 ⁻⁴	-
%Al _{C/M}	1.1-2.0x10 ⁻²	-
$\frac{d\%Al}{dt}$ (%/hr)	1.1-2.0x10 ⁻²	2 x 10 ⁻²

TABLE 6. Rates of Oxygen Transfer from Various Oxides.

Oxide	Author.	Conditions.	Charge wt. (gms)	%C + comments.	Temp. °C.	Rate of Oxygen Transfer \dot{n}_O /sq.cm/sec.
MgO	Fujii and Araki (109)	Surface decarburisation by argon-oxygen mixtures @ 1 atmos. Rate independent of carbon from .2-.8%	1400	.2-.8	1600	3.1×10^{-7}
MgO	Brotzmann (107)	Range of carbon contents pressures and temperatures.	25000	1.0%C 1 torr	1600	$3.1 \times 10^{-7} \uparrow$
			"	1.0%C 20 torr	1600	$1.5 \times 10^{-7} \uparrow$
			"	0.1%C 20 torr	1600	$0.67 \times 10^{-7} \uparrow$
MgO	Kraus (86)	Low carbon under vacuum.	27	-	1600	$4.4 \times 10^{-9} \#$
Al ₂ O ₃	Parlee et al (85)	Range of carbon contents; pressures near to 1 atmos.	153	0.44	1630	0.15×10^{-8}
			99	4.4	1630	1.3×10^{-8}
Al ₂ O ₃	Fischer & Hoffmann. (100)	High carbon under vacuum.	3500	-	-	3.8×10^{-8}
SiO ₂	Sharma & Ward (97)	3.5-4.5%C @ 1 atmos.	10	~4.0	1600	1.6×10^{-7}
			35	"	1600	1.5×10^{-7}
			60	"	1600	1.4×10^{-7}
SiO ₂	Graham & Argent. (99)	0.2%C under vacuum - alumino silicates.	12000	.2%C 95%Al ₂ O ₃	1600	$1.3 \times 10^{-7} \uparrow$
			"	.2%C 42%Al ₂ O ₃	1600	$6.6 \times 10^{-7} \uparrow$
SiO ₂	Turgdogan et al (94)	C saturated iron + silicate slag. CO gas @ interface.	6	^a SiO ₂ = 0.83	1600	10×10^{-7}
			"	^a SiO ₂ = 6.11.		5.28×10^{-7}
			"	^a SiO ₂ = 0.07	1600	4.12×10^{-7}

h calculated from charge weight and crucible diameter.

† assumed that h = 2D calculated from charge weight.

TABLE 7. Hydrogen removal by degassing.

Process.	Initial Hydrogen Content (ml/100g)	Hydrogen content after degassing. (ml/100g)		%Hydrogen removed.	Symbol.	Comments.
		Stream	Head.			
Tap Degassing (114)	4.1	1.1	1.5	73	⊙	fully killed. Bochumer 50T unit.
	2.3	0.65	1.0	72	⊙	" " Individual BEA heats.
	4.0	1.0	2.0	73	○	semi killed. (% removed calcd. on samples from streams)
	2.9	0.65	1.1	75	○	" " samples from streams)
	3.6	0.65	1.0	82	○	open
	1.9	0.50	0.60	74	○	
Vacuum casting (115)		Core	Head.			Unit @ E.S.C. % removed calcd. on samples from core of forging.
	4.0	0.74	1.6	82	×	AOH (mean of 33 casts) (60% on head)
	5.7	0.84	2.0	85	+	BEA (mean of 30 casts) (65% on head)
(116) D.H.	9.0	2.80		69	⊙	30T DH unit @ E.S.C. samples taken from ladle after degassing (Values derived from regression equation $F=0.25 H-0.04n-0.3X + 2.7$ where F=final [H] H = original [H] n = no. of cycles (25) X = recirculation factor (3.5)
	6.0	2.15		64	⊙	
	3.0	1.4		53	⊙	
D.H. (117)	10.0	4.0		60	□	100T DH unit @ Lancashire steel. (Values taken from best line drawn through points. B.O.H. furnaces)
	6.0	2.8		54	□	
	3.0	1.9		37	□	
R.H. (121)	6.0	1.9		68	△	Ruhrstahl - 30-100T BEA furnaces. Argon gas injection as part of process. (Values taken from best line drawn through points).
	4.0	1.8		55	△	
	3.0	1.5		50	△	
	2.0	1.1		45	△	

Static Ladle (118)	4.5	1.9	53	◆	70-80T heats. Beardmore. gas agitated. (Values taken from best line drawn through points) 70-80T heats. Not agitated. 20T heats. Not agitated.
	5.5	2.0	63	◆	
	4.5	2.9	35	■	
	5.5	3.1	44	■	
	4.5	2.0	56	♀	
	5.5	2.5	55	♀	
Static Ladle (119)	3.55	2.55	28	▲	100T. Domnarvet. agited with argon. Mean values from 190 heats.
Contin- uous vacuum degass- ing BISPA. (120)	9.0	4.8	47	▼	Operated @ Low Moor alloy steelworks. (Values taken from best line drawn through points) (30 heats)
	6.0	2.3	62	▼	

TABLE 8. Effect of ladle degassing on the oxygen and nitrogen contents of low alloy steels.

Steel type.	Treatment.	Oxygen content (ppm)	Nitrogen content (ppm)
0.20C, .3Si, .8Mn, .5Cr.	Double slag practice.	25-40	60-110
	Vacuum degassed.	15-30	30-60
1.0C, .5Si, .4Mn, 1.0Cr.	Double slag practice.	18-28	60-110
	Vacuum degassed.	8-16	30-70

TABLE 9. Analysis of iron base.

SUPPLIER.	C	Si	Mn	S	P	Ni	Cr	Mo	H(ml/100g)	O(w%)
B.I.S.R.A.	.025	.0076	.0079	.002	.002	.008	Nil	Nil	0.68	0.11
G.SENIOR LTD.	.018	.010	.045	.009	.001	.001	.01	.01	0.50	0.03

TABLE 10 Composition of crucibles.

Manufacturers Code Name.	SiO ₂	Al ₂ O ₃	MgO	Fe ₂ O ₃	CaO	TiO ₂	Loss	Hygroscopic water.
Silica	91.57	4.01	2.57	0.085	N.D.	0.03	N.D.	N.D.
M	55.80	41.45	0.22	1.14	0.10	0.13	0.05	0.05
P	36.80	61.20	0.07	0.57	0.10	1.20	0.10	0.05
HS	6.80	92.5	N.D.	0.29	N.D.	N.D.	N.D.	N.D.
MAG	8.00	0.33	89.80	0.29	N.D.	N.D.	0.05	0.10

N.D. = Not Determined

TABLE 11. Preparation and phases present in crucibles.

CRUCIBLE	PREPARATION.	FIRING TEMP. °C	PHASES PRESENT.
M	From molochite powder, precalcined at 1800°C.	1320	Mullite grains, silica glass + trace β quartz.
P	From silli- minite powder, precalcined at 1800°C.	1360	Mullite grains, small amount of silica glass + trace β quartz.
HS	From alumina, fused and reground.	1360	Corundum + very faint trace α quartz.
MAG	From periclase, fused at 3000°C, cast and re-ground.	1500	Periclase + faint trace of forsterite.

TABLE 12. Physical properties of crucibles.

Crucible	App. Porosity %	Bulk density (gm/cc)	Permeability(cc/ef	
			Circumfer- ential air flow.	Transverse air flow.
M	30.14	1.85	0.054	0.037
P	24.09	2.28	0.015	0.017
HS	29.86	2.68	0.116	0.079
MAG	29.83	2.45	0.054	0.036

TABLE 13.

The next 30 pages give details of the experimental method used and analytical results obtained on the 5lb laboratory heats.

Metal Samples Analysis % by weight					Gas Samples Analysis				
Δt	C	Si	O	Δ V.T. litres	Δt	CO ₂	H ₂ O	H ₂	CO
0	0.140	0.005	0.0126	-	15	7.25	0	5.79	86.96
40	0.134	0.005	0.0152	0.535	55	2.67	0	9.35	88.00
70	0.127	"	0.0099	0.405	85	0	0	16.00	84.00
100	0.123	"	-	0.400	115	0	0	19.35	80.65
130	0.115	"	0.0148	0.405	145	0	0	20.25	79.75
167	0.117	"	0.0336	0.430	175	0	0	6.12	91.40

Melt 19

Pressure 760 mm

Crucible 8% SiO₂
90% MgO

Metal Samples Analysis % by weight					Gas Samples Analysis				
Δt	C	Si	O	Δ V.T. litres	Δt	CO ₂	H ₂ O	H ₂	CO
0	0.111	0.010	0.0024	-	10	1.09	0	19.78	73.6
13	0.095	0.025	0.0032	.700	20	1.34	0	26.7	62.4
28	0.086	0.030	0.0025	.633	35	0	0	25.38	64.1
43	0.074	0.035	0.0025	.597	60	0	0	28.75	68.1
58	-	-	0.0024	.495	68	0	0	27.40	65.75
73	0.056	0.050	0.0037	.495	83	0	0	28.36	70.15
88	0.049	0.049	0.0040	.430	98	0	0	35.71	57.10
103	0.040	0.040	0.0037	.425	113	0	0	36.25	55.90

Melt 18

Pressure 76 mm

Crucible

8% SiO₂
90% MgO

Metal Samples Analysis % by weight					Gas Samples Analysis				
Δt	C	Si	O	Δ V.T. litres	Δt	CO ₂	H ₂ O	H ₂	CO
0	0.080	0.012	-	-	10	0	0	0	100
30	0.065	0.055	0.0013	1.205	40	0	0	15.3	84.7
60	0.040	0.075	0.0015	0.805	70	0	0	34.1	65.9
90	0.040	0.080	0.0022	0.480	100	0	0	26.4	73.6
120	0.035	0.089	0.0038	0.305	135	0	0	49.8	50.2
150	0.030	0.084	0.0022	0.210	170	0	0	49.9	50.1
180	0.030	0.105	0.0025	0.130	205	0	0	79.0	21.0
210	0.020	0.084	0.0030	0.105	235	0	0	81.5	18.5
240	0.035	0.077	0.0032	0.095					
270	0.040	0.070	-	0.060					

Melt 76

Pressure 3 mm

Crucible

8% SiO₂
90% MgO

Melt 82				Pressure 760 mm		Crucible 8% SiO ₂ 90% MgO			
Metal Samples Analysis % by weight					Gas Samples Analysis				
Δt	C	Si	O	Δ V.T. litres	Δt	CO ₂	H ₂ O	H ₂	CO
0	-	-	-	-	31	nil	nil	7.32	92.68
30	0.91	0.040	-	0.800	76	"	"	11.67	88.33
60	1.03	0.025	0.0024	0.540	161	"	"	20.33	79.67
90	1.015	0.020	0.0012 0.0025	0.440	191	"	"	27.84	72.16
120	0.965	0.045	0.0018 0.0024	0.380	221	"	"	28.44	71.56
150	0.985	0.055	0.0020 0.0023	0.380	241	"	"	31.08	68.92
180	0.980	0.040	0.0020	"					
210	0.970	0.050	0.0019	"					
240	0.945	0.055	-	"					
270	0.940	0.025	-	"					

Melt 37									
Pressure 76 mm					Crucible 8% SiO ₂ 90% MgO				
Metal Samples Analysis % by weight					Gas Samples Analysis				
Δt	C	Si	O	Δ V.T. litres	Δt	CO ₂	H ₂ O	H ₂	CO
0	0.780	0.075	-	-	-	0	0	4.32	93.73
42	0.716	0.125	0.0073	2.855	25	0	0	0	94.64
71	0.668	0.150	0.0052	1.457	55	0	0	3.39	96.61
108	0.514	0.175	0.0054	2.508	85	0	0	3.00	99.17
140	-	-	-	2.030	125	0	0	4.96	95.04
170	0.456	0.195	0.0057	0.600	150	0	0	7.20	91.20
200	0.456	0.21	0.0021	0.655	185	0	0	7.21	92.73
233	0.420	0.21	0.0018	1.100	210	0	0	7.38	91.80
266	0.448	0.22	0.0008	0.543	245	0	0	-	-
293	0.448	0.22	0.0016	0.382					

Metal Samples Analysis % by weight				Gas Samples Analysis					
Δt	C	Si	O	Δ V.T. litres	Δt	CO ₂	H ₂ O	H ₂	CO
0				-	0	0	0	0	100
30				2.580	20	0	0	0	100
60				1.770	50	0	0	0	100
90				1.480	70	0	0	0	100
120				1.300	90	0	0	0	100
150				1.120	160	0	0	0	100
180				1.210	180	0	0	0	100
210				1.070	200	0	0	0	100
240				1.060	210	0	0	0	100
270				1.110	260	0	0	0	100

Melt 90

Pressure 3 mm

Crucible

8% SiO₂

90% MgO

Melt 66				Pressure 76 mm.		Crucible			
						7% SiO ₂ 93% Al ₂ O ₃			
Metal Samples Analysis % by weight					Gas Samples Analysis				
Δt	C	Si	O	Δ V.T. litres	Δt	CO ₂	H ₂ O	H ₂	CO
0	0.13	0.03	0.00607 0.00657	-	25	1.38	1.58	9.47	87.30
30	0.10	0.055	0.00238 0.00260	1.536	225	0	0	35.18	64.70
60	0.075	0.070	0.00306	0.804	263	0	0	41.56	58.40
90	0.070	0.080	0.00316	0.582	285	0	0	44.85	55.00
120	0.060	0.090	0.00322	0.483					
150	0.050	0.095	0.00478	0.415					
180	0.050	0.100	0.00432	0.380					
210	0.050	0.095	0.00358	0.260					
240	0.050	0.095	-	0.186					
270	0.050	0.100	0.00336 0.00367	0.162					
300	0.050	0.095	0.00444						

Melt 71

Pressure 3 mm

Crucible $7\% \text{SiO}_2$
 $93\% \text{Al}_2\text{O}_3$

Metal Samples Analysis % by weight					Gas Samples Analysis				
Δt	C	Si	O	Δ V.T. litres	Δt	CO_2	H_2O	H_2	CO
0	0.095	0.035	0.0048	-	23	-	-	-	-
30	0.062	0.050	0.0017	1.280	108	0	0	24.84	75.16
60	0.052	0.070	-	0.630	153	0	0	24.96	75.04
90	0.053	0.060	0.0004	0.430	193	0	0	36.52	63.48
120	0.040	0.070	0.0006	0.250	213	0	0	40.81	59.19
150	0.035	0.075	0.0009	0.185					
180	0.032	0.080	0.0008	0.135					
210	0.030	0.080	0.0007	0.075					
240	0.030	0.085	0.0010	0.063					
270	0.030	0.080	-	0.050					

Metal Samples Analysis % by weight					Gas Samples Analysis				
Δt	C	Si	O	Δ V.T. litres	Δt	CO ₂	H ₂ O	H ₂	CO
0	-	-	0.012	-	10	nil	nil	8.91	91.09
30	0.96	0.065	-	1.605	40	"	"	11.19	88.81
60	0.92	0.11	-	1.165	75	"	"	20.46	79.54
90	0.89	0.125	0.014	0.870	155	"	"	25.62	74.38
120	0.90	0.13	-	0.750					
150	-	-	-	0.610					
180	0.84	0.14	-	0.410					
210	0.84	0.15	-	0.510					
240	0.825	0.16	-	0.610					
270	-	-	0.0043	0.540					

Melt 84

Pressure 76 mm

Crucible 7% SiO₂
93% Al₂O₃

Melt 57

Pressure 760

37% SiO₂
Crucible 61% Al₂O₃

Metal Samples Analysis % by weight				Gas Samples Analysis					
Δt	C	Si	O	Δ V.T. litres	Δt	CO ₂	H ₂ O	H ₂	CO
0	0.115	0.020	0.0282	-	3	2.79	0.56	5.03	91.60
30	0.105	0.025	0.0205	0.045	24	2.44	0.61	6.10	90.80
60	0.103	0.025	0.0195	0.126	58	2.17	0.54	8.15	89.20
90	0.105	0.025	0.0227	0.086	88	1.64	0.55	9.29	88.50
120	0.105	0.020	0.0216	0.022	128	0.70	0	10.42	88.80
150	0.104	0.025	0.0230	0.038	179	1.94	0	12.90	85.00
180	0.105	0.030	0.0248	0.036	210	1.2	0.64	14.19	83.88
210	0.105	0.030	0.0225	0.058	243	-	-	-	-
240	0.104	0.040	0.0267	0.044	274	2.35	0	15.88	81.77
270	0.105	0.040	0.0256	0.046					

Melt 79									
Pressure 3mm					Crucible 37% SiO ₂ 61% Al ₂ O ₃				
Metal Samples Analysis % by weight					Gas Samples Analysis				
Δt	C	Si	O	Δ V.T. litres	Δt	CO ₂	H ₂ O	H ₂	CO
0	0.10	0.084	-	-					
30	-	-	-	1.230					
60	0.045	0.145	-	1.020					
90	0.030	0.160	0.0036	0.820					
120	0.020	0.190	0.0064 0.0022	0.650					
150	0.015	0.185	0.0048 0.0044	0.210					
180	0.015	0.165	0.0044 0.0043	0.100					
210	0.010	0.155	-	0.095					
240	0.010	0.160	0.0055 0.0061	0.060					
270	0.010	0.150	0.0054	0.075					

Melt 67		Pressure 760			Crucible 37% SiO ₂ 61% Al ₂ O ₃				
Metal Samples Analysis % by weight					Gas Samples Analysis				
Δt	C	Si	O	Δ V.T. litres	Δt	CO ₂	H ₂ O	H ₂	CO
0	0.93	0.035	0.00185 0.00344	-	10	0	0	2.33	97.67
30	0.86	0.10	0.00262	2.928	45	0	0	5.19	94.81
60	0.80	0.13	-	1.747	110	0	0	7.29	92.71
90	0.80	0.155	0.00156	1.315	180	0	0	10.42	89.58
120	0.77	0.185	0.00462	1.100	270	0	0	9.83	90.17
150	0.745	0.205	0.00269	1.025	250	0	0	9.51	90.69
180	0.715	0.225	0.00222	0.985	280	0	0	12.00	88.00
210	0.690	0.250	-	0.650	315	0	0	11.99	88.01
240	0.680	0.265	-	0.655					
270	0.670	0.265	0.00753	0,315					
306	0.660	0.285	0.00287						
330	0.640	0.28	0.00220						

Melt 87

Pressure 3 mm

Crucible 37% SiO₂
61% Al₂O₃

Metal Samples Analysis % by weight					Gas Samples Analysis				
Δt	C	Si	O	Δ V.T. litres	Δt	CO ₂	H ₂ O	H ₂	CO
30				2.390	0	0	0	12.80	87.20
60				1.960	40	0	0	15.13	84.57
90				1.500	70	0	0	21.43	78.57
120				1.370	120	0	0	10.26	89.74
150				1.330	145	0	0	15.75	84.25
180				1.475	170	0	0	12.07	87.93
210				1.265	205	0	0	13.93	86.07
240				1.460	240	0	0	12.50	87.50
270				1.160	270	0	0	15.04	84.96

Melt 45

Pressure 76 mm.

Crucible 56% SiO₂
43% Al₂O₃

Metal Samples Analysis % by weight					Gas Samples Analysis				
Δt	C	Si	O	Δ V.T. litres	Δt	CO ₂	H ₂ O	H ₂	CO
0	0.126	0.04	0.0102	-					
29	0.058	0.09	0.0058	3.075					
62	0.029	0.12	0.0078	1.105					
90	0.022	0.125	0.0081	0.310					
120	0.021	0.130	0.0087	0.130					
180	0.019	0.135	0.0137	0.082					
210	0.019	0.135	0.0106	0.006					

Melt 86				Pressure 3 mm	Crucible 56% SiO ₂ 43% Al ₂ O ₃				
Metal Samples Analysis % by weight					Gas Samples Analysis				
Δt	C	Si	O	Δ V.T. litres	Δt	CO ₂	H ₂ O	H ₂	CO
30				0.810	15	0	0	0	100
60				0.440	75	0	0	0	100
90				0.200					
110				0.150					

Melt 44					Pressure 76 mm.		Crucible 56% SiO ₂ 43% Al ₂ O ₃		
Metal Samples Analysis % by weight					Gas Samples Analysis				
Δt	C	Si	O	Δ V.T. litres	Δt	CO ₂	H ₂ O	H ₂	CO
1	0.932	0.105	-	-					
32	0.873	0.170	0.0010	3.970					
62	0.750	0.210	-	2.740					
94	0.780	0.285	-	2.175					
123	0.745	0.330	0.0011	1.630					
155	0.724	0.370	0.0010	0.890					
184	0.705	0.380	0.0010	0.680					
213	0.662	0.390	0.0010	0.745					
242	0.670	0.420	0.0014	0.830					
274	0.645	0.420	-	0.670					

Melt 89									
Pressure 3 mm					Crucible 56% SiO ₂ 43% Al ₂ O ₃				
Metal Samples Analysis % by weight				Gas Samples Analysis					
Δt	C	Si	O	Δ V.T. litres	Δt	CO ₂	H ₂ O	H ₂	CO
30				3.750	0	0	0	3.82	96.18
60				3.700	20	0	0	1.27	98.73
90				3.550	40	0	0	0	100
120				3.300	60	0	0	0	100
150				2.950	80	0	0	0	100
180				2.600	100	0	0	0	100
210				2.250	160	0	0	0	100
240				2.150	190	0	0	0	100
270				2.150	210	0	0	0	100
					230	0	0	0	100

Melt 100 Pressure 140 mm Crucible 92% SiO ₂									
Metal Samples Analysis % by weight					Gas Samples Analysis				
Δt	C	Si	O	Δ V.T. litres	Δt	CO ₂	H ₂ O	H ₂	CO
0	-	-	-	-	5	0	0	0	100
50	0.55	0.59	0.0035	12.730	25	0	0	0	100
80	0.44	0.81	0.0103	5.200	95	0	0	0	100
110	0.34	0.82	0.0021	1.360	125	0	0	1.67	98.33
140	0.28	0.91	0.0026	2.760	155	0	0	5.00	95.00
170	0.23	0.95	0.0048 0.0049	1.900	185	0	0	5.88	94.12
200	0.18	0.96	0.0074 0.0077	1.990	220	0	0	7.87	92.13
230	0.12	0.97	0.0041	1.640	250	0	0	8.51	91.49
260	0.09	1.02	-	1.273					

Melt 109 Pressure 3 mm Crucible 92% SiO ₂									
Metal Samples Analysis % by weight					Gas Samples Analysis				
Δt	C	Si	O	Δ V.T. litres	Δt	CO ₂	H ₂ O	H ₂	CO
0				-	0	0	0	0	100
10				3.370	30	0	0	1.20	98.80
20				1.100	60	0	0	4.50	95.50
30				0.160					
60				0.210					
70				0.050					
80				0.025					

Melt 101

Pressure 760 mm

Crucible 92% SiO₂

Metal Samples Analysis % by weight				Gas Samples Analysis					
Δt	C	Si	O	Δ V.T. litres	Δt	CO ₂	H ₂ O	H ₂	CO
0	0.13	0.032	0.0234	-	10	2.20	0	3.30	94.50
30	0.13	0.045	0.0208	0.515	40	2.25	0	8.90	88.65
60	0.125	0.055	0.0169 0.0173	0.380	70	2.00	0	13.00	85.00
90	0.115	0.060	0.0134	0.440	130	0	0	19.00	81.00
120	0.105	0.061	0.0164 0.0168	0.270	150	0	0	19.40	80.60
150	0.089	0.076	ND	0.330	190	0	0	21.98	78.02
180	0.110	0.079	0.0205	0.185	220	0	0	23.26	76.74
210	0.10	0.081	0.0230 0.0250	0.185	250	0	0	22.73	77.27
240	0.08	0.10	0.0297	0.235					
270	0.08	0.085	0.0262 0.0284	0.250					

Melt 106

Pressure 140 mm

Crucible 92% SiO₂

Metal Samples Analysis % by weight				Gas Samples Analysis					
Δt	C	Si	O	Δ V.T. litres	Δt	CO ₂	H ₂ O	H ₂	CO
0	0.16	0.14	0.0066	-		ND	ND	ND	ND
30	0.102	0.20	0.0032	3.050					
60	0.084	0.21	0.722	1.260					
90	0.063	0.23	0.0144	1.050					
120	0.051	0.24	0.0096	0.725					
150	0.033	0.26	ND	0.635					
180	ND	ND	ND	0.425					

Melt 110

Pressure 3 mm

Crucible 92% SiO₂

Metal Samples Analysis % by weight					Gas Samples Analysis				
Δt	C	Si	O	Δ V.T. litres	Δt	CO ₂	H ₂ O	H ₂	CO
10				2.788	45	0	0	0	100
20				2.947					
30				2.363					
40				2.359					
45				0.800					

TABLE 14.

The next 30 pages give details of the oxygen balances carried out on the 5lb laboratory heats. Wherever possible the balance has been carried out using the results of metal samples but if these have not been available gas analysis plus flow measurement has been used.

Metal Samples Graphical Derivations N.T.P. Factor= 0.91		Melt 19 Pressure 760 m.m. Crucible 8% SiO ₂ 90% MgO			Initial % C= 0.1400 Initial % Si= 0.005 Initial % O= 0.0124		
Δt min	Mass gms	ΔC	ΔSi	ΔO	Δ V.T. N.T.P.	Δ VCO N.T.P.	Δ V.H. N.T.P.
40	2213	0.0072	0	0	0.4867	0.2974	0.1893
70	2178	0.0055	0	0	0.3686	0.2237	0.1449
100	2143	0.0043	0	0	0.3640	0.1721	0.1919
130	2108	0.0033	0	0	0.3686	0.1299	0.2387
167	2073	0.0026	0	0	0.3913	0.1006	0.2907
Δt min	ΔO H ₂ O	ΔO SiO ₂	ΔO C	ΣΔO H ₂ O	ΣΔO SiO ₂	ΣΔO C	
40	0.00611	0	0.00958	0.00611	0	0.00958	
70	0.00475	0	0.00732	0.01086	0	0.01690	
100	0.00639	0	0.00572	0.01725	0	0.02262	
130	0.00809	0	0.00439	0.02534	0	0.02701	
167	0.01001	0	0.00346	0.03534	0	0.03047	

Metal Samples Graphical Derivations N.T.P. Factor= 0.91		Melt Pressure Crucible	18 76 8% SiO ₂ 90% MgO	Initial % C= Initial % Si= Initial % O=	0.112 0.010 0.0024		
Δt min	Mass gms	ΔC	ΔSi	ΔO	Δ V.T. N.T.P.	Δ VCO N.T.P.	Δ V.H. N.T.P.
13	2135	0.0135	0.0105	0	0.6370	0.5381	0.0989
28	2075	0.0125	0.0090	0	0.5760	0.4843	0.0917
43	2015	0.0120	0.0080	0	0.5432	0.4514	0.0913
58	1955	0.0095	0.0070	0	0.4505	0.3467	0.1018
73	1895	0.0085	0.0060	+0.0002	0.4505	0.3008	0.1497
88	1835	0.0070	0.0050	+0.0004	0.3913	0.2399	0.1514
103	1775	0.0050	0.0045	+0.0006	0.3868	0.1822	0.2046
Δt min	ΔO H ₂ O	ΔO SiO ₂	ΔO C	ΣΔO H ₂ O	ΣΔO SiO ₂	ΣΔO C	
13	0.00331	0.01200	0.01796	0.00331	0.01200	0.01796	
28	0.00316	0.01029	0.01663	0.00647	0.02229	0.03459	
43	0.00325	0.00914	0.01596	0.00972	0.03143	0.05055	
58	0.00372	0.00800	0.01264	0.01344	0.03943	0.06319	
73	0.00564	0.00686	0.01131	0.01908	0.04629	0.07450	
88	0.00589	0.00572	0.00931	0.02497	0.05201	0.08381	
103	0.00823	0.00514	0.00732	0.03320	0.05715	0.09113	

Metal Samples Graphical Derivations N.T.P. Factor= 0.908		Melt 76 Pressure 3 m.m. Crucible 8% SiO ₂ 90% MgO		Initial % C= 0.0860 Initial % Si= 0.0200 Initial % O= 0.0010			
Δt min	Mass gms	ΔC	ΔSi	ΔO	Δ V.T. N.T.P.	Δ VCO N.T.P.	Δ V.H. N.T.P.
30	2147	0.0210	0.0350	+0.00025	1.0941	0.8418	0.2523
60	2113	0.0150	0.0180	+0.00025	0.7309	0.5918	0.1391
90	2073	0.0100	0.0050	+0.00025	0.4358	0.3870	0.0488
120	2030	0.0070	0.0030	+0.00025	0.2769	0.2653	0.0116
150	1988	0.0030	0.0010	+0.00025	0.1907	0.1113	0.0794
180	1944	0.0010	0	+0.00025	0.1180	0.0363	0.0317
210	1899	0.0005	0	+0.00025	0.0953	0.0177	0.0776
240	1857	0.0005	0	+0.00025	0.0863	0.0173	0.0690
270	1818	0.0005	0	+0.00025	0.0543	0.0170	0.0373
Δt min	ΔO H ₂ O	ΔO SiO ₂	ΔO C	ΣΔO H ₂ O	ΣΔO SiO ₂	ΣΔO C	
30	0.00839	0.04001	0.02793	0.00839	0.04001	0.02793	
60	0.00470	0.02057	0.01995	0.01309	0.06058	0.04788	
90	0.00168	0.00567	0.01330	0.01477	0.06625	0.06118	
120	0.00041	0.00343	0.00931	0.01518	0.06968	0.07049	
150	0.00285	0.00114	0.00399	0.01803	0.07082	0.07448	
180	0.00300	0	0.00133	0.02103	0.07082	0.07581	
210	0.00292	0	0.00067	0.02403	0.07082	0.07648	
240	0.00265	0	0.00067	0.02668	0.07082	0.07715	
270	0.00146	0	0.00067	0.02814	0.07082	0.07782	

Metal Samples Graphical Derivations N.T.P. Factor= 0.913		Melt 82 Pressure 760 m.m. Crucible 8% SiO ₂ 90% MgO ²			Initial % C= 1.065 Initial % Si= 0.017 Initial % O= 0.0025		
Δt min	Mass gms	ΔC	ΔSi	ΔO	Δ V.T. N.T.P.	Δ VCO N.T.P.	Δ V.H. N.T.P.
30	2190	0.020	0.013	0.00250	0.7306	0.7431	-
60	2157	0.015	0.010	0.00010	0.4931	0.6042	-
90	2117	0.015	0.007	0.00010	0.4019	0.5930	-
120	2072	0.015	0.003	0.00010	0.3479	0.5803	-
150	2022	0.015	0	0.00010	0.3471	0.5663	-
180	1972	0.005	0	0.00010	0.3471	0.1843	0.1628
210	1927	0.005	0	0.00010	0.3471	0.1800	0.1671
240	1877	0.005	0	0.00010	0.3471	0.1753	0.1718
270	1817	0.005	0	0.00010	0.3471	0.1697	0.1474
Δt min	ΔO H ₂ O	ΔO SiO ₂	ΔO C	ΣΔO H ₂ O	ΣΔO SiO ₂	ΣΔO C	
30	-	0.01486	0.02660	-	0.01486	0.02660	
60	-	0.01430	0.01995	-	0.02916	0.04655	
90	-	0.00800	0.01995	-	0.03716	0.06650	
120	-	0.00343	0.01995	-	0.04059	0.08645	
150	-	0	0.01995	-	0.04059	0.10640	
180	0.00589	0	0.00665	0.00589	0.04059	0.11305	
210	0.00619	0	0.00665	0.01208	0.04059	0.11970	
240	0.00654	0	0.00665	0.01862	0.04059	0.12635	
270	0.00580	0	0.00665	0.02442	0.04059	0.13300	

Metal Samples Graphical Derivations N.T.P. Factor= 0.925		Melt 37 Pressure 76 mm. Crucible 8% SiO ₂ 90% MgO			Initial % C= 0.845 Initial % Si= 0.063 Initial % O= 0.005		
Δt min	Mass gms	ΔC	ΔSi	ΔO	Δ V.T. N.T.P.	Δ VCO N.T.P.	Δ V.H. N.T.P.
30	2219	0.115	0.045	0.0012	2.6363	4.7646	-
60	2183	0.090	0.034	0.0010	2.0350	3.6687	-
90	2149	0.075	0.023	0.0050	1.7113	3.0008	-
120	2114	0.040	0.016	0.0035	1.4800	1.5787	-
150	2114	0.030	0.013	0	1.0638	1.1841	-
180	2084	0.020	0.013	0	0.8788	0.7782	0.1006
210	2035	0.015	0.009	0	0.6475	0.5699	0.0776
240	1997	0.007	0.008	0	0.4163	0.2597	0.1566
Δt min	ΔO H ₂ O	ΔO SiO ₂	ΔO C	ΣΔO H ₂ O	ΣΔO SiO ₂	ΣΔO C	
30	-	0.0514	0.15295	-	0.05140	0.15295	
60	-	0.0389	0.11970	-	0.09030	0.27265	
90	-	0.0263	0.9975	-	0.11660	0.37240	
120	-	0.0183	0.05990	-	0.13490	0.43230	
150	-	0.0149	0.03990	-	0.14980	0.47220	
180	0.0035	0.0080	0.02660	0.00350	0.15780	0.49880	
210	0.0027	0.0103	0.01995	0.00620	0.16810	0.51875	
240	0.0079	0.0091	0.00930	0.01410	0.17720	0.52805	

%Si 0.195, 0.190

%O 0.0026, 0.0018

Gas Samples Graphical Derivations			Melt 90 Pressure 3 mm Crucible 8% SiO ₂ 90% MgO			N.T.P. Factor = 0.937	
Δt	Mass	CO ₁	CO ₂	ΔC	ΔSi	Δ V.T. N.T.P.	Δ V.H. N.T.P.
30	2210	1.00	1.00	0.059	0.068	2.4180	0
60	2210	1.00	1.00	0.040	0.047	1.6585	0
90	2210	1.00	1.00	0.034	0.039	1.3868	0
120	2210	1.00	1.00	0.030	0.034	1.2181	0
150	2210	1.00	1.00	0.026	0.030	1.0635	0
180	2210	1.00	1.00	0.026	0.030	1.0635	0
210	2210	1.00	1.00	0.026	0.030	1.0635	0
240	2210	1.00	1.00	0.025	0.029	1.0307	0
270	2210	1.00	1.00	0.024	0.028	1.0000	0

Δt	ΔO H ₂ O	ΔO SiO ₂	ΔO C	ΣΔO H ₂ O	ΣΔO SiO ₂	ΣΔO C
30	0	0.07816	0.07812	0	0.07816	0.07812
60	0	0.05361	0.05358	0	0.13177	0.13171
90	0	0.04482	0.04479	0	0.17659	0.17650
120	0	0.03937	0.03935	0	0.21596	0.21585
150	0	0.03438	0.03436	0	0.25034	0.25021
180	0	0.03438	0.03436	0	0.28472	0.28457
210	0	0.03438	0.03436	0	0.31910	0.31893
240	0	0.03332	0.03329	0	0.35242	0.35222
270	0	0.03232	0.03231	0	0.38474	0.38453

Metal Samples Graphical Derivations N.T.P. Factor= 0.91		Melt 66 Pressure 76 mm Crucible 7% SiO ₂ 93% Al ₂ O ₃			Initial % C= 0.130 Initial % Si= 0.030 Initial % O= 0.012		
Δt min	Mass gms	ΔC	ΔSi	ΔO	Δ V.T. N.T.P.	Δ VCO N.T.P.	Δ V.H. N.T.P.
30	2019	0.0290	0.024	+ 0.00008	1.4090	1.0930	0.0316
60	1976	0.0193	0.015	+ 0.00008	0.7137	0.7120	0.0017
90	1916	0.0122	0.011	"	0.5399	0.4360	0.1039
120	1866	0.0100	0.009	"	0.4494	0.3480	0.1004
150	1816	0.0095	0.006	"	0.3843	0.3220	0.0623
180	1773	0	0	"	0.3203	0	0.3203
210	1713	0	0	"	0.2471	0	0.2471
240	1648	0	0	"	0.1922	0	0.1922
270	1604	0	0	"	0.1373	0	0.1373
Δt min	ΔO H ₂ O	ΔO SiO ₂	ΔO C	ΣΔO H ₂ O	ΣΔO SiO ₂	ΣΔO C	
30	0.00112	0.02743	0.03857	0.00112	0.02743	0.03857	
60	0.00006	0.01715	0.02567	0.00173	0.04458	0.06424	
90	0.00387	0.01257	0.01623	0.00561	0.05715	0.08047	
120	0.00384	0.1029	0.01330	0.00945	0.06744	0.09377	
150	0.00245	0.00686	0.01264	0.01190	0.07450	0.10641	
180	0.01295	0	0	0.02400	0.07430	0.10641	
210	0.01098	0	0	0.03498	"	"	
240	0.00833	0	0	0.04331	"	"	
270	0.00611	0	0	0.04942	0.07430	0.10641	

Metal Samples Graphical Derivations N.T.P. Factor= 0.921		Melt ⁶⁴ Pressure 760 mm Crucible 7% SiO ₂ 93% Al ₂ O ₃			Initial % C= 0.110 Initial % Si= 0.018 Initial % O= 0.021		
Δt min	Mass gms	ΔC	ΔSi	ΔO	Δ V.T. N.T.P.	Δ VCO N.T.P.	Δ V.H. N.T.P.
30	2206	0	0	0	0.2671	-	0.2671
60	2153	0	0	0	0.2118	-	0.2118
90	2103	0	0	0	0.1750	-	0.1750
120	2056	0	0	0	0.1474	-	0.1474
150	2008	0	0	0	0.1382	-	0.1382
180	1968	0	0	0	0.1289	-	0.1289
210	1923	0	0	0	0.1105	-	0.1105
240	1875	0	0	0	0.1105	-	0.1105
270	1828	0	0	0	0.1105	-	0.1105
Δt min	ΔO H ₂ O	ΔO SiO ₂	ΔO C	ΣΔO H ₂ O	ΣΔO SiO ₂	ΣΔO C	
30	0.00865	0	0	0.00865	0	0	
60	0.00703	0	0	0.01568	0	0	
90	0.00594	0	0	0.02162	0	0	
120	0.00512	0	0	0.02675	0	0	
150	0.00492	0	0	0.03166	0	0	
180	0.00468	0	0	0.03634	0	0	
210	0.00410	0	0	0.04044	0	0	
240	0.00421	0	0	0.04465	0	0	
270	0.00420	0	0	0.04885	0	0	

Metal Samples Graphical Derivations N.T.P. Factor= 0.92%		Melt 71 Pressure 3 mm Crucible 7% SiO ₂ 93% Al ₂ O ₃			Initial % C= 0.095 Initial % Si= 0.035 Initial % O= 0.0013		
Δt min	Mass gms	ΔC	ΔSi	ΔO	Δ V.T. N.T.P.	Δ VCO N.T.P.	Δ V.H. N.T.P.
30	1927	0.0330	0.0150	0.0013	1.1900	1.1900	0
60	1865	0.0100	0.0095	0.0010	0.5840	0.3500	0.2340
90	1775	0.0060	0.0069	0	0.3990	0.1990	0.2000
120	1715	0.0056	0.0056	0	0.2320	0.1770	0.0550
150	1669	0.0050	0.0043	0	0.1710	0.1560	0.0150
180	1619	0.0034	0.0027	0	0.1250	0.1030	0.0220
210	1575	0.0020	0.0010	0	0.0690	0.0590	0.0100
240	1532	0	0	0	0.0580	0	0.0580
270	1472	0	0	0	0.0460	0	0.0460
Δt min	ΔO H ₂ O	ΔO SiO ₂	ΔO C	ΣΔO H ₂ O	ΣΔO SiO ₂	ΣΔO C	
30	0	0.01715	0.04389	0	0.01715	0.04389	
60	0.00896	0.01086	0.01330	0.00896	0.02801	0.05719	
90	0.00805	0.00789	0.00798	0.01701	0.05590	0.06517	
120	0.00229	0.00640	0.00745	0.01930	0.04230	0.07262	
150	0.00064	0.00492	0.00665	0.01994	0.04722	0.07927	
180	0.00097	0.00309	0.00452	0.02091	0.05031	0.08379	
210	0.00045	0.00114	0.00266	0.02136	0.05145	0.08645	
240	0.00270	0	0	0.02406	0.05145	0.08645	
270	0.00223	0	0	0.02629	0.05145	0.08645	

Metal Samples Graphical Derivations N.T.P. Factor= 0.91		Melt 63 Pressure 760 m.m. Crucible 7% SiO ₂ 93% Al ₂ O ₃		Initial % C= 1.07 Initial % Si= 0.020 Initial % O= 0.0028			
Δt min	Mass gms	ΔC	ΔSi	ΔO	Δ V.T. N.T.P.	Δ VCO N.T.P.	Δ V.H. N.T.P.
30	2057	0.040	0.011	0.0006	0.8190	1.5362	-
60	2012	0.030	0.010	0.0002	0.5005	1.1269	-
90	1979	0.003	0.010	0	0.3549	1.1084	0.2441
120	1943	0.003	0.009	0	0.2730	0.1089	0.1642
150	1906	0.003	0.007	0	0.2366	0.1068	0.1297
180	1868	0.003	0.005	0	0.2184	0.1046	0.1138
210	1836	0.003	0.002	0	0.2184	0.1028	0.1156
240	1801	0.003	0.0015	0	0.2184	0.1009	0.1175
Δt min	ΔO H ₂ O	ΔO SiO ₂	ΔO C	ΣΔO H ₂ O	ΣΔO SiO ₂	ΣΔO C	
30	-	0.01257	0.05320	-	0.01257	0.05320	
60	-	0.01143	0.03990	-	0.02400	0.09310	
90	0.00881	0.01143	0.00399	0.00881 0.01484	0.03543	0.09709	
120	0.00603	0.01029	0.00399		0.04572	0.10108	
150	0.00486	0.00800	0.00399	0.01970	0.05372	0.10507	
180	0.00435	0.00572	0.00399	0.02405	0.05944	0.10906	
210	0.00450	0.00229	0.00399	0.02855	0.06173	0.11305	
240	0.00470	0.00171	0.00399	0.03325	0.06344	0.11704	

Metal Samples Graphical Derivations N.T.P. Factor= 0.93		Melt 84 Pressure 76 m.m. Crucible 7% SiO ₂ 93% Al ₂ O ₃			Initial % C= 1.025 Initial % Si= 0.045 Initial % O= 0.012		
Δt min	Mass gms	ΔC	ΔSi	ΔO	Δ V.T. N.T.P.	Δ VCO N.T.P.	Δ V.H. N.T.P.
30	2100	0.040	0.040	0.0006	1.4940	1.5683	-
60	2060	0.035	0.025	0.0006	1.0195	1.3461	-
90	2025	0.030	0.0125	0.0006	0.6889	1.1342	-
120	1990	0.030	0.0080	0.0006	0.6610	1.1146	-
150	1950	0.020	0.0065	0.0006	0.5865	0.7281	-
180	1915	0.015	0.0065	0.0005	0.4841	0.5364	-
210	1867	0.015	0.0065	0	0.4748	0.5228	-
240	1819	0.005	0.0065	0	0.4748	0.1698	0.3050
270	1819	0.005	0.0065	0	0.4748	0.1698	0.3050
Δt min	ΔO H ₂ O	ΔO SiO ₂	ΔO C	ΣΔO H ₂ O	ΣΔO SiO ₂	ΣΔO C	
30	-	0.04572	0.05320		0.04572	0.05320	
60	-	0.02858	0.04655		0.07430	0.09975	
90	-	0.01429	0.03990		0.08859	0.13965	
120	-	0.00914	0.03990		0.09773	0.17955	
150	-	0.00743	0.02660		0.10516	0.20615	
180	-	0.00743	0.01995		0.11259	0.22610	
210	-	0.00743	0.01995		0.12002	0.24605	
240	0.01197	0.00743	0.00665	0.01197	0.12745	0.25270	
270	0.01197	0.00743	0.00665	0.02394	0.13488	0.25935	

%Si 0.13, 0.145

%O 0.0009, 0.0005

Gas Samples Graphical Derivations		Melt 88 Pressure 3 mm Crucible 7% SiO ₂ 93% MgO		N.T.P. Factor = 0.933			
Δt	Mass	CO ₁	CO ₂	ΔC	ΔSi	Δ V.T. N.T.P.	Δ V.H. N.T.P.
30	2130	0.970	0.990	0.040	0.045	1.6328	0.0490
60	2130	0.990	1.00	0.031	0.035	1.2316	0.0122
90	2130	1.00	1.00	0.025	0.029	0.9938	0
120	2130	1.00	1.00	0.022	0.026	0.8864	0.0001
150	2130	0.990	0.975	0.0167	0.019	0.6718	0.0070
180	2130	0.975	0.975	0.015	0.017	0.6065	0.0150
210	2130	0.975	0.975	0.015	0.017	0.6065	0.0150
240	2130	0.975	0.975	0.0146	0.0166	0.5971	0.0150
270	2130	0.975	0.975	0.0137	0.0156	0.5598	0.0140
Δt	ΔO H ₂ O	ΔO SiO ₂	ΔO C	ΣΔO H ₂ O	ΣΔO SiO ₂	ΣΔO C	
30	0.00164	0.05149	0.05309	0.00164	0.05149	0.05309	
60	0.00040	0.04048	0.04087	0.00204	0.09197	0.09396	
90	0	0.03333	0.03331	0.00204	0.12530	0.12727	
120	0	0.02072	0.02971	0.00204	0.15502	0.15698	
150	0.00023	0.02207	0.02229	0.00227	0.17709	0.17927	
180	0.00050	0.01932	0.01982	0.00277	0.19641	0.19909	
210	0.00050	0.01932	0.01982	0.00327	0.21573	0.21891	
240	0.00050	0.01903	0.01951	0.00377	0.23476	0.23842	
270	0.00047	0.01784	0.01829	0.00424	0.25260	0.25671	

Metal Samples Graphical Derivations N.T.P. Factor= 0.92		Melt 57 Pressure 760mm. Crucible 37% SiO ₂ 61% Al ₂ O ₃		Initial % C= 0.115 Initial % Si= 0.020 Initial % O= 0.028			
Δt min	Mass gms	ΔC	ΔSi	ΔO	Δ V.T. N.T.P.	Δ VCO N.T.P.	Δ V.H. N.T.P.
30	2171	0.010	0.0015	0.0080	0.1049	0.4053	-
60	2138	0.001	"	+0.0070	0.0552	0.0399	0.0153
90	2081	"	"	"	0.0414	0.0389	0.0025
120	2041	"	"	"	0.0395	0.0381	0.0014
150	1991	"	"	"	0.0386	0.0372	0.0014
180	1936	"	"	"	0.0386	0.0362	0.0024
210	1904	0.001	0.0015	+0.0070	0.0386	0.0355	0.0031
Δt min	ΔO H ₂ O	ΔO SiO ₂	ΔO C	ΣΔO H ₂ O	ΣΔO SiO ₂	ΣΔO C	
30	-	0.00172	0.01330	-	0.00172	0.01330	
60	0.00051	"	0.00013	0.00051	0.00344	0.01463	
90	0.00009	"	"	0.00060	0.00516	0.01596	
120	0.00005	"	"	0.00065	0.00688	0.01729	
150	0.00005	"	"	0.00070	0.00860	0.01862	
180	0.00009	"	"	0.00079	0.01032	0.01995	
210	0.00012	0.00172	0.00013	0.00091	0.01204	0.02008	

Metal Samples Graphical Derivations N.T.P. Factor= 0.939		Melt 61 Pressure 76 mm. Crucible 37% SiO ₂ 61% Al ₂ O ₃			Initial % C= 0.090 Initial % Si= 0.030 Initial % O= 0.010		
Δt min	Mass gms	ΔC	ΔSi	ΔO	Δ V.T. N.T.P.	Δ VCO N.T.P.	Δ V.H. N.T.P.
30	2067	0.0260	0.0250	0	1.1830	1.0034	0.1796
60	2027	0.0140	0.0145	"	0.7136	0.5298	0.1838
90	1991	0.0045	0.0055	"	0.3380	0.1673	0.1707
120	1948	0.0005	0	"	0.2254	0.1818	0.0436
150	1901	0	"	"	0.1502	0	0.1502
180	1865	"	"	"	0.1221	"	0.1221
210	1822	"	"	"	0.1033	"	0.1033
240	1784	"	"	"	0.0939	"	0.0939
270	1745	"	"	"	0.0939	"	0.0939
Δt min	ΔO H ₂ O	ΔO SiO ₂	ΔO C	ΣΔO H ₂ O	ΣΔO SiO ₂	ΣΔO C	
30	0.00621	0.02860	0.03460	0.00621	0.02860	0.03460	
60	0.00648	0.01660	0.01860	0.01269	0.04520	0.05320	
90	0.00612	0.00629	0.00599	0.01881	0.05149	0.05919	
120	0.00127	0	0.00067	0.02008	"	0.05986	
150	0.00564	"	0	0.02572	"	"	
180	0.00468	"	"	0.03040	"	"	
210	0.00405	"	"	0.03445	"	"	
240	0.00376	"	"	0.03821	"	"	
270	0.00376	"	"	0.04197	0.05149	0.05986	

Metal Samples Graphical Derivations N.T.P. Factor= 0.885		Melt 79 Pressure 3 mm. Crucible 37% SiO ₂ 61% Al ₂ O ₃			Initial % C= 0.100 Initial % Si= 0.084 Initial % O= 0.005		
Δt min	Mass gms	ΔC	ΔSi	ΔO	Δ V.T. N.T.P.	Δ VCO N.T.P.	Δ V.H. N.T.P.
30	1933	0.0325	0.0360	0	1.1726	1.1728	-
60	1873	0.0225	0.0250	"	0.8186	0.7868	0.0318
90	1837	0.0150	0.0110	"	0.7257	0.5146	0.2111
120	1807	0.0100	0.0055	"	0.5399	0.3374	0.2025
150	1767	0.0060	0.0035	"	0.2213	0.1980	0.0233
180	1729	0.0040	0	"	0.0885	0.0692	0.0193
210	1689	0.0015	0	"	0.0841	0.0473	0.0368
240	1654	0	0	"	0.0531	0	0.0531
270	1600	0	0	"	0.0486	0	0.0486
Δt min	ΔO H ₂ O	ΔO SiO ₂	ΔO C	ΣΔO H ₂ O	ΣΔO SiO ₂	ΣΔO C	
30	-	0.04115	0.04323	-	0.04115	0.04323	
60	0.00121	0.02858	0.02979	0.00121	0.06973	0.07316	
90	0.00820	0.01257	0.02077	0.00941	0.08230	0.09311	
120	0.00800	0.00629	0.01429	0.01741	0.08859	0.10641	
150	0.00094	0.00400	0.00494	0.01835	0.09259	0.11439	
180	0.00080	0	0	0.01915	0.09259	0.11971	
210	0.00156	0	0	0.02071	"	0.12171	
240	0.00229	0	0	0.02330	"	0.12171	
270	0.00217	0	0	0.02517	0.09259	0.12171	

Metal Samples Graphical Derivations N.T.P. Factor= 0.913		Melt 67 Pressure 760 m.m. Crucible 37% SiO ₂ 61% Al ₂ O ₃			Initial % C= 0.930 Initial % Si= 0.035 Initial % O= 0.0034		
Δt min	Mass gms	ΔC	ΔSi	ΔO	Δ V.T. N.T.P.	Δ VCO N.T.P.	Δ V.H. N.T.P.
30	2083	0.060	0.065	0.001	2.6477	2.3333	0.3144
60	2026	0.040	0.030	0	1.5977	1.5130	0.0847
90	1971	0.033	0.030	0	1.2326	1.2144	0.0182
120	1917	0.027	0.025	0	1.0956	0.9663	0.0293
150	1857	0.025	0.024	0	0.9133	0.8668	0.0465
180	1807	0.024	0.023	0	0.8217	0.8097	0.0120
210	1754	0.020	0.018	0	0.6848	0.6549	0.0299
240	1705	0.016	0.014	0	0.5022	0.5020	0.0002
Δt min	ΔO H ₂ O	ΔO SiO ₂	ΔO C	ΣΔO H ₂ O	ΣΔO SiO ₂	ΣΔO C	
30	0.01078	0.07430	0.07980	0.01078	0.07430	0.07980	
60	0.00299	0.03429	0.05320	0.01377	0.10859	0.13300	
90	0.00066	0.03429	0.04389	0.01443	0.14288	0.17689	
120	0.00109	0.02858	0.03591	0.01552	0.17146	0.21280	
150	0.00179	0.02743	0.03325	0.01731	0.19889	0.24605	
180	0.00048	0.02629	0.03192	0.01779	0.22518	0.27797	
210	0.00122	0.02059	0.02660	0.01901	0.24577	0.30457	
240	0.00001	0.01600	0.02128	0.01902	0.26177	0.32586	

Metal Samples Graphical Derivations N.T.P. Factor= 0.928		Melt 68 Pressure 76 m.m. Crucible 37% SiO ₂			Initial % C= 0.960 Initial % Si= 0.070 Initial % O= 0.0007		
Δt min	Mass gms	ΔC	ΔSi	ΔO	Δ V.T. N.T.P.	Δ VCO N.T.P.	Δ V.H. N.T.P.
30	2065	0.070	0.106	0	2.7000	2.7000	0
60	2012	0.046	0.036	0	1.8096	1.7280	0.0820
90	1964	0.029	0.024	0	1.4384	1.0640	0.3744
120	1925	0.027	0.023	0	1.0208	0.9710	0.0498
150	1887	0.024	0.023	0	0.9280	0.8100	0.1180
180	1839	0.023	0.021	0	0.8352	0.8241	0.0111
210	1779	0.022	0.020	0	0.7340	0.7307	0.0033
240	1744	0.020	0.019	0	0.6496	0.6510	-
Δt min	ΔO H ₂ O	ΔO SiO ₂	ΔO C	ΣΔO H ₂ O	ΣΔO SiO ₂	ΣΔO C	
30	0	0.12116	0.09310	0	0.12116	0.09310	
60	0.00291	0.04115	0.06118	0.00291	0.16231	0.15428	
90	0.01360	0.02743	0.03857	0.01651	0.18974	0.19285	
120	0.00184	0.02629	0.03591	0.01835	0.21603	0.22876	
150	0.00447	0.02629	0.03192	0.02282	0.24232	0.26068	
180	0.00043	0.02400	0.03059	0.02325	0.26632	0.29127	
210	0.00014	0.02286	0.02926	0.02339	0.28918	0.32053	
240	0	0.02172	0.02660	0.02339	0.31090	0.34713	

%Si 0.445, 0.420

%O 0.0005, 0.008.

Gas Samples Graphical Derivations		Melt 87 Pressure 3 mm Crucible 37% SiO ₂ 61% Al ₂ O ₃				N.T.P. Factor = 0.932	
Δt	Mass	CO ₁	CO ₂	ΔC	ΔSi	Δ V.T. N.T.P.	Δ V.H. N.T.P.
30	2080	0.88	0.87	0.051	0.051	2.2275	0.2670
60	2080	0.87	0.865	0.041	0.041	1.8267	0.2380
90	2080	0.865	0.865	0.031	0.031	1.3980	0.1890
120	2080	0.865	0.865	0.029	0.029	1.3048	0.1760
150	2080	0.865	0.865	0.028	0.028	1.2582	0.1760
180	2080	0.865	0.865	0.028	0.028	1.2582	0.1700
210	2080	0.865	0.865	0.028	0.028	1.2582	0.1700
240	2080	0.865	0.865	0.028	0.028	1.2582	0.1700
270	2080	0.865	0.865	0.028	0.028	1.2582	0.1700
Δt	ΔO H ₂ O	ΔO SiO ₂	ΔO C	ΣΔO H ₂ O	ΣΔO SiO ₂	ΣΔO C	
30	0.00918	0.05814	0.06728	0.00918	0.05814	0.06728	
60	0.00816	0.04642	0.05455	0.01734	0.10456	0.12183	
90	0.00648	0.03505	0.04151	0.02382	0.13961	0.16334	
120	0.00605	0.03271	0.03874	0.02987	0.17232	0.20208	
150	0.00583	0.03154	0.03736	0.03570	0.20386	0.23944	
180	0.00583	0.03154	0.03736	0.04153	0.23540	0.27680	
210	0.00583	0.03154	0.03736	0.04736	0.26694	0.31416	
240	0.00583	0.03154	0.03736	0.05319	0.29848	0.35152	
270	0.00583	0.03154	0.03736	0.05902	0.33002	0.38888	

Metal Samples Graphical Derivations N.T.P. Factor= 0.90		Melt 49 Pressure 760 mm. Crucible 56% SiO ₂ 43% Al ₂ O ₃		Initial % C= 0.134 Initial % Si= 0.375 Initial % O= 0.0217			
Δt min	Mass gms	ΔC	ΔSi	ΔO	Δ V.T. N.T.P.	Δ VCO N.T.P.	Δ V.H. N.T.P.
30	2170	0.0055	0.0120	0.0014	0.1717	0.2229	-
60	2128	0.0035	0.0055	0.0013	0.1620	0.1391	0.0013
90	2087	0.0029	0.0035	0.0011	0.1395	0.0971	0.0424
120	2043	0.0013	0.0010	0.0005	0.0945	0.0496	0.0449
150	1983	0.0007	0.0005	0.0001	0.0585	0.0259	0.0326
180	1936	0.0005	0.0004	0	0.0495	0.0181	0.0314
210	1880	0.0004	0.0002	0	0.0495	0.0140	0.0355
240	1821	0.0004	0.0001	0	0.0450	0.0136	0.0314
270	1774	0.0003	0.0001	0	0.0450	0.0094	0.0366
Δt min	ΔO H ₂ O	ΔO SiO ₂	ΔO C	ΣΔO H ₂ O	ΣΔO SiO ₂	ΣΔO C	
30	-	0.01371	0.00732	-	0.01372	0.00732	
60	0.00077	0.00628	0.00466	0.00077	0.02000	0.07198	
90	0.00145	0.00400	0.00386	0.00222	0.02400	0.01584	
120	0.00150	0.00114	0.00173	0.00372	0.02514	0.01757	
150	0.00117	0.00057	0.00093	0.00489	0.02571	0.01850	
180	0.00116	0.00046	0.00067	0.00605	0.02617	0.01917	
210	0.00135	0.00023	0.00053	0.00740	0.02640	0.02023	
240	0.00123	0.00011	0.00053	0.00863	0.02651	0.02063	
270	0.00147	0.00011	0.00040	0.01010	0.02662	0.02103	

Metal Samples Graphical Derivations N.T.P. Factor= 0.90		Melt Pressure 45 76 mm. Crucible 56% SiO ₂ 43% Al ₂ O ₃			Initial % C= 0.126 Initial % Si= 0.040 Initial % O= 0.010		
Δt min	Mass gms	ΔC	ΔSi	ΔO	Δ V.T. N.T.P.	Δ VCO N.T.P.	Δ V.H. N.T.P.
29	2046	0.0680	0.050	0.004	2.7059	2.5976	0.1083
61	1999	0.0290	0.028	0.0006	1.0800	1.0823	-
90	1952	0.0070	0.012	+0.001	0.2552	0.2550	0.0002
120	1905	0.0024	0.004	+0.001	0.1170	0.0889	0.0281
150	1858	0.0005	0.001	+0.001	0.0630	0.0173	0.0457
180	1763	0.0000	0.000	+0.001	0.0720	0.0000	0.0120
Δt min	ΔO H ₂ O	ΔO SiO ₂	ΔO C	ΣΔO H ₂ O	ΣΔO SiO ₂	ΣΔO C	
29	0.00378	0.05715	0.09044	0.00378	0.04715	0.09044	
61	-	0.03200	0.03857	0.00378	0.08915	0.12901	
90	-	0.01372	0.00931	0.00378	0.10287	0.13832	
120	0.00105	0.00457	0.00319	0.00483	0.10744	0.14151	
150	0.00176	0.00114	0.00067	0.00639	0.10858	0.14218	
180	0.00049	0.0000	0.0000	0.00708	0.10858	0.14218	

%Si 0.29

%O 0.0196, 0.0197

Gas Samples Graphical Derivations		Melt 86 Pressure 3 mm Crucible 56% SiO ₂ 43% Al ₂ O ₃				N.T.P. Factor = 0.96	
Δt	Mass	CO ₁	CO ₂	ΔC	ΔSi	Δ V.T. N.T.P.	Δ V.H. N.T.P.
30	2170	1.00	1.00	0.019	0.022	0.7768	0
60	2170	1.00	1.00	0.010	0.012	0.4220	0
90	2170	1.00	1.00	0.006	0.007	0.2398	0
110	2170	1.00	1.00	0.002	0.003	0.0959	0

Δt	ΔO H ₂ O	ΔO SiO ₂	ΔO C	ΣΔO H ₂ O	ΣΔO SiO ₂	ΣΔO C
30	0	0.02557	0.02552	0	0.02557	
60	0	0.01389	0.01386	0	0.03946	0.03938
90	0	0.00789	0.00788	0	0.04735	0.04726
110	0	0.00315	0.00315	0	0.05050	0.05041

Metal Samples Graphical Derivations N.T.P. Factor= 0.95		Melt 41 Pressure 760 mm Crucible 56% SiO ₂ 37% Al ₂ O ₃			Initial % C= 0.955 Initial % Si=0.094 Initial % O= 0.0025		
Δt min	Mass gms	ΔC	ΔSi	ΔO	Δ V.T. N.T.P.	Δ VCO N.T.P.	Δ V.H. N.T.P.
30	2209	0.032	0.041	0	2.2430	1.3198	0.9232
60	2158	0.025	0.033	0	1.2910	1.0073	0.2837
90	2107	0.025	0.023	0	1.0042	0.9834	0.0208
120	2056	0.025	0.012	0	0.8066	0.9596	-
180	2005	0.046	0.021	0	1.3387	1.7219	-
210	1954	0.024	0.010	0	0.5216	0.8756	-
240	1903	0.023	0.010	0	0.4256	0.8172	-
270	1852	0.023	0.010	0	0.4256	0.7953	-
Δt min	ΔO H ₂ O	ΔO SiO ₂	ΔO C	ΣΔO H ₂ O	ΣΔO SiO ₂	ΣΔO C	
30	0.02990	0.04690	0.04260	0.02990	0.04690	0.04260	
60	0.00940	0.03770	0.03330	0.03930	0.08460	0.07590	
90	0.00070	0.02630	0.03330	0.04000	0.11090	0.10920	
120	-	0.01370	0.06120	-	0.12460	0.14250	
180	-	0.0240	0.03190	-	0.14860	0.20370	
210	-	0.01140	0.03060	-	0.16000	0.23560	
240	-	0.01140	0.03060	-	0.17140	0.26620	
270	-	0.01140	0.03060	-	0.18280	0.29680	

Metal Samples Graphical Derivations N.T.P. Factor= 0.94		Melt 44 Pressure 76 mm. Crucible 56% SiO ₂			Initial % C= 0.9350 Initial % Si= 0.1050 Initial % O= 0.001		
Δt min	Mass gms	ΔC	ΔSi	ΔO	Δ V.T. N.T.P.	Δ VCO N.T.P.	Δ V.H. N.T.P.
30	2189	0.0610	0.0630	0	3.7318	2.4930	1.2388
60	2142	0.0540	0.0570	"	2.5756	2.1596	0.4160
90	2095	0.0425	0.0530	"	2.0045	1.6624	0.3821
120	2048	0.0300	0.0495	"	1.3489	1.1471	0.2018
150	2001	0.0225	0.0385	"	0.9917	0.8405	0.1512
180	1954	0.0198	0.0220	"	0.7238	0.7223	0.0005
210	1907	0.0177	0.0120	"	0.6862	0.6301	0.0061
240	1860	0.0175	0.0100	"	0.6815	0.6077	0.0738
Δt min	ΔO H ₂ O	ΔO SiO ₂	ΔO C	ΣΔO H ₂ O	ΣΔO SiO ₂	ΣΔO C	
30	0.04041	0.07201	0.08113	0.04041	0.07201	0.08113	
60	0.01387	0.06515	0.07182	0.05428	0.13716	0.15295	
90	0.01302	0.06058	0.05653	0.06730	0.19774	0.20948	
120	0.00512	0.05658	0.03990	0.07242	0.25432	0.24938	
150	0.00540	0.04401	0.02993	0.07782	0.29833	0.27931	
180	0.00002	0.02515	0.02633	0.07784	0.32348	0.30564	
210	0.00210	0.01372	0.02354	0.07994	0.33720	0.32918	
240	0.00283	0.01143	0.02328	0.08277	0.34863	0.35246	

Gas Samples Graphical Derivations		Melt 89 Pressure 5 mm Crucible 56% SiO ₂ 43% Al ₂ O ₃		N.T.P. Factor = 0.031			
Δt	Mass	CO ₁	CO ₂	ΔC	ΔSi	Δ V.T. N.T.P.	Δ V.H. N.T.P.
30	2185	0.962	1.00	0.082	0.092	3.4913	0.132
60	2185	1.00	1.00	0.084	0.099	3.4447	0
90	2185	1.00	1.00	0.081	0.095	3.3051	0
120	2185	1.00	1.00	0.075	0.088	3.0723	0
150	2185	1.00	1.00	0.067	0.079	2.7465	0
180	2185	1.00	1.00	0.059	0.069	2.4206	0
210	2185	1.00	1.00	0.051	0.060	2.0948	0
240	2185	1.00	1.00	0.049	0.057	2.0017	0
270	2185	1.00	1.00	0.049	0.057	2.0017	0
Δt	ΔO H ₂ O	ΔO SiO ₂	ΔO C	ΣΔO H ₂ O	ΣΔO SiO ₂	ΣΔO C	
30	0.00430	0.10550	0.10976	0.00430	0.10550	0.10976	
60	0	0.11262	0.11256	0.00430	0.21812	0.22232	
90	0	0.10805	0.10799	0.00430	0.32611	0.33031	
120	0	0.10045	0.10039	0.00430	0.42662	0.43070	
150	0	0.08980	0.08975	0.00430	0.51642	0.52045	
180	0	0.07914	0.07909	0.00430	0.59556	0.59954	
210	0	0.06848	0.06845	0.00430	0.66404	0.66799	
240	0	0.06545	0.06541	0.00430	0.72949	0.73340	
270	0	0.06545	0.06541	0.00430	0.79494	0.79881	

Metal Samples Graphical Derivations N.T.P. Factor=		Melt 101 Pressure 760 mm Crucible 92% SiO ₂			Initial % C= 0.141 Initial % Si= 0.32 Initial % O= 0.0230		
Δt min	Mass gms	ΔC	ΔSi	ΔO	Δ V.T. N.T.P.	Δ VCO N.T.P.	Δ V.H. N.T.P.
30	2218	0.009	0.013	0.0024	0.4800	0.3727	0.1073
60	2177	0.0085	0.010	0.0034	0.3950	0.3456	0.0494
90	2124	0.0085	0.010	0.0038	0.3350	0.3350	0
120	2079	0.0075	0.0075	+0.0030	0.2900	0.2900	0
150	2044	0.0050	0.0050	+0.0031	0.2500	0.1908	0.0592
180	2004	0.0045	0.0025	+0.0027	0.2100	0.1684	0.0416
210	1969	0.0040	0.0025	+0.0023	0.1900	0.1470	0.0430
240	1921	0.0040	0.0025	+0.0025	0.1850	0.1435	0.0415
Δt min	ΔO H ₂ O	ΔO SiO ₂	ΔO C	ΣΔO H ₂ O	ΣΔO SiO ₂	ΣΔO C	
30	0.03454	0.01486	0.01197	0.03454	0.01486	0.01197	
60	0.01620	0.01430	0.01131	0.05074	0.02916	0.02328	
90	0	0.01430	0.01131	0.05074	0.04346	0.03459	
120	0	0.00857	0.00998	0.05074	0.05203	0.04457	
150	0.02068	0.00572	0.00665	0.07142	0.05775	0.05122	
180	0.01482	0.00286	0.00599	0.08624	0.06061	0.05721	
210	0.01559	0.00286	0.00532	0.10183	0.06347	0.06253	
240	0.01542	0.00286	0.00532	0.11725	0.06633	0.06785	

Metal Samples Graphical Derivations N.T.P. Factor= 0.94		Melt 100 Pressure 140 mm Crucible 92% SiO ₂		Initial % C= 0.885 Initial % Si= 0.160 Initial % O= 0.006			
Δt min	Mass gms	ΔC	ΔSi	ΔO	Δ V.T. N.T.P.	Δ VCO N.T.P.	Δ V.H. N.T.P.
30	1750	0.25	0.220	0.0017	8.836	8.1681	0.6679
60	1750	0.125	0.215	0.0012	4.4090	4.0841	0.3249
90	1720	0.110	0.215	0.0008	3.7030	3.5324	0.1706
120	1695	0.075	0.050	0.0002	2.3520	2.3500	0.0020
150	1675	0.065	0.040	+0.0007	2.0760	1.8763	0.1997
180	1635	0.055	0.040	+0.0012	1.7200	1.6789	0.0411
210	1595	0.045	0.010	+0.0013	1.7040	1.6378	0.0662
240	1555	0.035	0.010	+0.0015	1.3000	1.3000	0
Δt min	ΔO H ₂ O	ΔO SiO ₂	ΔO C	ΣΔO H ₂ O	ΣΔO SiO ₂	ΣΔO C	
30	0.02725	0.25146	0.33250	0.02725	0.25146	0.33250	
60	0.01326	0.24575	0.16625	0.04051	0.49721	0.49875	
90	0.00708	0.24575	0.14630	0.04759	0.74296	0.64505	
120	0.00008	0.05715	0.09975	0.04767	0.80011	0.74480	
150	0.00851	0.04572	0.07980	0.05618	0.84583	0.82460	
180	0.00180	0.04572	0.07315	0.05798	0.89155	0.89775	
210	0.00270	0.01143	0.07315	0.06068	0.90298	0.97090	
240	0	0.01143	0.05985	0.06068	0.01441	1.03075	

Final Ingot Analysis

%C 0.035

%Si 1.27

%O 0.0031, 0.0035

Gas Samples Graphical Derivations		Melt 110 Pressure 3 mm Crucible 92% SiO ₂		N.T.P. Factor = 0.93			
Δt	Mass	CO ₁	CO ₂	ΔC	ΔSi	$\Delta V.T.$ N.T.P.	$\Delta V.H.$ N.T.P.
10	880	1.00	1.00	0.162	0.19	2.6663	0
20	880	1.00	1.00	0.162	0.19	2.6663	0
30	880	1.00	1.00	0.144	0.168	2.1976	0
40	880	1.00	1.00	0.134	0.156	2.1939	0
45	880	1.00	1.00	0.049	0.057	0.7440	0
Δt	ΔO H ₂ O	ΔO SiO ₂	ΔO C	$\Sigma \Delta O$ H ₂ O	$\Sigma \Delta O$ SiO ₂	$\Sigma \Delta O$ C	
10	0	0.21630	0.21600	0	0.21630	0.21600	
20	0	0.21630	0.21600	0	0.43260	0.43200	
30	0	0.17840	0.17830	0	0.61100	0.61030	
40	0	0.19150	0.19140	0	0.80250	0.80170	
45	0	0.6494	0.06491	0	0.86744	0.86661	

Metal Samples Graphical Derivations N.T.P. Factor=		Melt 99 Pressure 750 mm Crucible 92% SiO ₂			Initial % C= 0.935 Initial % Si= 0.100 Initial % O= 0.024		
Δt min	Mass gms	ΔC	ΔSi	ΔO	Δ V.T. N.T.P.	Δ VCO N.T.P.	Δ V.H. N.T.P.
30	2045	0.058	0.065	0.0098	2.4544	2.2143	0.2401
60	2015	0.058	0.065	0.0058	2.1712	2.1825	-
90	1995	0.058	0.065	0.0034	2.1712	2.1601	0.0111
120	1950	0.058	0.065	0.0008	2.1712	2.1158	0.0554
150	1900	0.058	0.065	0.0002	2.1712	2.0574	0.0138
180	1856	0.058	0.065	0	2.0768	2.0108	0.0660
210	1810	0.058	0.065	0	1.6992	1.9604	-
Δt min	ΔO H ₂ O	ΔO SiO ₂	ΔO C	Σ ΔO H ₂ O	Σ ΔO SiO ₂	Σ ΔO C	
30	0.00838	0.07430	0.07980	0.00838	0.07430	0.07980	
60	-	0.07430	0.07980	0.00838	0.14860	0.15960	
90	0.00040	0.07430	0.07980	0.00878	0.22290	0.23940	
120	0.00203	0.07430	0.07980	0.01081	0.29720	0.31920	
150	0.00052	0.07430	0.07980	0.01133	0.37150	0.39900	
180	0.00254	0.07430	0.07980	0.01387	0.44580	0.47880	
210	-	0.07430	0.07980	0.01387	0.52010	0.55860	

Metal Samples Graphical Derivations N.T.P. Factor= 0.026		Melt 106 Pressure 140 mm Crucible 92% SiO ₂			Initial % C= 0.16 Initial % Si= 0.10 Initial % O= 0.003		
Δt min	Mass gms	ΔC	ΔSi	ΔO	Δ V.T. N.T.P.	Δ VCO N.T.P.	Δ V.H. N.T.P.
30	1960	0.048	0.055	+0.0044	2.8304	1.7565	1.0739
60	1900	0.029	0.020	+0.0036	1.1693	1.0287	0.1046
90	1870	0.020	0.015	+0.0010	0.9744	0.6983	0.2761
120	1835	0.016	0.015	0	0.6867	0.5482	0.1385
150	1800	0.013	0.015	0	0.5104	0.4369	0.0735
180	1770	0.011	0.015	0	0.4362	0.3635	0.0727
Δt min	ΔO H ₂ O	ΔO SiO ₂	ΔO C	ΣΔO H ₂ O	ΣΔO SiO ₂	ΣΔO C	
30	0.039121	0.04472	0.06384	0.03912	0.04472	0.06384	
60	0.00393	0.00449	0.03857	0.04305	0.04921	0.10241	
90	0.00154	0.00176	0.02660	0.04459	0.05097	0.12901	
120	0.00539	0.00616	0.02128	0.04998	0.05713	0.15029	
150	0.00292	0.00334	0.01729	0.05290	0.06047	0.16758	
180	0.00293	0.00334	0.01462	0.05583	0.06381	0.18220	

%Si 0.36

%O 0.0121, 0.0139

Gas Samples Graphical Derivations		Melt 109 Pressure 3 mm Crucible 92% SiO ₂		N.T.P. Factor = 0.94			
Δt	Mass	CO ₁	CO ₂	ΔC	ΔSi	Δ V.T. N.T.P.	Δ V.H. N.T.P.
10	860	1.00	0.94	0.197	0.230	3.1678	0.006
20	860	0.94	0.88	0.061	0.066	1.0340	0.063
30	860	0.88	0.815	0.008	0.008	0.1510	0.019
60	860	0.815	0.63	0.010	0.009	0.197	0.038
70	860	0.63	0.57	0.002	0.008	0.047	0.018
80	860	0.57	0.51	0.0008	0.0016	0.024	0.011

Δt	ΔO H ₂ O	ΔO SiO ₂	ΔO C	ΔO H ₂ O	ΔO SiO ₂	ΔO C
10	0.00005	0.26304	0.26294	0.00005	0.26304	0.26294
20	0.00520	0.07548	0.08064	0.00525	0.33852	0.34358
30	0.00156	0.00942	0.01098	0.00681	0.34794	0.35456
60	0.00318	0.0100	0.01318	0.00999	0.35794	0.36774
70	0.00149	0.00914	0.00241	0.01148	0.36708	0.37015
80	0.00091	0.00018	0.00109	0.01239	0.36726	0.37124

TABLE 15. Comparison of oxygen balances carried out by 2.1. Flowmeasurement plus gas analysis and 2.2.

Metal sampling.

Melt No.	Crucible.	wt. % C I	P _{CO} (torr)	OXYGEN BALANCE.							
				Flow Measurement.				Metal Sampling.			
				$\Sigma \Delta O_{SiO_2}$ (wt. %)	$\Sigma \Delta O_C$ (wt. %)	$\Sigma \Delta O_{H_2O}$ (wt. %)	$\Sigma \Delta O_{SiO_2}$ (wt. %)	$\Sigma \Delta O_C$ (wt. %)	$\Sigma \Delta O_{H_2O}$ (wt. %)		
82	8SiO ₂	1.0	760	0.0361	0.0766	0.0414	0.0406	0.1330	0.0244		
51	-MgO	1.0	760	0.0489	0.0679	0.0187	0.0194	0.1064	-		
54		1.0	760	0.0316	0.0453	0.0109	0.0172	0.0519	0.0041		
53		1.0	76	0.1376	0.1658	0.0283	0.1074	0.1769	0.0170		
37		1.0	76	0.3609	0.3722	0.0111	0.1772	0.5281	0.0141		
90		1.0	3	0.3847	0.3845	0	-	-	-		
19		0.1	760	0.0129	0.0403	0.0276	0	0.0305	0.0353		
76		0.1	3	0.0647	0.0797	0.0264	0.0708	0.0778	0.0281		
59	37SiO ₂	1.0	760	0.2126	0.2351	0.0226	0.2172	0.2848	0.0201		
67	-Al ₂ O ₃	1.0	760	0.3052	0.3325	0.0302	0.2618	0.3251	0.0190		
62		1.0	760	0.3395	0.3436	0.0041	0.3716	0.4389	0.0477		
68		1.0	76	0.3339	0.3513	0.0175	0.3109	0.3471	0.0234		

OXYGEN BALANCE.

Flow Measurement.

Metal Sampling.

P_{CO}
(torr)

wt. % C_I

Crucible.

Melt No.

$\Sigma \Delta^{0}_{SiO_2}$
(wt. %)

$\Sigma \Delta^{0}_{C}$
(wt. %)

$\Sigma \Delta^{0}_{H_2O}$
(wt. %)

$\Sigma \Delta^{0}_{SiO_2}$
(wt. %)

$\Sigma \Delta^{0}_{C}$
(wt. %)

$\Sigma \Delta^{0}_{H_2O}$
(wt. %)

57	0.1	760	0.0009	0.0040	0.0083	0.0120	0.0201	0.0009
61	0.1	76	0.0646	0.0861	0.0221	0.0515	0.0598	0.0419
52	1.0	760	0.1545	0.1624	0.0100	0.1875	0.2527	0.0048
49	0.1	760	0.0199	0.0251	0.0049	0.0267	0.0210	0.0116
27	0.1	76	0.0168	0.0416	0.0288	0	0.0352	0.0349
85	1.0	760	0.0618	0.0960	0.0366	0.0629	0.1064	0.0261
84	1.0	76	0.1433	0.1762	0.0457	0.1349	0.2593	0.1588
71	0.1	3	0.0833	0.0981	0.0236	0.0515	0.0864	0.0263
99	1.0	760	0.4663	0.5072	0.0411	0.5457	0.5586	0.0139
100	1.0	140	1.1006	1.1206	0.0206	0.9163	1.0773	0.0625
101	0.1	760	0.0186	0.0526	0.0340	0.0852	0.0732	0.0134

TABLE 16. Analysis of deposit with melts in magnesia crucibles.

Melt No.	%C	torr.	Crucible.	Chemical Analysis of Deposit.										X-Ray phases present.			
				%SiO ₂	%MgO	%Al ₂ O ₃	%C	%MnO	%FeO	%Fe	%Fe ₂ O ₃	MgO/C ratio.	Melt No.	Major	Minor.		
40	1.00	760	90%MgO	N.D.	N.D.	N.D.	0.60	N.D.	N.D.	N.D.	N.D.	N.D.	N.D.	-	M.30	MgO(periclase)	unable
50	1.00	76	"	2.40	33.89	1.34	N.D.	0.22	59.50	N.D.	N.D.	N.D.	2.49	-		α Fe	determi
30	1.00	76	"	0.20	47.20	0.30	N.D.	1.00	N.D.	N.D.	N.D.	N.D.	N.D.	-		MgO.Fe ₂ O ₃ (spinel)	
53	1.00	76	"	2.10	23.26	Nil	4.70	N.D.	N.D.	N.D.	69.7	N.D.	N.D.	4.96			
90	1.00	3	"	0.90	N.D.	N.D.	N.D.	N.D.	N.D.	N.D.	N.D.	N.D.	0.57	-			
77	1.00	3	"	0.08	16.44	1.00	4.74	Trace	N.D.	N.D.	71.00	N.D.	N.D.	3.47	M.77	α Fe	trace
76	0.10	3	"	4.50	5.50	0.11	N.D.	Trace	88.85	N.D.	N.D.	0.85	-		MgO		trace
94	1.00	3	97%MgO	0.20	34.50	0.33	14.18	17.11	N.D.	N.D.	N.D.	33.44	2.43		M.94	α Fe	trace
96*	1.00	3	"	0.02	8.25	Trace	4.47	0.37	N.D.	83.00	N.D.	N.D.	1.85				
97	0.10	3	"	2.60	4.20	0.08	0.55	Trace	N.D.	N.D.	89.20	N.D.	7.64			MgO	
98*	0.10	3	"	2.30	4.06	0.08	0.88	Trace	N.D.	N.D.	90.40	N.D.	4.61				

* ½ Ferrostatic Head.

Average MgO/C ratio = 4.09

TABLE 17. Dissociation rates for magnesia.

Melt No.	Crucible.	Initial %C	Pressure (torr)	Average w/o Oxygen.	V _{CO MgO} (litres)	Δt (mins)	Rate of oxygen transfer from magnesia (\dot{n}_O /sq.cm/sec)
37	92%MgO	1.0	76	0.00165	7.565	150	1.87×10^{-7}
90	92%MgO	1.0	3	0.0018	9.485	240	1.47×10^{-7}
82	92%MgO	1.0	760	0.0022	1.949	150	0.48×10^{-7}
94	97%MgO	1.0	3	0.0014	8.296	210	1.47×10^{-7}
96*	97%MgO	1.0	3	0.0019	3.848	210	1.10×10^{-7}

* Height of metal in crucible was reduced by 50% giving $A_R = 124 \text{ cm}^2$.

TABLE 18.

Contribution of oxygen from silica and
water in 8%SiO₂-MgO crucibles in 200 mins.

Melt No.	W/O _C _I	P _{CO} torr	Static [O ₂] ^{W/O}	ΣΔO _{SiO₂} (wt.%)	ΣΔO _{H₂O} (wt.%)	ΣΔO _C (wt.%)
51	1.0	760	0.0022	0.019	N.D.	0.093
40	1.0	760	0.0020	N.D.	N.D.	0.106
37	1.0	76	0.0016	0.168	0.017	0.479
94	1.0	3	0.0014	0.103	0.016	0.293
96	1.0	3	0.0019	0.114	0.012	0.322
82	1.0	760	0.0022	0.041	0.012	0.120
90	1.0	3	0.0018	0.222	N.D.	0.395
76	0.1	3	0.0020	0.071	0.024	0.076
55	0.1	76	0.0037	0.030	0.022	0.069
97	0.1	3	0.010	0.011	0.004	0.048
19	0.1	760	0.012	0	0.055	0.036
18	0.1	76	0.0024	0.057	0.033	0.091

TABLE 19. Dissociation rates for alumina.

Melt No.	Crucible.	Pressure and Initial Carbon Content %.	Aluminium Content at end of melt %.	$V_{CO}^{Al_2O_3}$ (litres)	Rate of oxygen transfer (Based on Al pickup.)	Rate of oxygen transfer (Based on $V_{CO}^{Al_2O_3}$) $\times 10^{-8}$
62	37SiO ₂ -	76 mm, 1.0	0.019	1.32	0.96	5.0
68	63Al ₂ O ₃	76 mm, 1.0	0.025	0.66	1.2	1.65
87	- " -	3 mm, 1.0	0.105	-	4.8	
65	7SiO ₂ -	76 mm, 1.0	0.064	4.27	3.15	6.6
84	93Al ₂ O ₃	76 mm, 1.0	0.050	3.84	2.4	5.3
78	- " -	3 mm, 1.0	0.175	-		
88	- " -	3 mm, 1.0	0.130	4.84	4.8	6.7

TABLE 20. Contribution of oxygen from silica and water in aluminosilicate crucibles in 200 mins.

Melt No.	wt. % G I	P _{CO} (torr)	Static [O] _M (wt. %)	Crucible.	ΣΔO _{SiO₂} (wt. %)	ΣΔO _{H₂O} (wt. %)	ΣΔO _C (wt. %)
67	1.0	760	0.0025	37SiO ₂	0.246	0.019	0.305
62	1.0	76		-Al ₂ O ₃	0.343	0.033	0.426
68	1.0	76	0.00075		0.300	0.023	0.321
57	0.1	760	0.020		0.012	0.013	0.020
61	0.1	76	0.010		0.052	0.042	0.060
79	0.1	3	0.005		0.093	0.021	0.122
59	1.0	760	0.002		0.208	0.006	0.280
44	1.0	76	0.0010	56SiO ₂	0.337	0.0199	0.329
41	1.0	760	0.0025	-Al ₂ O ₃	0.160	N.D.	0.230
52	1.0	760	0.0030		0.173	0.005	0.233
49	0.1	760	0.0173		0.026	0.007	0.020
45	0.1	76	0.006		0.109	0.007	0.142
48	0.1	76	0.0055		0.123	0.029	0.119
27	0.1	76	0.0115		0	0.032	0.035

Melt No.	wt. % C _I	P _{CO} (torr)	Static [O _M] (wt. %)	Crucible.	$\Sigma \Delta O_{SiO_2}$ (wt. %)	$\Sigma \Delta O_{H_2O}$ (wt. %)	$\Sigma \Delta O_C$ (wt. %)
63	1.0	760	0.0020	7SiO ₂	0.062	0.029	0.113
85	1.0	760	0.0020	-Al ₂ O ₃	0.063	0.025	0.093
84	1.0	76	0.0013		0.120	N.D.	0.246
65	1.0	76			0.086	N.D.	0.255
64	0.1	760	0.021		0	0.040	0
66	0.1	76	0.0032		0.074	0.035	0.106
83	0.1	76	0.0039		0.079	0.035	0.128
71	0.1	3	0.0007		0.052	0.021	0.086

TABLE 21. Analysis of scrapings from crucible wall after melt.

Melt No.	Pressure (torr)	wt. % Finish.	wt. % Finish x 10 ⁻³	Crucible Wall Scrapings (Analysis by wt.)					Surface Loss % SiO ₂	Crucible	
				%Fe	%FeO	%Fe ₂ O ₃	%SiO ₂	%Al ₂ O ₃			%MgO
41	760	0.689	2.50	25.81	7.97	-	16.20	75.97	N.D.	70.80	56%SiO ₂
44	76	0.670	1.00	14.59	6.17	-	3.66	89.67	N.D.	93.50	43%Al ₂ O ₃
89	3	0.250	1.20	N.D.	N.D.	1.57	4.40	92.75	N.D.	92.10	
49	760	0.119	19.00	0.47	8.36	-	45.44	37.33	N.D.	18.90	
45	76	0.019	10.00	38.87	9.32	-	18.60	57.91	N.D.	60.80	
67	760	0.685	2.50	N.D.	4.05	0.29	6.25	87.87	N.D.	83.10	37%SiO ₂
68	76	0.699	0.75	N.D.	1.54	0	2.10	95.10	N.D.	94.30	61%Al ₂ O ₃
57	760	0.104	26.00	N.D.	5.02	0	32.20	59.59	N.D.	11.30	
61	76	0.045	12.50	N.D.	3.62	0	30.00	63.71	N.D.	18.90	
79	3	0.010	6.00	N.D.	2.19	0	21.70	71.74	N.D.	41.30	
63	760	0.980	2.00	N.D.	1.11	0.14	1.50	97.05	N.D.	78.60	7.0%SiO ₂
84	76	0.830	3.00	N.D.	0.20	0.36	1.40	-	N.D.	80.0	33.0%Al ₂ O ₃
88	3	0.64	0.70	5.96	-	0.31	4.50	94.70	N.D.	35.70	
78	3	0.82	N.D.	N.D.	0.13	0.14	1.40	98.20	N.D.	80.00	After 2 only.

Melt No.	Pressure (torr)	wt. % C Finish.	wt. % Fe Finish x 10 ⁻³	Crucible Wall Scrapings (Analysis by wt.)						Surface Loss % SiO ₂	Crucible
				%Fe	%FeO	%Fe ₂ O ₃	%SiO ₂	%Al ₂ O ₃	%MgO		
64	760	0.110	2.10	N.D.	0.95	0.09	4.10	94.55	N.D.	41.40	
66	76	0.050	3.20	N.D.	0.26	0.13	1.70	97.70	N.D.	75.70	
71	3	0.030	1.00	N.D.	0.36	0.13	3.10	96.30	N.D.	55.770	
82	760	0.965	2.45	N.D.	-	1.28	3.40	-	-	57.50	8.0%SiO ₂
37	76	0.453	2.00	2.32	1.60	0	1.18	-	98.00	85.20	90%MgO
90	3	0.525	1.80	N.D.	-	0.57	0.90	N.D.	-	88.70	
19	760	0.117	12.40	N.D.	1.50	-	8.00	-	89.80	0	
18	76	0.044	3.30	6.25	4.82	-	2.80	-	92.00	65.00	
76	3	0.028	3.00	N.D.	1.39	0.29	4.00	-	-	50.00	
99	76	0.51	4.00	-	1.29	Nil	88.10	5.18	N.D.	6.29	92.0%SiO ₂
101	760	0.086	27.40	-	2.06	0.29	88.80	3.84	N.D.	3.48	
109	3	< 0.01	13.00	-	0.86	0.04	90.44	3.68	N.D.	1.70	

TABLE 22. Diffractometer Analysis of Crucible sections after melting.

Four samples of refractory material were vacuum mounted in araldite and polished. They were then examined on the Philips 1310 diffractometer. The samples were then re-polished and 20 thous. removed from the surface, they were re-examined and repolished repeatedly until a total of 100 thous. had been removed. The results were as follows:-

Sample		Phases Present.
No.41. 56%SiO ₂ -Al ₂ O ₃ 1.00%C @ 760 mm	Surface.	Major phases, alumina and α iron. Minor phase mullite.
	20 Thous. below surface.	Alumina, iron and mullite in fairly equal proportions.
	40 Thous. below surface.	Major phase mullite- some alumina and α iron may be present.
No.44. 56%SiO ₂ -Al ₂ O ₃ 1.00°C @ 76 mm	Surface.	Major phase alumina, minor phase α iron.
	10 thou. below surface.	Major phase alumina, minor phase mullite and α iron.
	20 thou. below surface.	Approx. equal quantities of mullite, alumina and α iron.
	40 thou. below surface.	Major phase mullite, minor phase α iron, possible trace alumina.
	60 thou. below surface.	Major phase mullite, small quantity α iron.
80 thou. below surface.	Major phase mullite, even less α iron.	
No.57. 37%SiO ₂ -Al ₂ O ₃ 0.10%C 760 mm.	Surface.	Only mullite detected, but alumina could be present - as results were very poor.
	20 thou. below surface.	Almost pure mullite with trace alumina and small quantity α iron.
	40 thou. below surface.	- ditto -

	60 thou. below surface.	Almost pure mullite, trace alumina.
	80 thou. below surface.	Almost pure mullite, possible trace alumina.
	100 thou. below surface.	Pure mullite.
No.68. 37%SiO ₂ -Al ₂ O ₃ 1.00%C 76 mm	Surface.	Alumina + slight trace α iron.
	20 thou. below surface.	- ditto -
	40 thou. below surface.	Major phase alumina and α iron trace mullite.
	60 thou. below surface.	Major phase mullite and alumina, minor phase α iron.
	80 thou. below surface.	Major phase mullite, minor phase alumina, α iron.
	100 thou. below surface.	Major phase, mullite, minor phase alumina, trace α iron.

TABLE 23. Relationship between wt. % silica in crucible surface layer and calculated $\% \text{SiO}_2$

Crucible & Melt No.	Final [%Si _M]	Final [%O _M]	a _{SiO₂} cal'd from Eq. 33.	Analysed %SiO ₂ in surface layer.	mole fraction SiO ₂ †	%SiO ₂ Loss
MAG 82 ^E	0.05	0.0024	0.0115	3.4	0.023	57.5
37	0.21	0.0020	0.0336	1.18 ^{u53}		85.2
90	0.195 [*]	0.0018 [*]		0.9	0.006	88.7
19 ^E	< .005	0.0124	0.0307	8.0 [⊙]	0.055	0
18 ^E	0.06	0.0033	0.0264	2.8	0.019	65.0
76 ^E	0.085	0.0030	0.0306	4.0	0.027	50.0
P 67	0.28	0.0025	0.07	6.25	0.102	83.1
68	0.355	0.00075	0.0079	2.1	0.035	94.3
87	0.445 [*]	0.00070 [*]		4.2 ?		
57 ^E	0.04	0.026	1.08	32.8	0.456	11.3
61 ^E	0.085	0.0125	0.528	30.0	0.421	18.9
79 ^E	0.165	0.006	0.237	21.7	0.319	41.3
M 89	0.66	0.0012	0.038	4.4	0.074	92.1
44	0.42	0.0010	0.017	3.66	0.062	93.5

E denotes an approach to equilibrium as shown by $\frac{d\text{Si}}{dt} \rightarrow 0$

^u analysis from similar melt.

† mole fraction calc'd on assumption that final surface is composed solely of (SiO₂ + Al₂O₃) or (SiO₂ + MgO)³

⊙ No analysis - since no measurable reaction assumed no loss.

* ingot analysis only.

? queried result.

Crucible & Melt No.	Final [%Si _M]	Final [%O _M]	a _{SiO₂} from Eq. 33.	Analysed %SiO ₂ in surface layer.	mole fraction SiO ₂	%SiO ₂ Loss
41	0.28	0.0025	0.07	16.2	0.251	70.8
86 ^E	0.29 [*]	0.020 [*]	4.64			
45 ^E	0.135	0.010	0.54	41.4 ^R 48	0.2	26.1
49 ^E	0.06	0.019	0.868	45.4	0.591	18.9
HS 63 ^E	0.08	0.002	0.0128	1.5	0.0252	72.6
84	0.16	0.003 [*]		1.4 ^R 65	0.042	80.0
88	0.145 [*]	0.0007 [*]		4.5 ?	0.067	35.7
64 ^E	0.018	0.021	0.31	4.1	0.067	41.4
66 ^E	0.095	0.0032	0.039	1.7	0.028	75.7
71 ^E	0.08	0.0010	0.0032	3.1	0.051	55.7

TABLE 24. Effect of melt oxygen content on the total silicon transfer and the calculated thickness of eroded silica.

Melt No.	Crucible.	Static oxygen content (wt. % x 10 ⁻³)	Final silicon content w/o	Total silicon transfer (moles/unit area of silica) x 10 ⁻³	Calculated thickness of eroded silica -- w (cms)
90	8%SiO ₂	1.8	0.195	15.3	-
37	92%MgO	1.65	0.21	16.5	-
82	(N _{SiO₂} = .055)	2.20	0.05	3.93	-
76		2.00	0.085	6.68	-
18		2.45	0.06	4.72	-
19		12.4	<.005	0.39	-
88	7%SiO ₂	0.70	0.145	4.31	0.117
84	93%Al ₂ O ₃	1.30	0.16	4.76	0.129
63	(N _{SiO₂} = .12)	2.00	0.08	2.38	0.065
71		0.70	0.08	2.38	0.065
66		3.20	0.095	2.83	0.077
64		21.00	0.018	0.54	0.015
87	37%SiO ₂	0.70	0.445	3.18	0.086
68	93%Al ₂ O ₃	0.75	0.355	2.54	0.069
67	(N _{SiO₂} = .5)	2.50	0.280	1.99	0.054

X

Melt No.	Crucible.	Static oxygen content (wt.% x 10 ⁻³)	Final silicon content ^{w/o}	Total silicon transfer (moles/unit area of silica) x 10 ⁻³	Calculated thickness of eroded silica - w (cms)
79		5.00	0.165	1.18	0.032
61		10.00	0.085	0.61	0.016
57		20.00	0.04	0.29	0.008
89	56%SiO ₂	1.20	0.66	3.41	0.093
44	44%Al ₂ O ₃	1.00	0.42	2.17	0.059
41	(N _{SiO₂} = .69)	2.50	0.28	1.45	0.039
86		-	0.29	1.50	0.041
45		6.00	0.135	0.70	0.019
49		17.30	0.06	0.31	0.008
100	95%SiO ₂ 5%Al ₂ O ₃ (N _{SiO₂} = 1)	2.20	1.02	3.64	-
99		4.00	0.54	1.93	-
106		6.60	0.26	0.93	-
101		20.00	0.082	0.29	-

TABLE 25.

Effect of melt oxygen content on the specific rate of silicon transfer at t = 600s.

Melt No.	Crucible.	Rate of Silicon Pick-up @ t=600s(\dot{n}_{Si} /sq.cm.silica/ sec) x 10^{-7}	Oxygen Content @ t=600s(ppm)
82	8SiO ₂ 92MgO	4.54	24.5
37	"	17.50	16.5
90	"	-	-
19	"	too low to measure.	124
18	"	6.50	25.0
76	"	9.70	11.0
63	7SiO ₂ 93Al ₂ O ₃	1.79	26.0
84	"	5.94	13.0
88	"	-	-
64	"	too low to measure	210
66	"	3.86	29.0
71	"	1.78	35.0
67	37SiO ₂ 63Al ₂ O ₃	3.07	31.0
68	"	2.22	7.5
87	"	2.14	6.5
57	"	0.072	200
61	"	1.43	100
79	"	1.50	50
41	56SiO ₂ 44Al ₂ O ₃	1.34	25.0
44	"	2.85	10.0
89	"	2.85	12.0
49	"	0.257	210
45	"	1.34	80
86	"	0.88	19.6

100	$95\text{SiO}_2 \cdot 5\text{Al}_2\text{O}_3$	3.86	55
99		1.25	170
106		1.19	66
101		0.205	225

TABLE 26. Rates of silicon transfer calculated by various models at t = 600s.

Melt No.	Crucible.	Bulk [Si] at t = 600s (w/o)	Bulk [O] at t = 600s (w/o)	Measured transfer rate for silicon (w/o/s) x 10 ⁻⁵	Rates of silicon transfer calculated by various models (w/o /s x 10 ⁻⁵)				
					Model I (a)	Model I (b)	Model II	Model III	Model IV
82	8SiO ₂ -	.0125	.00245	0.7	0.55	1.61	2.58	2.02	-
37	MgO	.08	.00165	2.7	0.21	0.66	0.79	0.78	-
19		<.005	.0124	0	0.87	-	1.34	0.61	-
18		.015	.0025	1.0	0.49	1.48	2.26	1.85	-
76		.04	.0011	1.5	0.31	0.84	1.53	1.44	-
63	7SiO ₂ -	.020	.0026	0.6	0.63	1.54	3.08	2.56	1.61
84	Al ₂ O ₃	.060	.0013	2.0	0.37	1.10	1.84	1.77	1.16
64		.020	.021	0	0.63	-	0	0	0.14
66		.0375	.0029	1.3	0.46	1.19	1.92	1.78	1.26
71		.045	.0035	0.6	0.45	0.88	1.49	1.39	1.11
67	37SiO ₂ -	.05	.0031	4.3	0.83	3.86	4.07	3.65	3.76
68	Al ₂ O ₃	.1275	.00075	3.1	0.52	2.41	2.93	2.85	2.94
87		.17	.00065	3.0	0.45	1.96	2.53	2.49	2.57
57		.02	.020	0.1	1.31	1.13	1.59	1.08	1.19

Melt No.	Crucible.	Bulk[Si] at t = 600s (w/o)	Bulk[O] at t = 600s (w/o)	Measured transfer rate for silicon (w/o/s) x 10 ⁻⁵	Rates of silicon transfer calculated by various models (w/o / s x 10 ⁻⁵)				
					Model I (a)	Model I (b)	Model II	Model III	Model IV
61		.03	.010	2.0	1.06	0.76	3.33	2.67	2.79
79		.097	.005	2.1	0.59	0.65	2.02	1.94	2.03
41	56SiO ₂ -	.087	.0025	2.6	0.73	3.95	3.69	3.48	3.52
44	Al ₂ O ₃	.103	.001	5.5	0.68	3.25	3.83	3.67	3.71
89		.04	.0012	5.5	1.08	4.64	6.25	5.33	5.37
49		.04	.021	0.5	1.08	0.37	0	0	0.56
45		.06	.008	2.6	0.88	0.97	2.86	2.58	2.62
99	92SiO ₂ -	.123	.017	3.5				0	0
100	Al ₂ O ₃	.237	.0055	10.8				1.49	1.49
110		.760	.0045	18.7				0.39	0.39
101		.036	.0225	0.57				0.99	0.99
106		.167	.0066	3.3				1.75	1.75
109		.267	.0047	13.3				1.57	1.57

TABLE 27.

Effect of calculated gas/metal interfacial area on the total rate of silicon transfer.

Melt No.	Crucible.	$\left[\frac{O_R}{W}\right] \times 10^{-3}$	$\left[\frac{O_M}{W}\right] \times 10^{-3}$	$\left[\frac{O}{W}\right] \times 10^{-3}$	Gas/metal interfacial area $A_g(\text{cm}^2)$	measured total rate of silicon transfer ($\dot{V}_{Si}/\text{sec.} \times 10^{-5}$)
82	8SiO ₂ -	4.01	2.45	2.06	183	0.499
37	92MgO	7.68	1.65	0.24	198	1.93
18		4.73	2.50	1.95	187	0.714
76		4.44	1.10	0.11	156	1.07
67	37SiO ₂ -	12.68	3.10	2.39	623	3.07
68	63Al ₂ O ₃	7.66	0.75	0.23	616	2.21
87		7.34	0.65	0.012	484	2.14
57		20.22	20.00	19.64	3	0.071
61		14.46	10.0	2.53	27	1.43
79		9.68	5.0	0.099	44	1.49
63	7SiO ₂ -	3.94	2.60	2.07	117	0.428
84	93Al ₂ O ₃	5.76	1.30	0.21	188	1.43
66		5.80	2.90	1.82	135	0.928
71		4.84	3.50	0.11	94	0.428
41	56SiO ₂	8.30	2.50	2.3	1340	1.86
44	-44Al ₂ O ₃	13.26	1.00	0.24	743	3.93
89		13.46	1.20	0.0099	475	3.93
49		22.11	21.0	16.4	11	0.357
45		13.80	8.0	1.36	44	1.36

TABLE 28. Theoretical oxygen transfer rates from silica and mullite.

Melt No.	Crucible.	Static Oxygen (wt.%)	Transfer rates calculated from Model IV			Measured specific transfer rate fr crucible. (\dot{n}_0 /sq crucible/s $\times 10^{-7}$)
			Specific transfer rate from silica (\dot{n}_0 /sq.cm.SiO ₂ /s $\times 10^{-7}$)	Specific transfer rate from mullite (\dot{n}_0 /sq.cm.mullite/ s $\times 10^{-7}$)	Specific transfer rate from crucible (\dot{n}_0 /sq.cm.crucible/s $\times 10^{-7}$)	
67	37SiO ₂	.0031	3.86	2.38	2.69	3.07
68	-Al ₂ O ₃	.00075	2.96	1.88	2.10	2.21
87		.00065	2.59	1.64	1.84	2.14
57		.020	2.24	0.46	0.85	0.07
61		.010	3.32	1.64	1.99	1.43
79		.005	2.39	1.19	1.45	1.50
41	56SiO ₂	.0025	3.12	1.87	2.51	1.86
44	-Al ₂ O ₃	.0010	3.21	2.04	2.65	3.93
89		.0012	4.58	3.04	3.83	3.93
49		.021	0.74	0	0.39	0.36
45		.008	2.54	1.11	1.83	1.86
63	7SiO ₂	.0026	-	1.76	1.15	0.43
84	-Al ₂ O ₃	.0013	-	1.28	0.83	1.43
64		.021	-	0.15	0.09	0

Melt No.	Crucible.	Static Oxygen (wt.%)	Transfer rates calculated from Model IV			Measured specific transfer rate crucible/s x 10 ¹⁰
			Specific transfer rate from silica (\dot{n}_0 /sq.cm.SiO ₂ /s x 10 ⁻⁷)	Specific transfer rate from mullite (\dot{n}_0 /sq.cm.mullite/ \bar{s} x 10 ⁻⁷)	Specific transfer rate from crucible (\dot{n}_0 /sq.cm.crucible/S.crucible. (\dot{n}_0 x 10 ⁻⁷))	
66		.0029	-	1.38	0.89	0.93
71		.0035	-	1.21	0.79	0.43

TABLE 29. Effect of change of a_{SiO_2} on driving force for diffusion and rate of transfer.

No.	Crucible.	Assumed a_{SiO_2}	time t (s)	Rate of SiO_2 pickup, wt/o/sec $\times 10^{-5}$	\dot{n}_{Si} Si/sec $\times 10^{-5}$	[Si _M] w/o	[Si _R] w/o	[O _M] w/o	Calculation of oxygen gradients by method B.		Calculation of oxygen gradient by method A.	
									$\frac{[\text{O}_R]}{w/o}$	$\frac{(\text{O}_R - \text{O}_M)}{w/o}$	$\frac{[\text{O}_R]}{w/o}$	$\frac{(\text{O}_R - \text{O}_M)}{w/o}$
82	8SiO ₂ -	0.055	600	0.7	0.499	0.0125	0.0262	0.0025	0.0072	0.0047	0.0040	0.0016
37	92MgO			2.7	1.93	0.08	0.1326	0.0016	0.00316	0.00156	0.0077	0.0060
19				0	0	<0.005	0.005	0.0124	0.0166	0.0042	0.0124	0
18				1.0	0.714	0.015	0.0345	0.0025	0.0062	0.0037	0.0047	0.0022
76				1.5	1.07	0.04	0.0693	0.0011	0.0044	0.0033	0.0044	0.0033
82			6000	0.3	0.214	0.0425	0.0484	0.00225	0.0053	0.0030	0.0029	0.00067
37				0.9	0.643	0.17	0.1875	0.00165	0.0026	0.0009	0.0037	0.0020
19				0	0	<0.005	0.005	0.0124	0.0166	0.0042	0.0124	0
18				0.4	0.286	0.055	0.0628	0.0037	0.0046	0.0009	0.0046	0.00089
76				0.3	0.214	0.035	0.0908	0.00156	0.0039	0.0023	0.0022	0.00067
82			12000	0	0	0.05	0.05	0.0020	0.0052	0.0032	0.002	0
37				0.3	0.214	0.203	0.208	0.0016	0.0025	0.0009	0.0023	0.0007
19				0	0	<0.005	0.005	0.0122	0.0166	0.0044	0.0122	0
18				0	0	0.065	0.065	0.0037	0.0046	0.0009	0.0037	0

No.	Crucible.	Assumed a_{SiO_2}	time t (s)	Rate of silicon pickup.		$[Si_M]$ w/o	$[Si_R]$ w/o	$[O_M]$ w/o	Calculation of oxygen gradient by method B		Calculation of oxygen gradient by method A.	
				wt/o/sec $\times 10^{-5}$	$\dot{M}_{Si}/sec \times 10^{-5}$				$[O_R]$ w/o	$(O_R - O_M)$ w/o	$[O_R]$ w/o	$(O_R - 0)$ w/o
76			0	0	0.085	0.085	0.0028	0.004	0.0012	0.0028	0	
63	7SiO ₂	0.12	600	0.6	0.02	0.0317	0.0026	0.0097	0.0071	0.00394	0.0013	
84	93Al ₂ O ₃			2.0	0.06	0.099	0.0013	0.0055	0.0042	0.00576	0.0045	
64				0	0.02	0.02	0.021	0.0122	-0.0087	0.021	0	
66				1.3	0.037	0.0628	0.0029	0.0068	0.0039	0.0053	0.0029	
71				0.6	0.045	0.0567	0.0035	0.0072	0.0037	0.0043	0.0013	
63			6000	0.6	0.0575	0.0692	0.0020	0.0066	0.0046	0.0033	0.0013	
84				0.5	0.1275	0.1372	0.0013	0.0045	0.0032	0.0024	0.0011	
64				0	0.02	0.02	0.021	0.0122	-0.0087	0.021	0	
66				0.5	0.085	0.0948	0.0032	0.0056	0.0024	0.0043	0.0011	
71				0.2	0.076	0.0799	0.0007	0.0061	0.0054	0.0011	0.0004	
63			12000	0.1	0.0725	0.0744	0.0020	0.0063	0.0043	0.0022	0.0002	
84				0.028	0.15	0.1505	0.0013	0.0044	0.0031	0.0014	0.0000	
64				0	0.02	0.02	0.021	0.0122	-0.0087	0.021	0	
66				0	0.095	0.095	0.0034	0.0056	0.0022	0.0034	0	

No.	Crucible.	Assumed a_{SiO_2}	time t (s)	Rate of silicon pickup.		$[\text{Si}_M]$ w/o	$[\text{Si}_R]$ w/o	$[\text{O}_M]$ w/o	Calculation of oxygen gradient by method B.		Calculation of oxygen gradient by method A.	
				$\frac{\text{wt}/\text{o}/\text{sec}}{\times 10^{-5}}$	$\dot{m}_{\text{Si}}/\text{sec} \times 10^{-5}$				$[\text{O}_R]$ w/o	$(\text{O}_R - \text{O}_M)$ w/o	$[\text{O}_R]$ w/o	$(\text{O}_R - \text{O}_M)$ w/o
71				0	0	0.08	0.08	0.0007	0.0061	0.0054	0.0007	0
67	37SiO ₂	0.50	600	4.3	3.07	0.05	0.1338	0.0031	0.0096	0.0065	0.0127	0.0096
68	63Al ₂ O ₃			3.1	2.21	0.1275	0.1879	0.00075	0.0081	0.0074	0.0077	0.0069
87				3.0	2.14	0.17	0.2285	0.00065	0.0073	0.0067	0.0073	0.0067
57				0.1	0.071	0.02	0.0219	0.020	0.0238	0.0038	0.0202	0.0002
61				2.0	1.43	0.03	0.069	0.010	0.0134	0.0034	0.0145	0.0045
79				2.1	1.49	0.097	0.1385	0.005	0.0095	0.0045	0.0097	0.0047
67			6000	1.3	.929	0.165	0.1903	0.0025	0.0031	0.0056	0.0053	0.0028
68				1.3	.929	0.24	0.2653	0.00075	0.0069	0.0061	0.0037	0.0029
87				1.6	1.14	0.285	0.3162	0.00065	0.0062	0.0056	0.0042	0.0036
57				0.1	.071	0.025	0.0269	0.0228	0.0215	-0.0013	0.023	0.0002
61				0.1	.071	0.075	0.0769	0.010	0.0127	0.0027	0.010	0.0002
79				0.3	.214	0.16	0.1653	0.005	0.0037	0.0037	0.0057	0.0007
67			12000	1.07	.764	0.235	0.2508	0.0025	0.0070	0.0045	0.0049	0.0024
68				1.00	.714	0.305	0.3245	0.0007	0.0062	0.0055	0.0029	0.0022
87				1.50	1.07	0.325	0.3542	0.0007	0.0059	0.0052	0.010	0.0032

No.	Crucible.	Assumed a_{SiO_2}	time t (s)	Rate of silicon pickup.		$[Si_M]$ w/o	$[Si_R]$ w/o	$[O_M]$ w/o	Calculation of oxygen gradient by method B.		Calculation of oxygen gradient by method A.	
				wt/o/sec $\times 10^{-5}$	\dot{n}_{Si}/sec $\times 10^{-5}$				$[O_R]$ w/o	$(O_R - O_M)$ w/o	$[O_R]$ w/o	$(O_R - O_M)$ w/o
57				0.10	.071	0.032	0.0339	0.024	0.0192	-0.0048	0.024	0.00022
61				0	0	0.075	0.0750	0.010	0.0129	0.0029	0.010	0
79				0	0	0.165	0.1650	0.005	0.0087	0.0037	0.005	0
41	56SiO ₂	0.69	600	2.6	1.86	0.0875	0.1382	0.0025	0.0111	0.0086	0.0083	0.0058
44	-44Al ₂ O ₃			5.5	3.93	0.1025	0.2097	0.0010	0.0091	0.0081	0.0133	0.0123
89				5.5	3.93	0.040	0.1473	0.0012	0.0108	0.0096	0.0135	0.0123
49				0.5	0.36	0.040	0.0497	0.021	0.0186	-0.0024	0.0221	0.0011
45				2.6	1.86	0.060	0.1107	0.008	0.1107	0.0044	0.0138	0.0053
41			6000	1.2	0.86	0.1350	0.2084	0.0025	0.0091	0.0066	0.0052	0.0027
44				2.7	1.93	0.2425	0.2976	0.0010	0.0075	0.0065	0.0070	0.0060
89				5.3	3.78	0.3250	0.4283	0.0012	0.0063	0.0051	0.0130	0.0118
49				0.1	0.071	0.0575	0.0595	0.0180	0.0170	-0.001	0.0132	0.0002
45				0.2	0.143	0.0800	0.0839	0.0080	0.0143	0.0063	0.0159	0.00045
41			12000	0.6	0.429	0.24	0.2517	0.0025	0.0082	0.0057	0.0038	0.0013
44				0.6	0.429	0.393	0.4042	0.0010	0.0065	0.0055	0.0023	0.0013
89				3.3	2.36	0.570	0.6344	0.0012	0.0051	0.0039	0.0086	0.0074

No.	Crucible.	Assumed $\% \text{SiO}_2$	time t (s)	Rate of silicon pickup.		$[\text{Si}_M]$ w/o	$[\text{Si}_R]$ w/o	$[\text{O}_M]$ w/o	Calculation of oxygen gradient by method B.		Calculation of oxygen gradient by method A.	
				wt/o/sec $\times 10^{-5}$	\dot{m} Si/sec $\times 10^{-5}$				$[\text{O}_R]$ w/o	$(\text{O}_R - \text{O}_M)$ w/o	$[\text{O}_R]$ w/o	$(\text{O}_R - \text{O}_M)$ w/o
49	56SiO ₂	.69	12000	.005	.0036	.06	.06	.017	-.0001	.017	0	
45	-44AL ₂ O ₃			0	0	.135	.135	.010	.0013	.010	0	
100	95SiO ₂	1.0	600	10.83	7.73	0.238	0.666	0.0055	0.0043	0.0295	0.024	
106	5AL ₂ O ₃			3.33	2.38	0.167	0.237	0.0066	0.0038	0.0145	0.0079	
99				3.51	2.51	0.123	0.139	0.017	-0.0055	0.0247	0.0077	
101				0.575	0.410	0.036	0.024	0.0224	0.0019	0.0237	0.0013	
100			6000	3.47	2.48	0.833	0.872	0.0035	0.0020	0.0112	0.0077	
106				0.83	0.59	0.235	0.252	0.0066	0.0033	0.0084	0.0018	
99				3.51	2.51	0.313	0.380	0.0040	0.0043	0.0117	0.0077	
101				0.490	0.350	0.069	0.034	0.0144	0.0035	0.0155	0.0011	
100			12000	0.66	0.47	0.958	0.971	0.0035	0.0015	0.00497	0.0014	
99				3.51	2.51	0.520	0.537	0.0040	0.0025	0.0117	0.0077	
101				0.094	0.067	0.030	0.044	.023	-0.0054	0.0232	0.0002	

No.	Crucible.	a _{SiO₂} obtained from analysis of scrap- ings.	time t (s)	Rate of silicon pickup.		[Si _M] w/o	[Si _R] w/o	[O _M] w/o	Calculation of oxygen gradient by method G.	
				wt%/sec x 10 ⁻⁵	n _{Si} /sec x 10 ⁻⁵				[O _R] w/o	(O _R - O _M) w/o
37	8SiO ₂ -	0.0196	12000	0.3	0.214	0.202	0.2083	0.00165	0.00152	-0.0001
90	92MgO	0.006		0	0	0.190	0.190	0.0018	0.00084	-0.0009
84	7SiO ₂	0.042		.028	0.0199	0.15	0.1505	0.0013	0.0026	0.0013
88	93MgO	0.067		0	0	0.145	0.145	0.0007	0.0034	0.0027
67	37SiO ₂ -	0.102		1.07	0.764	0.235	0.256	0.0025	0.0031	0.00065
68	63Al ₂ O ₃	0.035		1.00	0.714	0.305	0.325	0.00070	0.0016	0.0009
87		0.063		1.50	1.07	0.325	0.354	0.00070	0.0022	0.0015
89	56SiO ₂	0.074		3.3	2.36	0.57	0.634	0.0012	0.0017	0.0005
44	-44Al ₂ O ₃	0.062		0.6	0.429	0.392	0.404	0.001	0.00195	0.0009
41		0.251		0.6	0.429	0.24	0.252	0.0025	0.0050	0.0025

TABLE 30. Values of experimental equilibrium quotient, K_4^1 , for the carbon-oxygen reaction.

Melt No.	Pressure (torr)	w/o C Finish.	w/o O 10^{-3} Finish	$\frac{dSi}{dt}$ wt. % per. s. $\times 10^{-5}$ at t =		K_4^1 at t =		Crucible.		
				600 (s)	12000 (s)	600 (s)	12000 (s)			
41	760	0.689	2.50	2.600	1.200	0.600	416.6	459	517.0	56%SiO ₂
44	76	0.670	1.00	5.500	2.700	0.600	108.7	129.9	145.0	43%Al ₂ O ₃
89	3	0.250	1.20	5.500	5.200	3.300	3.788	5.330	5.350	
49	760	0.119	17.50	0.500	0.100	0.005	348.3	426.3	451.0	
45	76	0.019	10.00	2.600	0.200	0	106.0	565.5	539.0	
86	3	0.007	1.96	1.700	0.300	-	17.50	29.00	-	
67	760	0.685	2.50	4.300	1.300	1.070	343.0	469.4	510.0	37%SiO ₂
68	76	0.699	0.70	3.100	1.300	1.000	135.0	156.3	184.0	61%Al ₂ O ₃
87	3	0.430	0.70	3.000	1.600	1.500	7.320	8.439	9.226	
57	760	0.104	25.00	0.100	0.100	0.100	395.1	384.5	350.0	
61	76	0.045	10.00	2.000	0.100	0	N.D.	N.D.	N.D.	
79	3	0.010	5.00	2.100	0.300	0	5.360	10.15	22.40	
63	760	0.980	2.00	0.600	0.600	0.100	344.7	462.0	456.4	7%SiO ₂
84	76	0.830	1.30	2.00	0.500	0.028	7.412	9.890	19.11	93%Al ₂ O ₃
88	3	0.640	0.70	-	-	-	-	-	9.290	

Melt No.	Pressure (torr)	w/o C Finish.	w/o O 10^{-3} Finish	$\frac{dSi}{dt}$ wt. % per. s. x 10^{-5} at t =		K_4^1 at t =			Crucibles.	
				600 (s)	6000 (s)	12000 (s)	600 (s)	6000 (s)		12000 (s)
64	760	0.110	21.00	0	0	0	381.0	342.0	312.0	
66	76	0.050	3.40	1.300	0.500	0	N.D.	N.D.	N.D.	
71	3	0.030	0.70	0.600	0.200	0	13.93	10.26	11.64	
82	760	0.965	2.00	0.700	0.300	0	372.0	361.2	367.4	8.0%SiO ₂
37	76	0.455	1.65	2.700	0.900	0.300	13.76	27.05	12.60	90%MgO
90	3	0.515	1.65	-	-	-	-	-	3.810	
19	760	0.117	12.20	0	0	0	489.0	525.0	636.0	
18	76	0.044	3.70	1.00	0.400	0	261.0	323.0	450.5	
76	3	0.028	3.50	1.50	0.300	0	43.70	39.66	13.83	
99	760	0.515	4.00	3.510	3.510	3.510	60.0	305.4	467.5	92%SiO ₂
100	140	0.075	8.00	10.83	3.470	0.660	42.59	143.7	328.6	
110	3	0.035	4.50	18.75	-	-	1.11	-	-	
101	760	0.086	27.50	0.575	0.490	0.094	318.5	509.3	358.2	
106	140	0.023	12.00	3.33	0.830	-	N.D.	N.D.	N.D.	
109	3	< 0.01	4.70	13.33	0	-	9.00	46.50	N.D.	

TABLE 31.

Comparison of theoretical and actual
rates of oxygen transfer from the silica
of the ladle lining. using Model III.

$$(\delta = .0075 \text{ cm})$$

Cast No.	Measured Rate of Oxygen Transfer (\dot{n}_o /sq.cm/sec) $\times 10^{-7}$	Calculated Rate of Oxygen Transfer (\dot{n}_o /sq.cm/sec $\times 10^{-7}$)	Source of Data.
VB I	8.4	10.1	80T Hoesc
VB II	8.6	8.8	" "
VB III	12.6	11.0	" "
VB IV	12.6	12.0	" "
VB V	5.14	9.6	" "
VB VI	14.2	10.6	" "
VB VII	5.2	6.0	" "
VB XII	6.5	7.2	" "
VB XVI	12.7	13.5	" "
VB XVIII	8.0	10.6	" "
LM 2117	5.6	4.4	30T E.S.C
LM 3426	0	0	" "

TABLE 32. Relationship between silicon, carbon and oxygen contents prior to the degassing of E.S.C. 30 t. melts.

Code No.	Cast No.	Analysed carbon content (wt.%)	Analysed silicon content (wt.%)	Analysed oxygen content (wt.%)	Cal'd oxygen in equilibrium with carbon at $P_{CO} = 760$ torr (wt.%)	Cal'd oxygen in equilibrium with silicon at $a_{SiO_2} = 1$ (wt.%)
1	LM 3355	0.035	0.01	0.11	0.057	0.056
2	LM 3364	0.042	0.01	0.068	0.043	0.056
3	LM 3398	0.066	0.05	0.028	0.030	0.025
4	LM 3426	0.076	0.13	0.026	0.026	0.016
5	LM 3553	0.032	0.0125	0.068	0.063	0.05
6	LM 3612	0.65	0.125	0.010	0.003	0.016
7	LM 3649	0.345	0.12	0.0084	0.0058	0.016
8	LM 3722	0.017	0.015	0.090	0.117	0.046
9	LM 3775	0.16	0.14	0.020	0.0125	0.015
10	LL 1179	0.032	0.01	0.060	0.063	0.056
11	RZ 7599	1.12	0.12	0.0035	0.0018	0.016

TABLE 33.

Effect of Carbon content on yield of
silicon for E.S.C. 50t Melts.

Cast No.	Carbon Content. wt %	Silicon Yield. (%)
LM 3398	0.066	26.6
LM 3426	0.076	67.5
LM 3775	0.16	79.5
LM 3649	0.35	72.5
LM 3612	0.65	72.0

TABLE 34.

Comparison of methods of obtaining the
carbon loss during the degassing of
30 ton heats.

Melt No.	Cycles.	%wt.C.loss x 10^{-3} from pressure graphs.	%wt.C.loss x 10^{-3} from analysis graphs.
LM 3426	6-22	5.10	7.00
LM 3355	7-16	5.10	7.30
LM 1179	8-18	3.50	5.30
LM 3398	8-25	7.20	10.01

TABLE 35. Oxygen balance and rate measurements for E.S.C., 30 ton and Hoesch, 80 ton heats.

Melt Cycles. No.	ts (s from middle of C_T)	Δt (s)	[Si] (wt.%)	[C] (wt.%)	ΔG (wt.%)	ΔO_c (wt.%)	[O] _s (wt.%)	ΔO (wt.%)	Total [O] donation rate (wt. %/sec)	Total Oxygen donation (moles/sec $\times 10^{-2}$)	Theoretical [O] donation rate from SiO ₂ in ladle (\dot{m}_O $\times 10^{-2}$)	[O] donation rate from other sources (\dot{m}_O /s $\times 10^{-2}$)	Effic of de ing
LM3649.6-16	97	210	.119	.348	.0056*	.0074*	.007	.0	3.5×10^{-5}	63.0	5.4	57.6	0
LM3775 4-20	60	300	.140	.165	.010	.0133	.020	.0144.	0	0	1.50	0	72.0
LM3398 8-25	161	330	.050	.063	.0101	.01348	.0243	.0148	0 ^{to}	0	0	0	61.0
LM3426 6-22	96	335	.134	.073	.007	.009	.021	.009	0 ^o	0	0	0	44.0
LM3355 7-16	108	158	.01	.0207	.0073	.0097	.109	.0062	2.21×10^{-5}	39.8	0	39.8	55.0
LM3722 23-32	455	185	.0167	.008	.002	.0026	.097	.0205	-	-	0	-	-
LM3364 9-20	142	218	.01	.0230	.0145	.0193	.057	.015	1.97×10^{-5}	35.4	0.45	34.9	26.4
LM1179 21-31	480	170	.01	.0230	.0053	.0070	.0473	.0008	3.65×10^{-5}	65.8	0.90	64.9	1.7
LM3553 2-23	25	430	.015	.032	.021	.028	.0671	.0063	5.05×10^{-5}	91.0	0	91.0	9.4
LM4207 11-23	175	140	.08	.1600	.0057*	.0077*	.0153	.0010	4.78×10^{-5}	86.0	2.10	83.9	24.70
LM4246 7-22	120	230	.225	.12	.0030*	.0040*	.0099	.0026	0.61×10^{-5}	11.0	1.50	9.5	30.00
LM4199 7-16	110	140	.13	.222	.0038*	.0051*	.0136	.0026	1.79×10^{-5}	32.0	1.50	30.5	19.00
LD1569 8-17	140	172	.072	.243	.0034*	.0045*	.0090	.0010	2.16×10^{-5}	38.8	6.0	32.8	55.50
LM4204 7-15	110	140	.10	.270	.0051*	.0067*	.0110	.0029	2.718×10^{-5}	48.6	3.90	44.7	50.00
LM4227 6-16	100	160	.290	.490	.0039*	.0053*	.006	Nil	3.31×10^{-5}	59.4	2.40	57.0	0

Melt Cycles. No.	t s. (s from middle of C _I)	Δt (s)	[Si _s] (wt.%)	[C _s] (wt.%)	ΔC (wt.%)	ΔO _G (wt.%)	[O _s] (wt.%)	ΔO (wt.%)	Total [O] donation rate (wt. %/sec)	Total Oxygen donation rate (moles/sec x 10 ⁻²)	Theoretical [O] donation rate from SiO ₂ in ladle (n ₀ /s x 10 ⁻²)	[O] donation rate from other sources (n ₀ /s x 10 ⁻²)	Efficiency of degassing O ₂
LD1580	9-17	150	125	.120	.30	.0032	.0043	.0110	2.96x10 ⁻⁵	54.0	2.70	51.3	5.50
LD1561	5-19	80	235	.174	.40	.0040	.0053	.0144	0	0	1.50	0	50.00
<u>R.T.B.</u>													
LM2117	1-24	20	460	.0057	.058	.039	.052	.043	8.05x10 ⁻⁵	140.0	5.70	134.3	35.0
LM2108	1-24	20	460	.005	.076	.035	.047	.042	4.78x10 ⁻⁵	86.0	7.80	78.2	59.5
LM2171	1-29	20	560	.005	.046	.033	.044	.058	5.53x10 ⁻⁵	99.5	2.40	97.1	22.2
LM2203	1-15	20	280	.005	.073	.028	.037	.038	7.5x10 ⁻⁵	135.0	7.80	127.2	42.0
<u>Hoesch.</u>													
I	1-26		1125	.0050	.07		0	.022	.0137	0	25.5	0	68.0
II	1-21		900	.005	.08	.027	.036	.025	2.44x10 ⁻⁵	125.9	22.5	123.4	57.0
III			875	.005	.17	.0075	.010	.0158	0.45x10 ⁻⁵	23.5	27.9	0	50.0
IV			875	.010	.48	.0225	.030	.0030	3.24x10 ⁻⁵	166.6	30.4	136.2	45.0
V	1-20		849	.005	.10	.0165	.022	.018	1.45x10 ⁻⁵	74.6	24.3	50.3	49.5
VI	1-20		849	.005	.06	.00561	.0076	.0146	0	0	26.7	0	71.5
VII	1-23		613	.005	.05	0	0	.038	.0170	0	15.2	0	65.5
VIII	1-30		712	.005	.04	0	0	.0336	.0216	0	19.5	0	72.0
IX	1-30		664	.004	.064	.0170	.0227	.022	2.0x10 ⁻⁵	103.2	25.5	77.7	48.0

Melt No.	Cycles.	t_s (s from middle of C_I)	Δt (s)	$[Si_s]$ (wt.%)	$[C_s]$ (wt.%)	ΔC (wt.%)	ΔO_c (wt.%)	$[O_s]$ (wt.%)	ΔO (wt.%)	Total $[O]$ donation rate (wt. %/sec)	Total Oxygen donation (moles/sec $\times 10^{-2}$)	Theoretical $[O]$ donation rate from SiO_2 in ladle ($\dot{n}_O/s \times 10^{-2}$)	$[O]$ donation rate from other sources ($\dot{n}_O/s \times 10^{-2}$)	Efficiency of degassing $\frac{\Delta O}{O_s}$
X		666"	.010	.53	.0087	.0116	.008	.0034	1.23×10^{-5}	63.4	30.4	33.0	47.6	
XI		666"	.011	.14	.0087	.0116	.021	.0104	0.188×10^{-5}	9.7	21.9	0	57.0	
XII	1-24	616	.003	.05	.00943	.0126	.038	.0210	0	0	18.2	0	57.7	
XIII		666"	.005	.091	.0036	.0048	.024	.0119	0	0	25.5	0	54.5	
XIV		666"	.011	-	-	-	.0070	-	-	-	-	-	14.3	
XV		666"	.0081	.47	.00875	.0117	.0090	.0282	0	0	30.4	0	35.5	
XVI		666"	.009	.55	.0239	.0319	.0070	.0016	4.55×10^{-5}	234.3	30.9	203.4	28.6	
XVII		666"	.005	.09	.0264	.0351	.0290	.0158	2.90×10^{-5}	149.4	20.1	129.3	62.0	
XVIII	1-34	724	.005	.136	.0164	.0218	.0270	.0190	0.386×10^{-5}	19.9	24.3	0	64.7	

† MgO wash on ladle.

* calc'd from pressure curves.

⊙ MgO to ladle cover.

⊠ double slag heat.

⚡ Estimated times.

TABLE 36. Analysis of slag samples taken from E.S.C. 30 ton casts.

Cast No.	Stage sample taken.	(wt.%) SiO ₂	(wt.%) FeO	(wt.%) Al ₂ O ₃	(wt.%) MnO	(wt.%) CaO	(wt.%) MgO	(wt.%) Cr ₂ O ₃	(wt.%) TiO ₂	Double slag or single slag.
LM 3649.										S.S.
LM 3775										S.S.
LM 3398	Ladle after tap.	29.94								S.S.
	After Degas.	30.76								S.S.
LM 3426	B.D.	26.92			5.47					S.S.
	A.D.	22.04			3.65					S.S.
LM 3355	During Deg.	33.1	13.76	23.45	4.09	13.20	5.21	1.98	5.18	S.S.
	A.D.	33.0	13.63	24.16	3.72	13.20	5.14	1.90	5.18	S.S.
	During Teeming.	30.3	19.87	23.94	4.46	12.40	4.85	2.28	1.86	S.S.
LM 3722										S.S.
LM 3364	During Deg.	30.34	11.91	14.59	11.24	22.08	7.68	-	1.03	S.S.
LL 1179	B.D.	21.17	13.37	9.86	4.80	30.55				S.S.
	A.D.	31.14	4.28	14.11	4.69	23.19				S.S.

Cast No.	Stage sample taken.	(wt.%) SiO ₂	(wt.%) FeO	(wt.%) Al ₂ O ₃	(wt.%) MnO	(wt.%) CaO	(wt.%) MgO	(wt.%) Cr ₂ O ₃	(wt.%) TiO ₂	Double slag or single slag.
LM 3553										S.S.
LM 4207	Prior to Block.	20.49	8.09	4.73	6.06	51.67	7.78			S.S.
	ladle glaze.	30.98	0.70	13.61	3.32	38.72	9.49			
	ladle after tap.	31.26	2.13	6.30	6.23	43.42	10.27			
	B.D.	31.26	1.82	6.52	5.72	41.54	9.82			
	C ₄	31.92	1.82	7.09	5.75	41.20	9.82			
	C ₅	32.05	1.62	8.86	5.68	39.54	9.47			
	C ₇	37.75	1.72	9.22	5.25	30.83	7.54			
	C ₁₀	33.78	1.72	7.09	6.30	40.48	9.13			
	C ₁₄	34.31	1.72	7.94	6.45	38.27	10.36			
	C ₁₉	34.44	1.82	9.00	7.27	33.10	9.70			
C ₂₄	33.25	1.41	8.29	6.37	37.58	10.82				
LM 4246	ladle glaze 'A'	66.50	1.33	6.52	9.10	6.31	2.76			D.S.
	ladle glaze 'B'	55.74	1.50	9.57	6.39	16.01	4.64			

Cast No.	Stage sample taken.	(wt.%) SiO ₂	(wt.%) FeO	(wt.%) Al ₂ O ₃	(wt.%) MnO	(wt.%) CaO	(wt.%) MgO	(wt.%) Cr ₂ O ₃	(wt.%) TiO ₂	Double slag or single slag.
	ladle after tap.	29.98	0.52	6.37	1.70	45.08	12.55			
	C ₄	33.81	0.40	7.86	1.87	41.68	11.55			
	C ₁₀	33.81	0.20	8.58	1.95	39.33	11.79			
	C ₁₄	38.81	0.20	8.43	2.06	39.33	11.82			
	C ₁₅	34.21	0.20	8.36	2.10	39.33	11.86			
	After teeming.	38.45	0.20	10.15	2.14	32.14	11.13			
LM 4199	Prior to Block.	15.68	8.96	5.87	6.30	49.06	10.71			S.S.
	ladle glaze.	38.17	1.51	9.79	5.02	34.85	11.49			
	ladle after tap.	27.40	1.82	8.01	4.61	41.28	15.05			
	B.D.	29.76	1.72	8.36	4.50	40.85	14.91.			
	C ₆	30.53	1.43	9.37	4.65	38.03	14.24			
	C ₈	30.53	1.31	9.94	4.58	36.61	14.72			
	C ₁₁	34.65	1.51	13.54	4.99	27.79	11.30			
	C ₁₆	31.35	1.00	11.17	4.76	34.48	15.69			
	A.D.	33.87	1.41	15.74	5.30	29.21	12.63			

Cast No.	Stage sample taken.	(wt.%) SiO ₂	(wt.%) FeO	(wt.%) Al ₂ O ₃	(wt.%) MnO	(wt.%) CaO	(wt.%) MgO	(wt.%) Cr ₂ O ₃	(wt.%) TiO ₂	Double slag or single slag.
ID 1569	Prior to Block.	16.37	11.88	2.72	7.79	41.64	7.55			S.S.
	B.D.	27.16	3.97	5.22	8.44	38.35	9.47			
	C ₂	28.20	3.77	5.80	8.83	38.24	9.59			
	C ₃	27.03	3.40	7.01	8.37	35.87	9.21			
	C ₆	28.07	3.30	8.65	8.44	35.42	9.30			
	C ₉	31.11	3.40	7.72	8.44	36.08	9.26			
	C ₁₃	31.90	2.95	10.66	7.66	29.10	8.88			
	C ₁₉	31.11	3.05	8.22	8.44	33.75	9.13			
	LM4204	Prior to Block.	18.36	10.38	4.81	8.59	39.94	7.04		
ladle after tap.		36.01	2.23	7.15	9.45	27.38	10.82			
C ₁		38.66	2.03	9.50	8.75	24.37	9.89			
C ₅		38.93	1.62	8.43	8.75	23.76	9.80			
C ₆		41.44	1.72	8.93	8.56	23.63	9.51			
C ₈		40.78	1.72	9.65	8.68	22.96	9.85			
C ₁₃		39.99	1.62	9.50	9.10	22.53	9.97			
C ₂₁		39.99	1.51	10.44	9.34	20.93	10.25			

Cast No.	Stage sample taken.	(wt.%) SiO ₂	(wt.%) FeO	(wt.%) Al ₂ O ₃	(wt.%) MnO	(wt.%) CaO	(wt.%) MgO	(wt.%) Cr ₂ O ₃	(wt.%) TiO ₂	Double sleg or single sleg.
IM 4227	C ₂₄	40.25	1.62	10.52	9.21	21.13	10.06			
	A.D.	40.65	1.72	12.04	9.41	19.76	9.80			
	P.T.T.	21.42	0.5	4.30	0.10	59.12	6.80			D.S.
	ladle glaze.	36.03	0.7	8.80	1.76	40.17	10.43			
	B.D.	32.53	0.10	7.44	0.61	45.95	10.32			
	C ₇	31.92	0.00	8.08	0.89	43.43	10.84			
	C ₁₆	34.04	0.20	8.53	1.06	40.76	9.59			
	C ₁₃	32.93	0.10	8.22	1.06	46.20	10.80			
	C ₂₆	34.31	0.40	9.15	1.52	45.01	10.65			
	A.D.	32.85	0.10	8.93	1.17	44.89	10.49			
ID 1530	Prior to Block.	25.39	6.20	6.00	7.02	44.76	6.62			S.S.
	ladle after tap	32.32	1.30	6.42	5.93	41.43	9.52			
	B.D.	33.24	1.90	7.17	5.73	39.91	9.20			
	C ₄	33.33	3.30	8.35	5.36	37.72	8.42			
ID 1561	P.T.T.	23.12	0	6.15	0.21	47.32	13.93			D.S.

TABLE 37.

Dimensions for E.S.C. 30t and Hoesch
80t. ladles.

Ladles.	80T	30T
Metal Height (cm)	274	147
Top. I.D. (cm)	247	204
Bottom I.D. (cm)	220	176
Metal Volume (cm ³)	11800000	4100000
Ladle/metal area (cm ²)	243000	120200
Slag/metal area (cm ²)	47922	32689

TABLE 38. Calibration of Toepler Gauge.

Small bulb V_1 ($f_{P1} = .0739$)					top two bulbs (V_1+V_2) ($f_{P12} = .263$)				
h_{1a}	P_a	h_{1b}	P_b	V_x	h_{12a}	P_a	h_{12b}	P_b	V_x
22.8	1.685	3.3	.244	87.99	6.4	1.683	0.8	.210	74.24
20.5	1.515	2.8	.207	82.26	5.7	1.499	0.7	.184	72.83
15.6	1.153	2.2	.163	85.40	4.9	1.288	0.45	.118	52.5
31.8	2.35	4.8	.355	92.67	8.8	2.31	1.0	.263	66.64
16.0	1.18	2.4	.177	91.89	4.4	1.160	0.4	.105	51.80
8.6	0.636	1.3	.096	92.68	2.4	0.631	0.25	.066	60.39
24.2	1.79	3.3	.244	82.26	6.7	1.760	0.8	.210	70.55

TABLE 39. Calibration of pressure transducer.

McLeod Reading.		Calculated pressure in system P_o (torr)	Output from transducer (mV)
for volume V_1 h_1 (cms) ($f_1 = .0739$)	for volumes V_1+V_2 h_{12} (cms) ($f_{12} = .263$)		
0	0	0	0
13.6		1.005	1.7
14.4		1.064	1.75
23.3		1.722	2.92
26.4		1.951	3.28
29.6		2.187	3.68
	9.4	2.472	4.29
	10.9	2.867	4.92
	12.2	3.209	5.65
	13.1	3.445	6.05
	14.6	3.839	6.78
	16.5	4.339	7.66

Figure 1. Ellingham diagram giving the standard free energies of formation of oxides. (1)

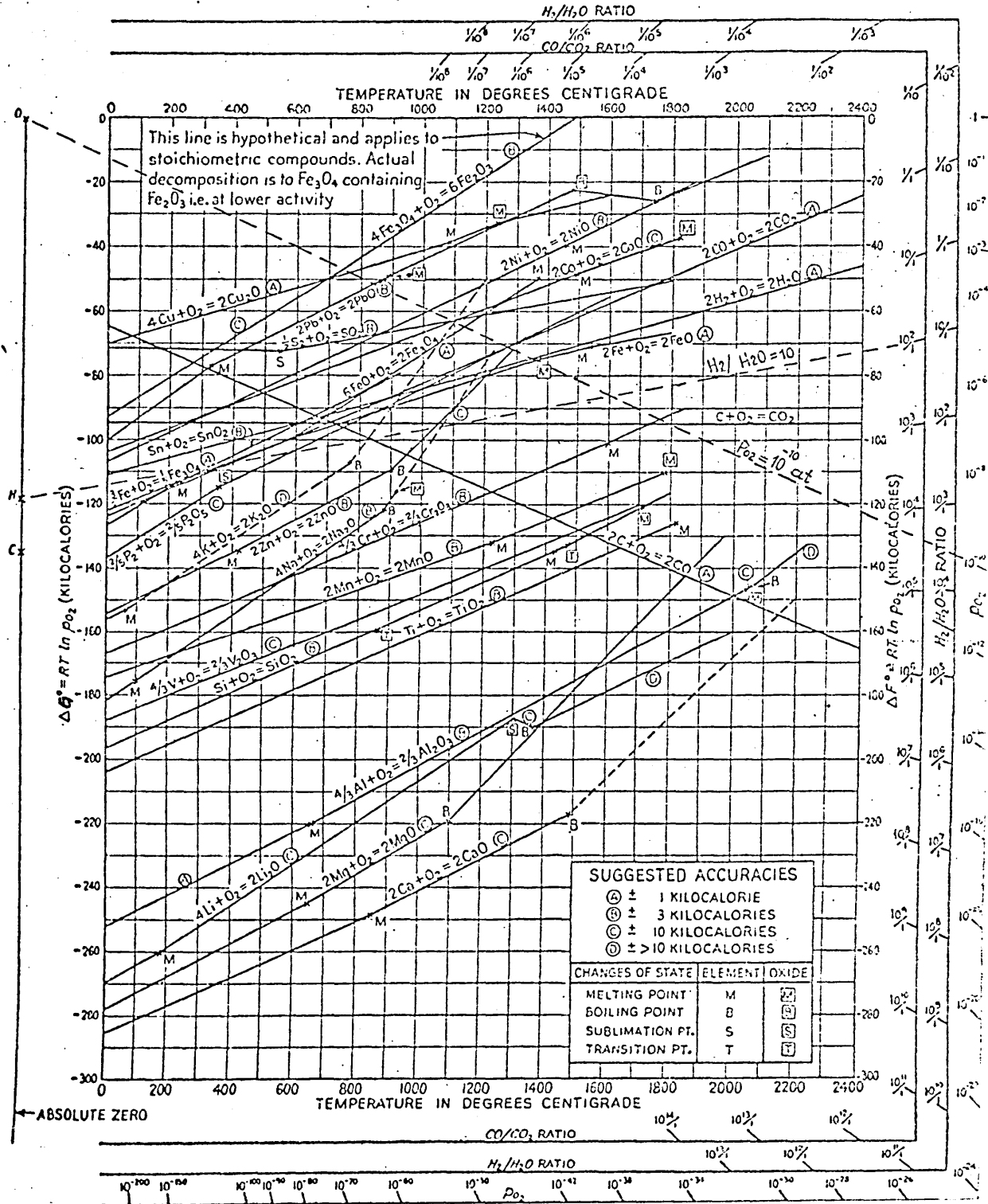


Figure 2.

Temperature dependence of the oxygen pressure
of iron containing 1000 p.p.m. oxygen. (1)

Figure 3.

Concentration of oxygen in iron at 1540° C
and 1600° C as a function of oxygen
pressure. (3)

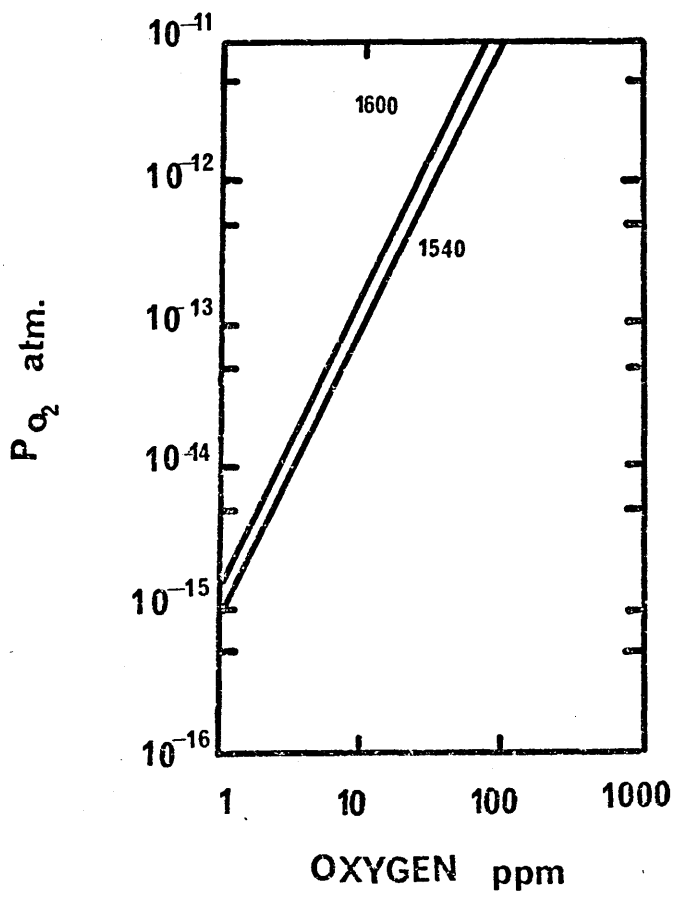
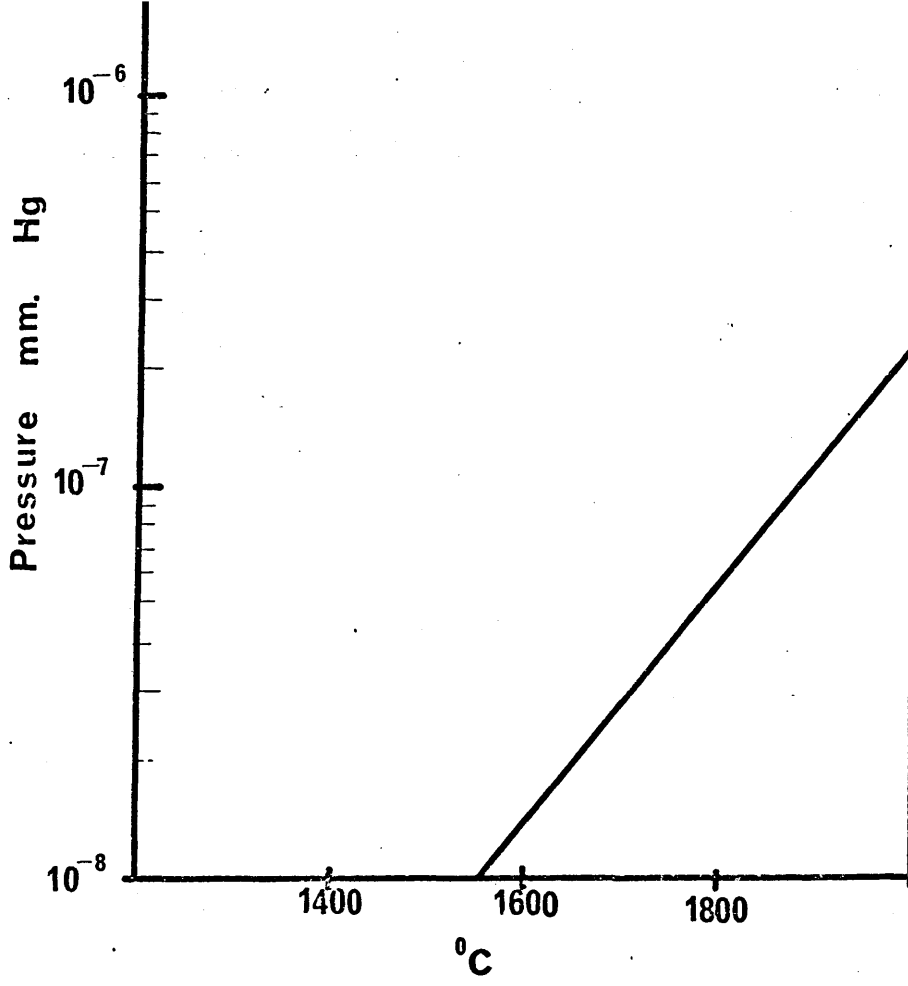


Figure 4. Pressure dependence of nitrogen and hydrogen contents of liquid iron. (1)

Figure 5. Deoxidation equilibria in liquid iron at 1600° C. (3)

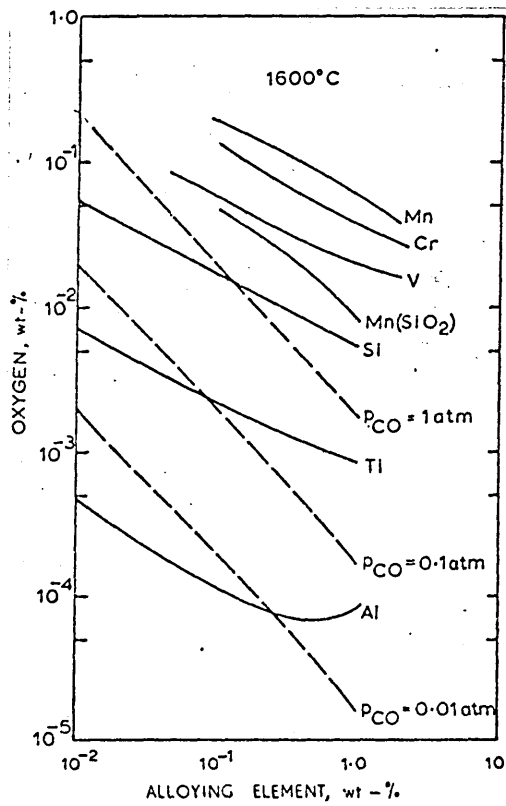
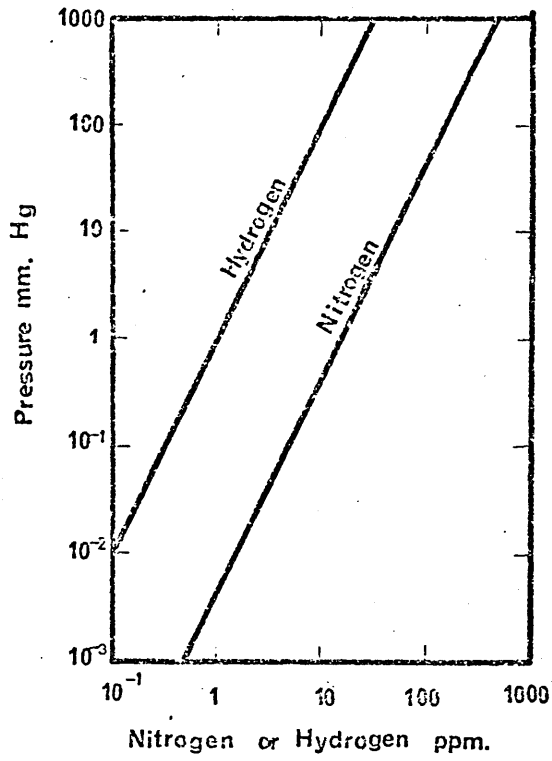


Figure 6. Effect of temperature on the equilibrium between carbon monoxide, carbon dioxide and oxygen in liquid iron. Reference list numbers are given against each line. (7)

Figure 7. Effect of temperature on the equilibrium between carbon monoxide, carbon dioxide and carbon in liquid iron. Reference list numbers are given against each line. (7)

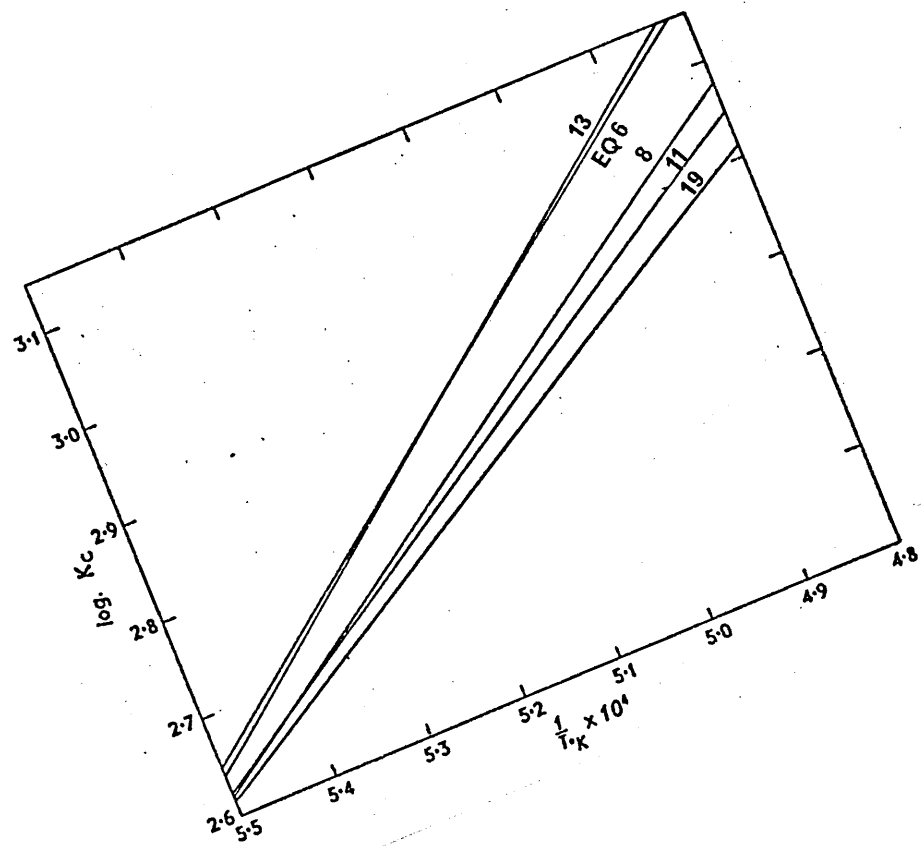
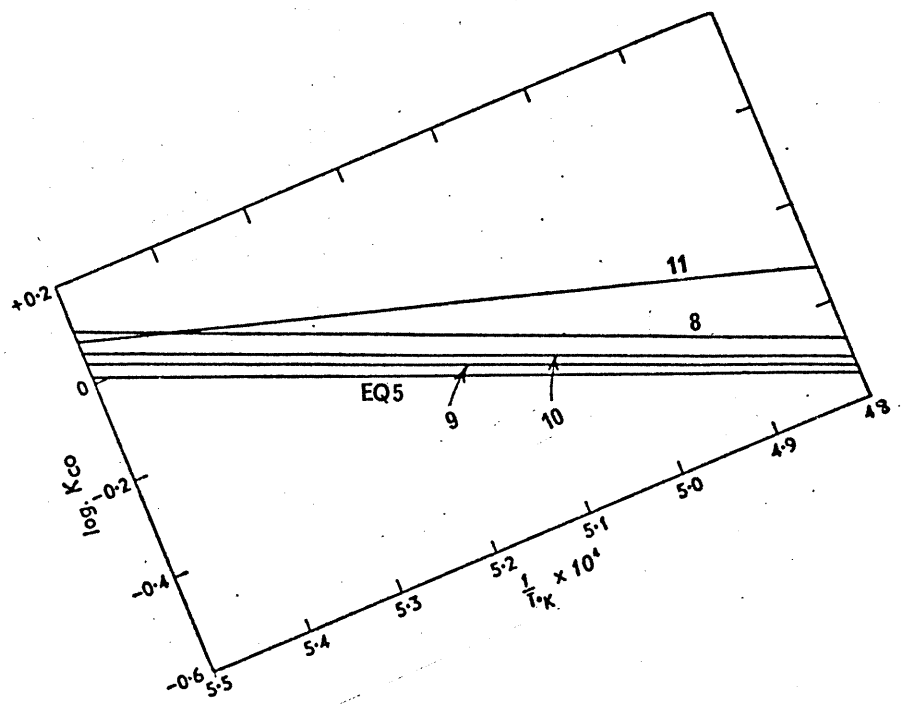


Figure 8.

Plot of the data (10) for the product

$[\%C][\%O] \times 10^{-3}$ against temperature.

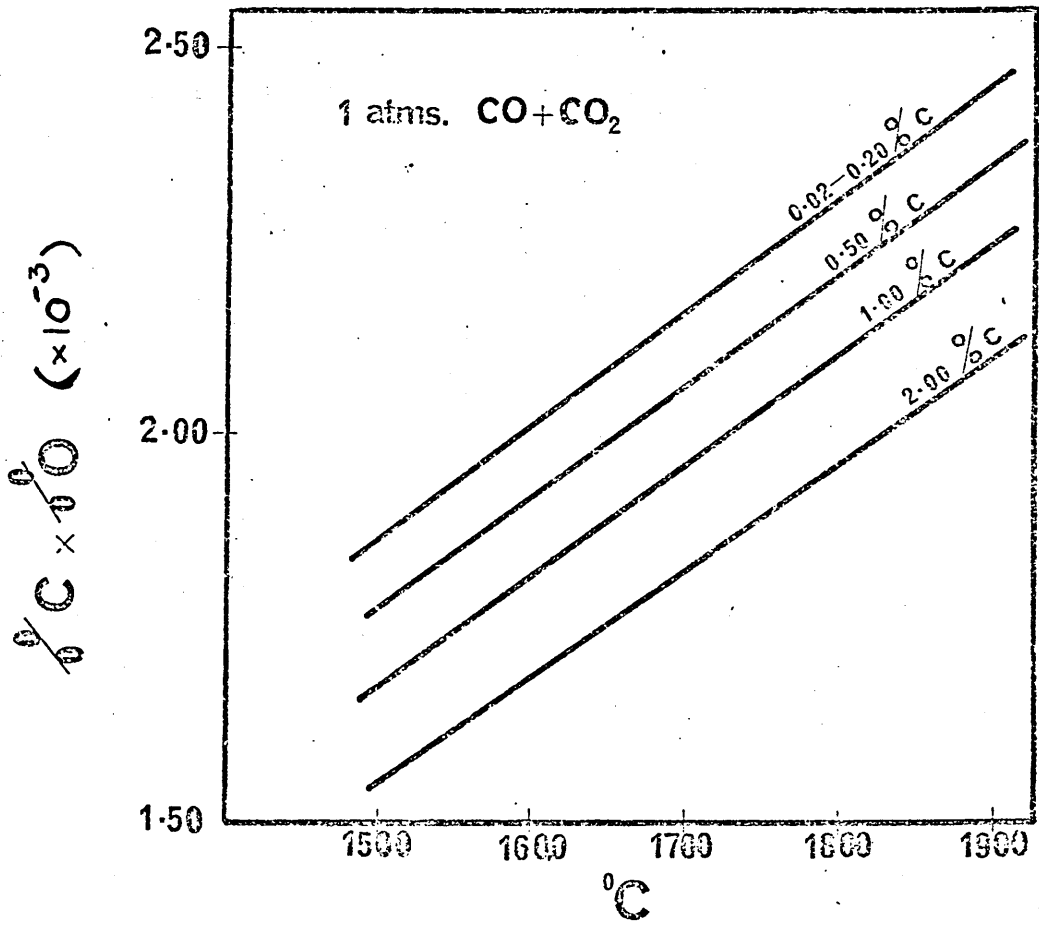


Figure 9. Theoretical carbon-oxygen equilibrium curves
for iron-carbon-oxygen alloys. (20)

Figure 10. Per cent CO_2 in CO-CO_2 mixtures at various
pressures vs. per cent carbon in liquid
iron. (20)

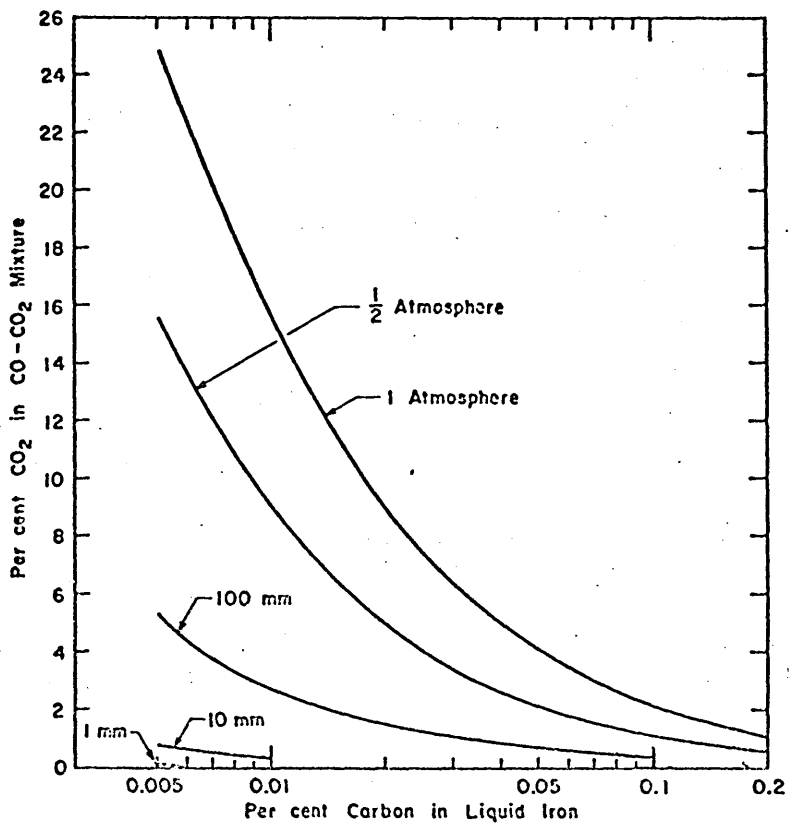
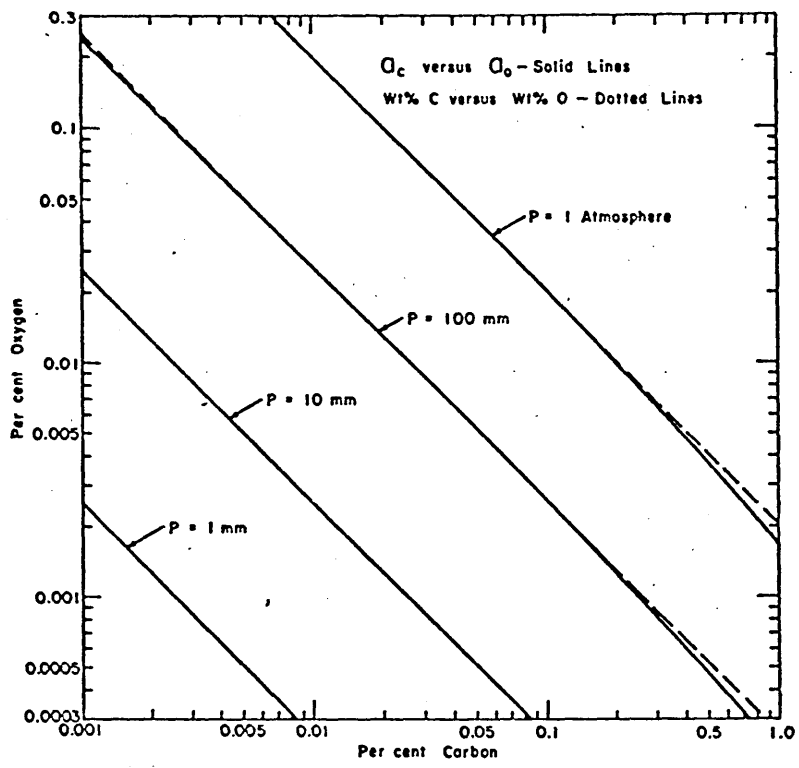


Figure 11.

Solubility of oxygen in liquid iron. (23)
(Chipman and Fletters (24), Taylor and
Chipman (25)).

Figure 12.

The effect of various elements on the activity
coefficient of oxygen in dilute solution in
liquid iron. The numbers in parantheses
against each line relate to the references
for the interaction coefficients given in
Appendix I, Table 10 of Bodsworth. (7)

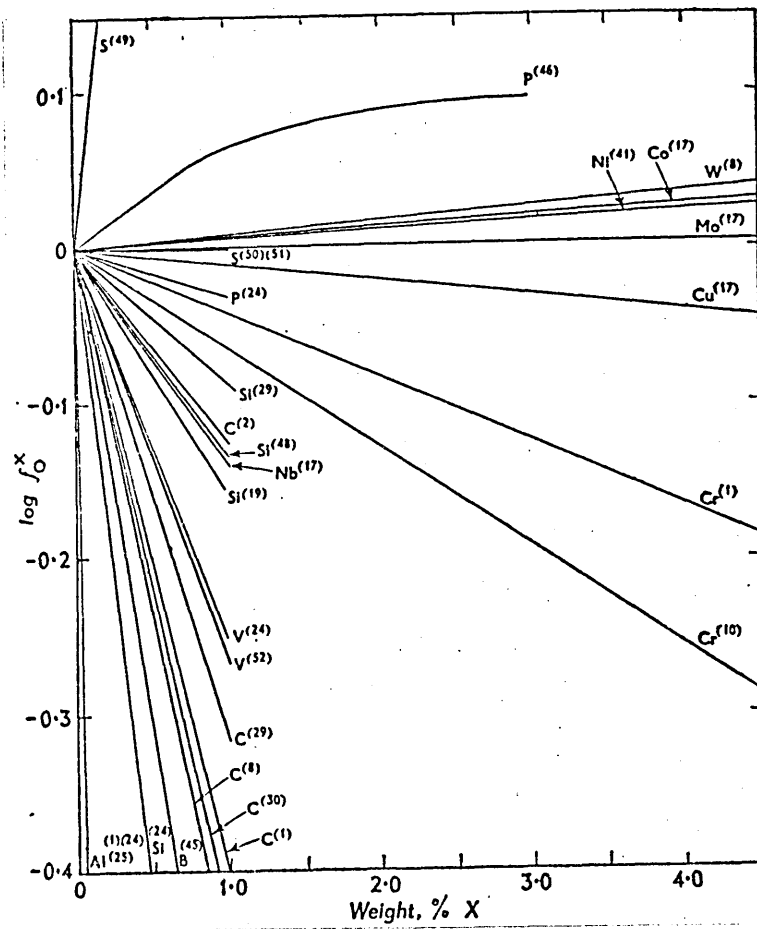
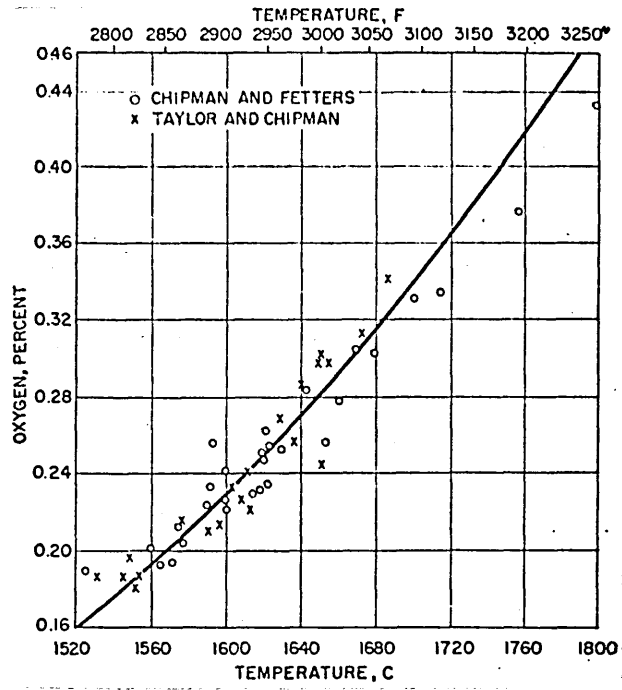


Figure 13.

The activities of carbon in pure liquid iron-carbon alloys with reference to pure graphite and dilute, weight-per cent carbon, standard states. (7)(8).

Figure 14.

The effect of carbon on the activity coefficient of oxygen in pure iron-carbon-oxygen alloys.

Curve I	Elliott (8)
" II	Matoba and Banya (30)
" III	Chipman (29)
" IV	Schenck and Gerdorn (11)
" V	Turkdogan et al (15)
" VI	Fuwa and Chipman (10)

Figure 15.

The effect of various elements on the activity coefficient of carbon in dilute solution in liquid iron. The numbers in parentheses against each line relate to the references in Appendix I, Table 3 of Bodsworth.

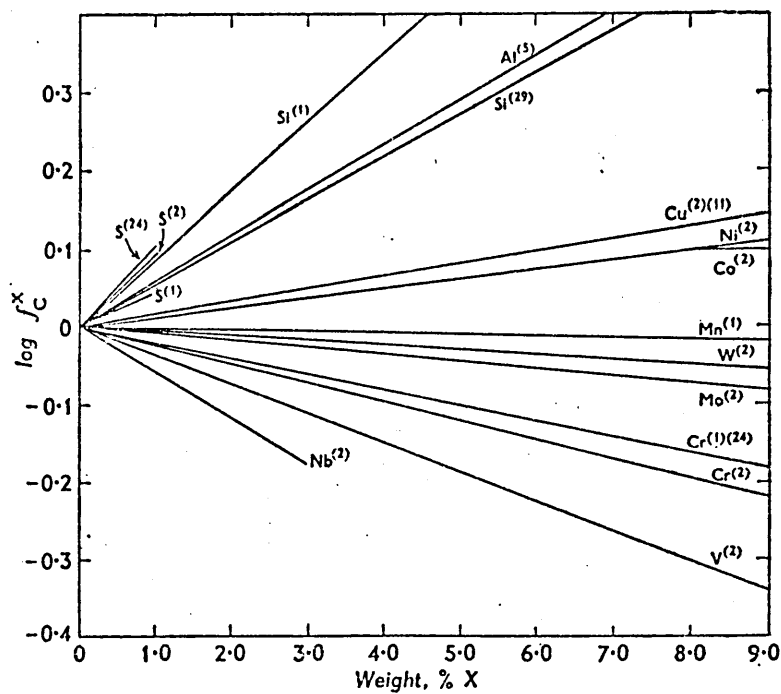
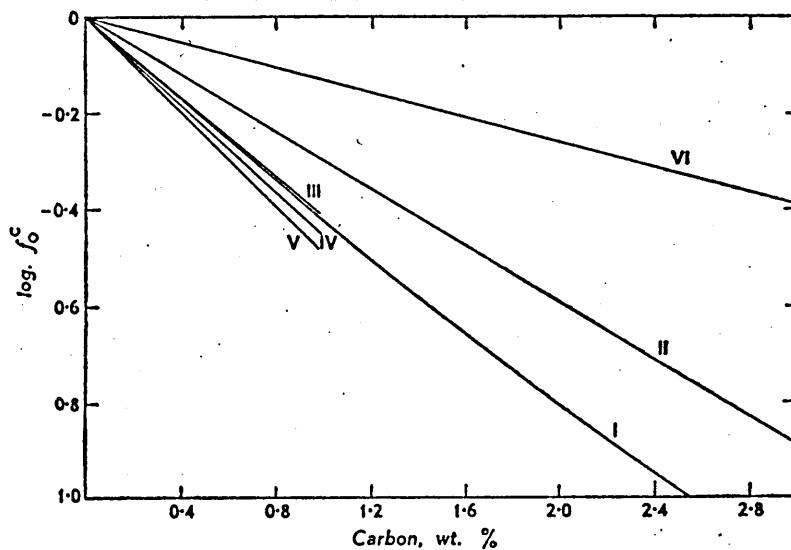
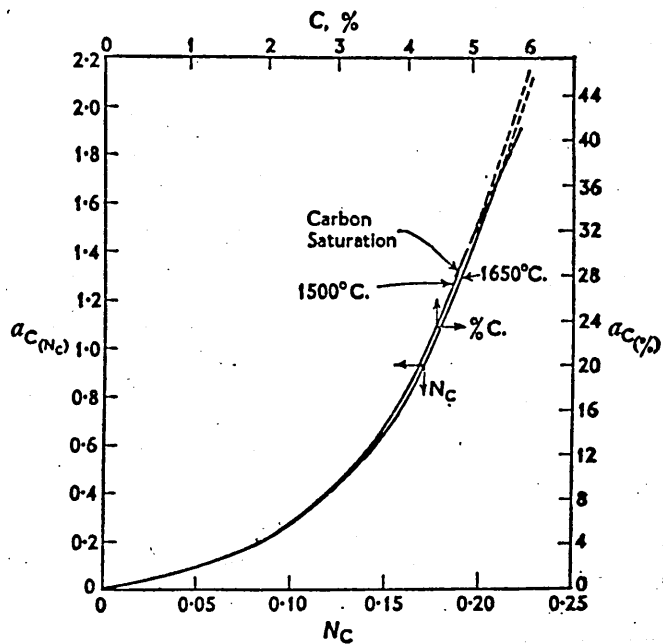


Figure 16.

Comparison of the true (full lines) and apparent (dotted lines) equilibrium constants for the dissociation of solid alumina to form aluminium and oxygen dissolved in liquid iron (7). Reference numbers are given against each line.

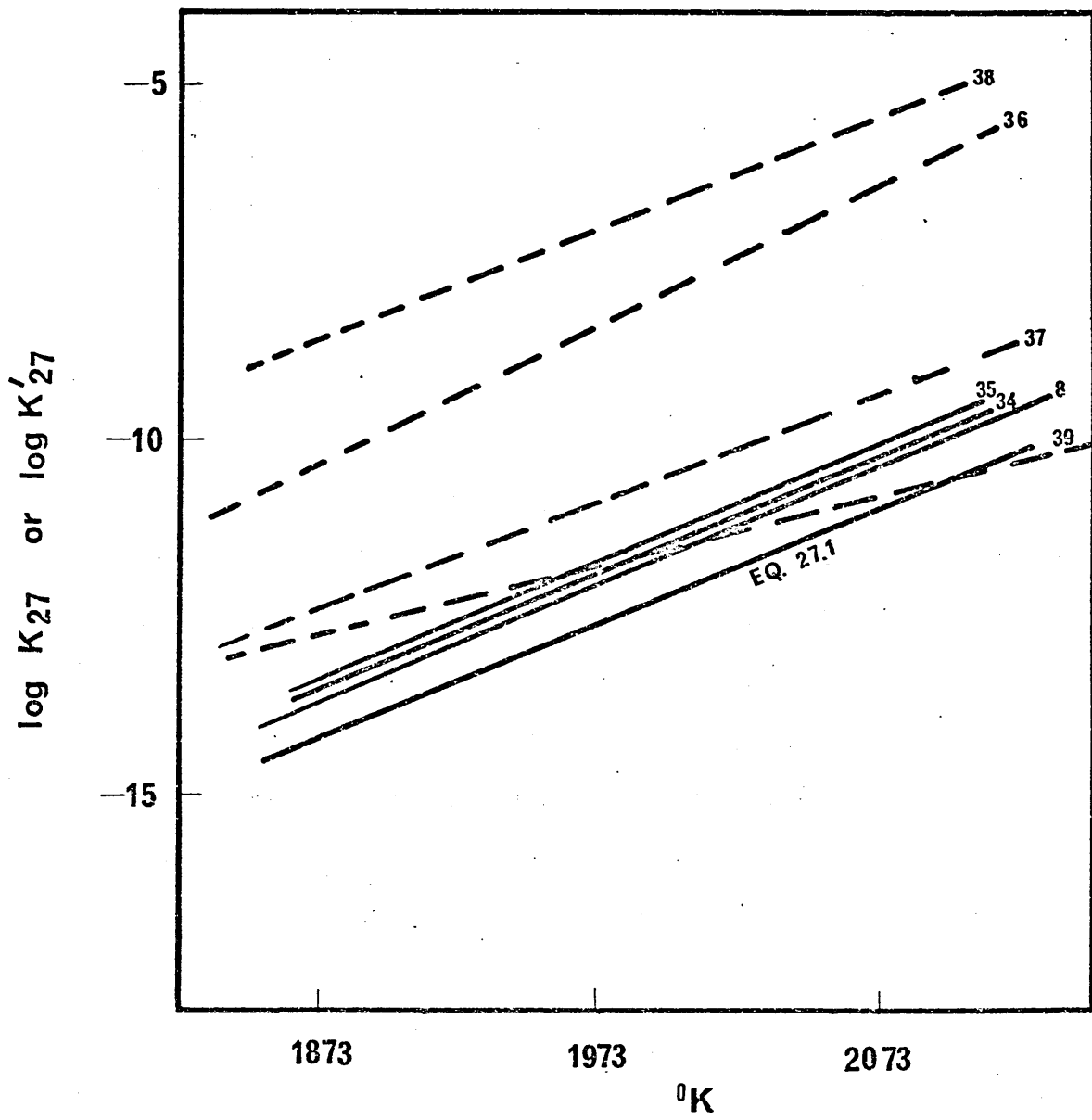
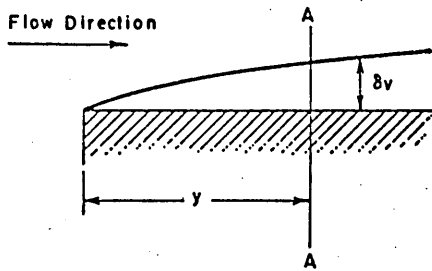
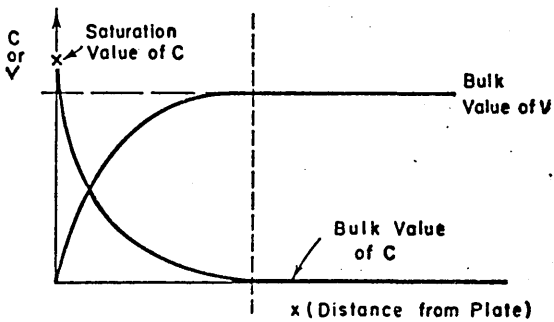


Figure 17. (a) Velocity and concentration boundary layers
next to a flat plate in streamline flow.
(b) Development of concentration boundary
layer along a tube. (23)

Figure 18. Effective diffusion boundary layer
thickness, .



FLAT PLATE IN STREAMLINE FLOW - SIDE ELEVATION



FLAT PLATE IN STREAMLINE FLOW - SECTION AT A-A
(a)



(b)

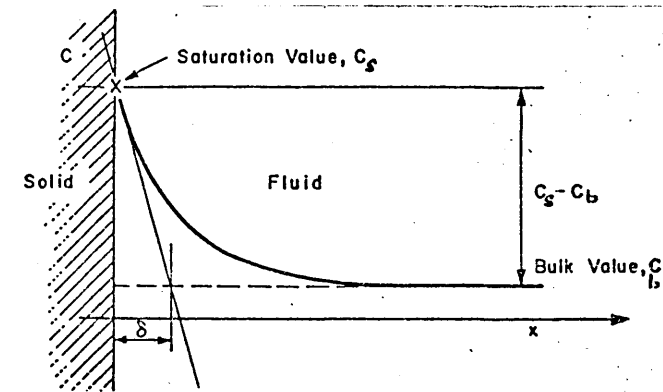


Figure 19. Summary of theories of mass transport from melt to gas-melt interface. (65).

Model	Description	Schematic Representation	Mass Transfer Coefficient (\bar{k})	Rate Equation $\frac{dn}{dt}$	Conditions under which Model is Valid
Static Boundary Layer	Melt consists of a convectively stirred homogeneous bulk and a static surface layer. Transport to the surface takes place by diffusion across the surface layer.		D/δ	$2A_{gm}(C_b - C_e)$	All conditions since δ is a function of the convective stirring.
Theory of Dankwerts	Elements of surface are renewed in a random fashion by packets of fluid arriving from the bulk. Mean rate of renewal of surface is constant. Fluid packet at the surface discharges its contents by unsteady state diffusion until replaced.		$(DS)^{1/2}$	$2A_{gm}(C_b - C_e)$	All since 'S' is a function of the convective stirring.
Rigid Flow model of Machlin	A surface layer exists in which streamline rigid flow parallel to the surface takes place. Flow pattern has the form indicated. Fluid packet is brought to the surface at the centre and removed at the boundary. During its stay on the surface an element discharges its contents by unsteady state diffusion.		$2 \left(\frac{D^2 V}{\pi} \right)^{1/2}$	$2A_{gm}(C_b - C_e)$	An inductively stirred melt in a cylindrical crucible.
Free convection Model of Kraus	A fluid element is brought to the surface by convection currents, arising from density differences due to heat loss by radiation from the melt surface. An element remains on the surface for a time λ/v during which it discharges its contents by unsteady state diffusion.		$D^{1/2} \left[\frac{g \Delta T \rho}{\nu \rho C_p} \right]^{1/4}$	$2A_{gm}(C_b - C_e)$	A melt stirred by natural convection currents caused by heat losses from the melt surface.

Figure 20. Flow lines in the vicinity of a plane contact surface. (60)(93).

Figure 21. Diagrammatic representation of flow in an induction melting furnace. (93)

Figure 22. Probability of homogeneous nucleation J of CO bubbles in an iron melt in relation to the oxygen content of the bath, (1%O, 1600°C) (approximate values) (72).

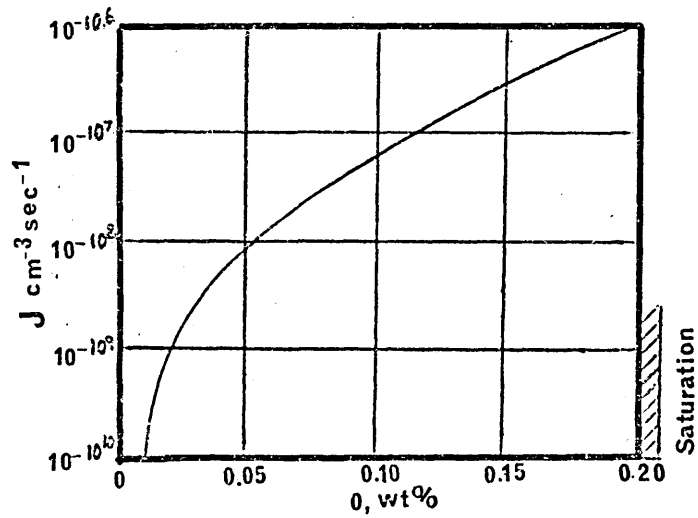
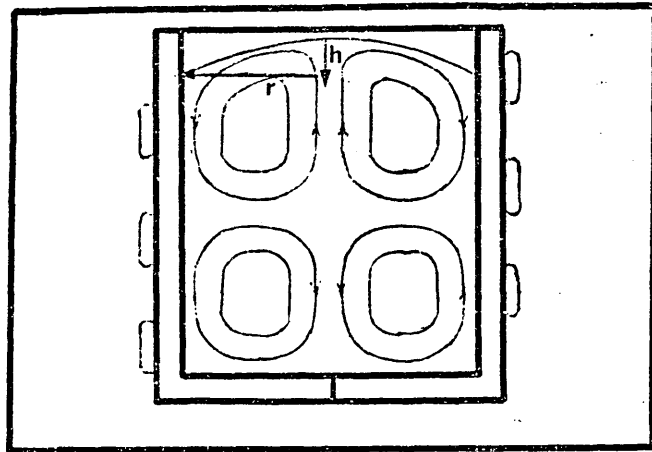
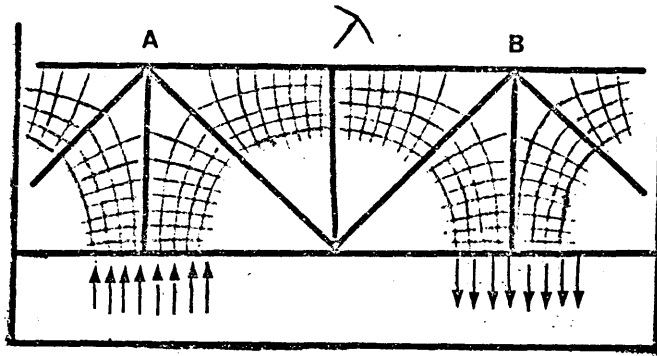


Figure 23.

Schematic representation of a spherical cap bubble and its supposed growth as it rises through metal in the open hearth furnace (79).

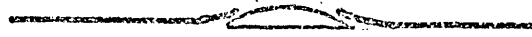
Figure 24.

The effect of bubble size on their rising velocity in a variety of liquids (e.g. ethyl alcohol and mercury). The velocity is uninfluenced by the density of the liquid and the surface tension at the gas-liquid interface. (82)

air in water	+
nitrogen in ethyl alcohol	x
air in mercury	o
air in P.D.A. solutions, (54 c.p.)	Δ
212 c.p. solution	●

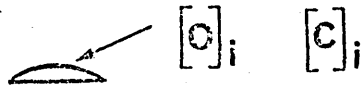
✓.

slag



$[C]_b$ $[C]_b$

Metal



$[C]_i$ $[C]_i$

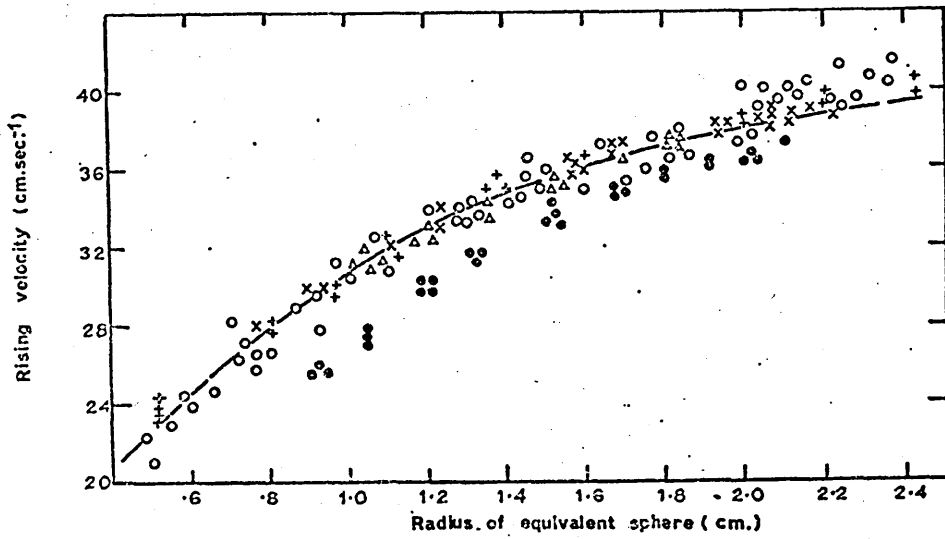
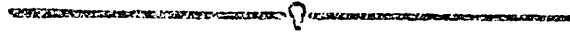


Figure 25.

Increase in mean silicon content of graphite-saturated melts with time, when reacting with silicate melts at 1600° C and CO at 1.0 atm. Bubbled through slag at the slag-metal interface. (94)

Figure 26.

The plot of $\frac{R}{a_{\text{SiO}_2}}$ against R results in a straight line with a negative slope as equation (94) predicts (94).

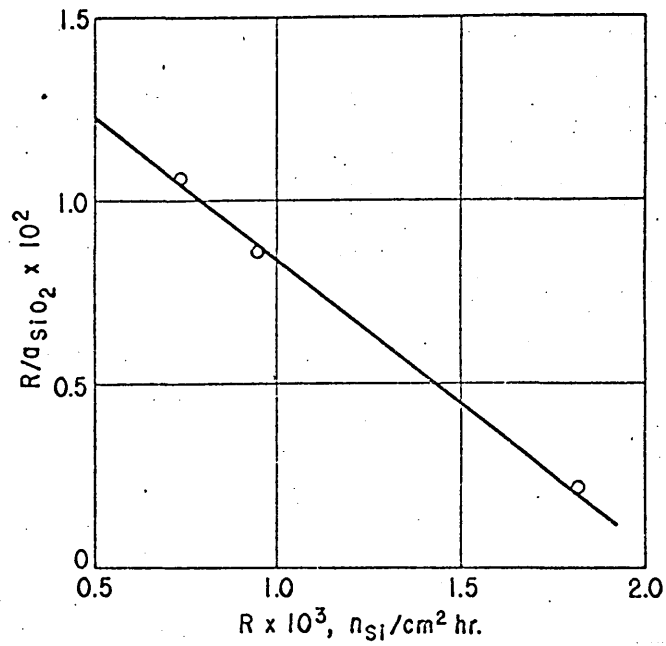
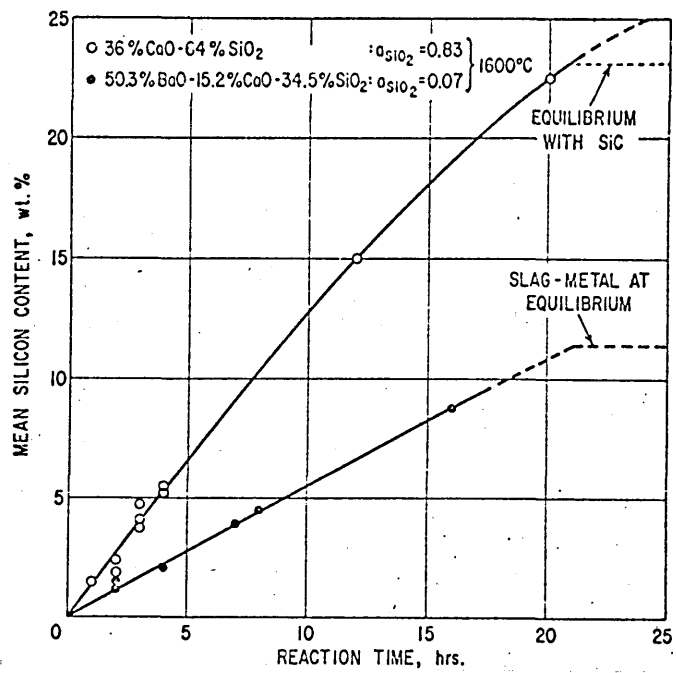


Figure 27.

Rate of silica reduction
at 1450° C in simple graphite
cells and sleeved cells. (96)

Figure 28.

Schematic oxygen concen-
tration profile in liquid
iron. (97)

Figure 29.

Arrhenius plots of rate constants and
temperature for melts saturated with
carbon. (97)

Figure 30.

Arrhenius plot of rate constant and
temperature for melts unsaturated with
carbon. (97)

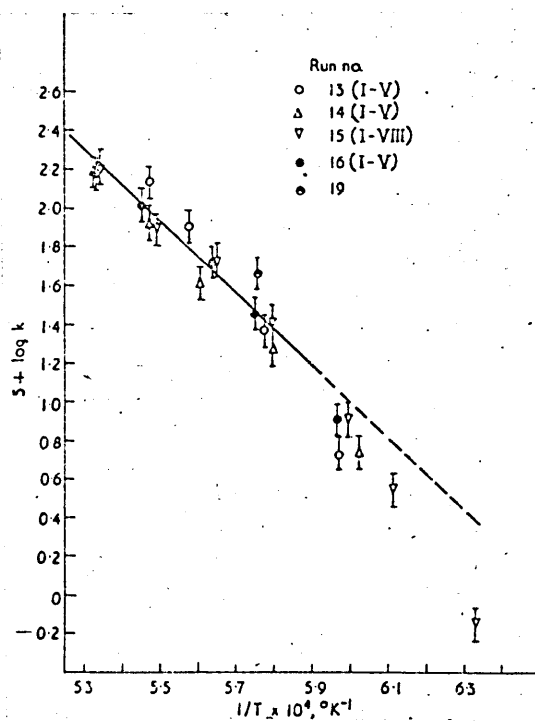
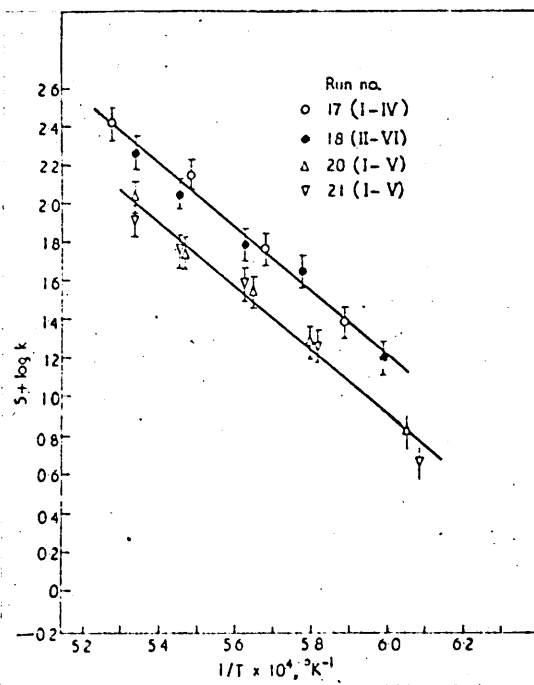
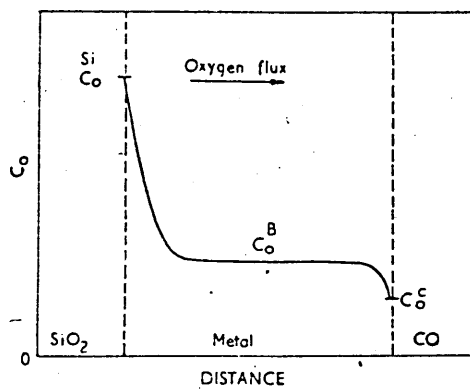
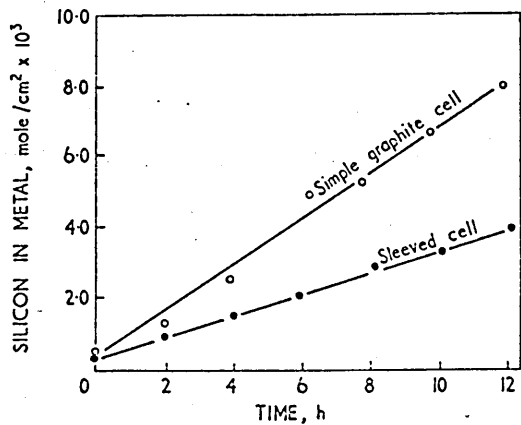


Figure 31.

Increase in silicon content and reduction
in carbon content of steels containing
initially 0.2% C during vacuum melting in
 $4\frac{3}{8}$ in. diameter alumino-silicate crucibles. (99)

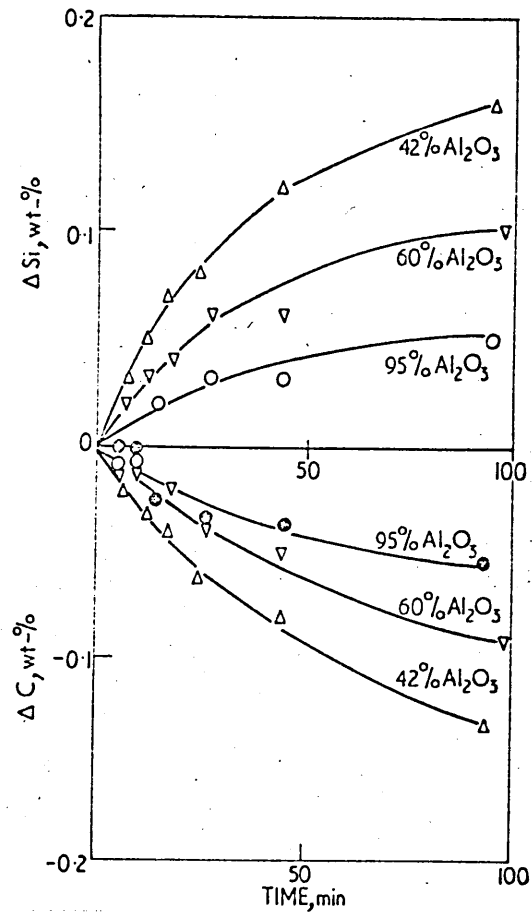
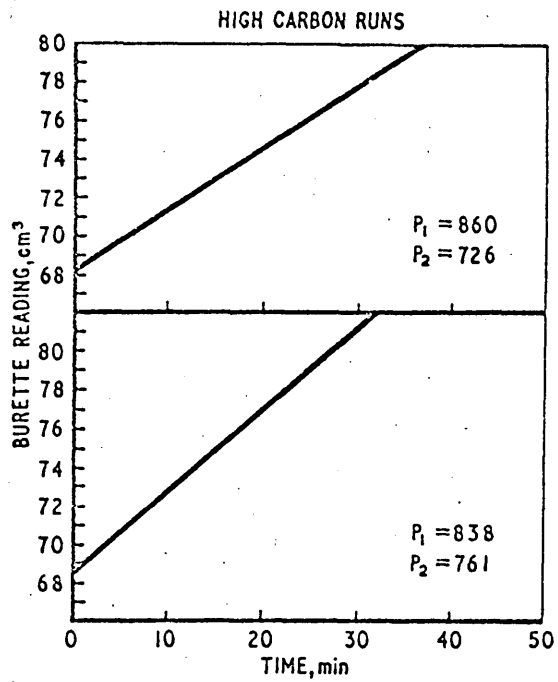


Figure 32.

Results of experiments of Parlee et al (85)
showing evolution of CO with time.

Figure 33.

Variation of mass transfer coefficient β
with $W/o C$.



P_1 = Equilibrating pressure
 P_2 = Pressure during run

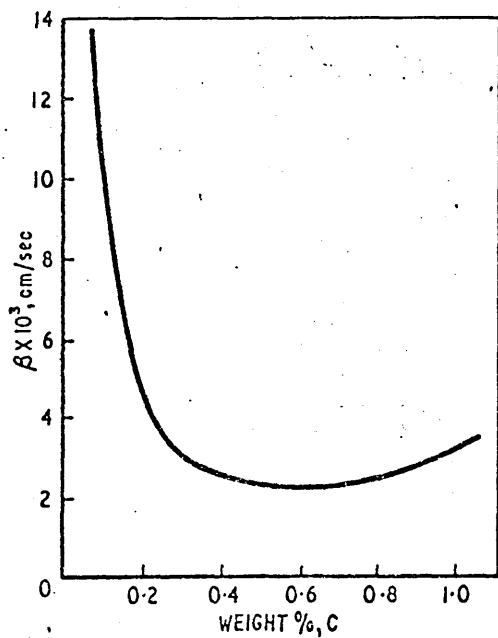
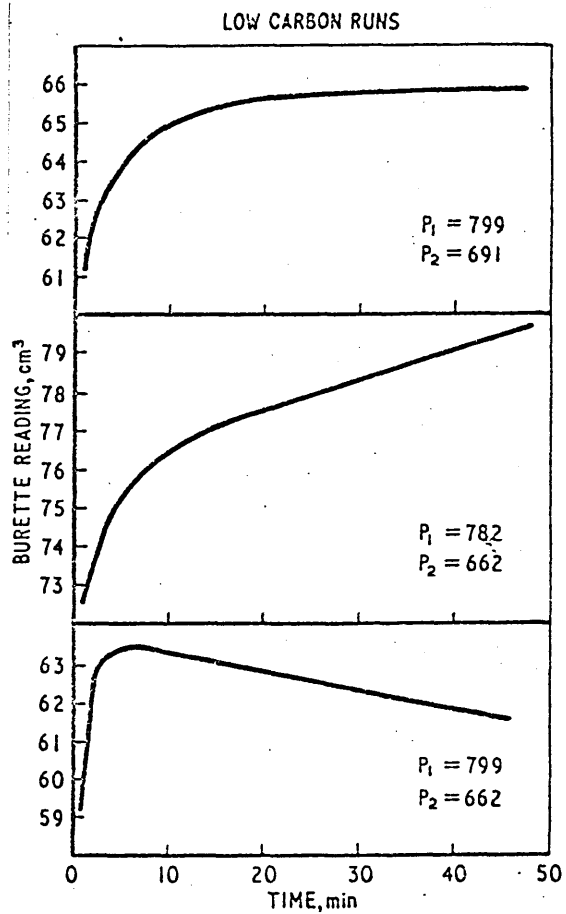


Figure 34.

Reduction of oxide inclusions
by carbon saturated iron at
1700°C. (101)

Figure 35.

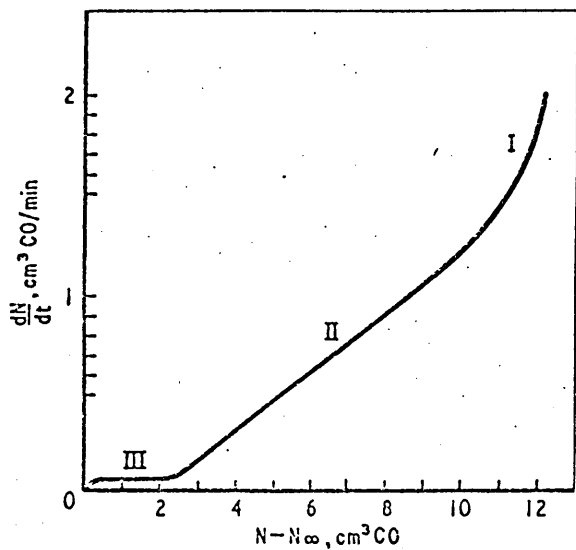
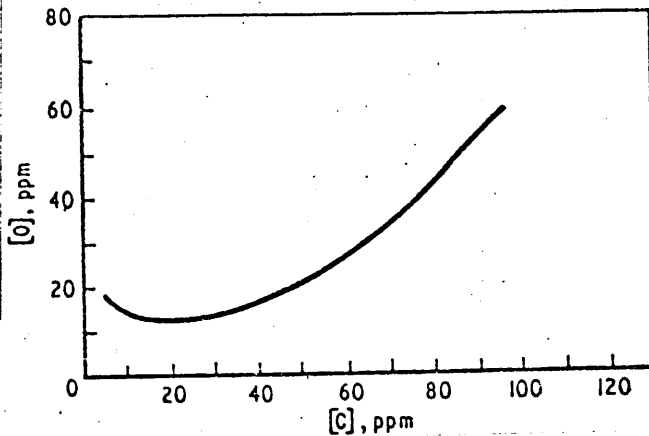
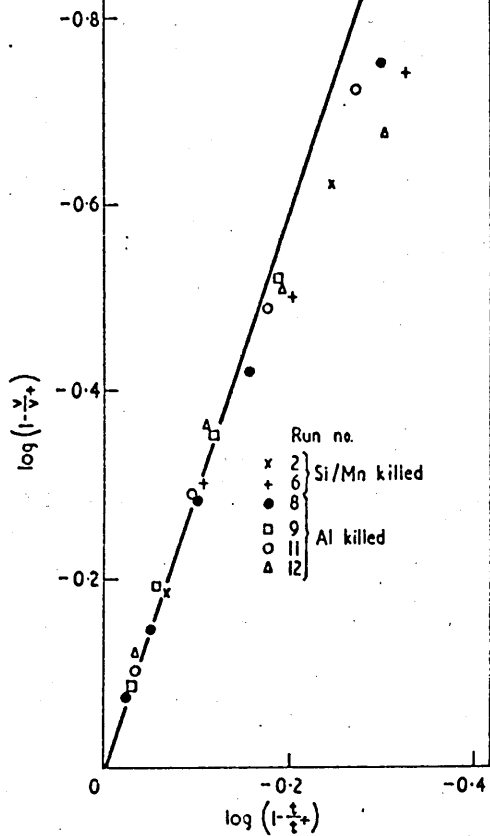
Change of carbon-oxygen
contents during degassing
of an iron melt (86).

Figure 36.

Rate of evolution of carbon
monoxide against gas content
of melt. (86)

Figure 37.

Evolution of carbon
monoxide from molten iron
with time. (86)



N = gas content of the melt at time t ,
in cm^3 of CO at 10^{-3} mm Hg

$N_{\infty} = N_{t \rightarrow \infty}$ = gas content of the melt in cm^3 of
 CO at 10^{-3} mm Hg that would be
in equilibrium with CO gas at
 10^{-3} mm Hg

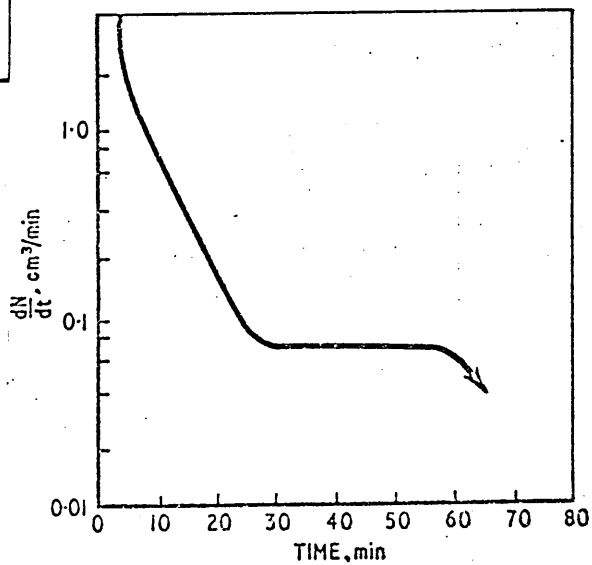


Figure 38. Quantity of gas formed as a function of temperature for different carbon contents of iron in magnesia crucibles and at pressures of 1, 5, 10 and 20 Torr. (107)

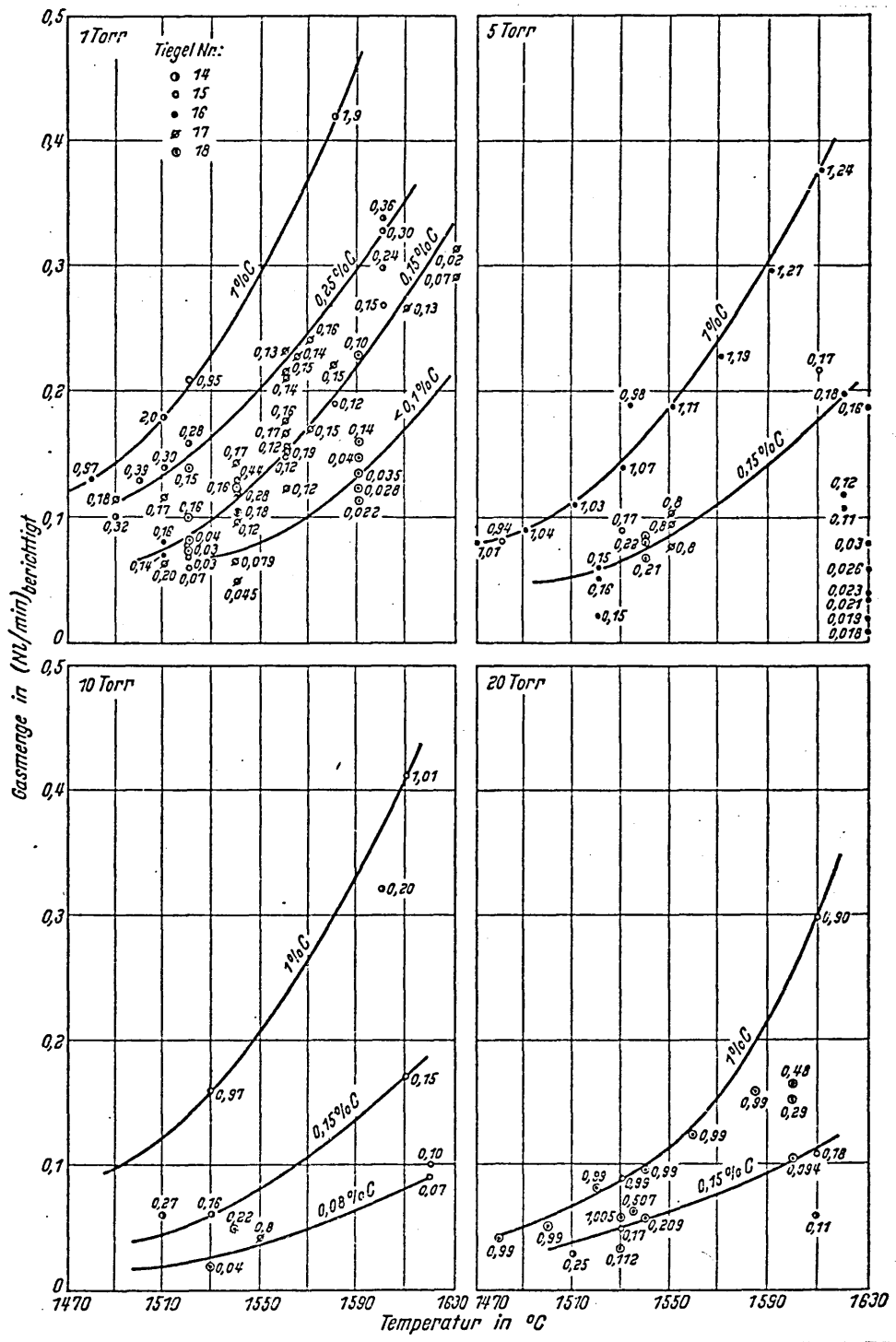


Figure 39. Theoretical quantity of gas evolved (equations 104, 105) at different pressures as a function of carbon content. (107)

Figure 40. Theoretical quantity of gas evolved (equations 104, 105) from melts containing 0.1 and 1% carbon as a function of pressure.

Figure 41. Decarburisation rate vs carbon content in a high frequency induction furnace. (109).

Figure 42. Effect of the free surface area on decarburisation.

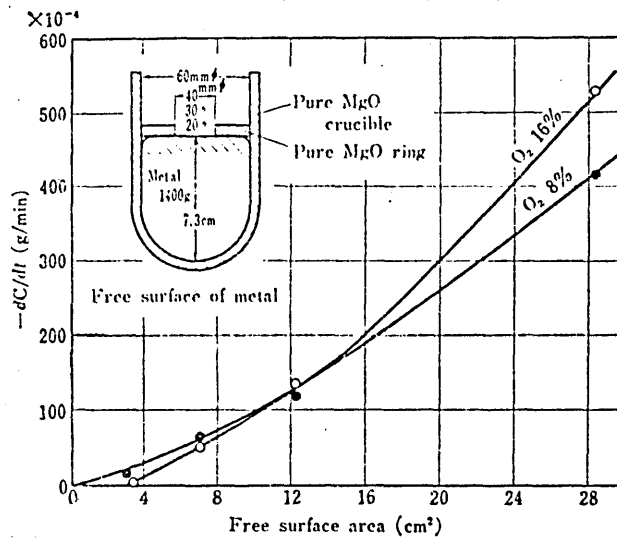
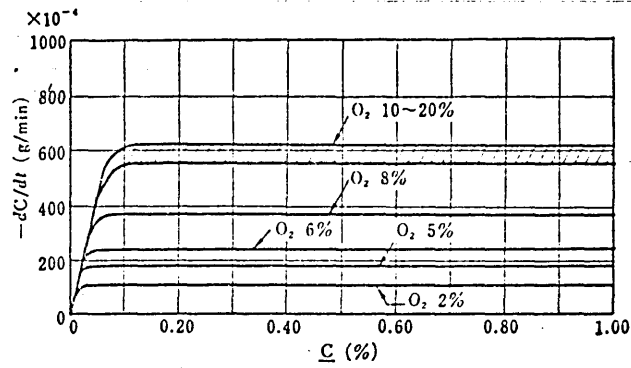
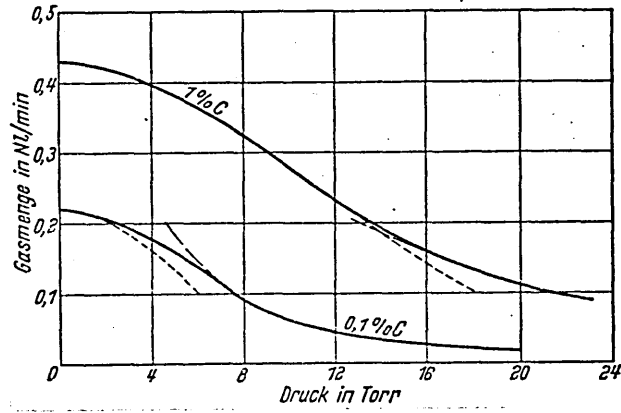
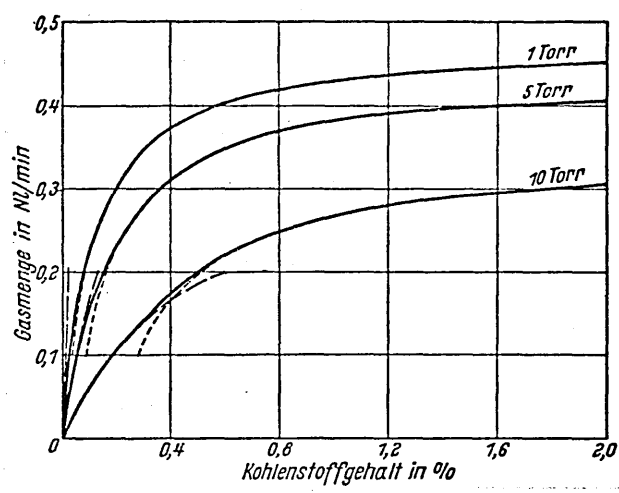
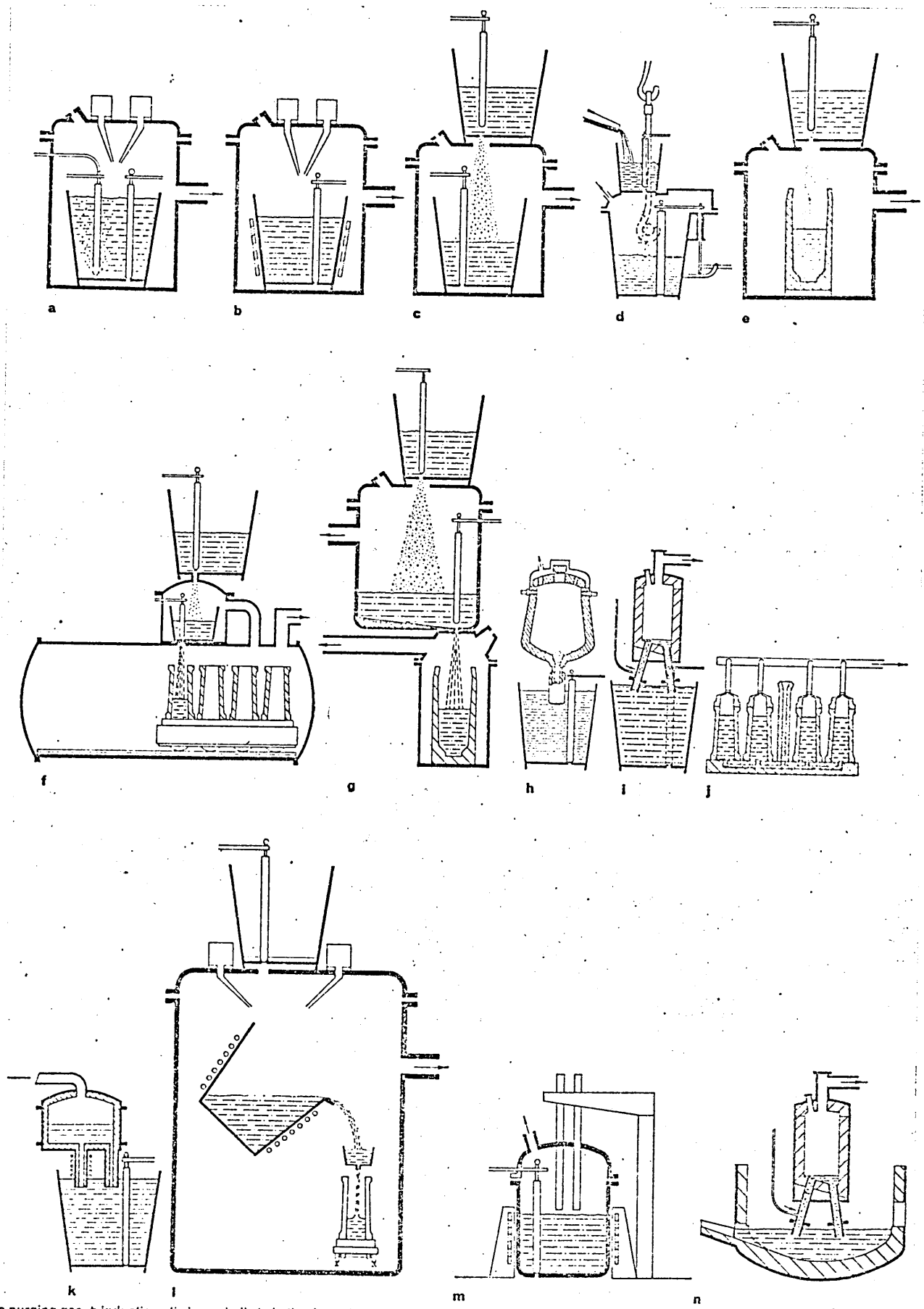


Figure 43.

Schematic illustration of the various methods
of degassing. (112)



a purging gas b induction stirring c ladle to ladle d tap degassing e ladle to mould f ladle to multiple mould g two-stage treatment h vacuum lift
 i circulation by gas lift j ingot degassing k circulation by induction l combination process m arc heating n treatment in the furnace

Figure 44.

Survey of the efficiency of the various degassing processes in terms of hydrogen removal. (present work)(See Table 7 for key to this diagram).

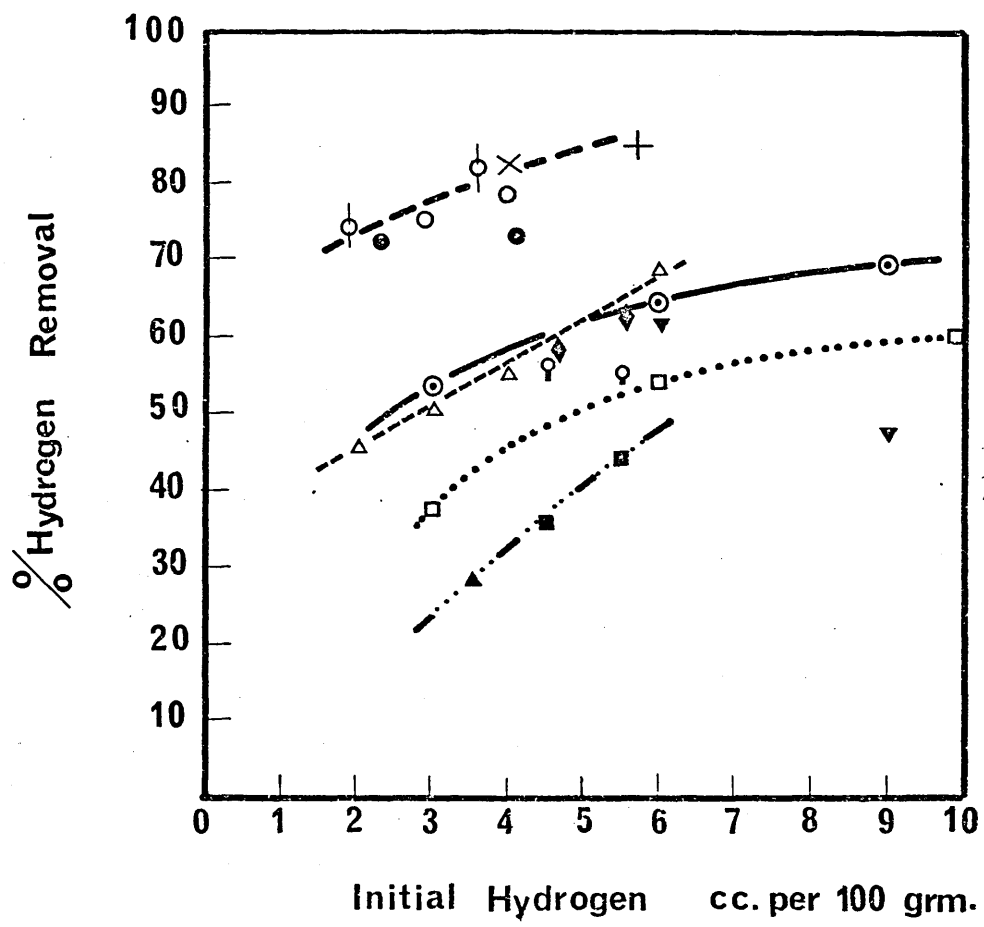


Figure 45. Final oxygen content against initial level for steels in various states of oxidation degassed by the RH method.

Figure 46. Variation in the oxygen content from furnace to ingot mould with partial preliminary deoxidation before the carbon addition and with complete deoxidation with Si and Al. (113). (RH technique).

Figure 47. Percentage of total samples analysed which contained more oxygen than the corresponding amount shown on the abscissa. (125).

Key. Method A: standard double slag, Si deox, air cast.
Method B: double slag, Si + Al deox, air cast.
Method C: standard double slag A plus vac. deg.
Method D: single slag, fce. block with silicon pig iron plus vac. deg.
Method E: double slag, ~~no~~ Si or Al added to fce, vac, deg. with Si to chamber ladle.
Method F: double slag, balanced with Si addition to fce, vac. deg. with Si and Al to chamber ladle.

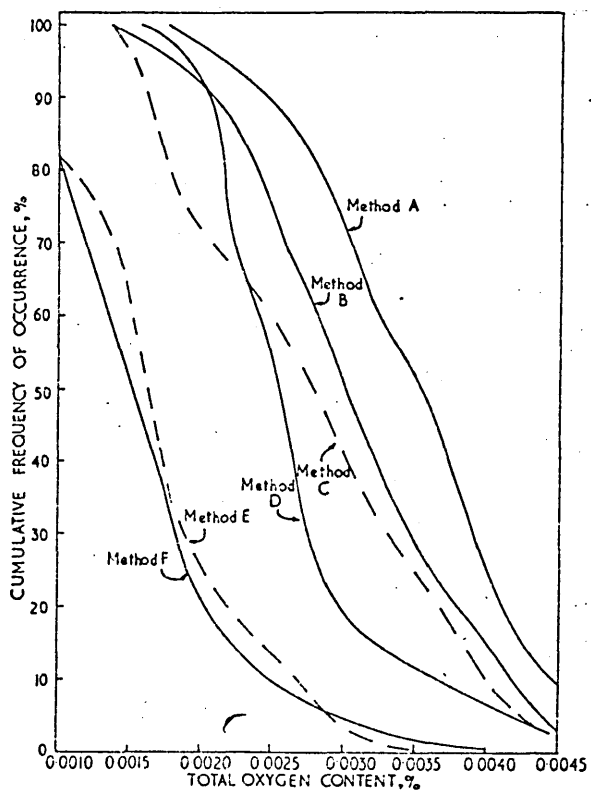
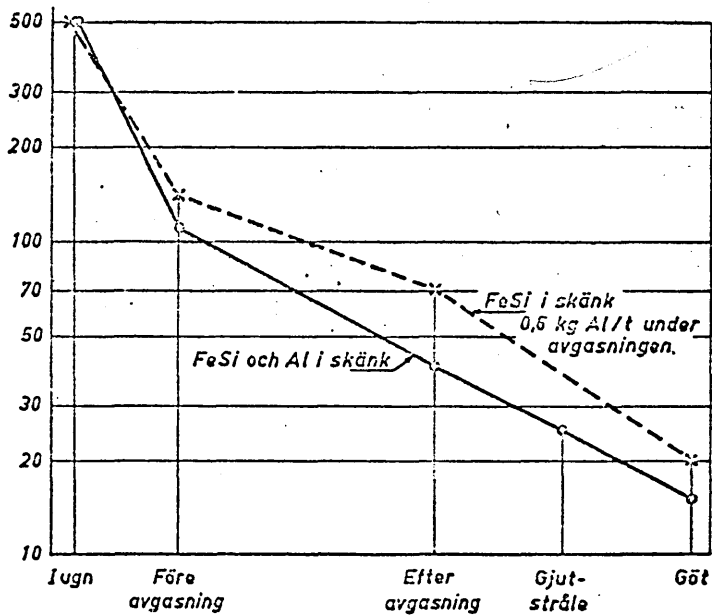
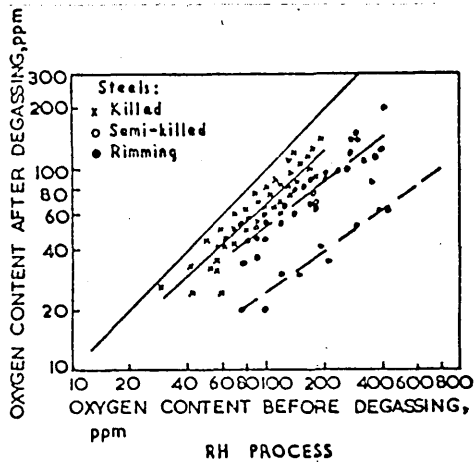


Figure 48.

Deoxidation equilibria in iron at 1600°C. (3)

Figure 49.

Carbon/oxygen relationships obtained by three methods of vacuum treatment. (present work).

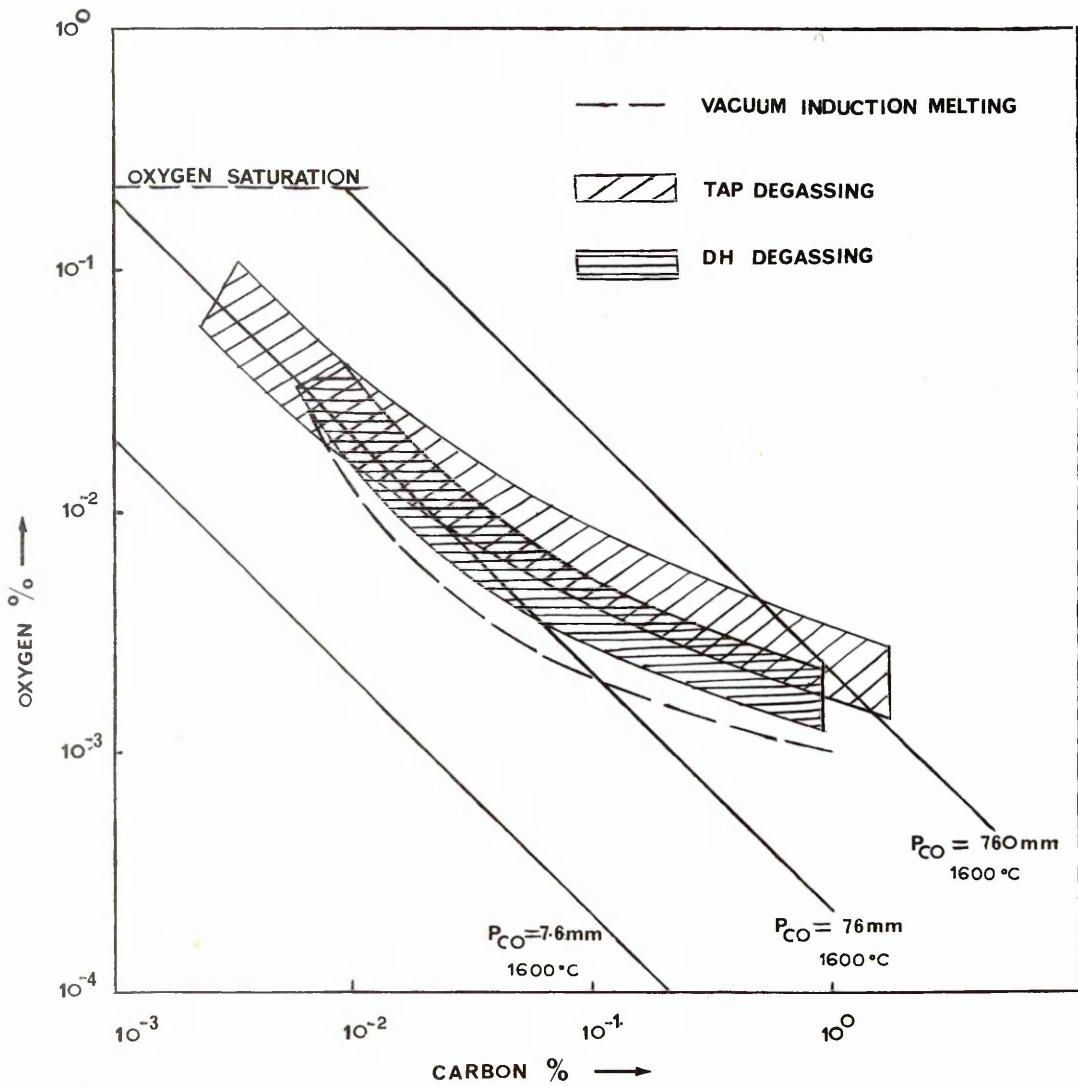
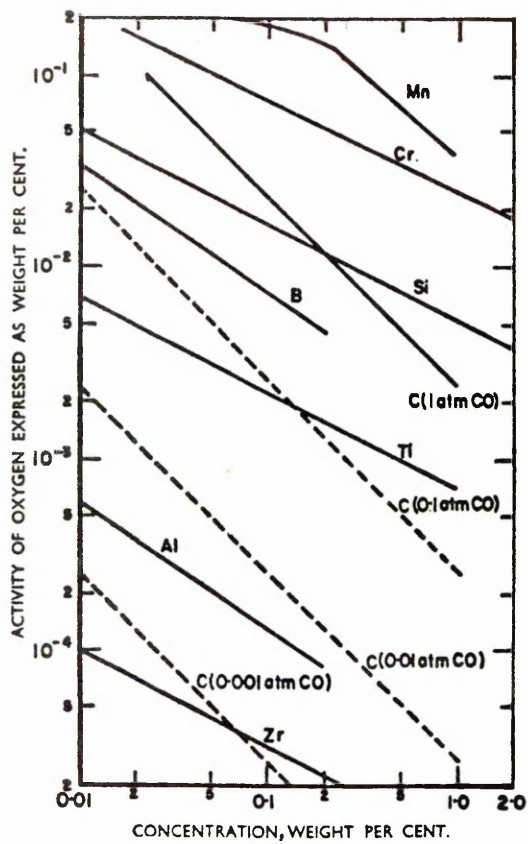


Figure 50.

The 5lb vacuum furnace plus ancillary gear for sampling and temperature measurement. The gas analyser is shown to the left of the main equipment.

Figure 51.

A closer view of the furnace showing electromagnetic valves and switches for control of the gas in the sampling lock and main vessel. A mercury manometer and McLeod gauge can be seen, mounted on the main panel.

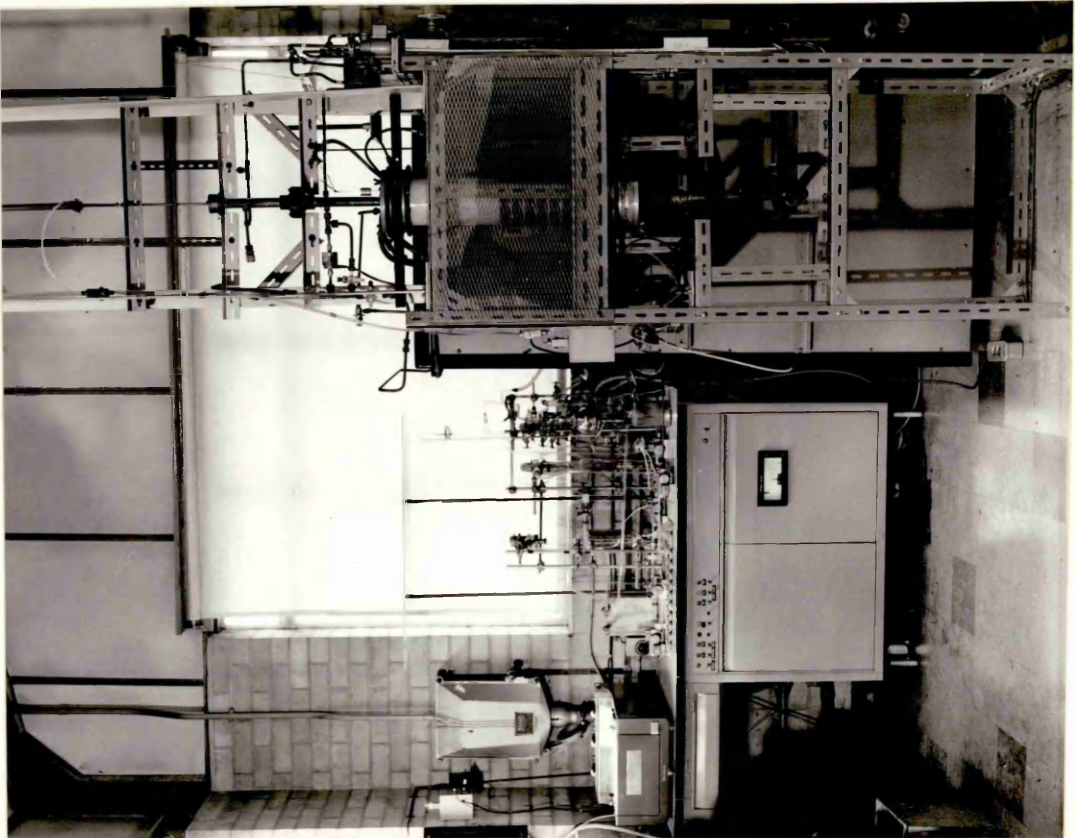
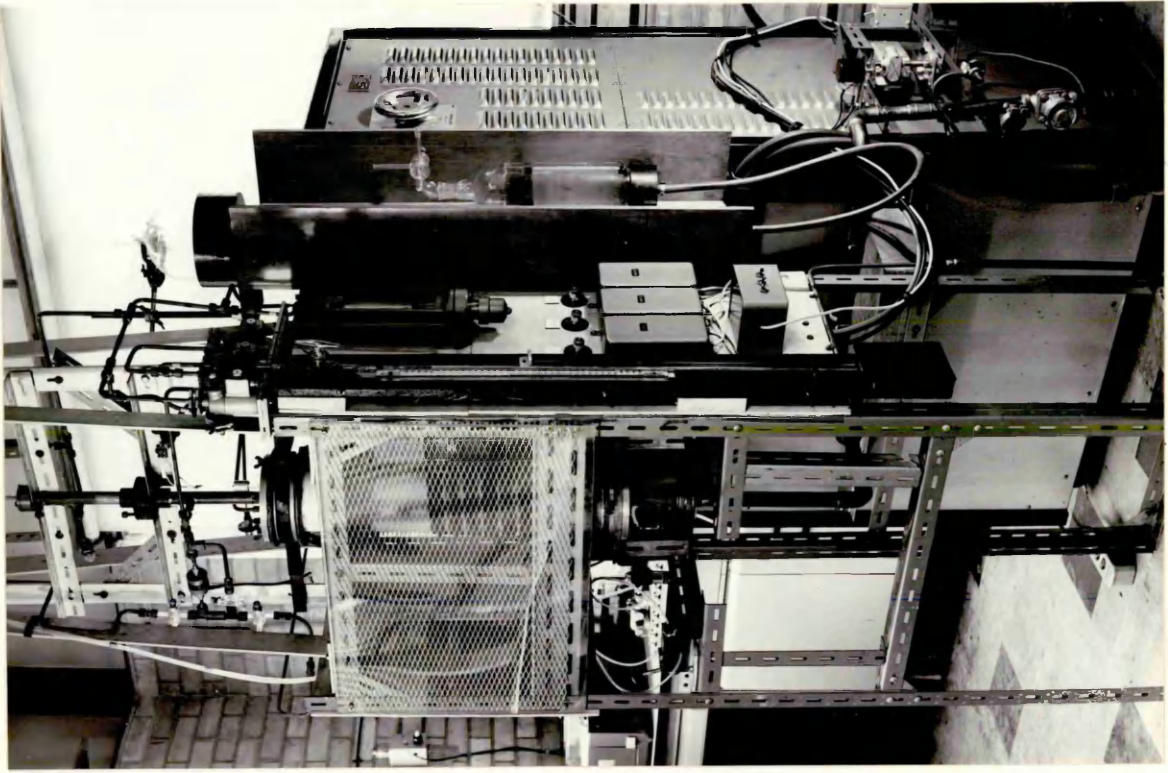


Figure 52.

A schematic diagram of the experimental assembly, indicating the lines for pressure measurement and gas analysis.

Figure 53.

A schematic representation of the crucible assembly.

Figure 54.

Photograph showing the fail-safe design of the vacuum pump layout which uses electromagnetic valves to seal off the system in the event of a leak.

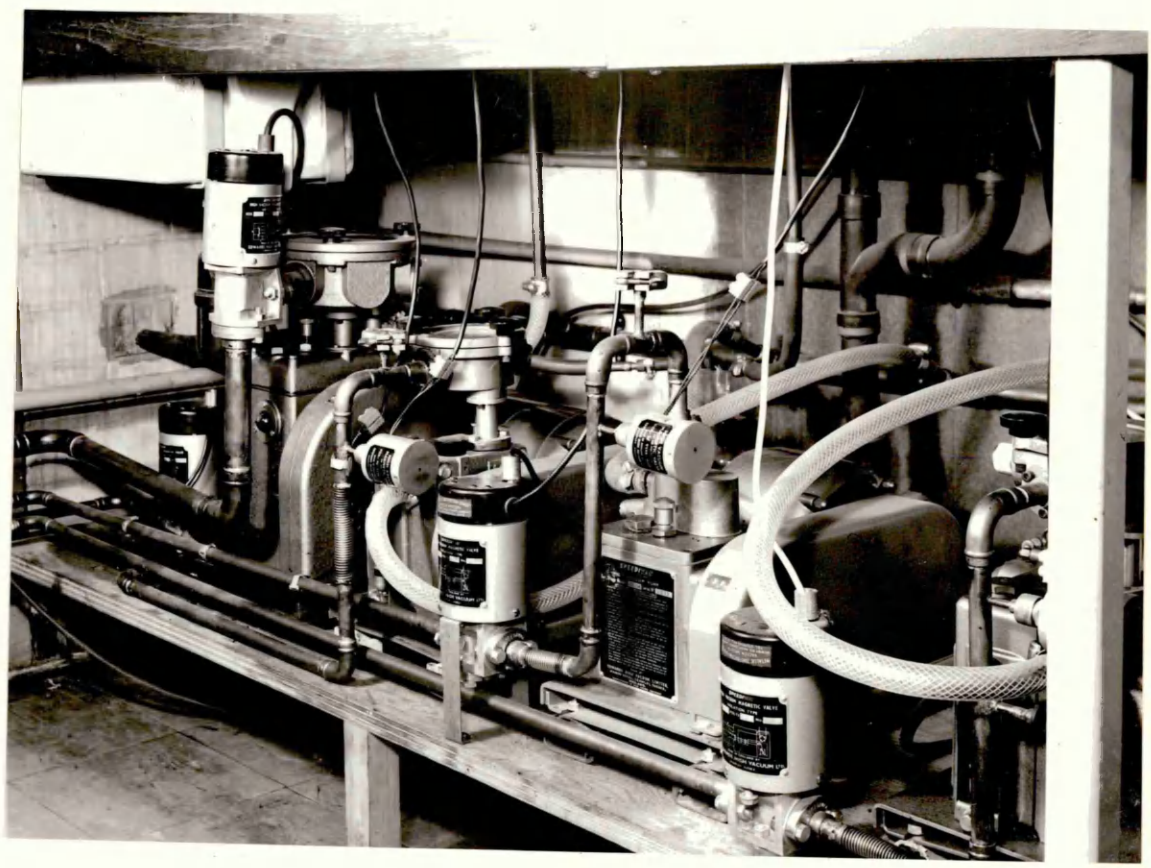
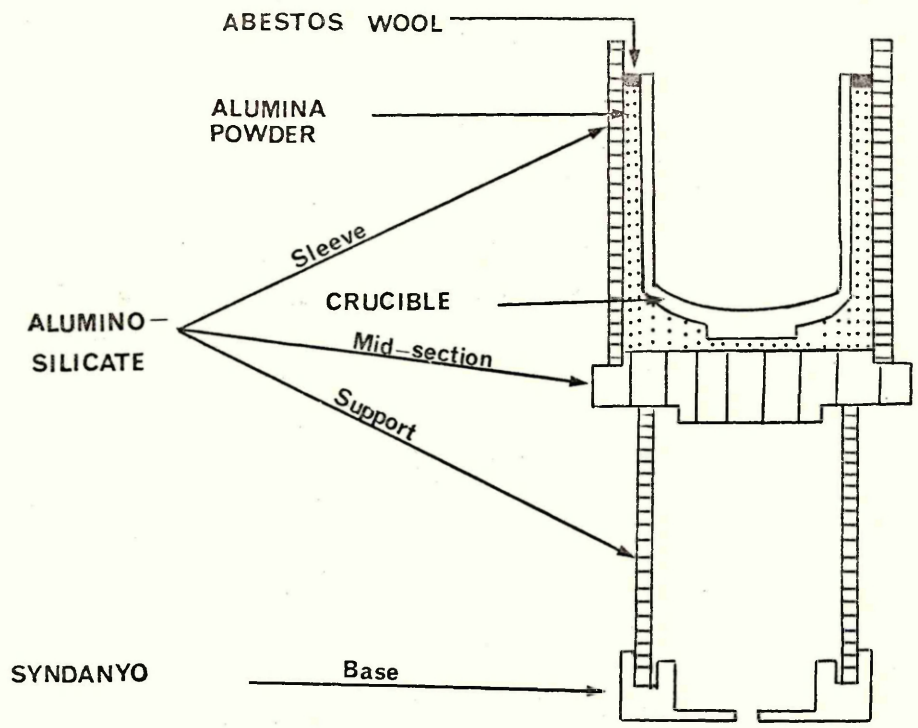


Figure 55.

The thermocouple design evolved from preliminary trials which gave accurate temperature measurement for periods up to 6 hours.

Figure 57. Photograph of the

sampling lock showing the ball valve seal and gas and vacuum connections. A sampling tube is about to be loaded into the lock.

Figure 56.

The device finally chosen to take samples from the liquid melt without fear of contamination or significant temperature changes.

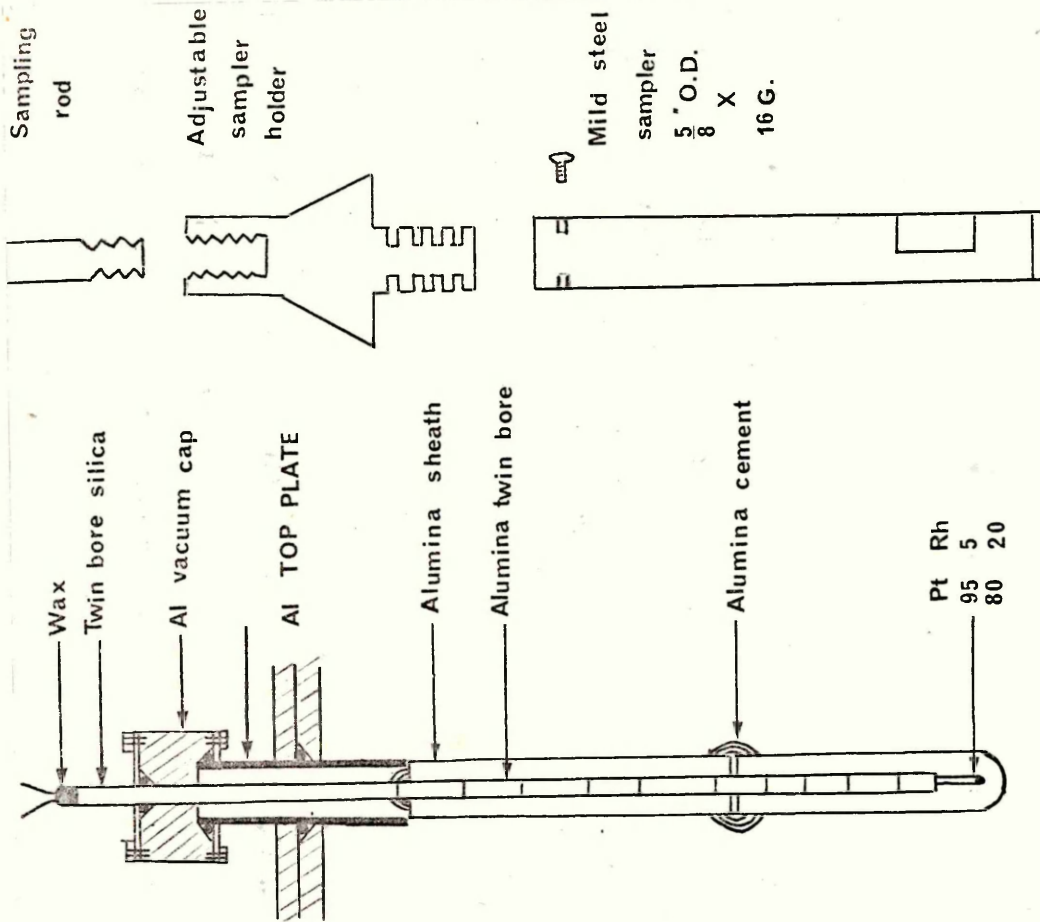
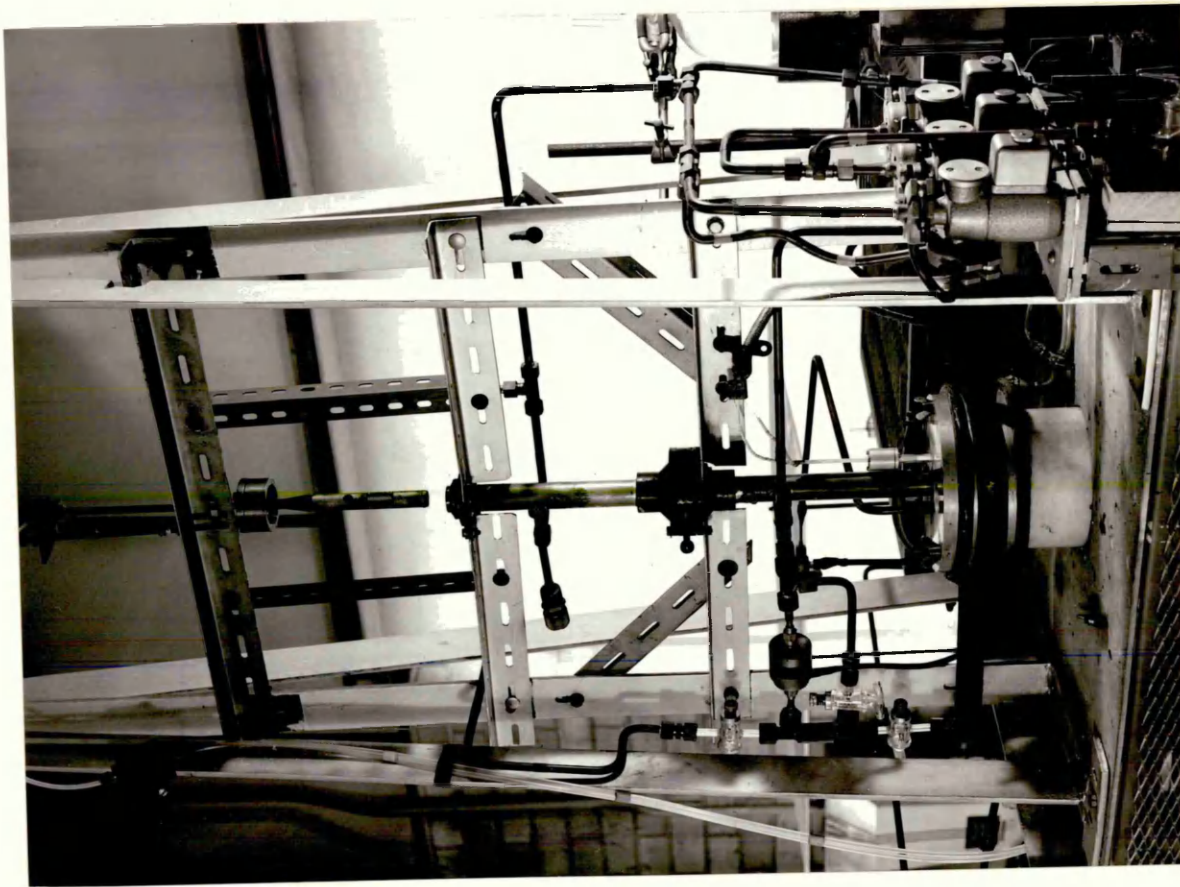
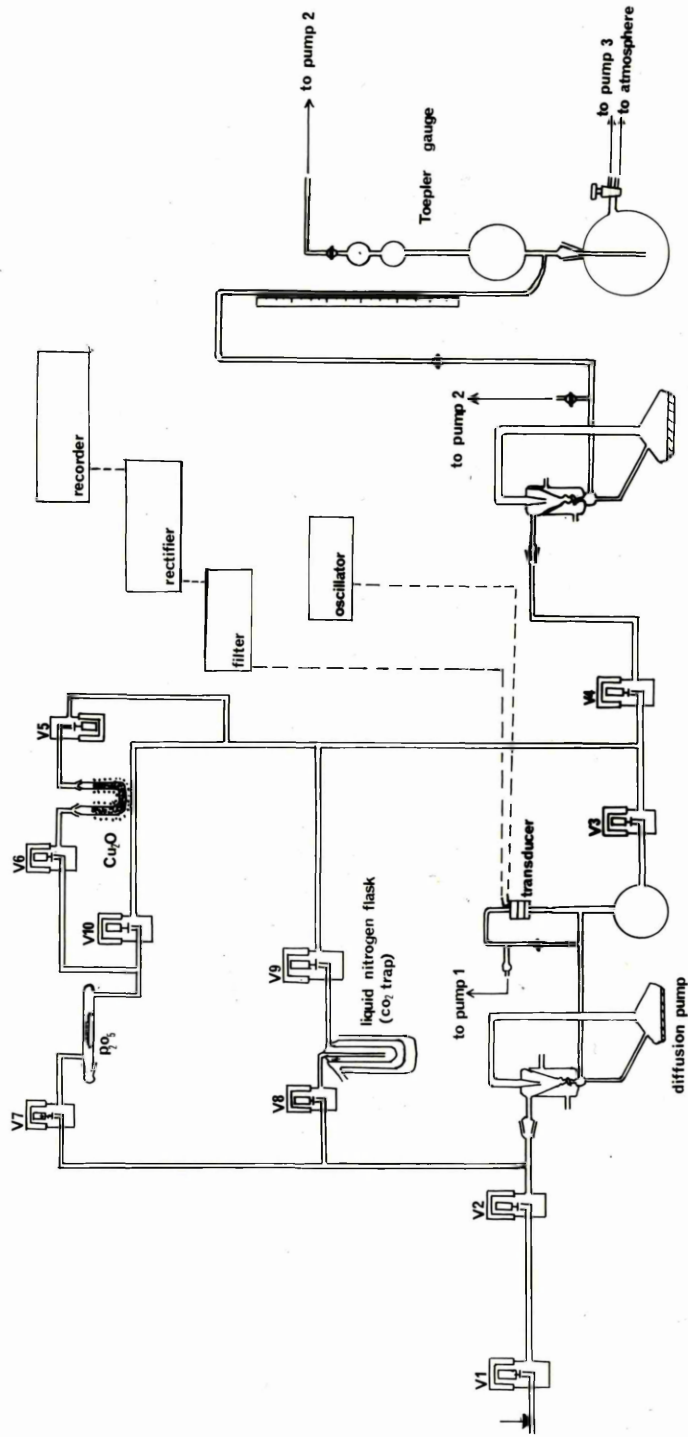


Figure 58. Schematic diagram of the gas analysis unit. The electromagnetic valves used to select the analysis circuit are numbered VI to VIO.

GAS ANALYSIS UNIT



GAS ANALYSIS UNIT

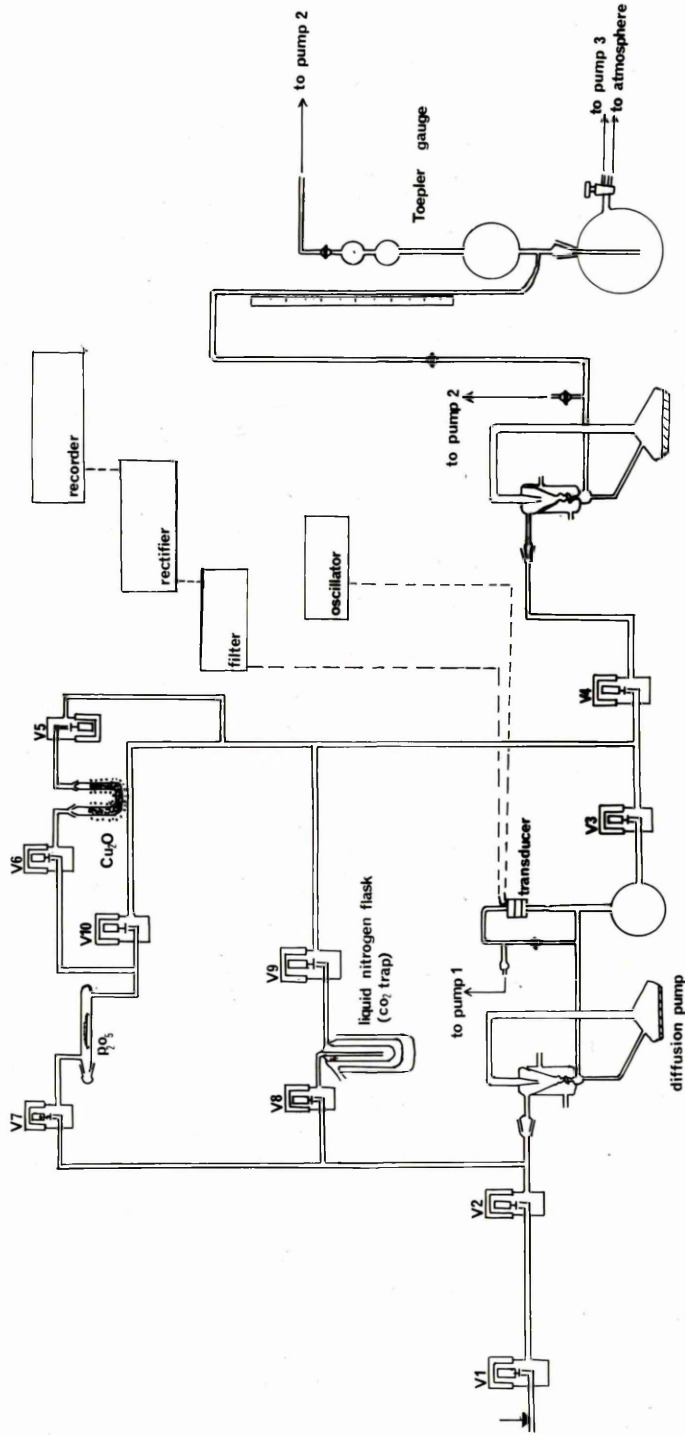


Figure 59.

The gas analysis unit showing on the left hand side the Rikadenki mV recorder on the bench top and the rectifier and zero-adjust controls for the transducer.

Figure 60.

The individual analysis circuits can be clearly identified from this photograph. The transducer has been surrounded with cotton wool and an earthed copper-mesh to reduce temperature fluctuations and electrical pick-up.

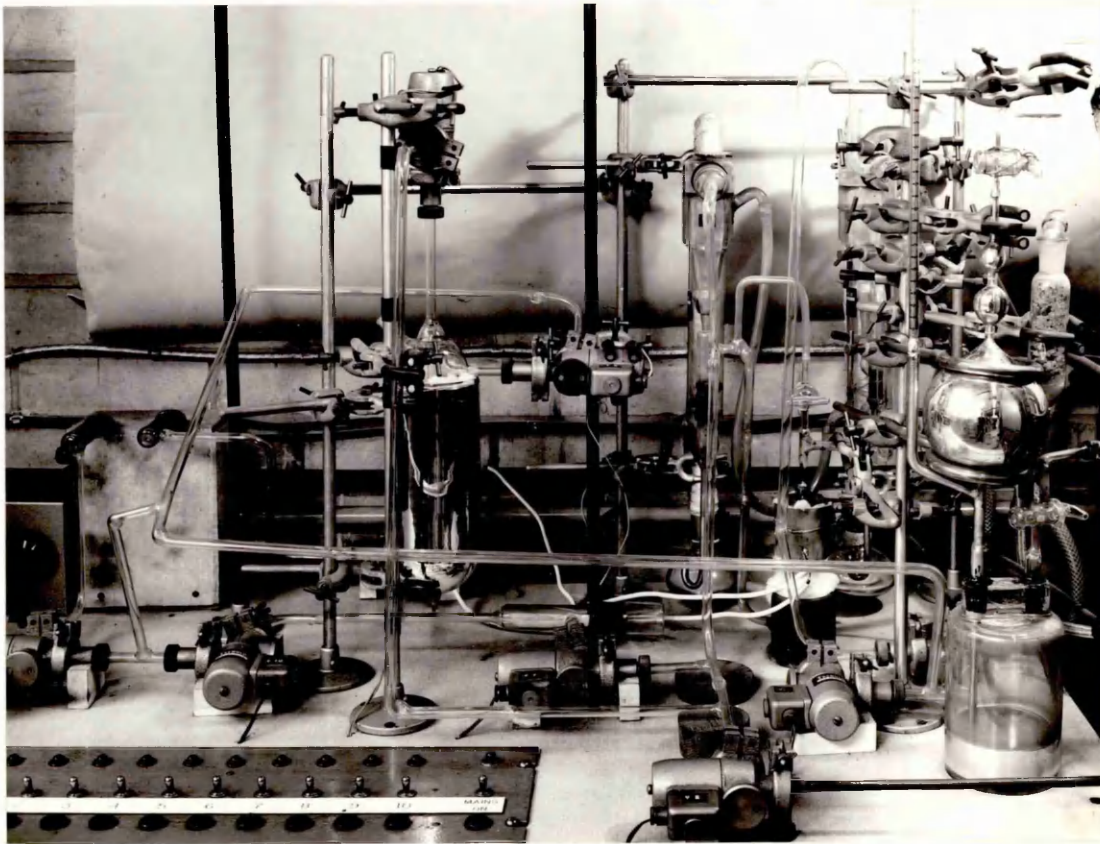
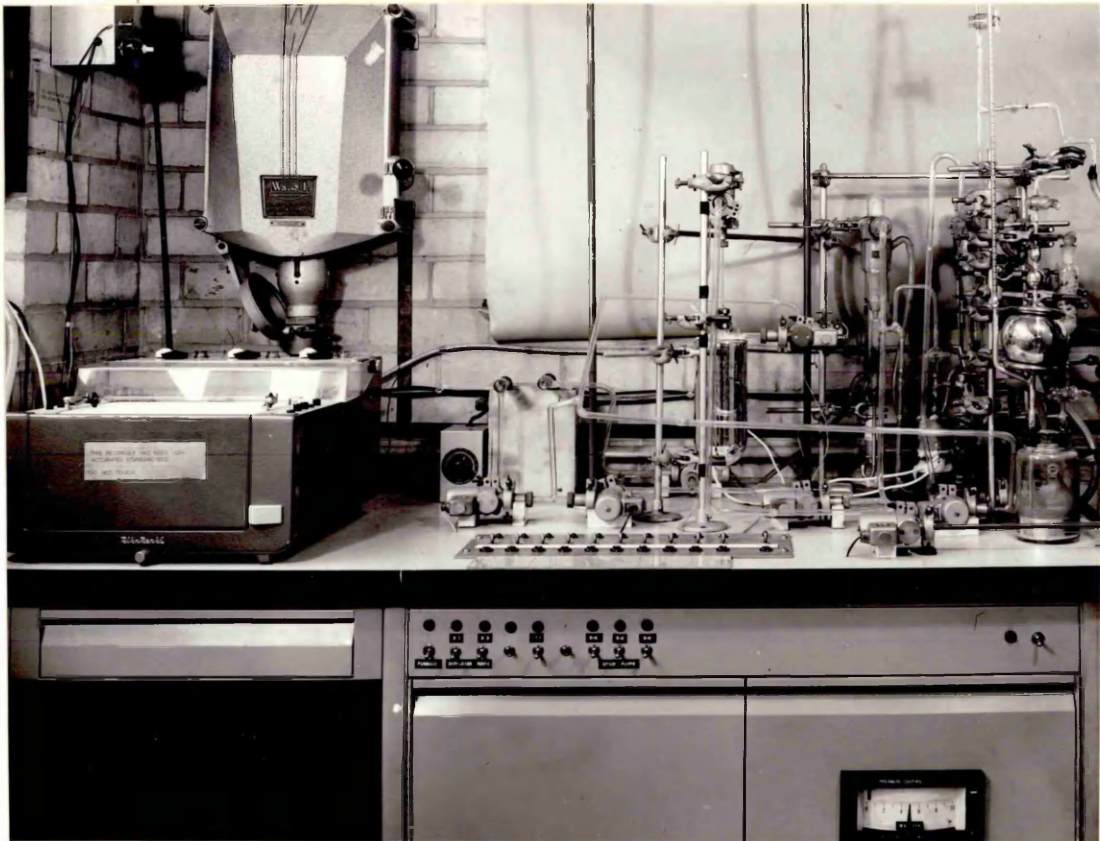


Figure 61.

The calibration graph for the ± 50 m.b. transducer used in the gas analyser (see Appendix I).

Figure 62.

A typical trace for the analysis of a sample of gas taken from the furnace chamber. The chart speed in this case was 5 mm/min or one division every 2 minutes. The temperature trace has been zeroed at 1.0 mV giving a recorded value of 6.35 mV for 1600°C

Figure 63.

The effect of the melt oxygen content on the amount of oxygen transferred from MgO - 8%SiO₂ crucibles in 200 minutes, showing the separate contributions of oxygen from water, silica and magnesia.

TOTAL OXYGEN TRANSFER, wt% IN 200 min.

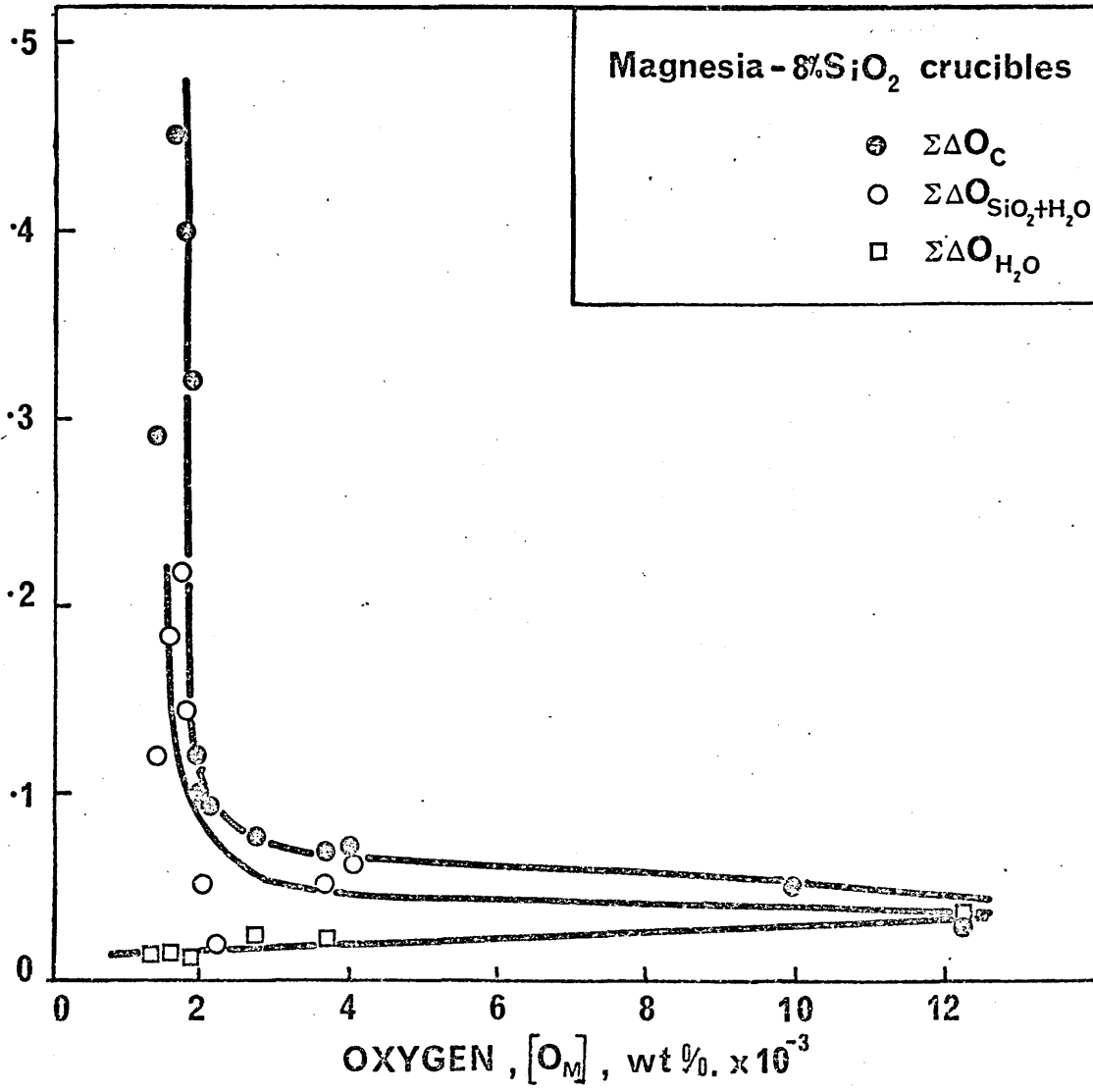


Figure 64.

The effect of the melt oxygen content on the amount of oxygen transferred from aluminosilicate crucibles in 200 minutes. The contribution from alumina can be found by comparing the top curves for the measured donation from silica and water with the bottom curves for the measured removal of oxygen from the melt by reaction with carbon.

TOTAL OXYGEN TRANSFER, wt% IN 200 min.

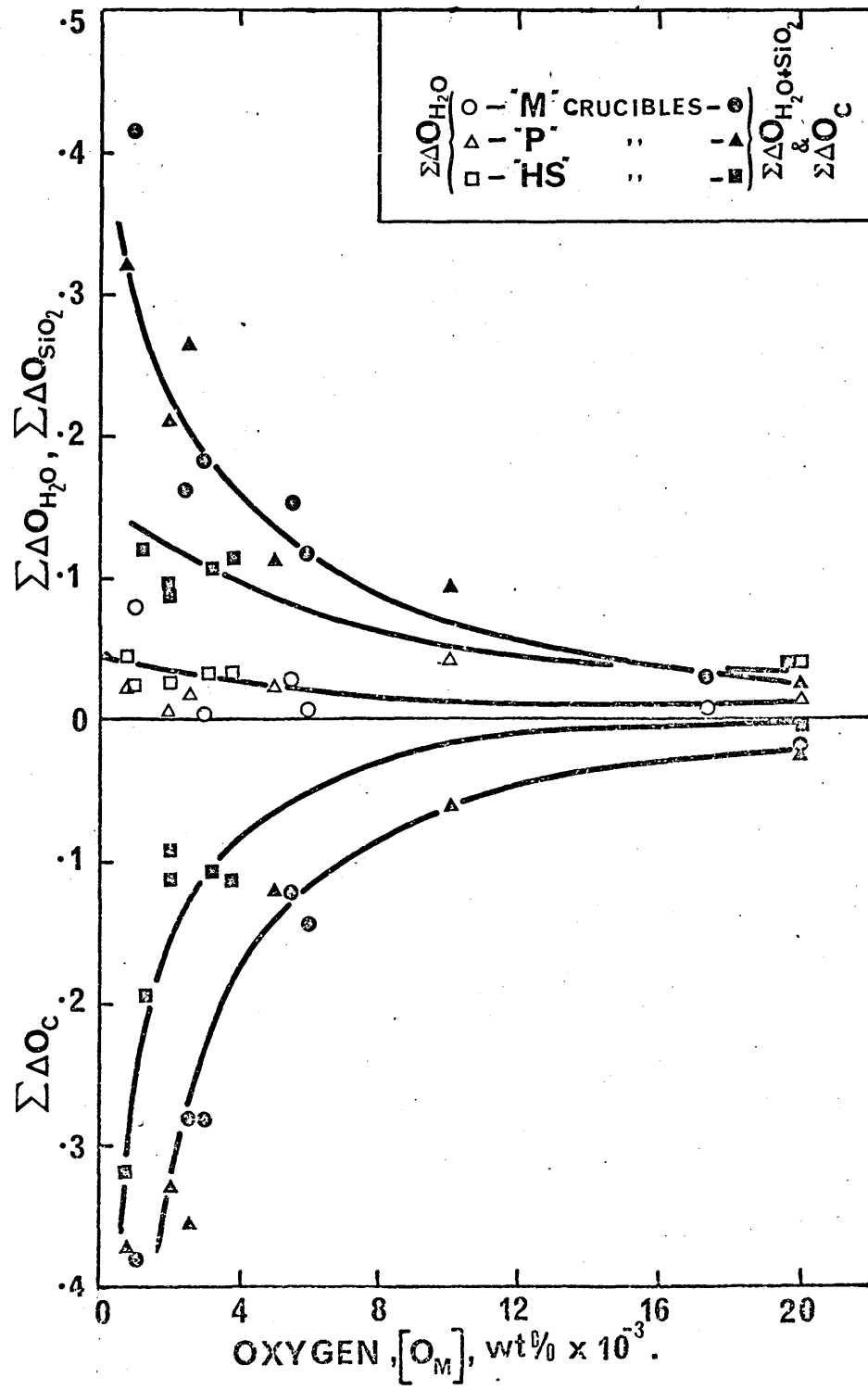
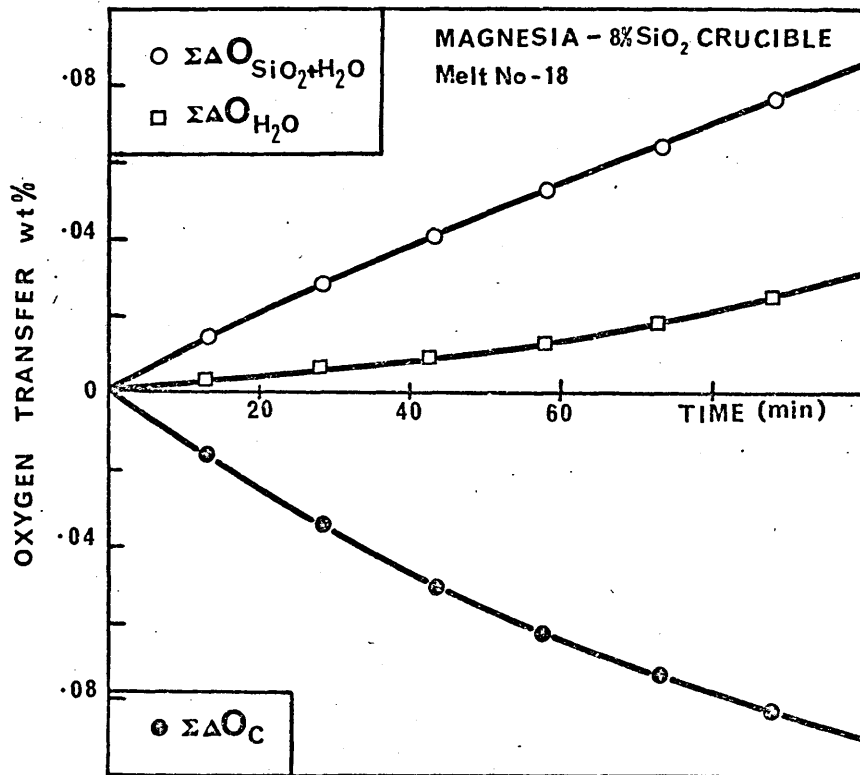


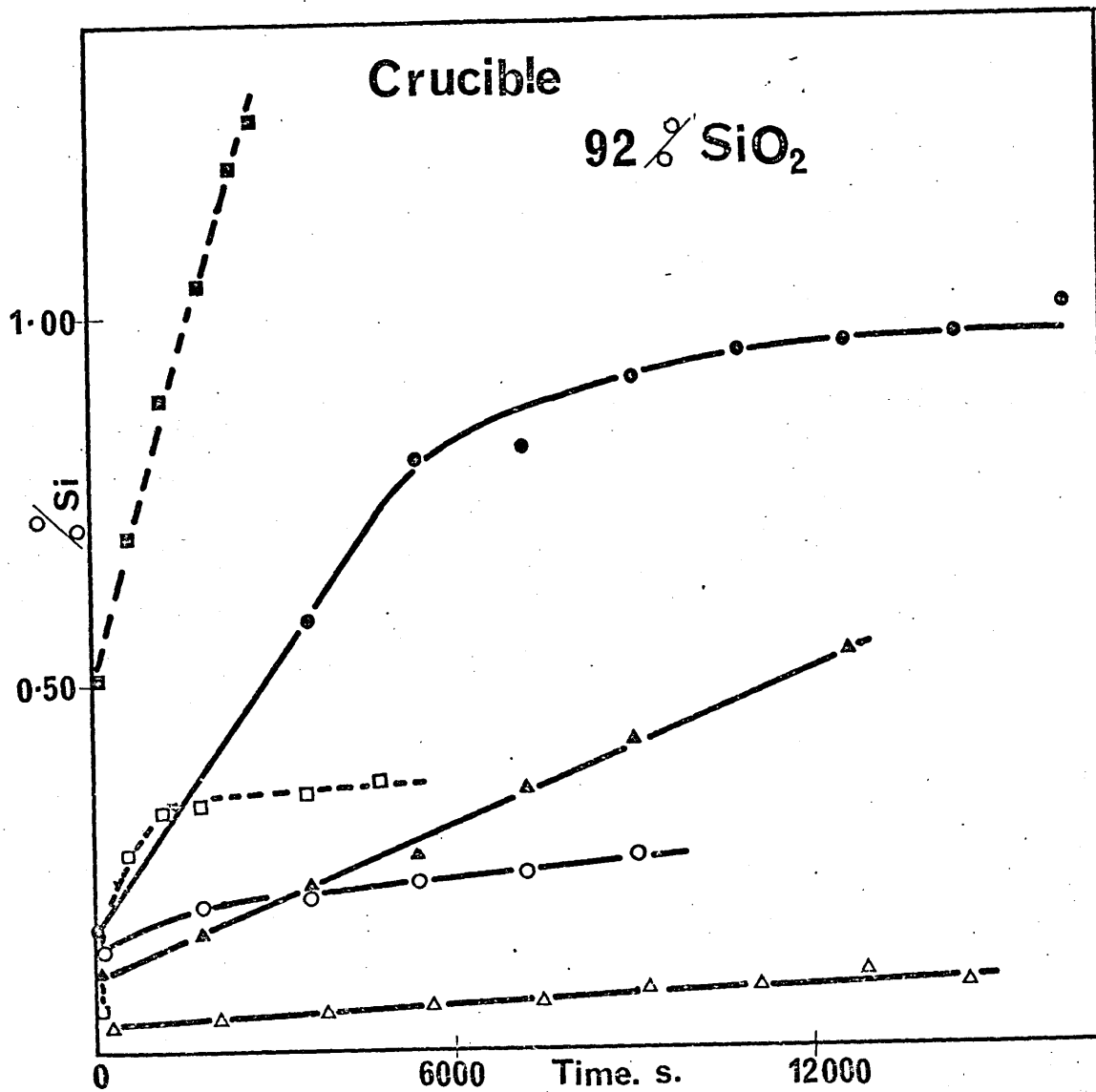
Figure 65.

This diagram shows the amount of oxygen picked up or removed as time progresses. Melt 18, in a crucible of MgO-8\%SiO_2 initially contained approximately 0.1%C and was controlled at a total pressure of 76 torr. Under these conditions it is apparent that the oxygen contributed from water and silica alone is sufficient to account for all the carbon removed from the melt. Silica dissociation alone, however, accounts for only two-thirds of the total oxygen donated.



Handwritten note: 2/1 (as 7.0)

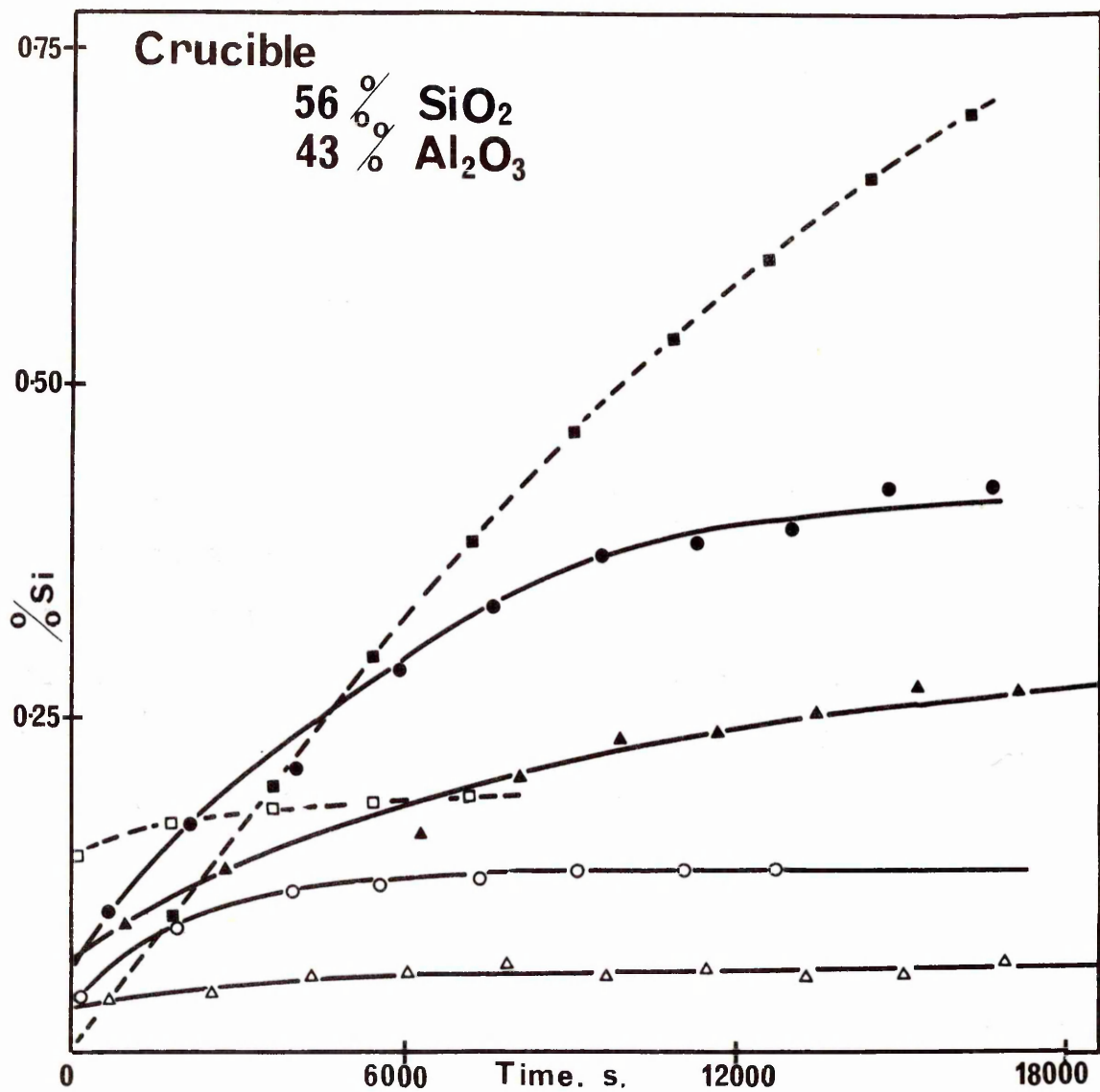
Figure 66. Silicon pickup from crucibles consisting of 92 wt.%SiO₂ - 4 wt.%Al₂O₃. The extent and rate of reaction is increased by increasing carbon content and decreasing pressure. The key for the curves is given in the table below the diagram.



Melt No	Key	Initial % C	Static Oxygen ₃ x 10 ⁻³	Control Pressure mm.Hg.	$\frac{\Delta Si}{\Delta t}$ % per s. x 10 ⁻⁵ at t =			
					600 s	6000s	12000s	
110	■	0.786	4.50	3	18.75	-	-	
100	●	0.885	2.20	140	10.83	3.47	0.66	
99	▲	0.935	4.00	760	3.510	3.51	3.51	
109	□	0.288	4.70	3	13.33	0	-	
106	○	0.16	6.60	140	3.33	0.83	-	
101	△	0.141	20.00	760	0.575	0.49	0.094	
	---	Calculated						

Figure 67.

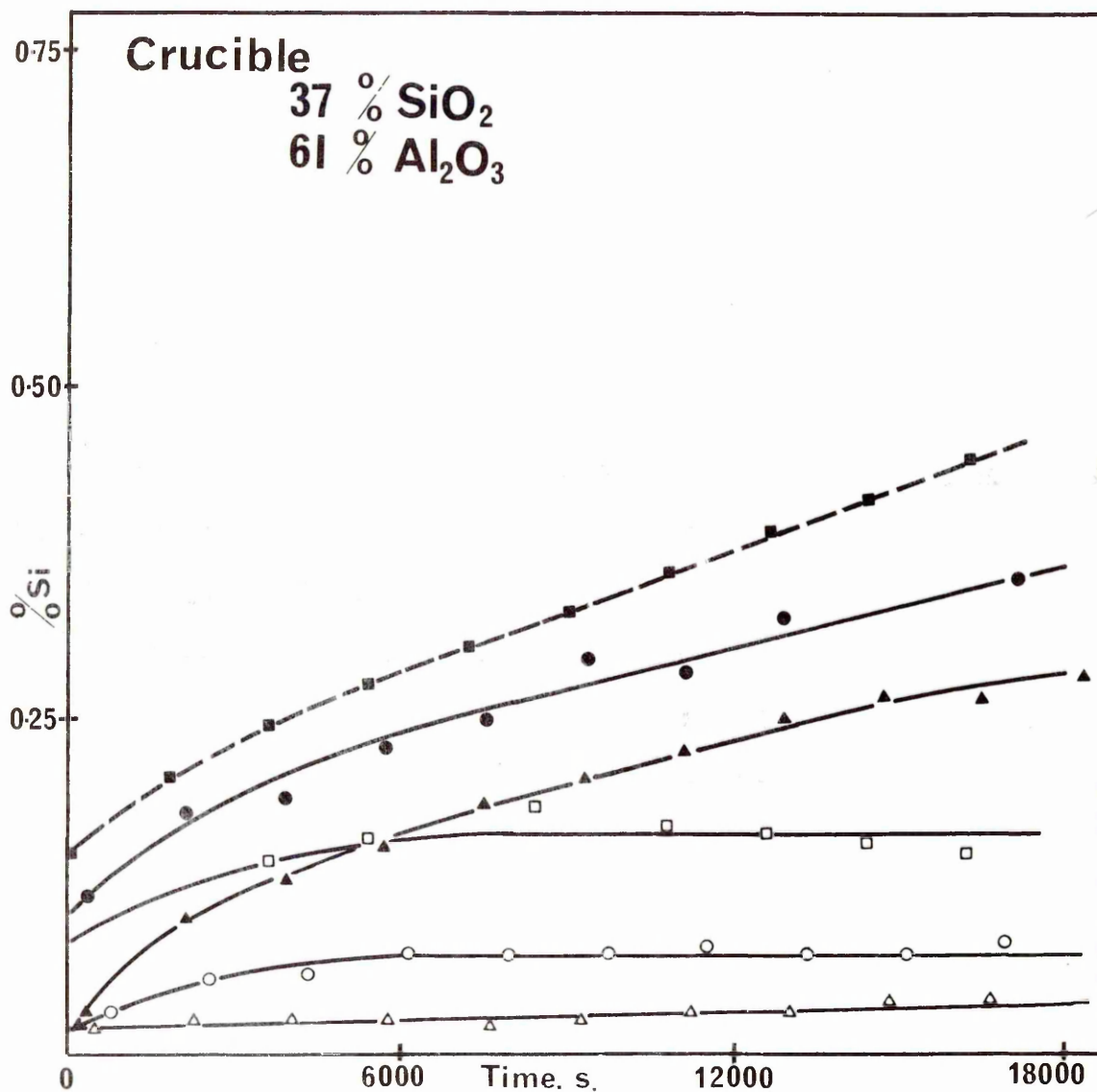
The extent and rate of silicon donation from 56 wt.%SiO₂ - Al₂O₃ crucibles is seen to depend on the oxygen concentration achieved by the carbon-oxygen reaction. In the table below the graph the rate of silicon transfer is given for three values of time (t).



Melt No	Key	Initial % C	Static Oxygen x 10 ⁻³	Control Pressure m.m.Hg.	$\frac{\Delta Si}{\Delta t}$ % per.s. x 10 ⁻⁵ at t =		
					600 s.	6000 s.	12000 s.
89	■	0.853	1.20	3	5.50	5.30	3.30
44	●	0.935	1.00	76	5.50	2.70	0.60
41	▲	0.955	2.50	760	2.60	1.20	0.60
86	□	0.037	-	3	1.70	0.30	-
45	○	0.126	6.00	76	2.60	0.20	0
49	△	0.134	17.30	760	0.50	0.10	0.005
	---	Calculated					

Figure 68.

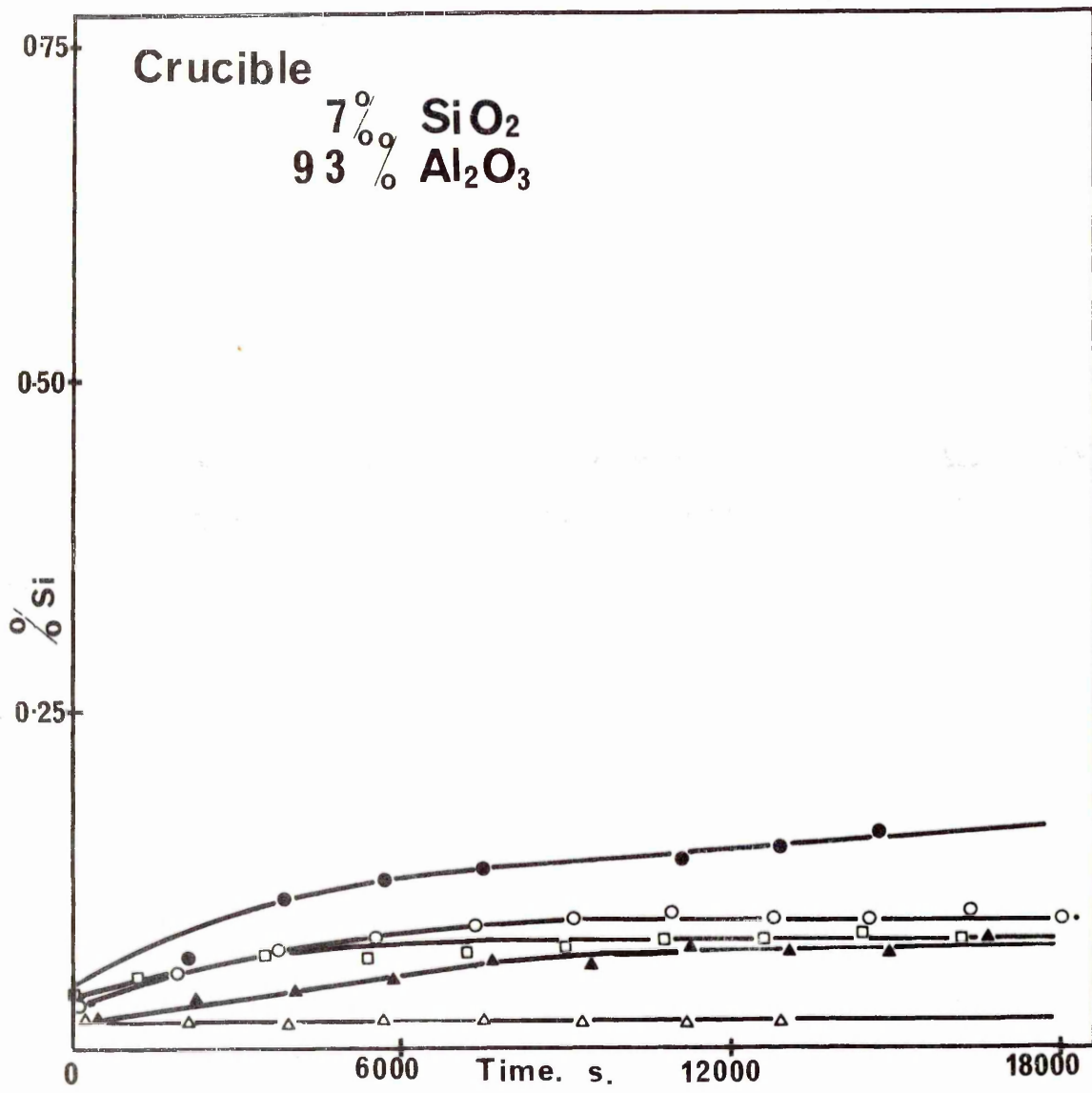
The extent and rate of silicon transfer from 37 wt.%SiO₂ - Al₂O₃ crucibles. The effect of carbon content and the partial pressure of carbon monoxide is evident both from the static oxygen value and the amount of silicon picked up by the metal.



Melt No	Key	Initial % C	Static Oxygen x 10 ⁻³	Control Pressure m.m.Hg.	$\frac{\Delta \text{Si}}{\Delta t}$ % per.s. x 10 ⁻⁵ at t =		
					600 s.	6000 s.	12000 s.
87	■	0.760	0.70	3	3.00	1.60	1.50
68	●	0.960	0.75	76	3.10	1.30	1.00
67	▲	0.930	2.50	760	4.30	1.30	1.07
79	□	0.100	5.00	3	2.10	0.20	0
61	○	0.090	10.00	76	2.00	0.10	0
57	△	0.115	20.00	760	0.10	0.10	0.10
	---	Calculated					

Figure 69.

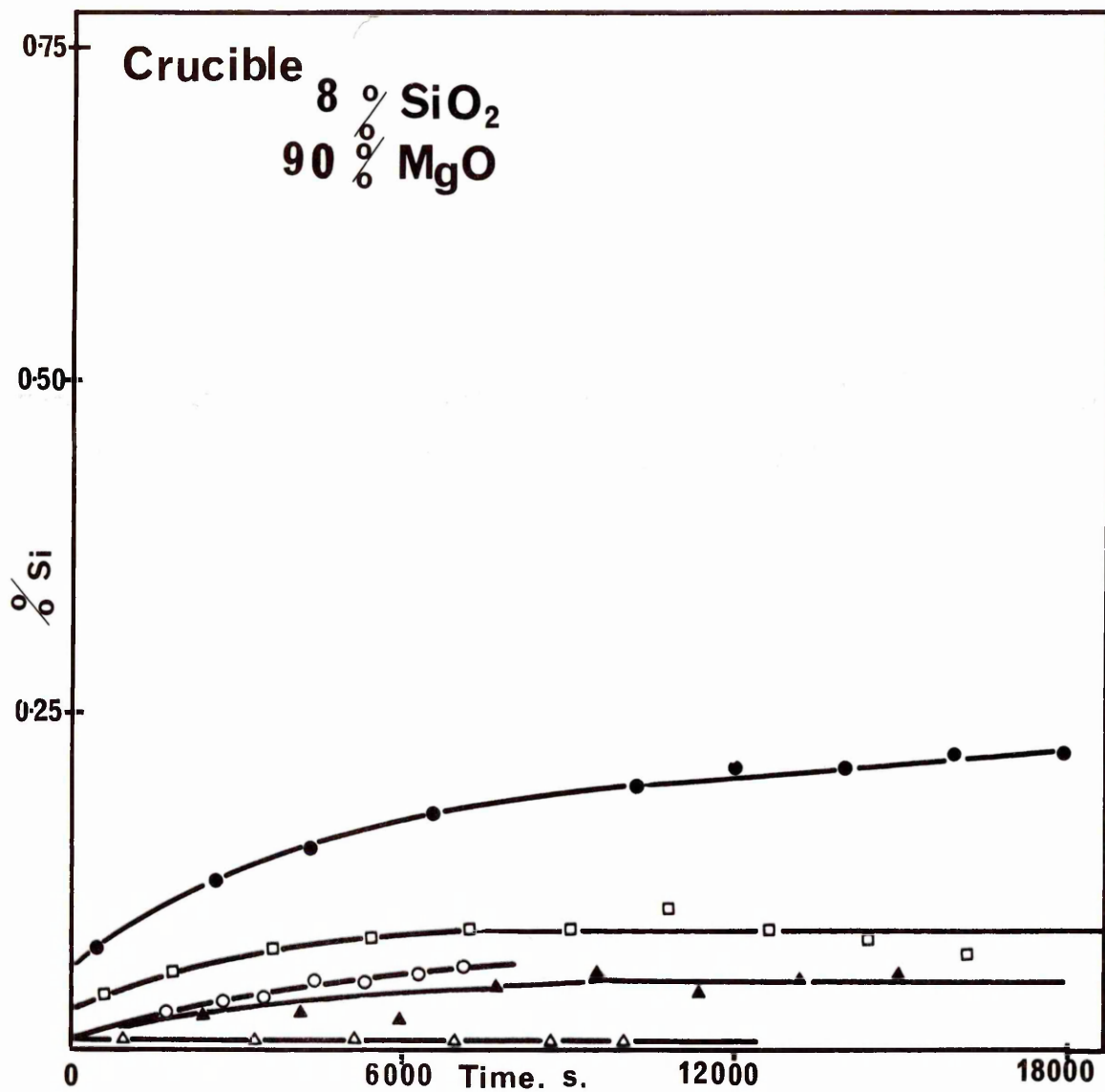
Silicon pickup from 7 wt.%SiO₂ - Al₂O₃
crucibles for various oxygen contents.



Melt No	Key	Initial % C	Static Oxygen x 10 ⁻³	Control Pressure m.m. Hg	$\frac{\Delta \text{Si}}{\Delta t}$ % per s. x 10 ⁻⁵ at t =		
					600 s.	6000 s.	12000 s.
88	■	0.846	0.70	3	-	-	-
84	●	1.025	1.30	76	2.00	0.50	0.028
63	▲	1.070	2.00	760	0.60	0.60	0.10
71	□	0.075	0.70	3	0.60	0.20	0
66	○	0.130	3.20	76	1.30	0.50	0
64	△	0.110	21.00	760	0	0	0

Figure 70.

The effect of metal oxygen content on the rate
and extent of silicon donation from a 8 wt.%SiO₂
- MgO crucible.



Melt No.	Key	Initial % C	Static Oxygen x 10 ⁻³	Control Pressure m.m.Hg	$\frac{\Delta Si}{\Delta t}$ % per s. x 10 ⁻⁵ at t =		
					600 s.	6000 s.	12000 s.
90	■	0.813	1.80	3	-	-	-
37	●	0.845	1.65	76	2.70	0.90	0.30
82	▲	1.065	2.20	760	0.70	0.30	0
76	□	0.086	2.00	3	1.50	0.30	0
18	○	0.112	2.45	76	1.00	0.40	0
19	△	0.142	12.40	760	0	0	0
	---	Calculated					

Figure 71.

The relationship between the activity of silica at the crucible-metal interface (calculated from the final bulk silicon and oxygen contents by equation 33) and the wt.% silica in the surface layers analysed from crucible scrapings.

On this and most of the following diagrams up to Figure 94 the crucibles have been coded by their trade names as follows:-

	%SiO ₂	%Al ₂ O ₃	%MgO.
'SiO ₂ '	91.57	4.01	2.57
'M'	55.80	41.45	0.22
'P'	36.80	61.20	0.07
'HS'	6.80	92.5	N.D.
'MAG'	8.00	0.33	89.80

Figure 72.

The quantity of silica removed from the interface, by the dissociation process, increases with decreasing oxygen content.

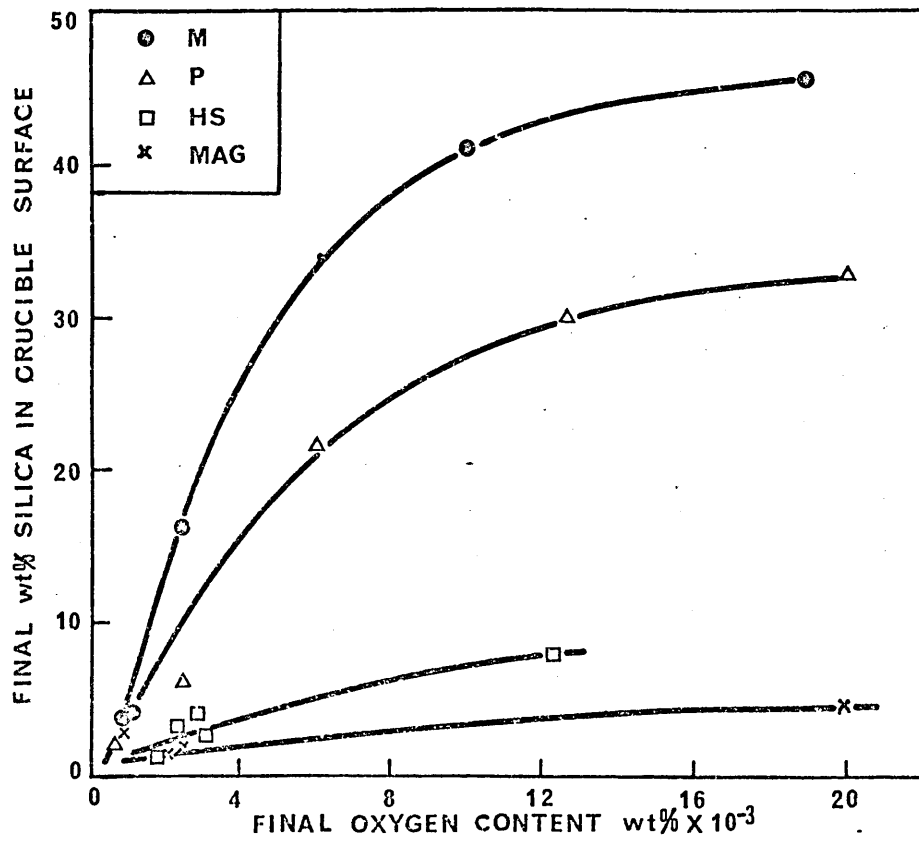
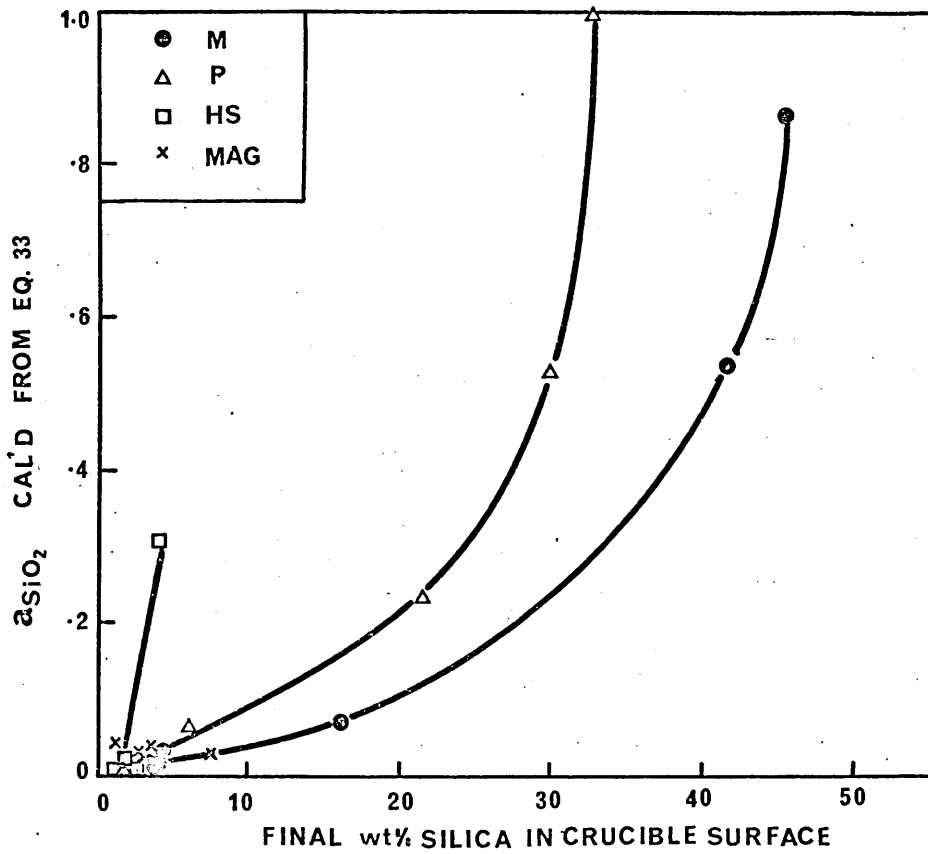


Figure 73.

When the wt.% silica loss from Figure 72 is plotted as a percentage of the original silica content all points appear to lie on the same curve, irrespective of the original crucible composition.

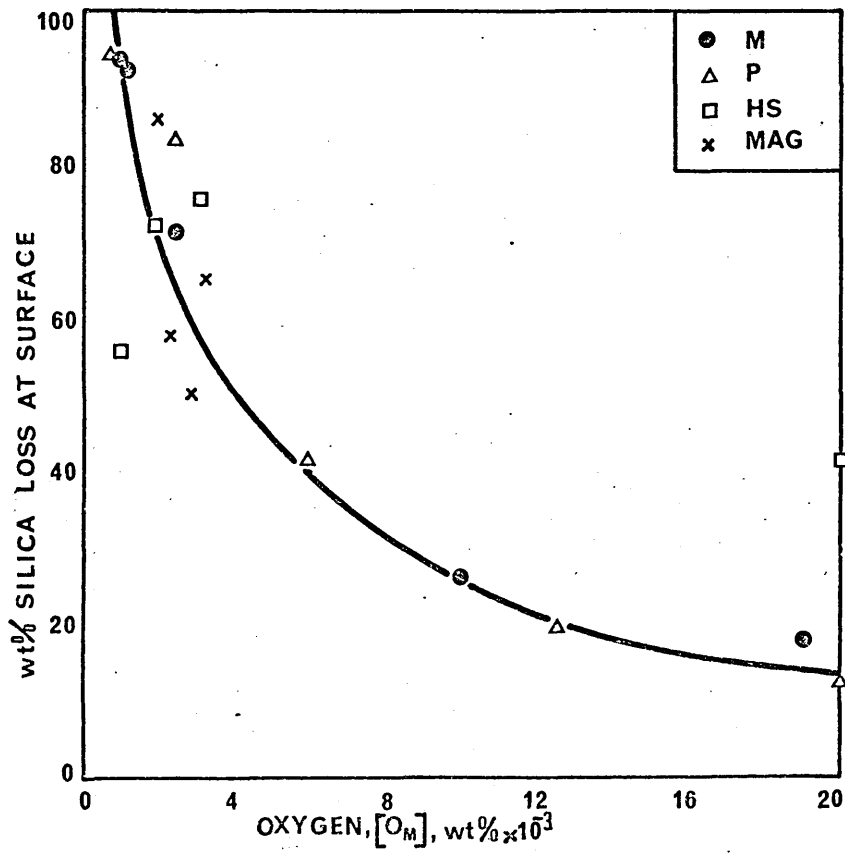


Figure 74.

The extent of silica dissociation is illustrated by the plot of the final silicon content (wt.%) against the bulk static oxygen content (wt.%). The amount of silicon picked up, for a given oxygen level, increases with increasing silica content of the crucible.

Figure 75.

The effect of the initial silica content of the crucible is better shown by this diagram of final silicon content wt.%/initial N_{SiO_2} .

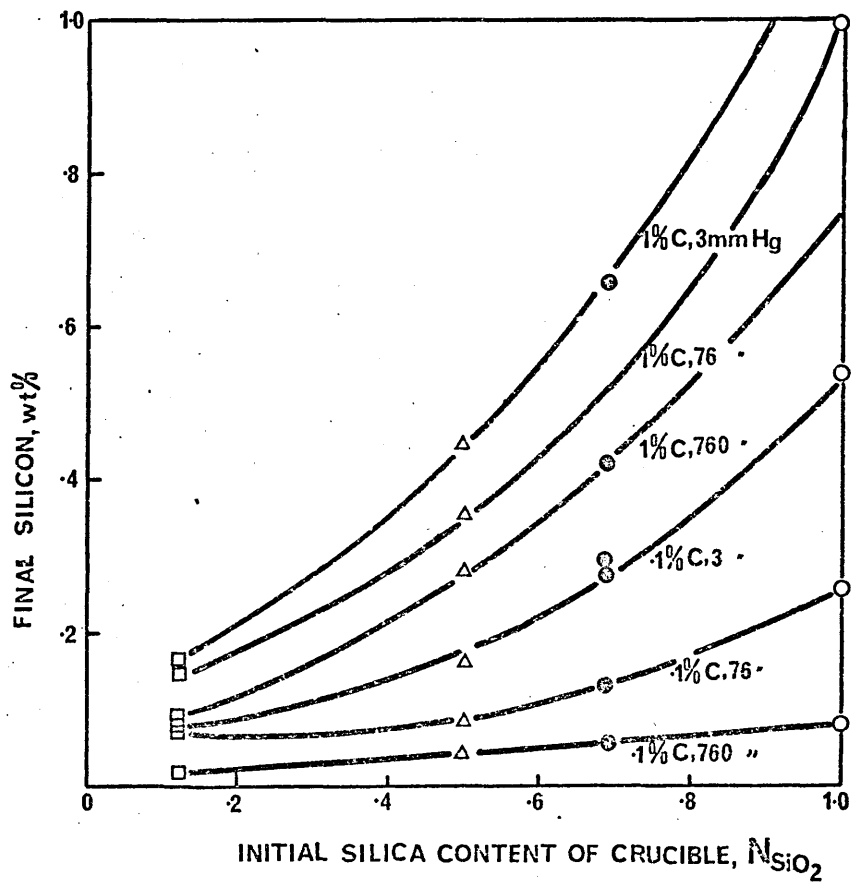
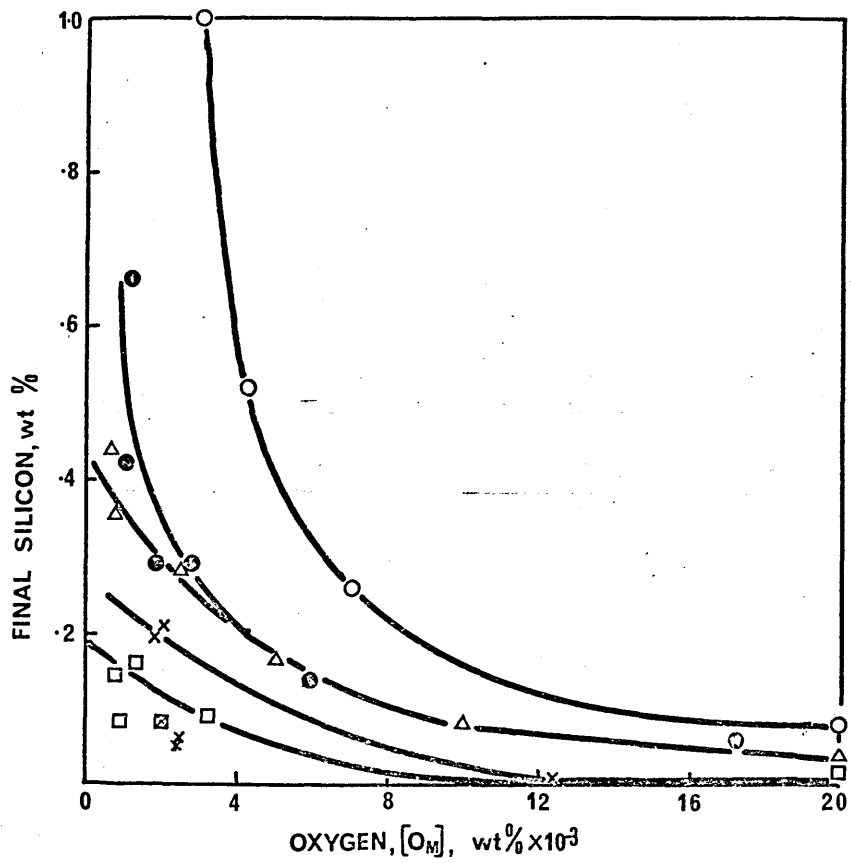


Figure 76.

M crucible (56 wt.%SiO₂-Al₂O₃). Held at 1600°C in vacuo for 4 hours and gas quenched. Vacuum mounted in Araldite and, after polishing, etched in a 5% HF solution. Photographed on a Zeiss Ultraphot at a magnification of X 100.

Figure 77.

P crucible (37 wt.%SiO₂-Al₂O₃). Held at 1600°C in vacuo for 4 hours and gas quenched. Magnification X 200.

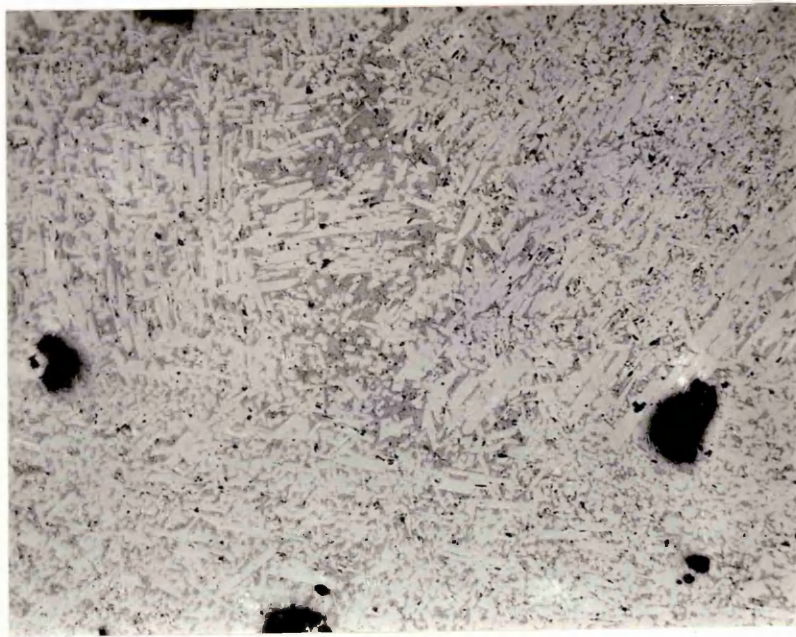
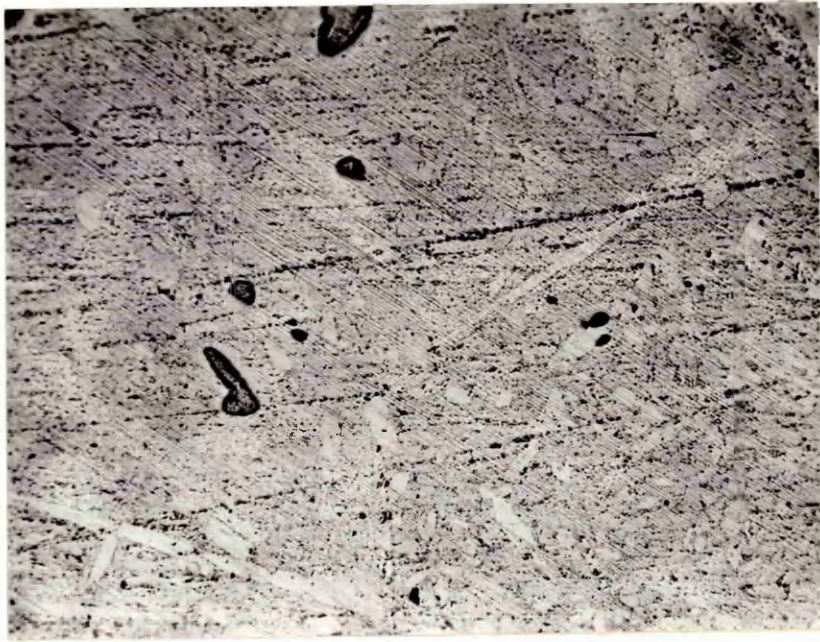


Figure 78. HS crucible (7 wt.%SiO₂-Al₂O₃). Held at 1600°C
in vacuo for 4 hours and gas quenched.
Magnification X 50.

Figure 79. MAG crucible (8 wt.%SiO₂-MgO). Held at 1600°C
in vacuo for 4 hours and gas quenched.
Magnification X 50.

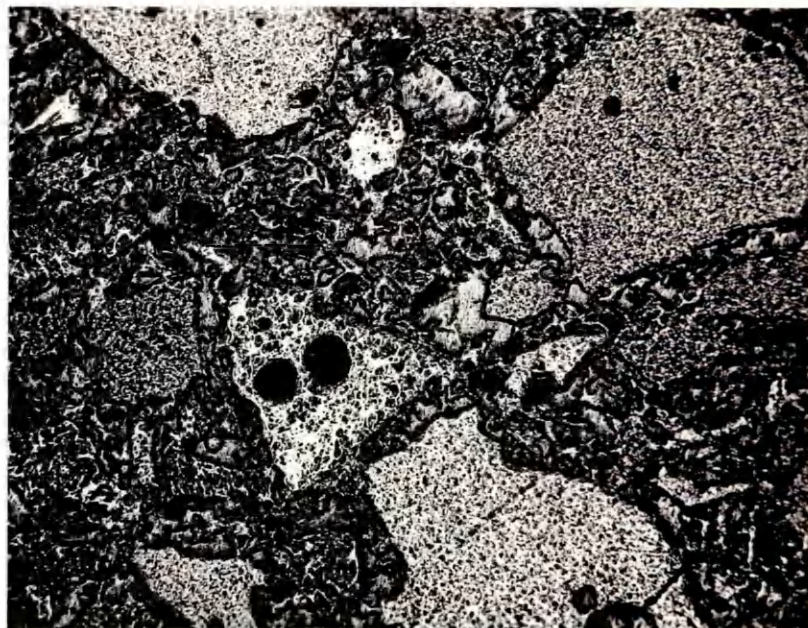


Figure 80.

$\text{SiO}_2 - \text{Al}_2\text{O}_3$ equilibrium diagram. (134)

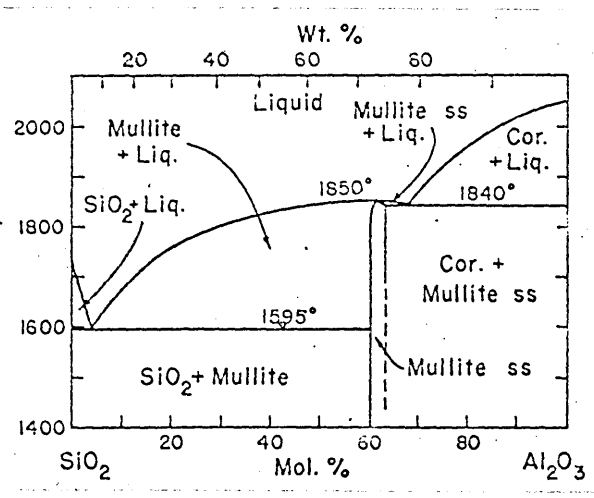


Figure 81.

The effect of the bulk oxygen content on the total silicon transfer, calculated as the number of moles of silicon transferred to the melt from unit area of silica assuming the conditions shown in Figure 82 apply.

Figure 82.

The crucible surface is schematically represented by separate areas of silica and alumina. The effect of time is to increase the surface area of alumina exposed to the melt.

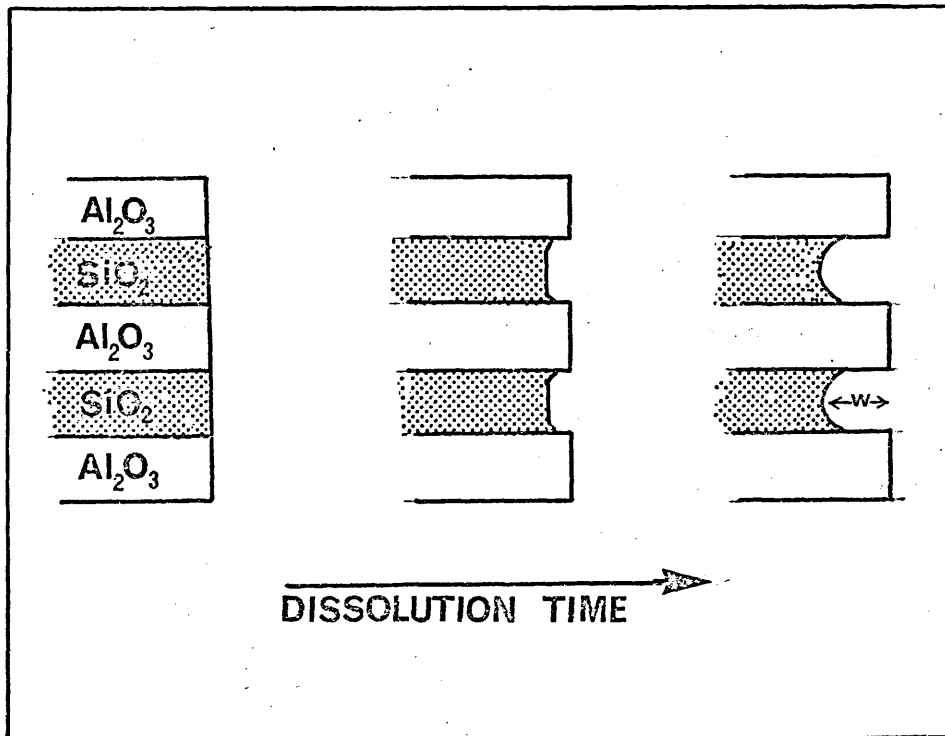
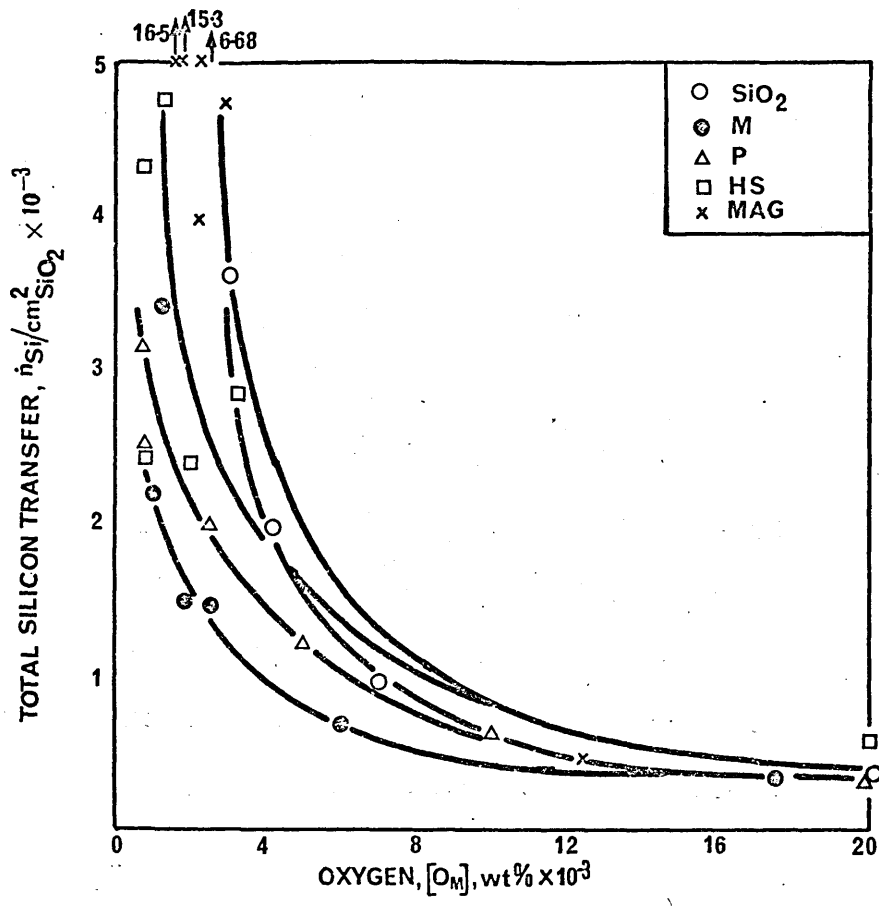


Figure 83.

The depth of silica erosion achieved by the end of the melt, assuming Figure 82 to apply, increases with decreasing melt oxygen and decreasing a_{SiO_2} . These calculated values are in good agreement with Xray studies carried out on the as-used crucibles.

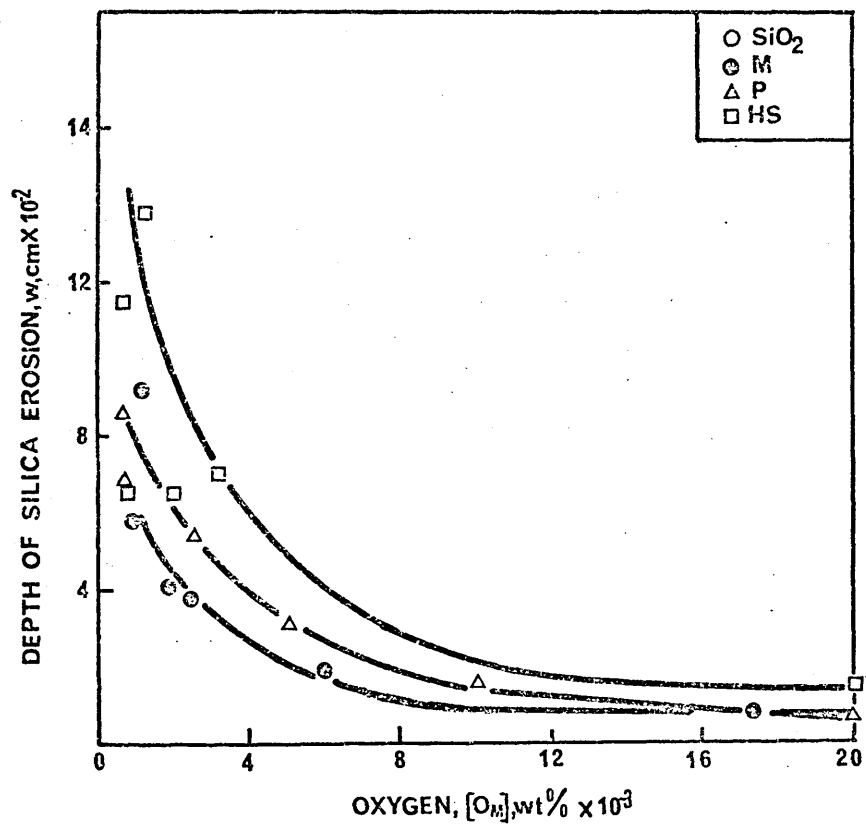


Figure 84.

The specific rate of silicon pickup at $t=600s$ (calculated as the number of moles of silicon transferred from each sq.cm. of silica in one second) is seen to increase with decreasing bulk oxygen content. The specific rates are higher in the low silica crucibles possibly as a result of the larger local driving force with the lower values of bulk silicon.

Figure 8.5. The effect of varying, in turn, the parameters in rate equation (71). The wt.% silicon in the bulk metal is calculated in each case feeding in values for the rate of Silicon pickup,

$\delta = 0.013$ cm, $\frac{V}{A} = 1.5$, $D_{Si} = 4 \times 10^{-4}$ and $a_{SiO_2} = 1$. The sensitivity of each parameter can be estimated from this diagram.

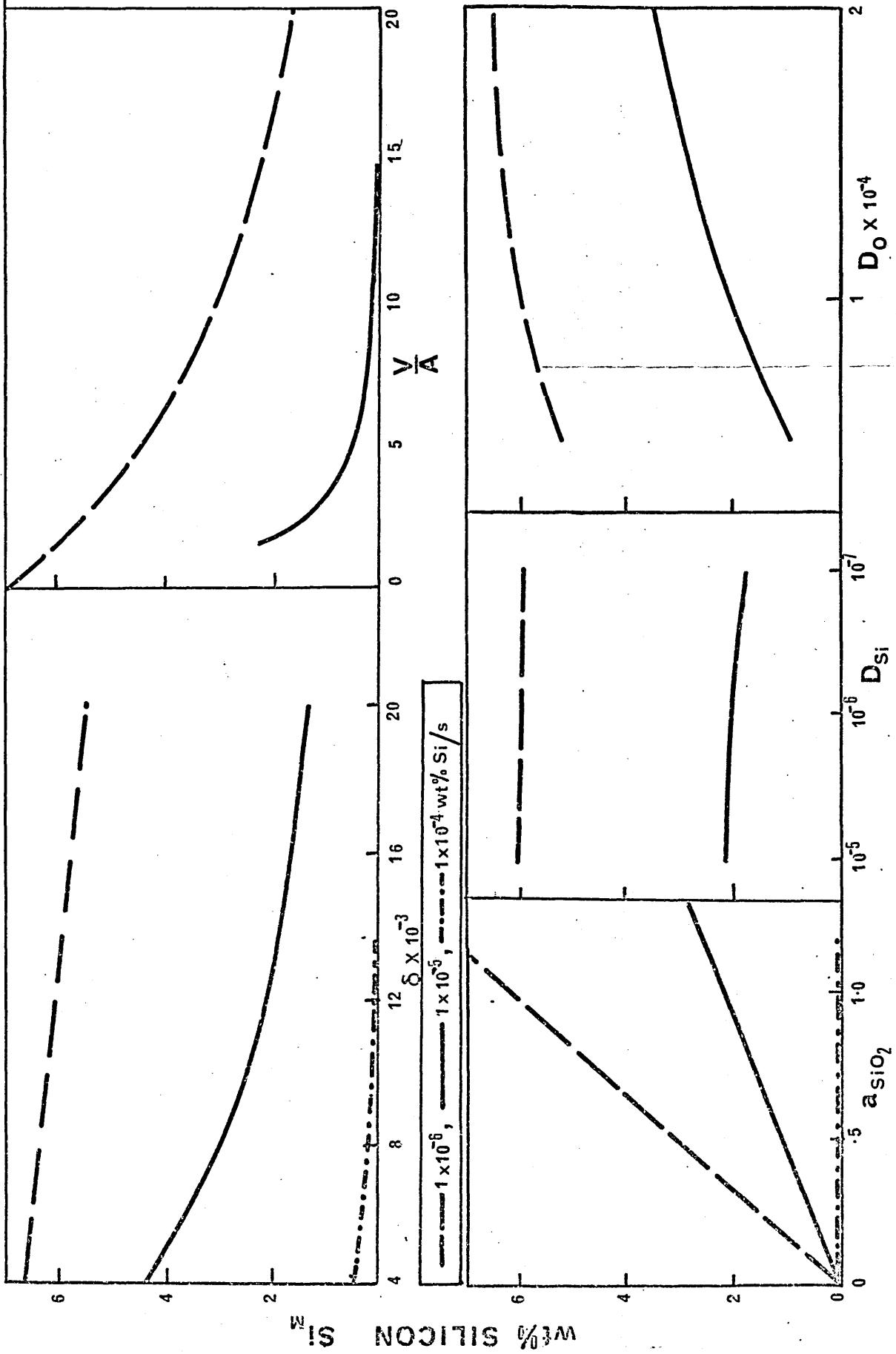


Figure 86(a).

Comparison of measured rates of silicon transfer with those calculated from Model I (a) (equation 130, table 26) after Ward (97). There is virtually no correlation.

Figure 86(b).

Comparison of measured rates of silicon transfer with those calculated from Model I (b). Here the value for the gas-metal interfacial area has been calculated from equation 132 and the agreement with the measured rates can be seen to be much better.

- M
- △ P
- HS
- x MAG

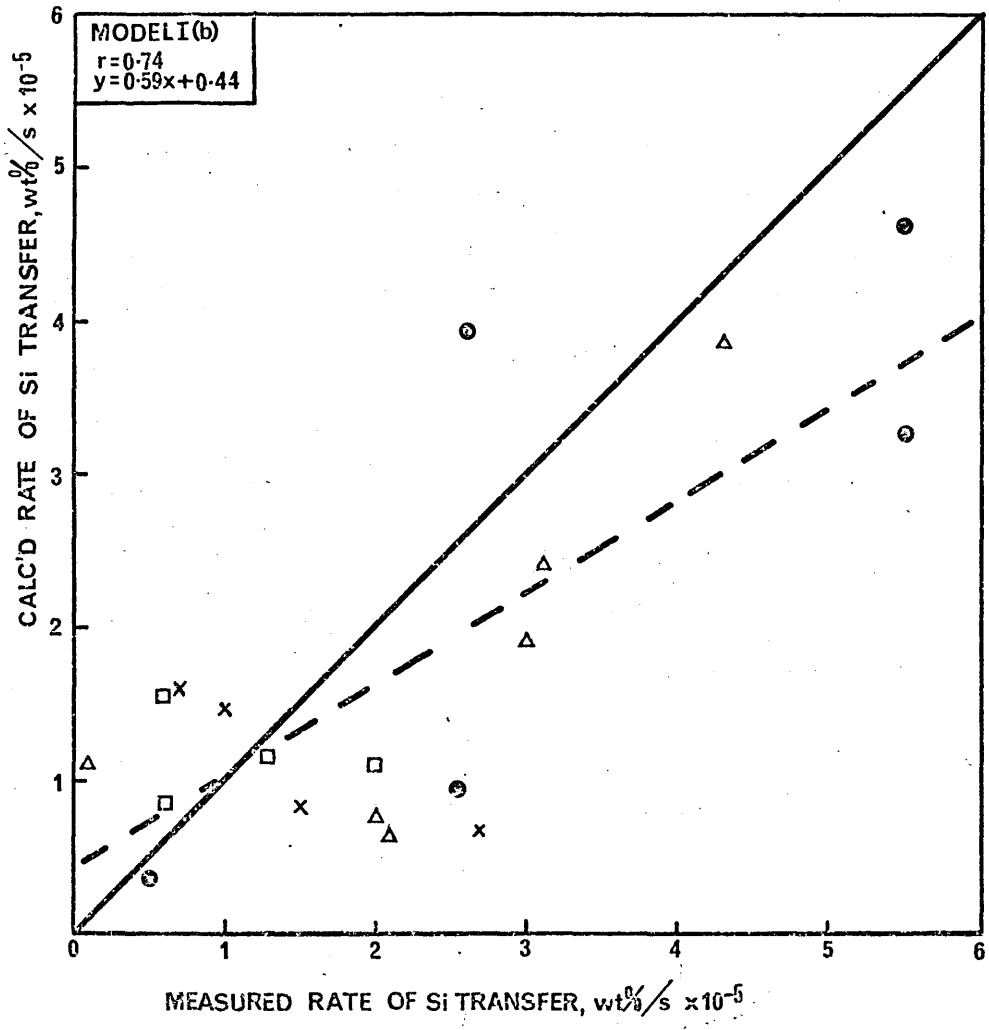
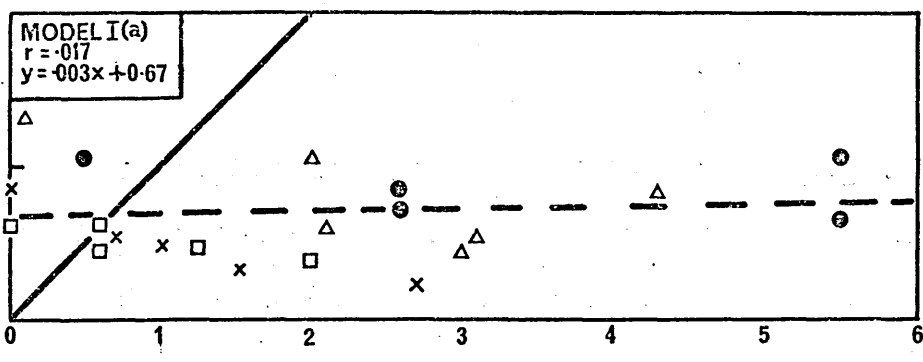


Figure 87.

The gas-metal surface area (A_g) calculated from equation (132) and listed in Table 27 is shown to increase with decreasing oxygen content and

Figure 88.

..... increasing rate of silicon transfer. This is a reflection of the effect of increasing the carbon content and decreasing the pressure.

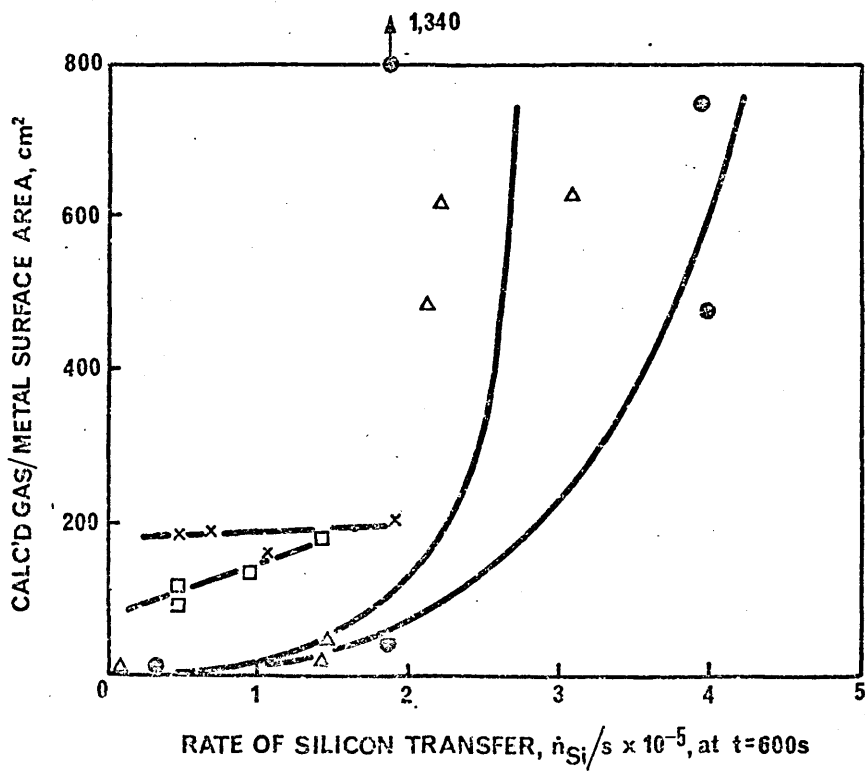
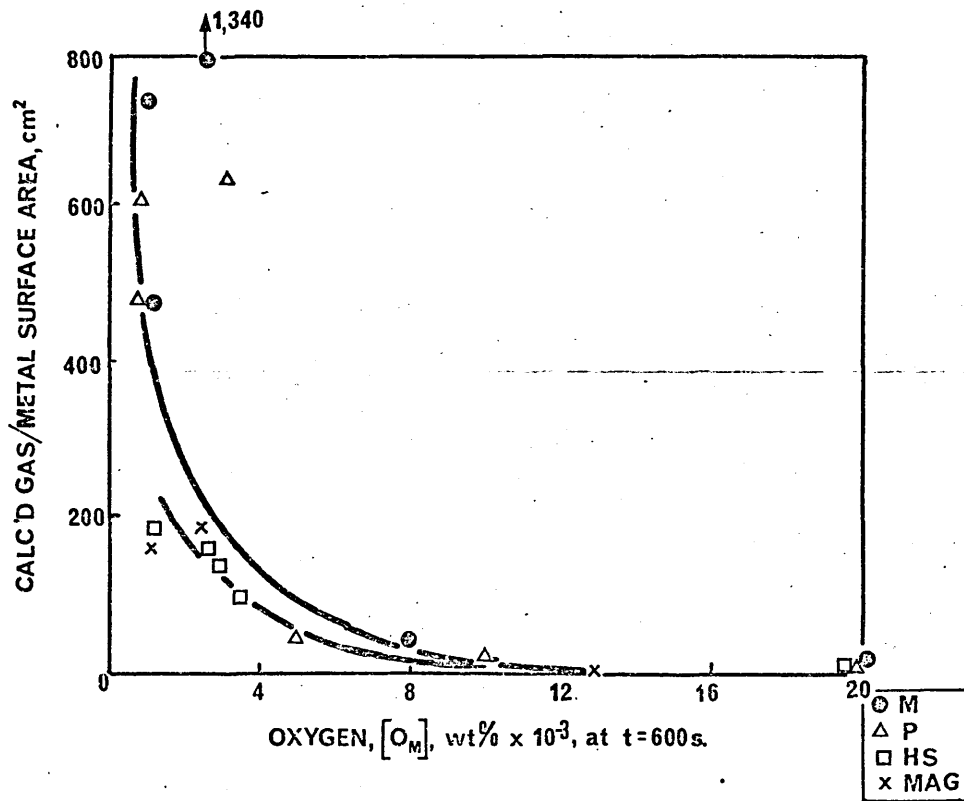
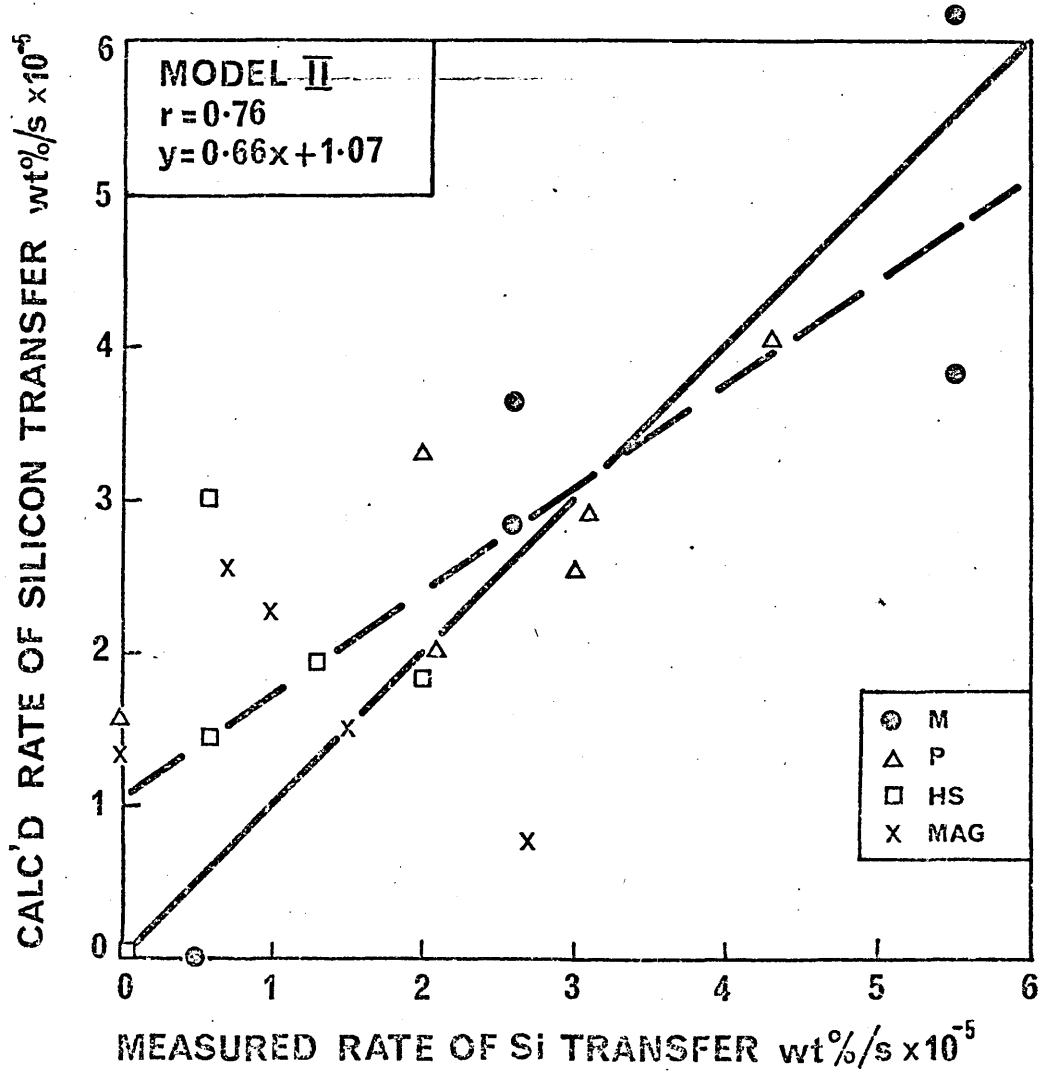


Figure 89.

Comparison of measured rates of silicon transfer with those calculated from Model II (equation 133, table 26).



7

Figure 90. Comparison of measured rates of silicon transfer with those calculated from Model III (equation 124, Table 26).

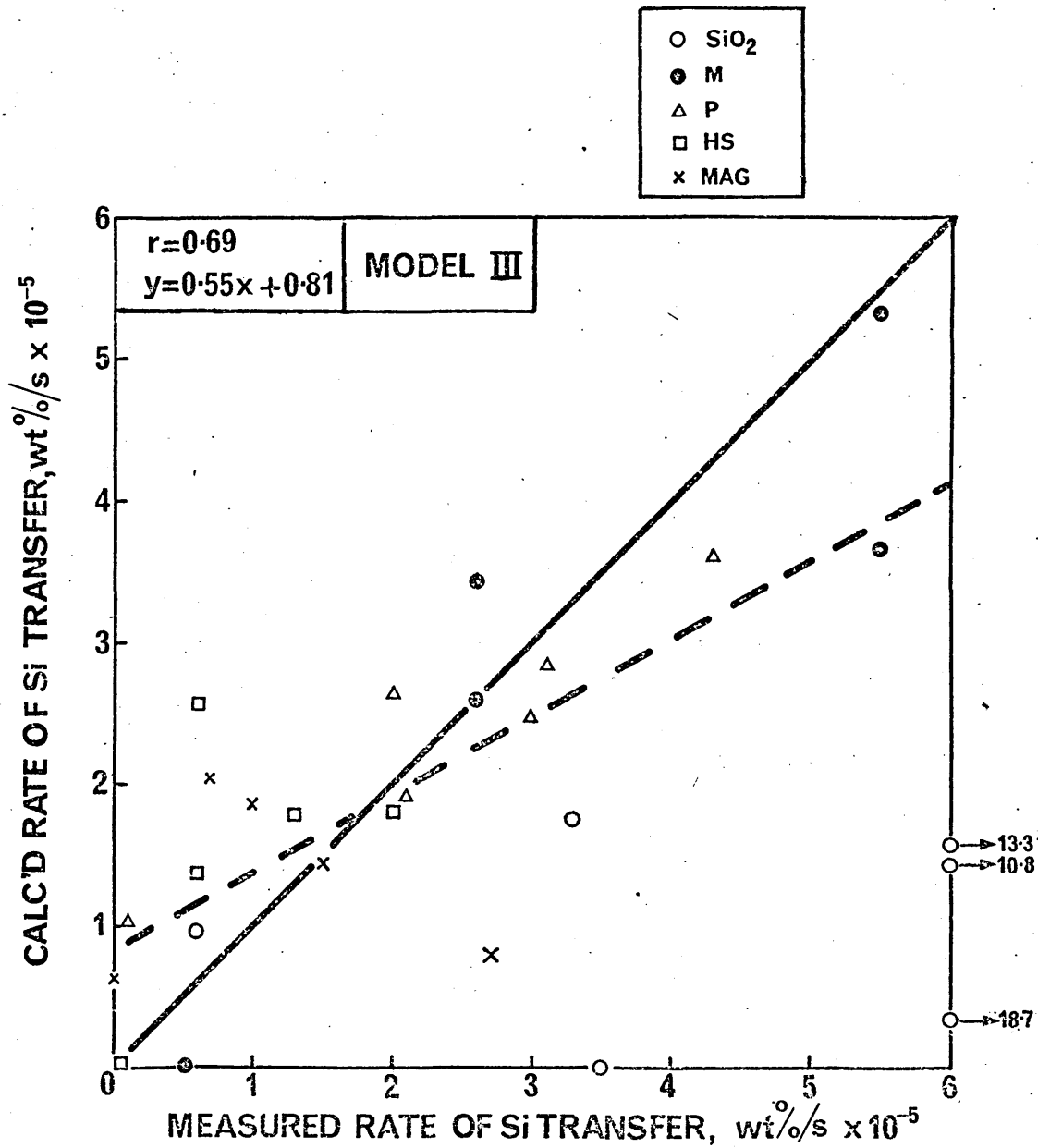


Figure 91.

Comparison of measured rates of silicon transfer with those calculated from Model IV. (separate phase model; equation 124, table 26)

- SiO₂
- ⊙ M
- △ P
- HS

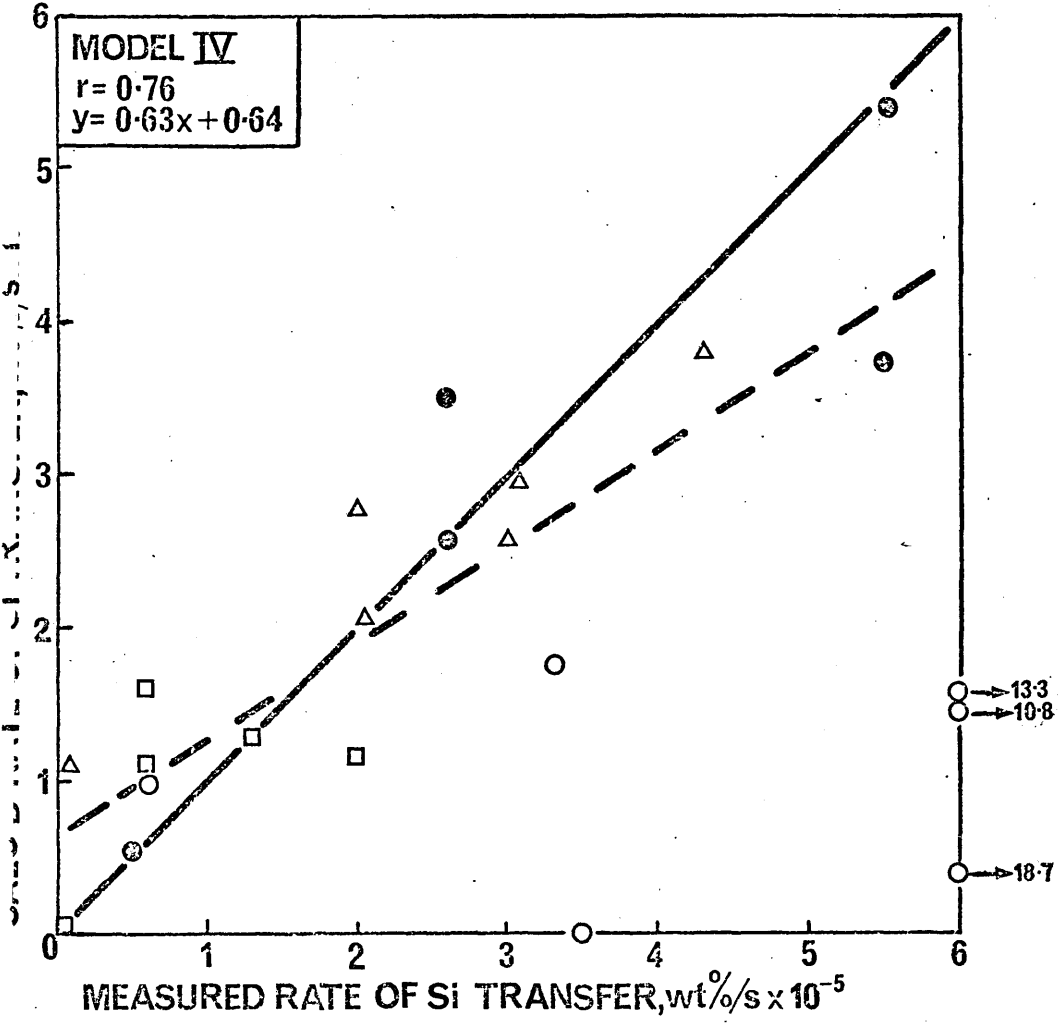


Figure 92.

The influence of the bulk oxygen content on the separate specific rates of oxygen transfer from silica and mullite. From this diagram mullite appears to have roughly twice the stability of silica.

Figure 93.

The theoretical trend from Model IV is seen to give good agreement with the measured rate of transfer over the whole range of metal oxygen contents.

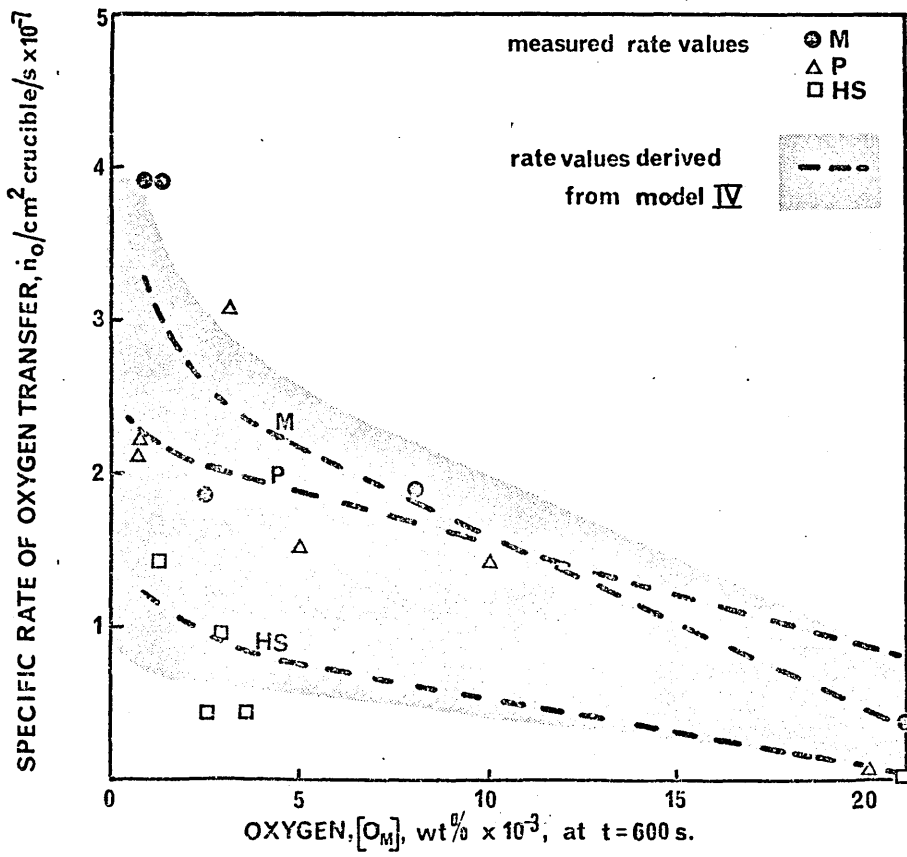
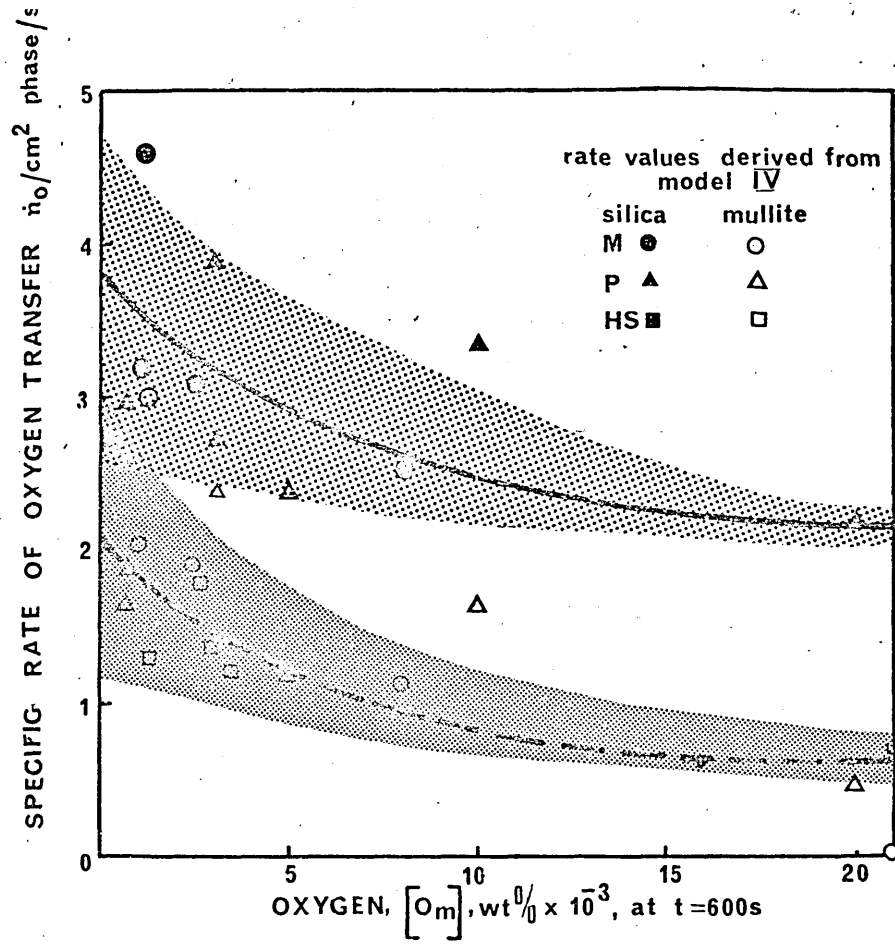
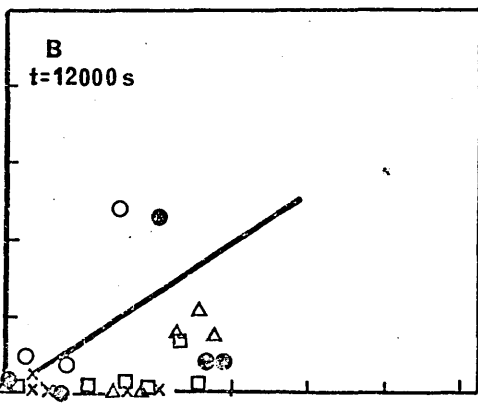
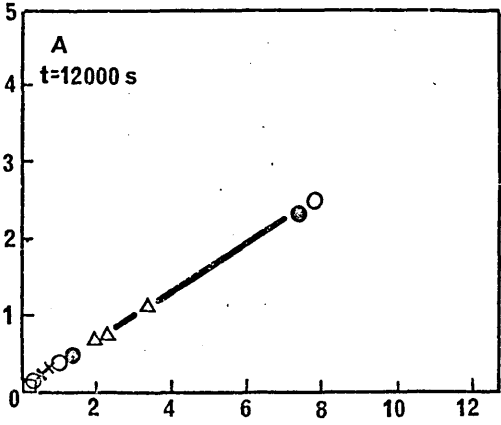
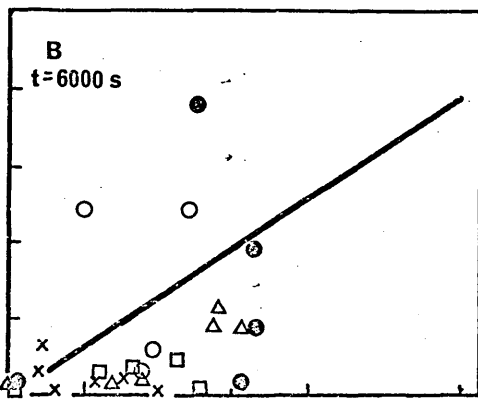
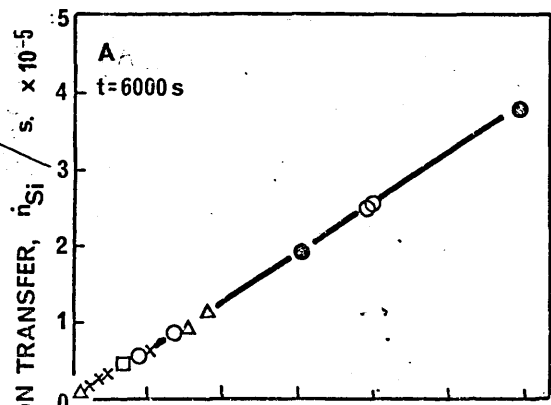
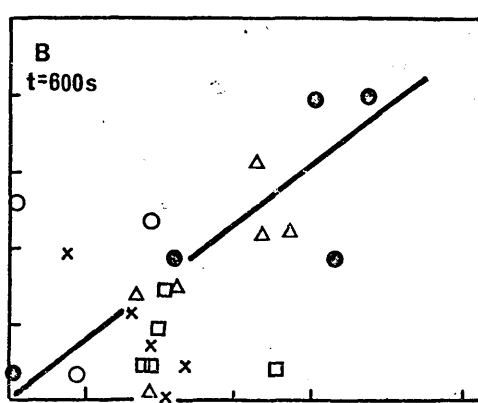
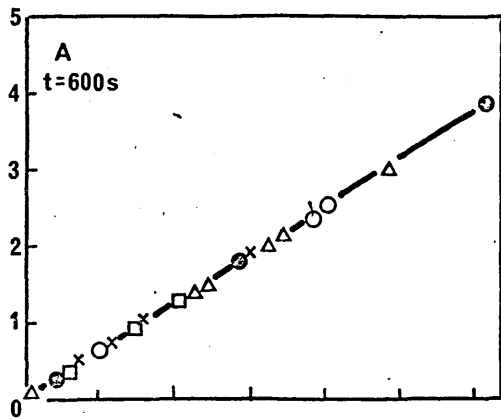


Figure 94.

The relationship between the transfer rate of silicon and the driving force for oxygen diffusion across the boundary layer as calculated by methods A and B outlined in Chapter 2, section 4.3.2.6. and Table 29. Method B, by equation (140), becomes more inaccurate as time progresses because of the uncertainty of the value for silica activity at the crucible-metal boundary. The results are brought more into line with the expected relationship when the analysed value for N_{SiO_2} is used for method C.



OXYGEN GRADIENT ACROSS
BOUNDARY LAYER, $(O_R - O_M), \text{wt}\% \times 10^{-3}$

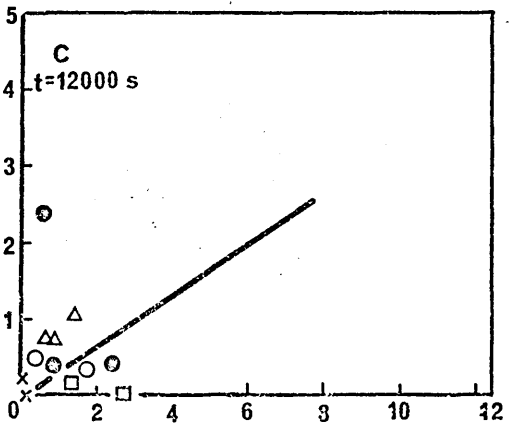


Figure 95(a).

The effect of oxygen and silicon contents
on the specific rate of oxygen transfer
calculated from Model III (equation (124)).

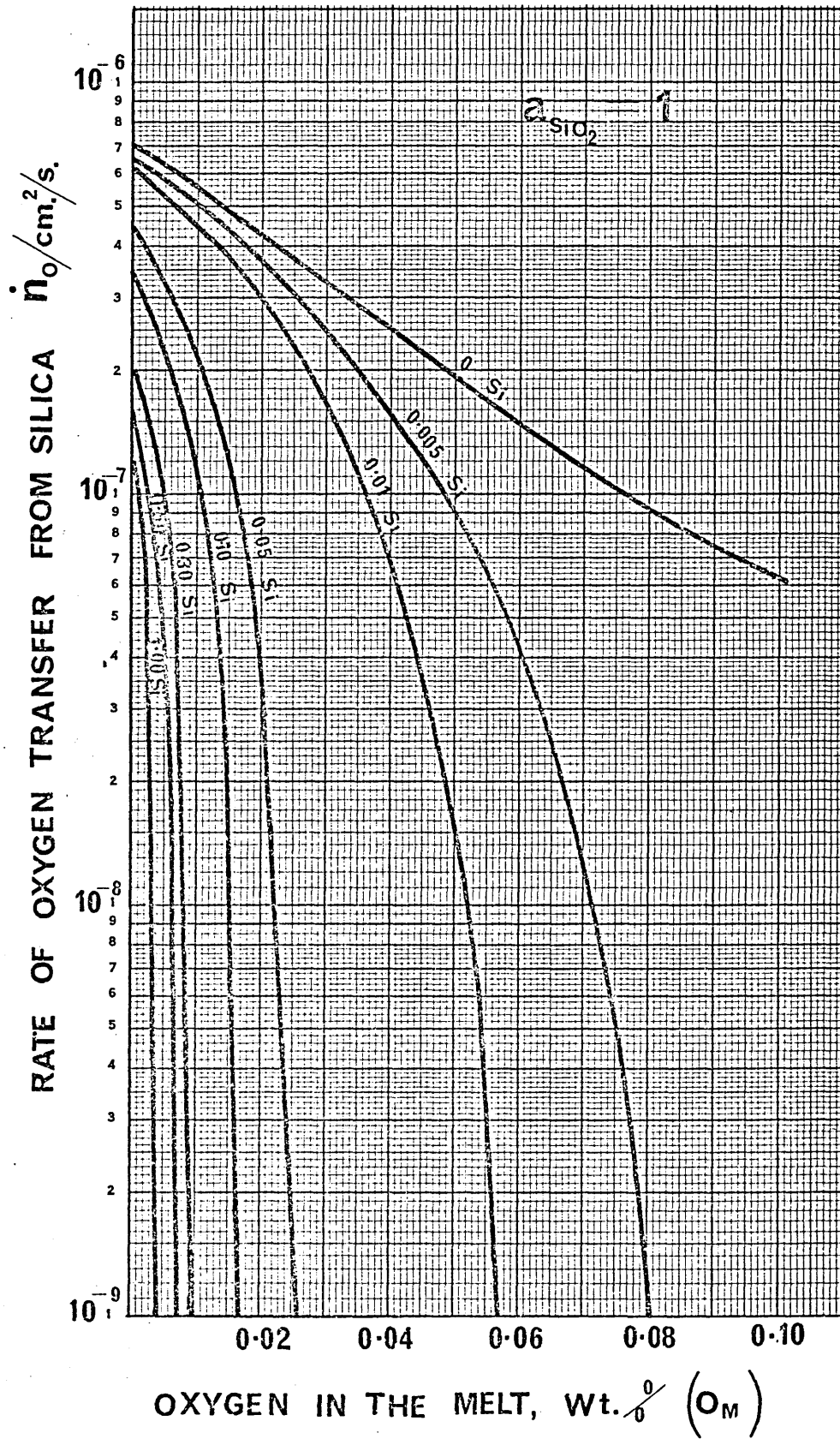


Figure 95(b).

This diagram shows the effect of decreasing the activity of silica in the crucible surface upon the specific rate of oxygen transfer. From this the oxygen donation rate can be estimated for a wide range of melt and crucible conditions.

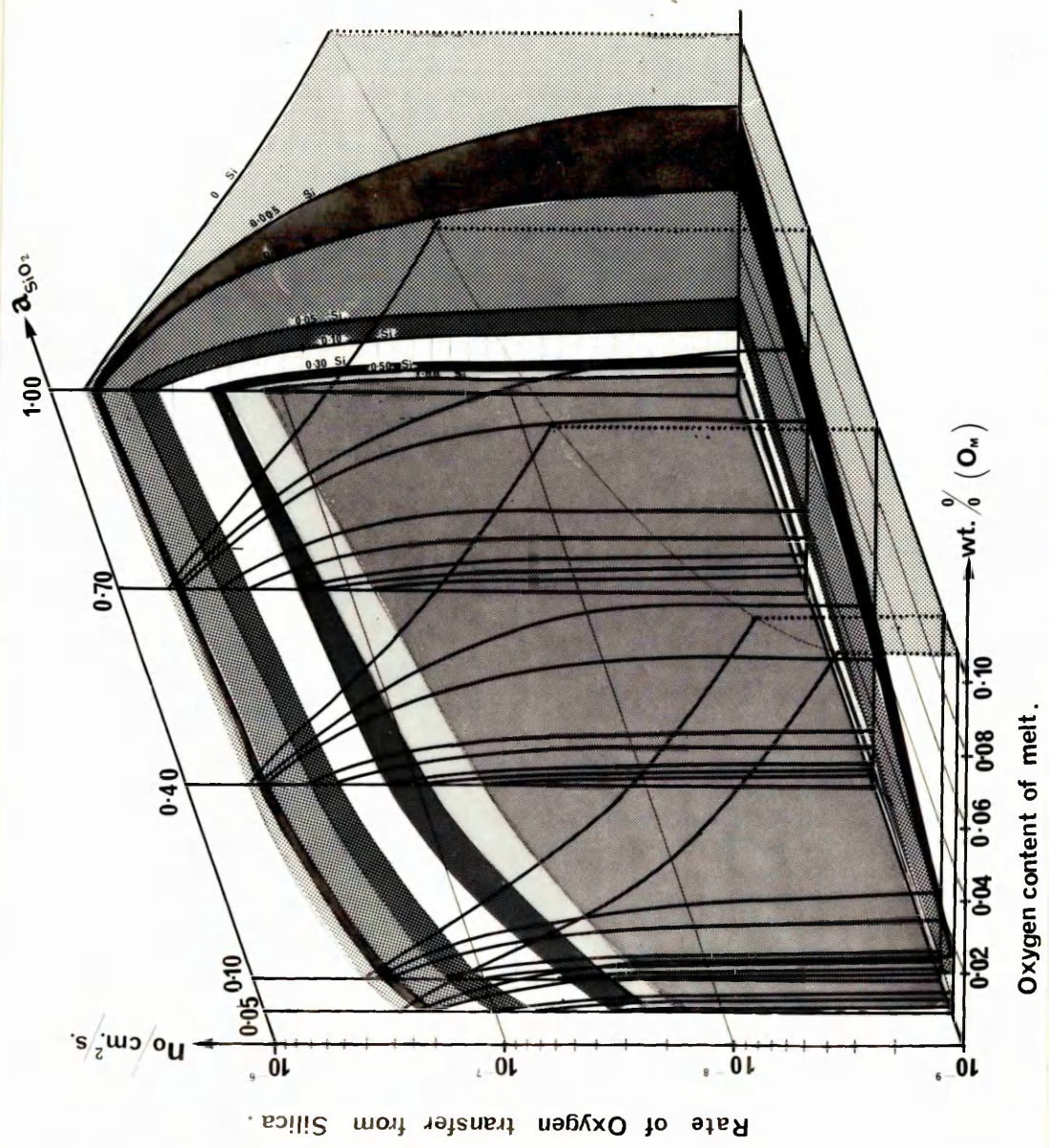


Figure 96.

The effect of bubble radius and atmospheric pressure upon the partial pressure of carbon monoxide, p_{CO_x} , at the surface of bubbles nucleated on the crucible bottom of the present 5lb melts. (equations 141 and 142).

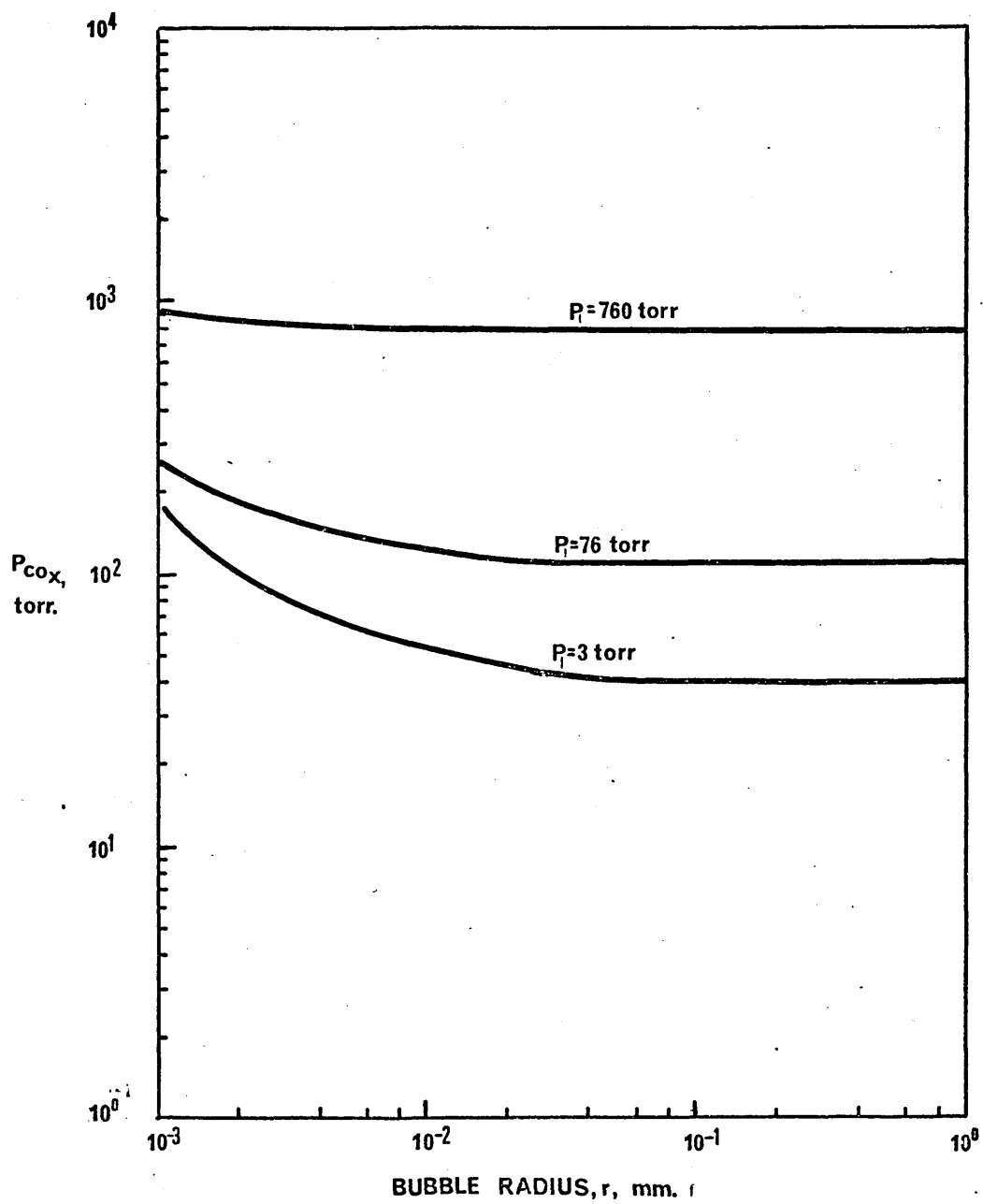
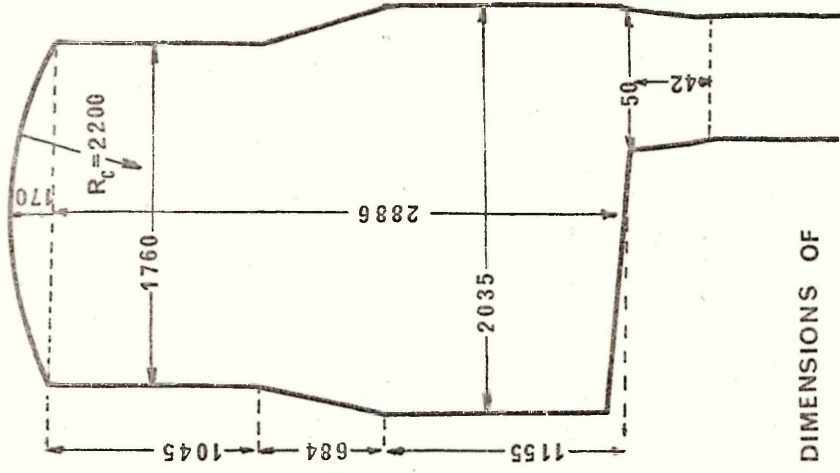
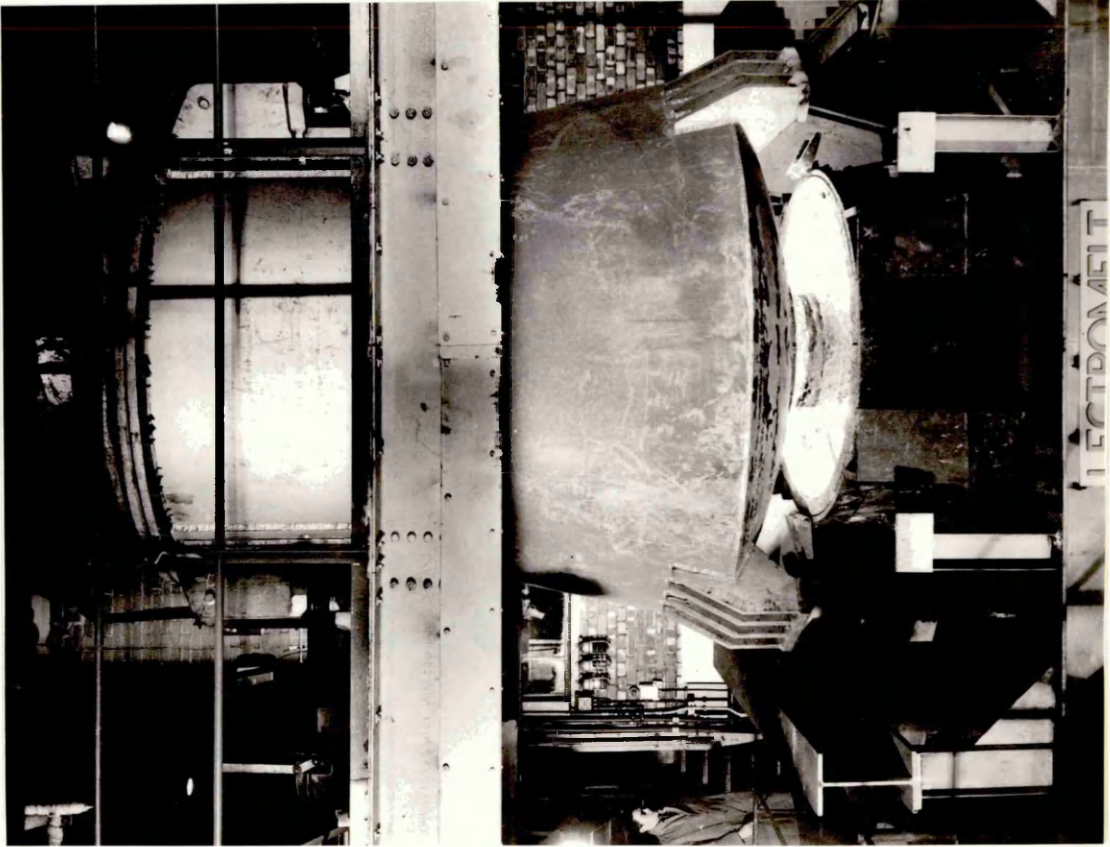


Figure 97.

Photograph of the 30 ton Dortmund-
Horder vacuum treatment unit in
operation at the Openshaw works of
English Steel Corporation Ltd.

Figure 98.

A schematic diagram of the E.S.C.
30 t. D.H. vessel showing the
internal dimensions.

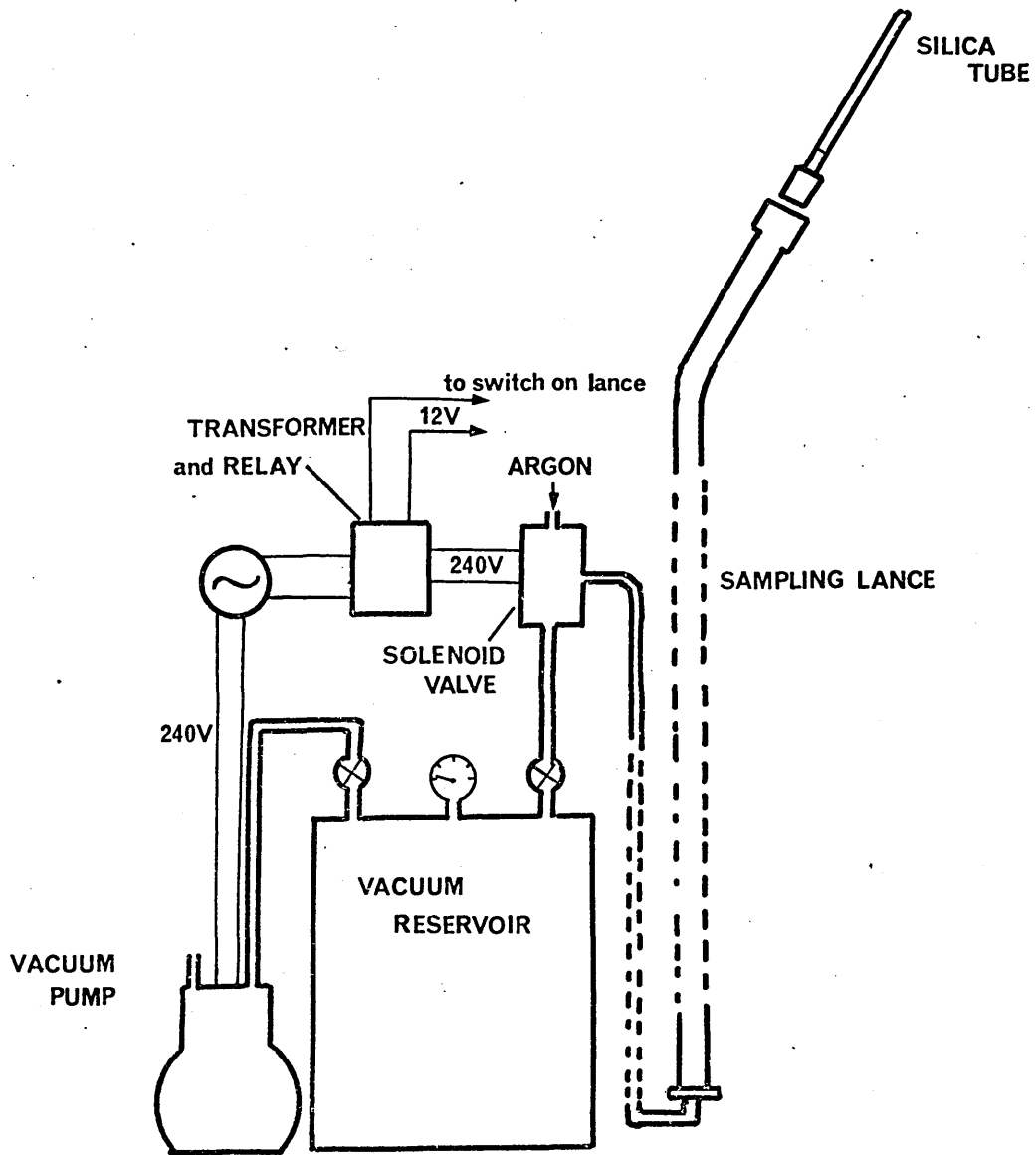


INTERNAL DIMENSIONS OF
E.S.C., 30t. D.H. VESSEL (mm.)

Figure 99.

The argon-suction device used to take samples of metal from the ladle before and during vacuum degassing. This equipment was designed to be operated by one man. A switch on the lance operates the solenoid valve which shuts off the supply of argon and opens the lines to vacuum.

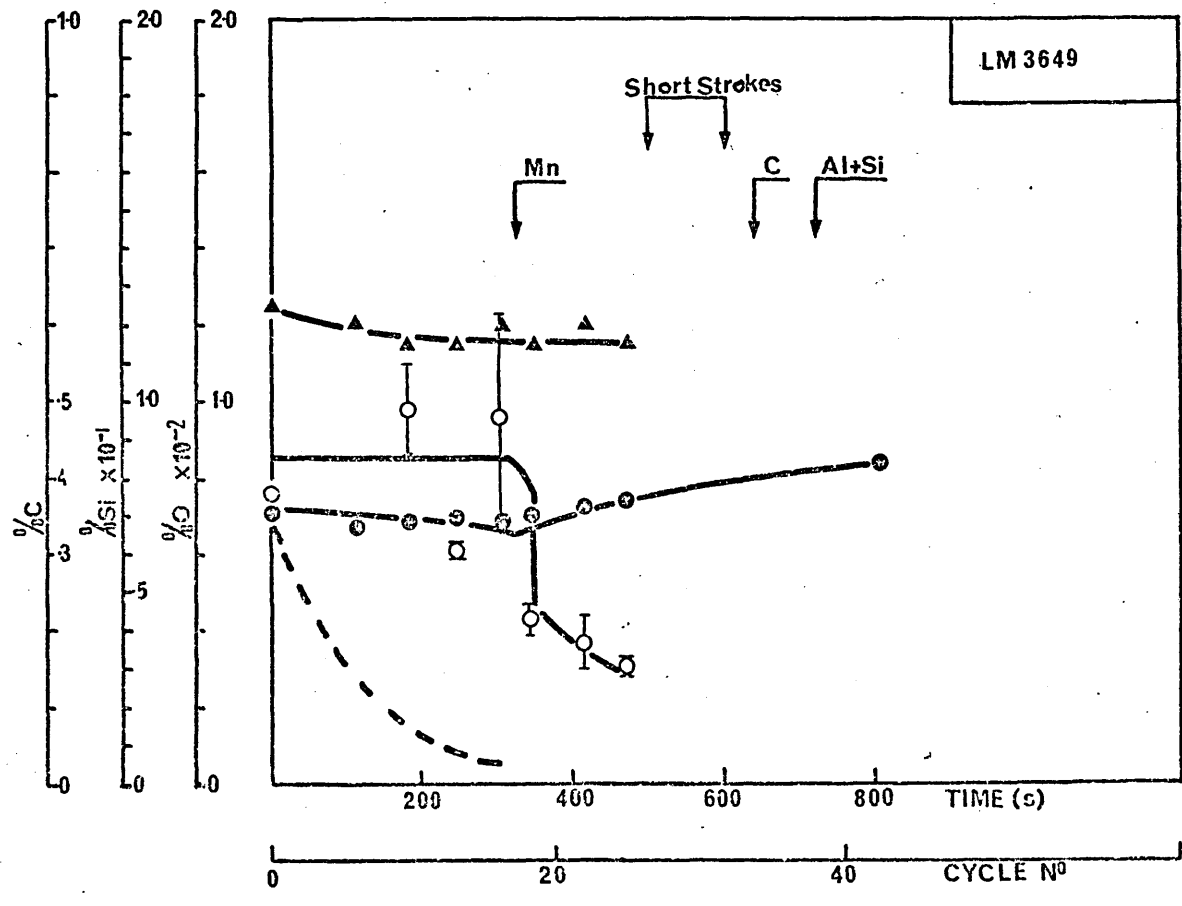
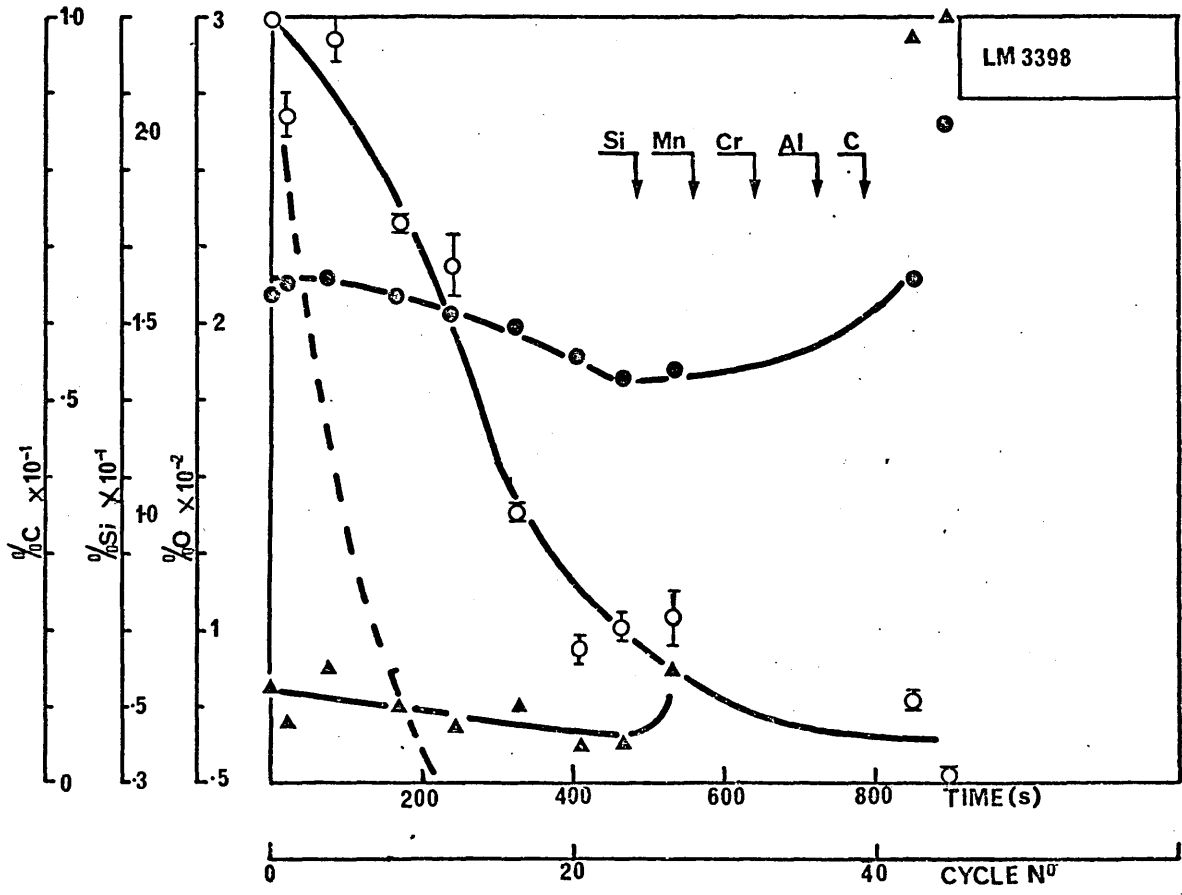
at 1000

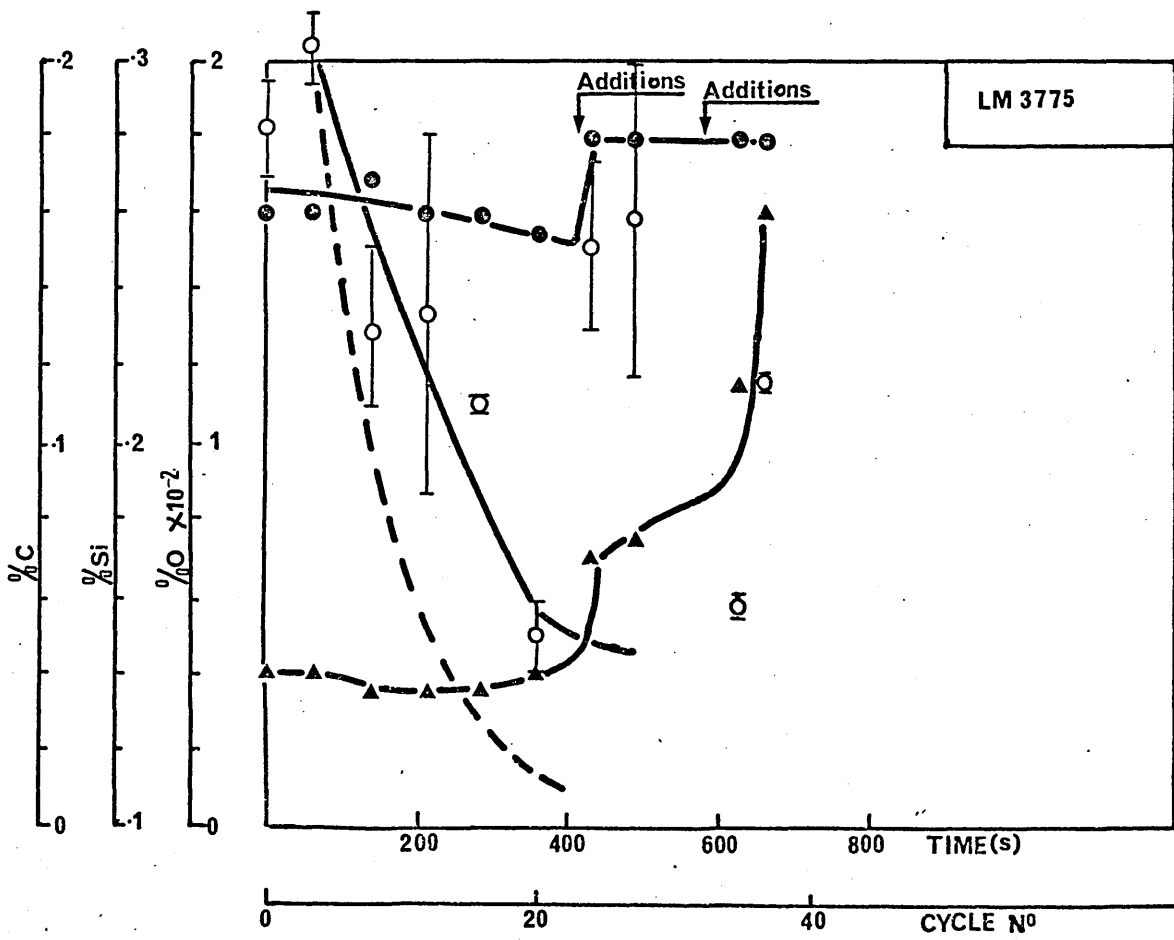
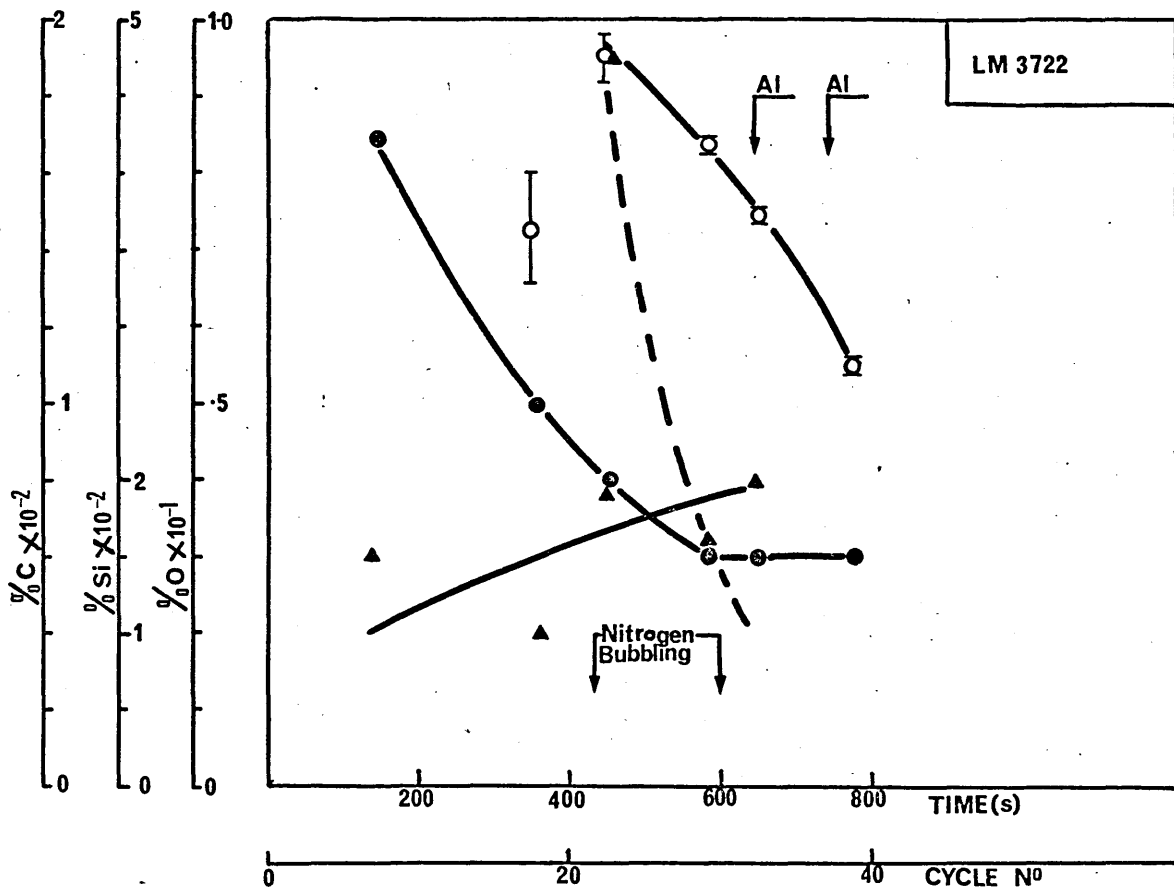


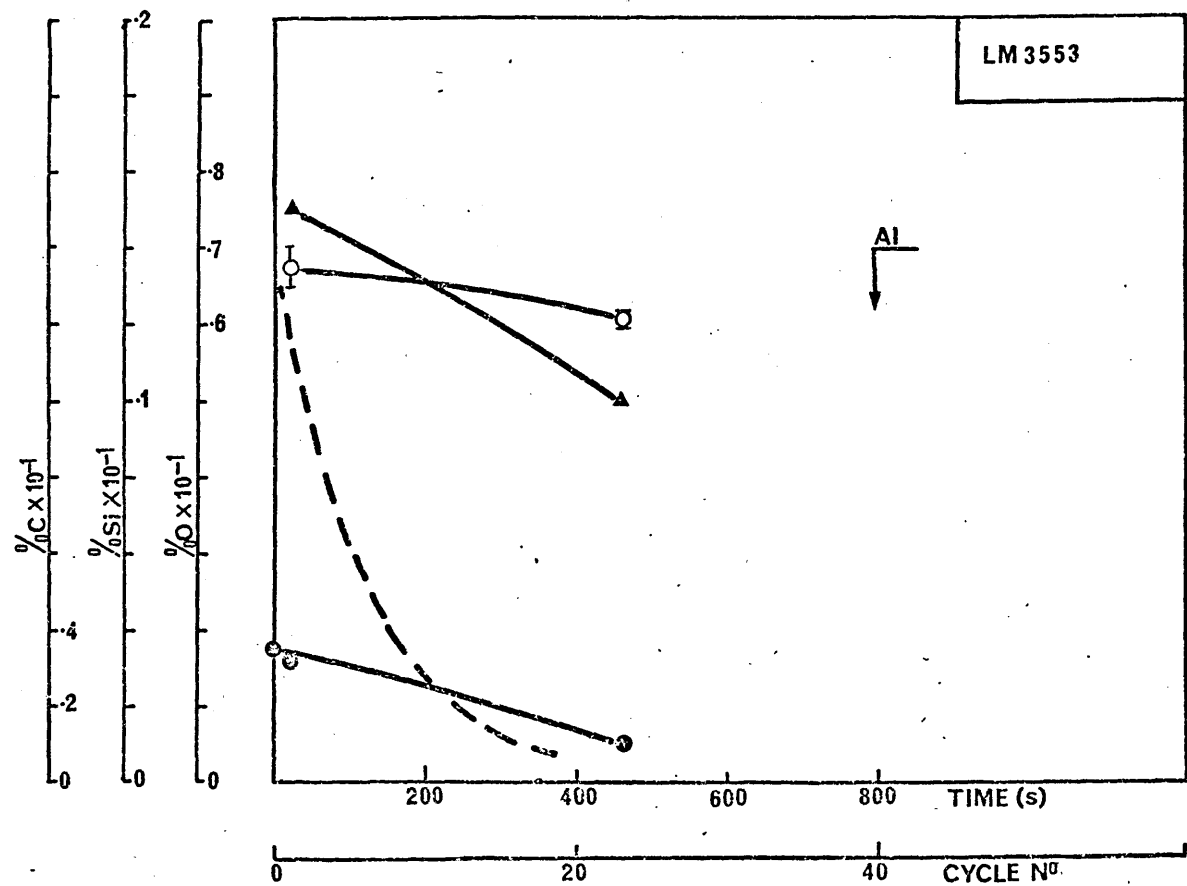
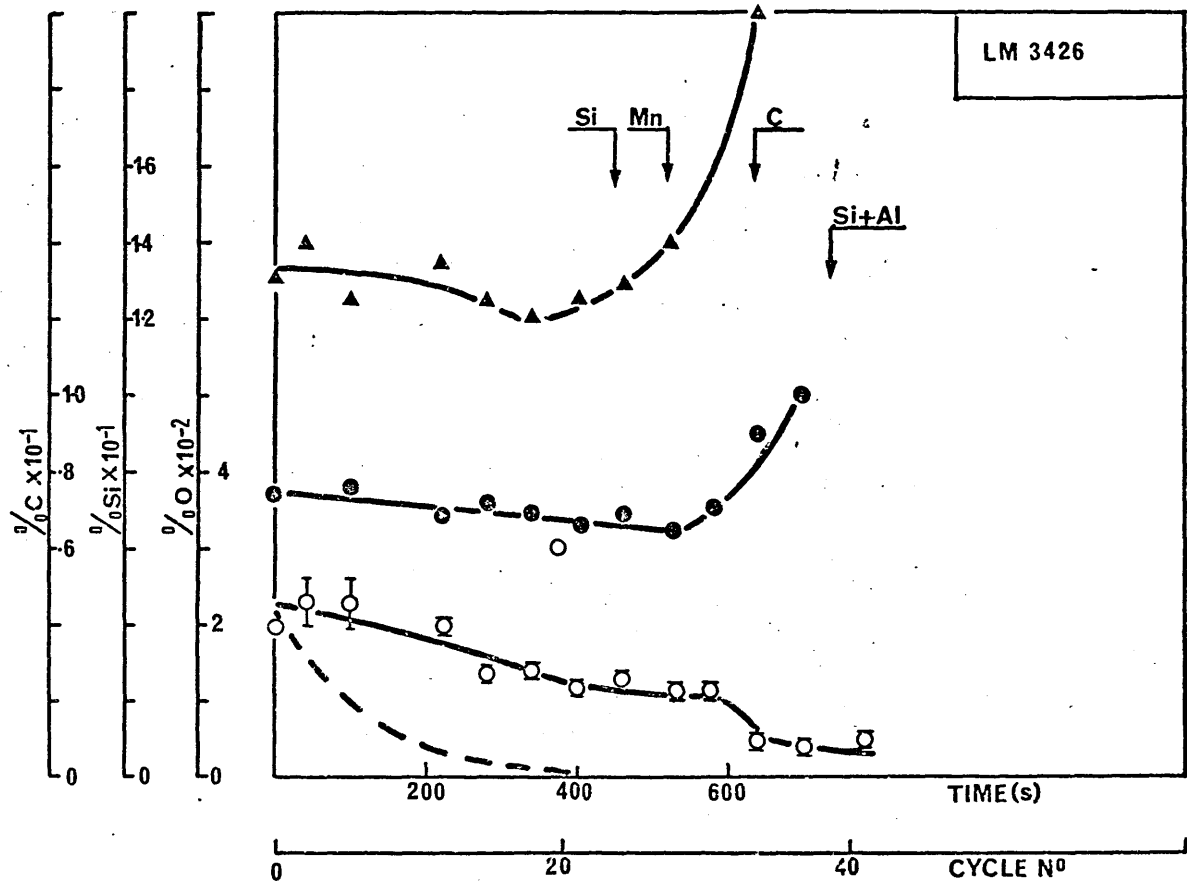
Figures 100-116.

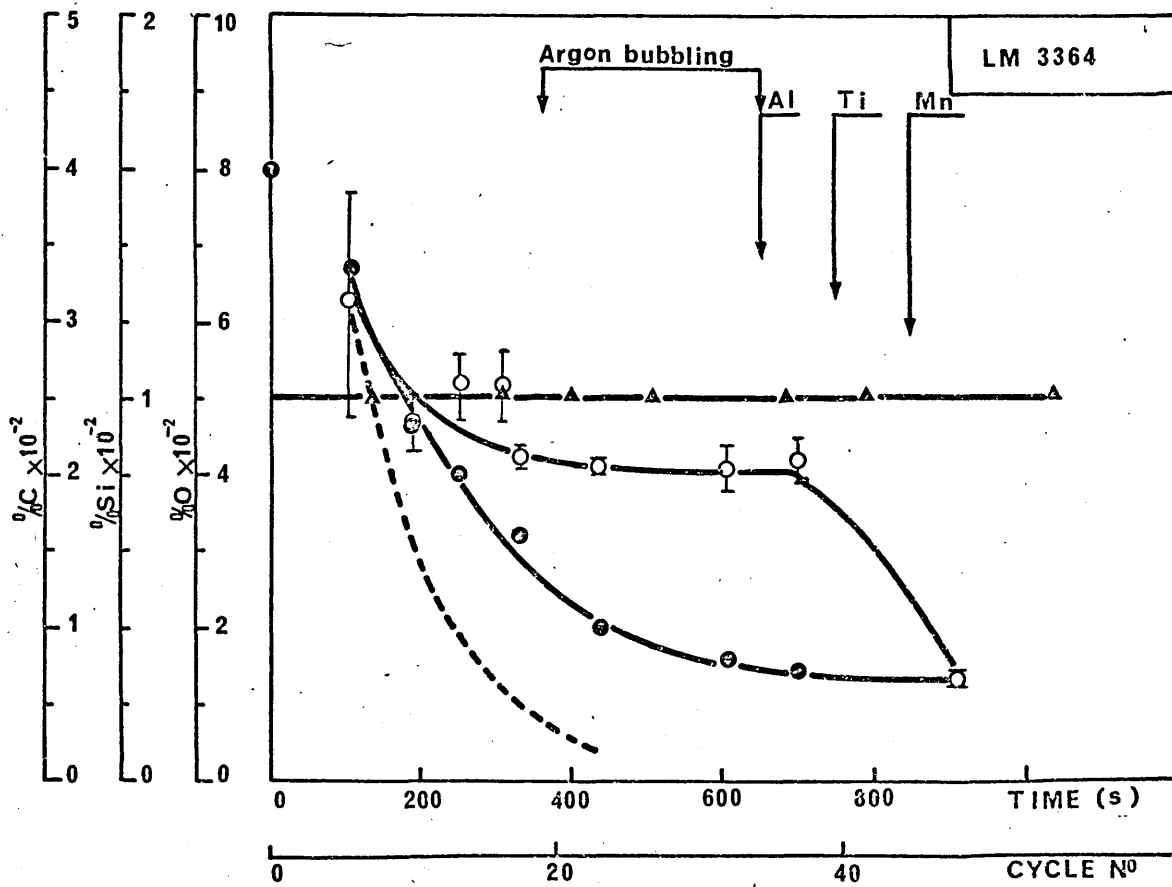
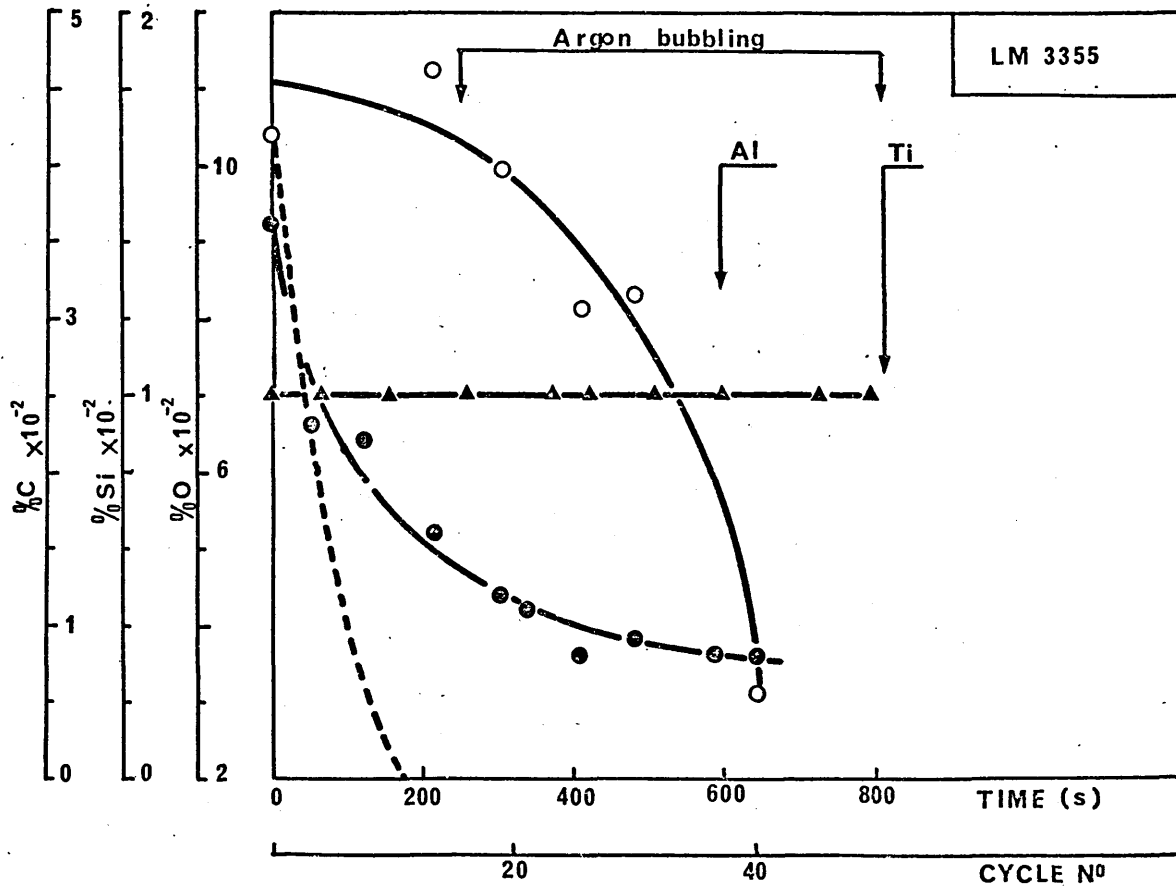
The next seventeen diagrams represent the changes in oxygen, silicon and carbon contents which took place during the vacuum treatment of the experimental **30t** heats. The dashed line on each figure represents the theoretical oxygen path had equilibrium been obtained between carbon and oxygen at each degassing cycle (equation (143)). Alloying and deoxidant additions are indicated in each case.

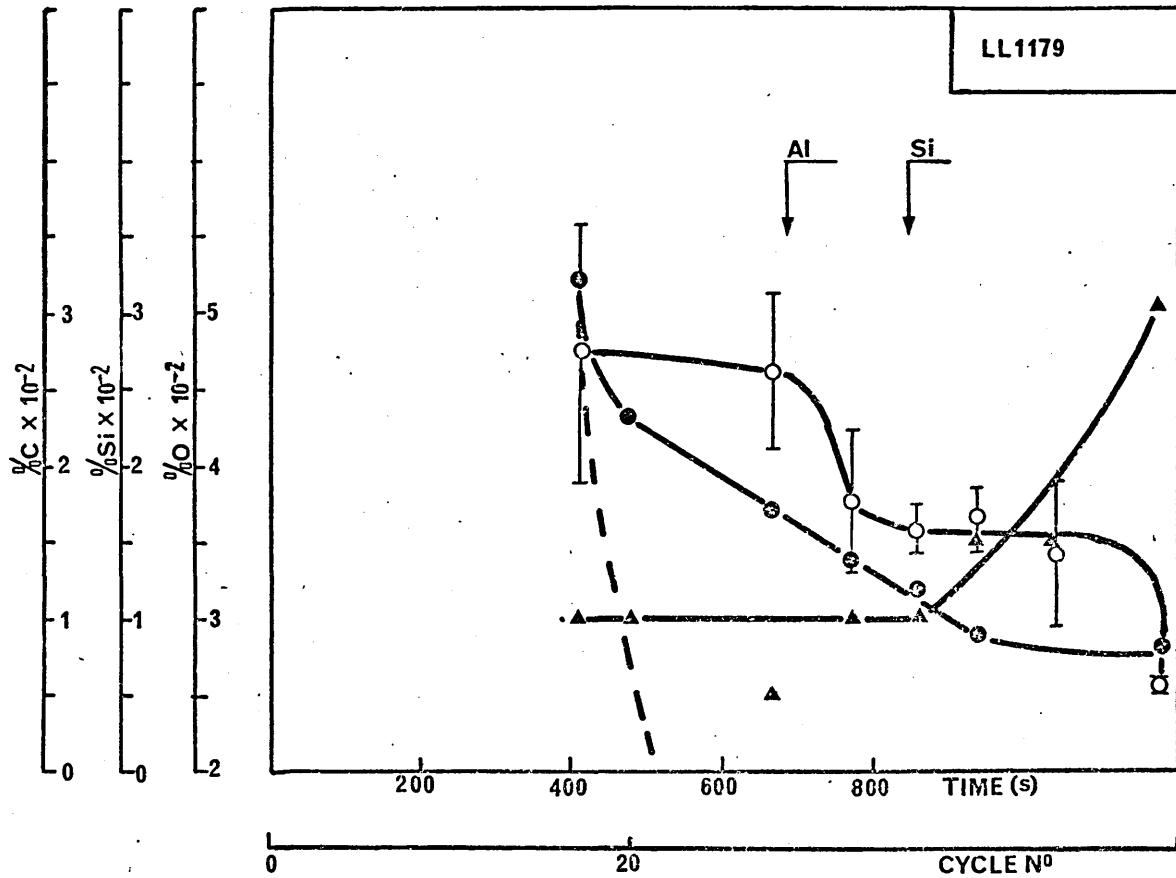
oxygen (wt.%) ○
carbon (wt.%) ●
silicon (wt.%) ▲

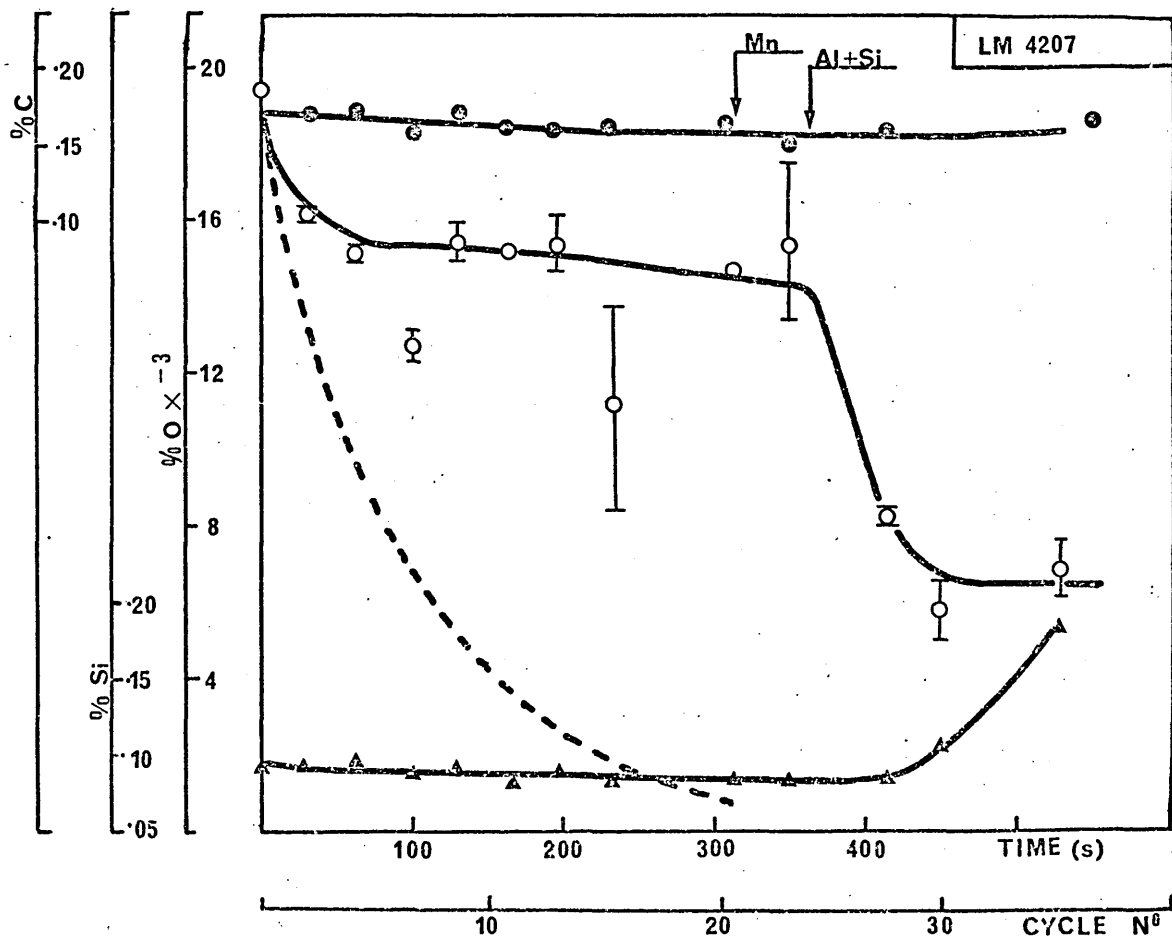
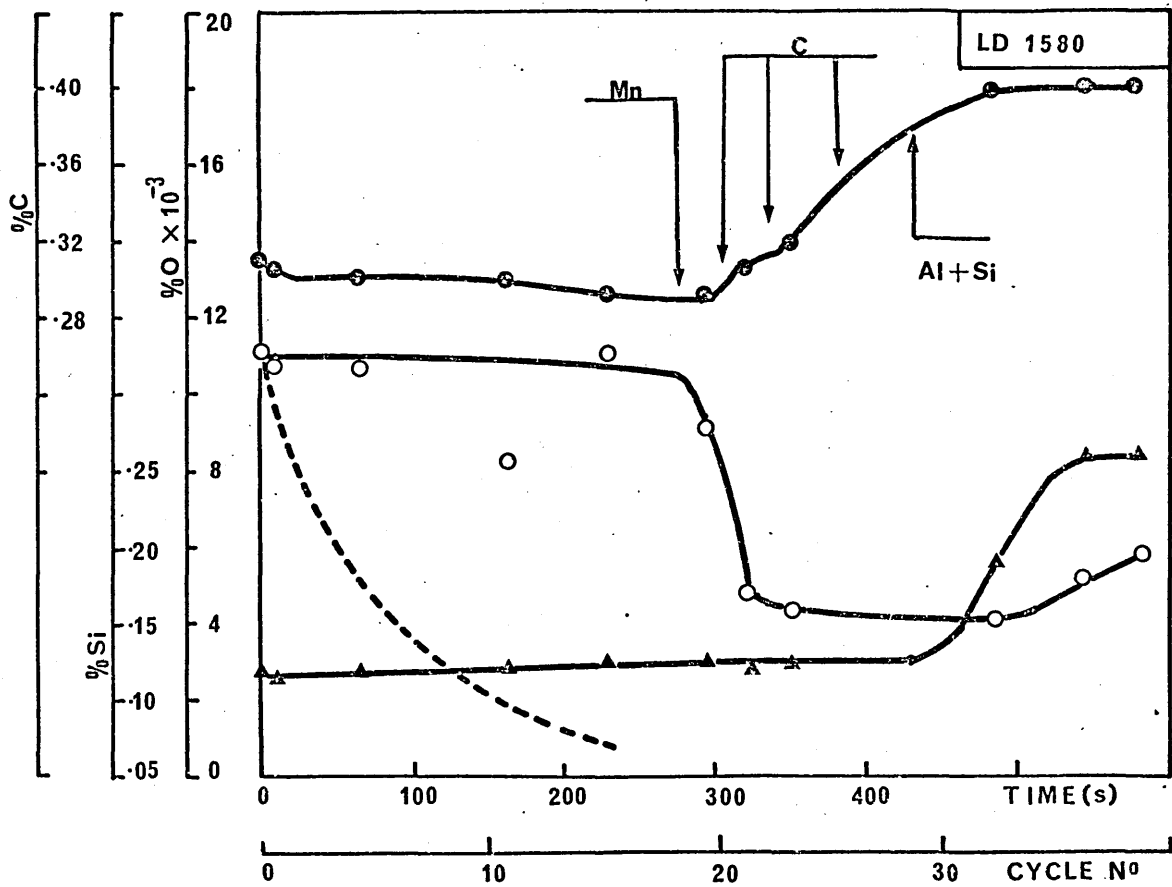


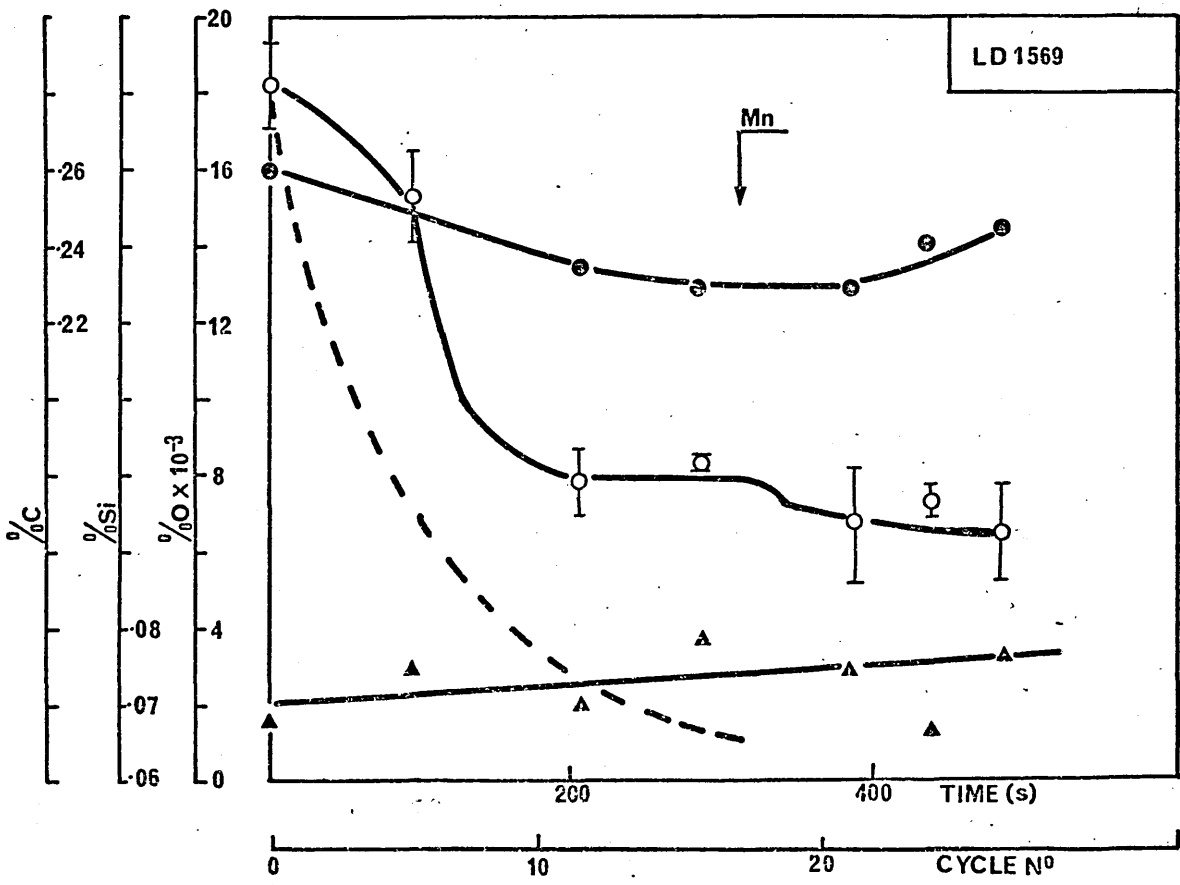
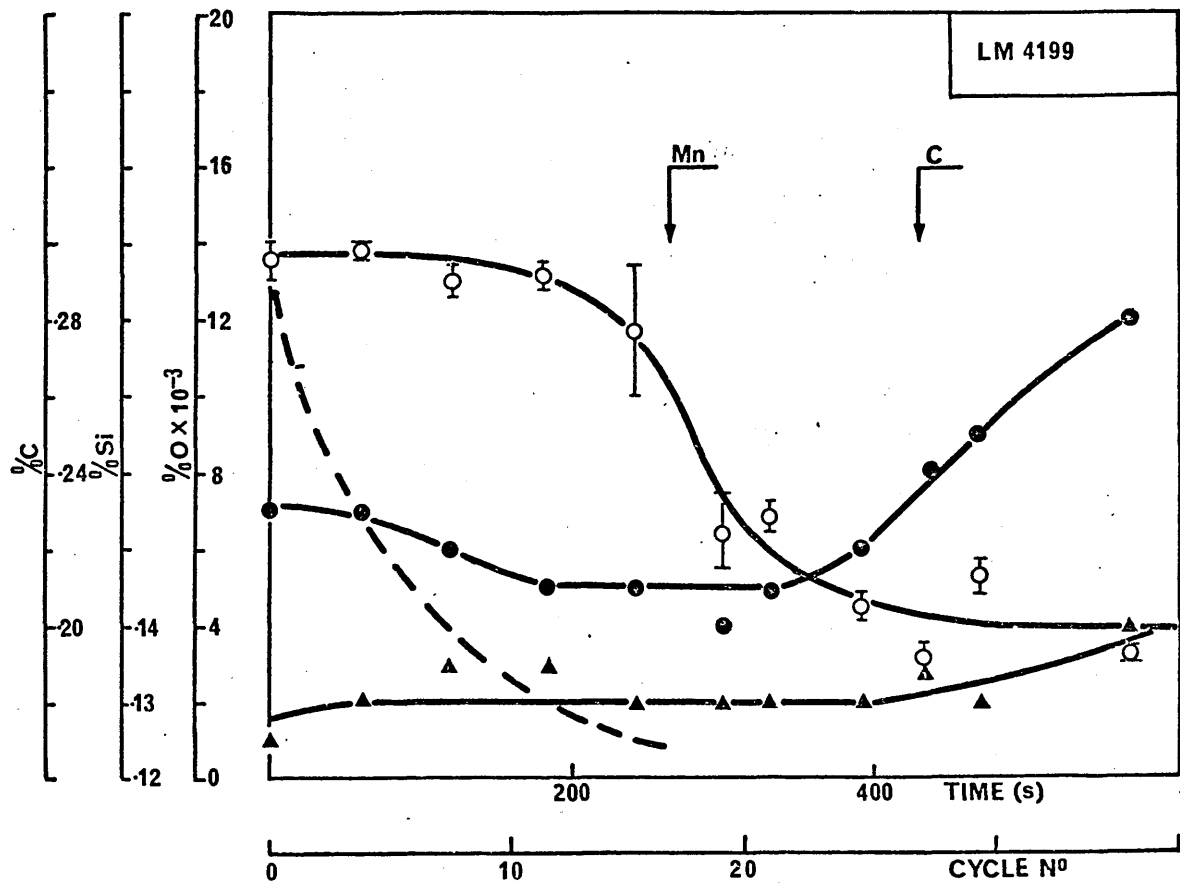


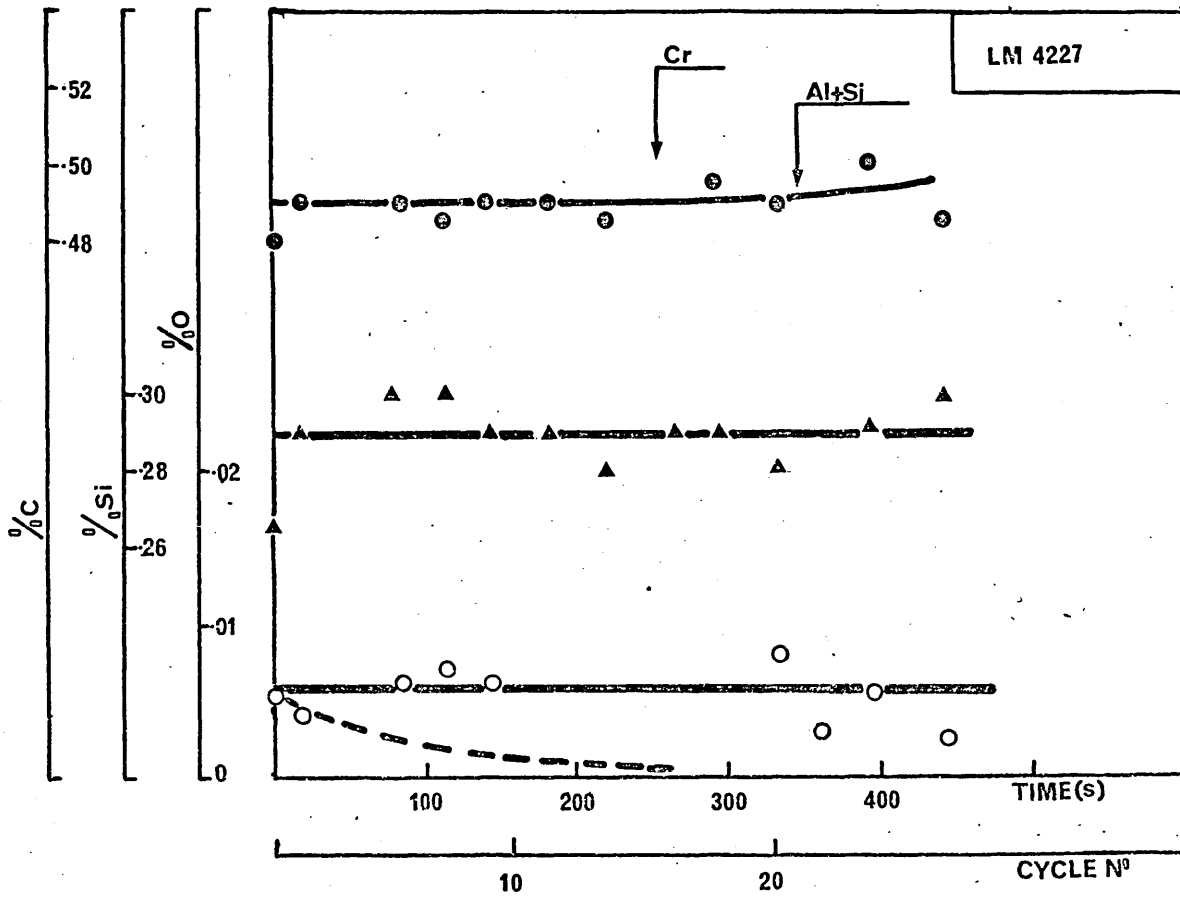
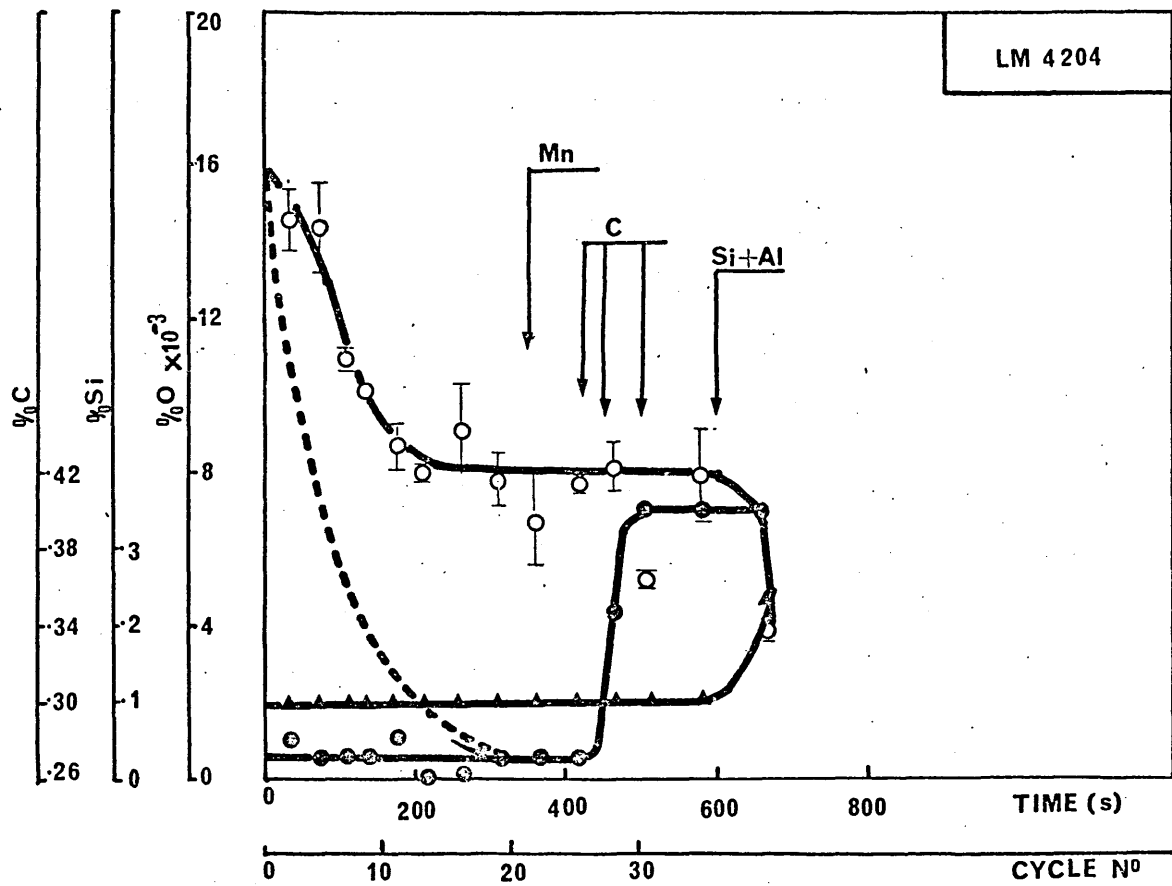












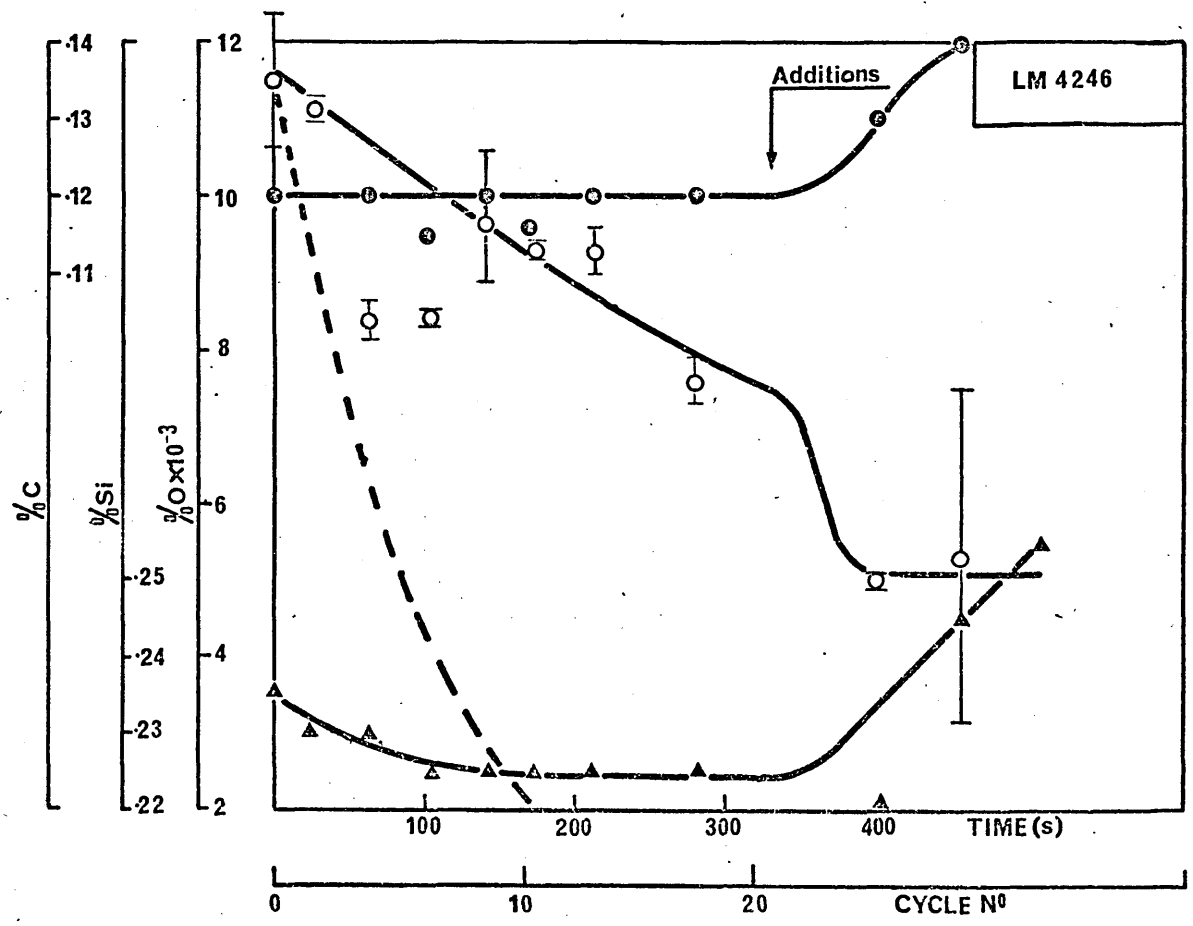
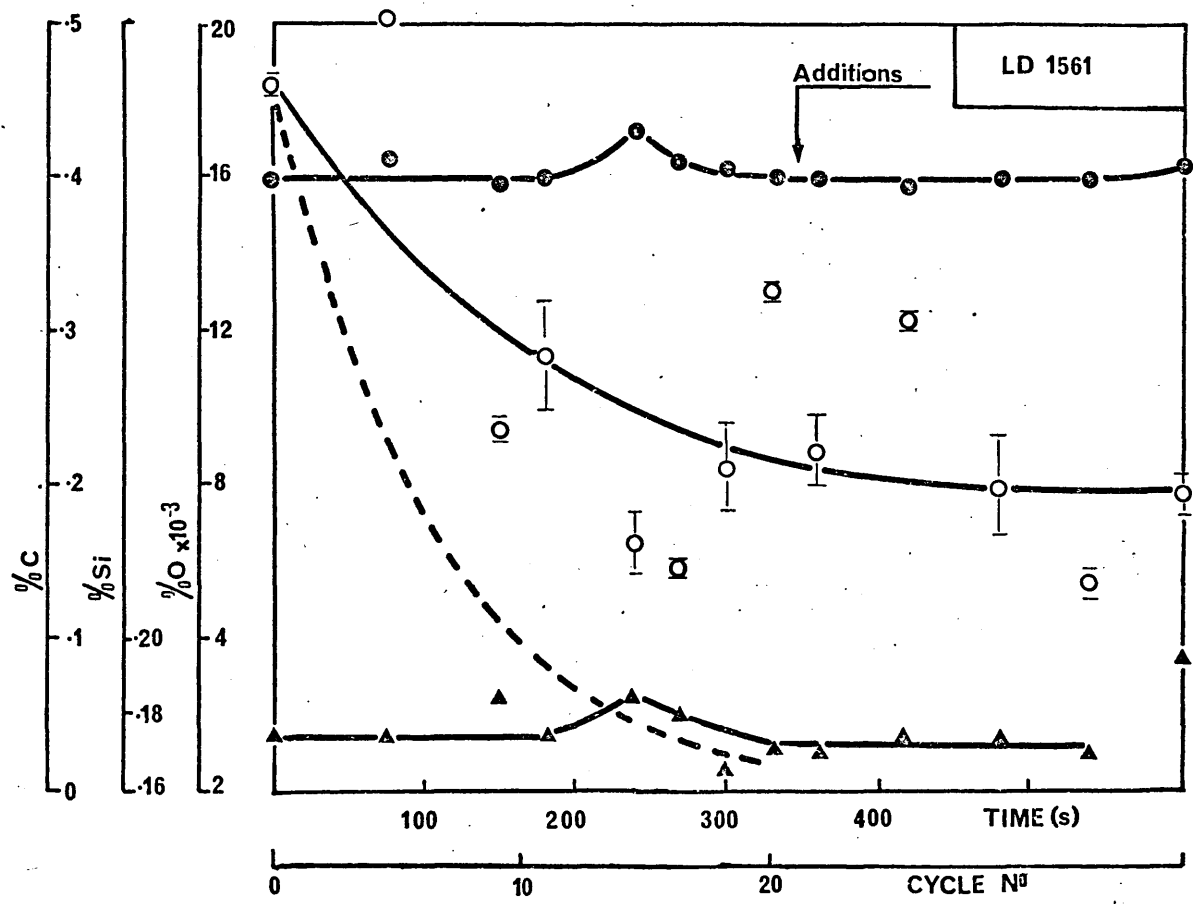


Figure 117 (116).

Typical DH record charts showing the synchronization and form of (a) the pressure in the vessel/time, (b) the ladle stroke/time, and (c) the weight of steel in the vessel/time.

Figure 118.

Calibration curve for the effect of pressure on the flow rate of gas evacuated from the vessel. This curve was produced by evacuating the vessel and, with the main vacuum valve open, measuring the steady pressure obtained when air was allowed to flow into the vessel at a known rate through calibrated nozzles.

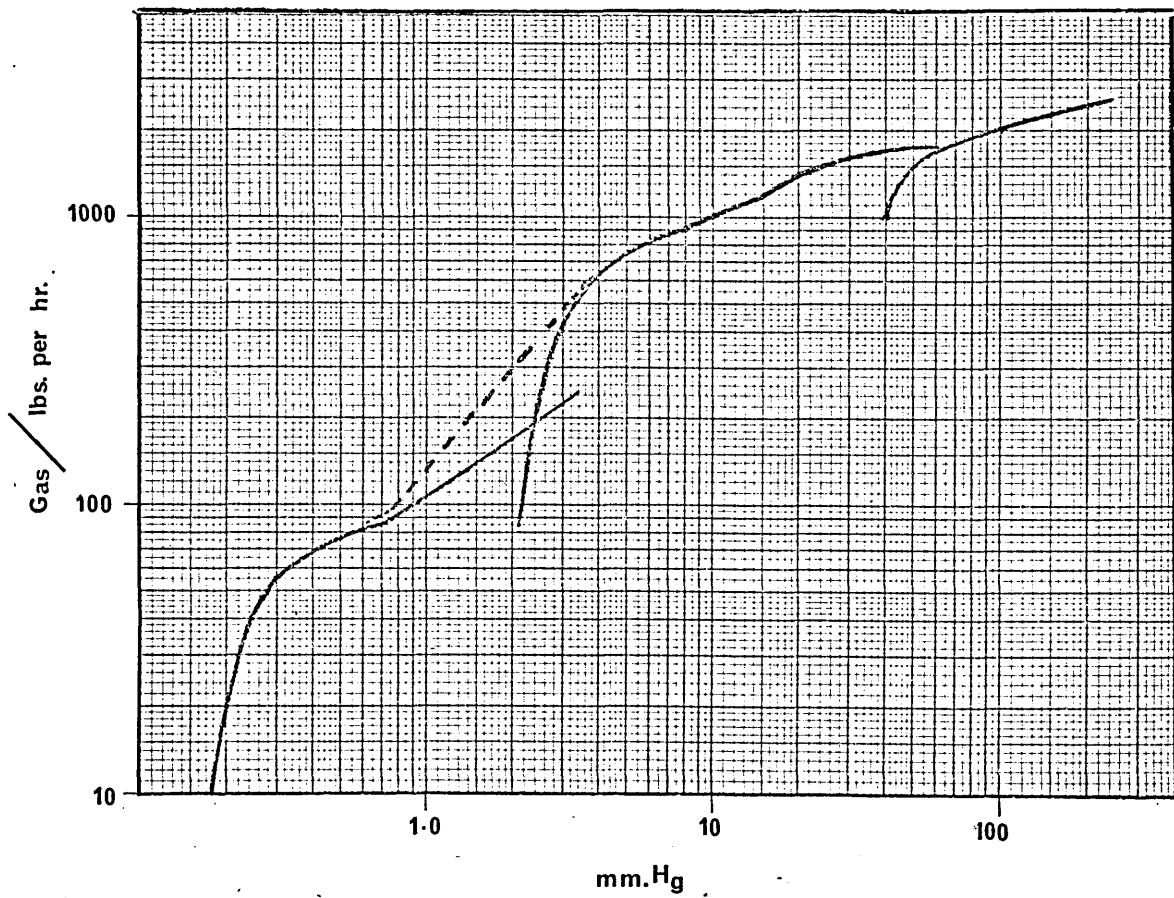
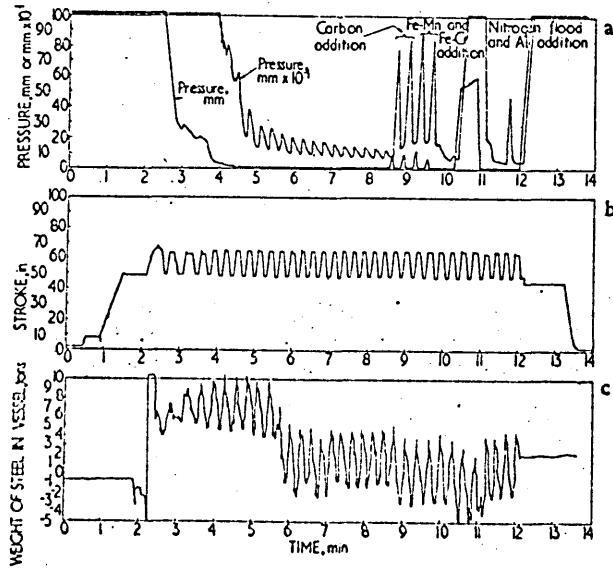
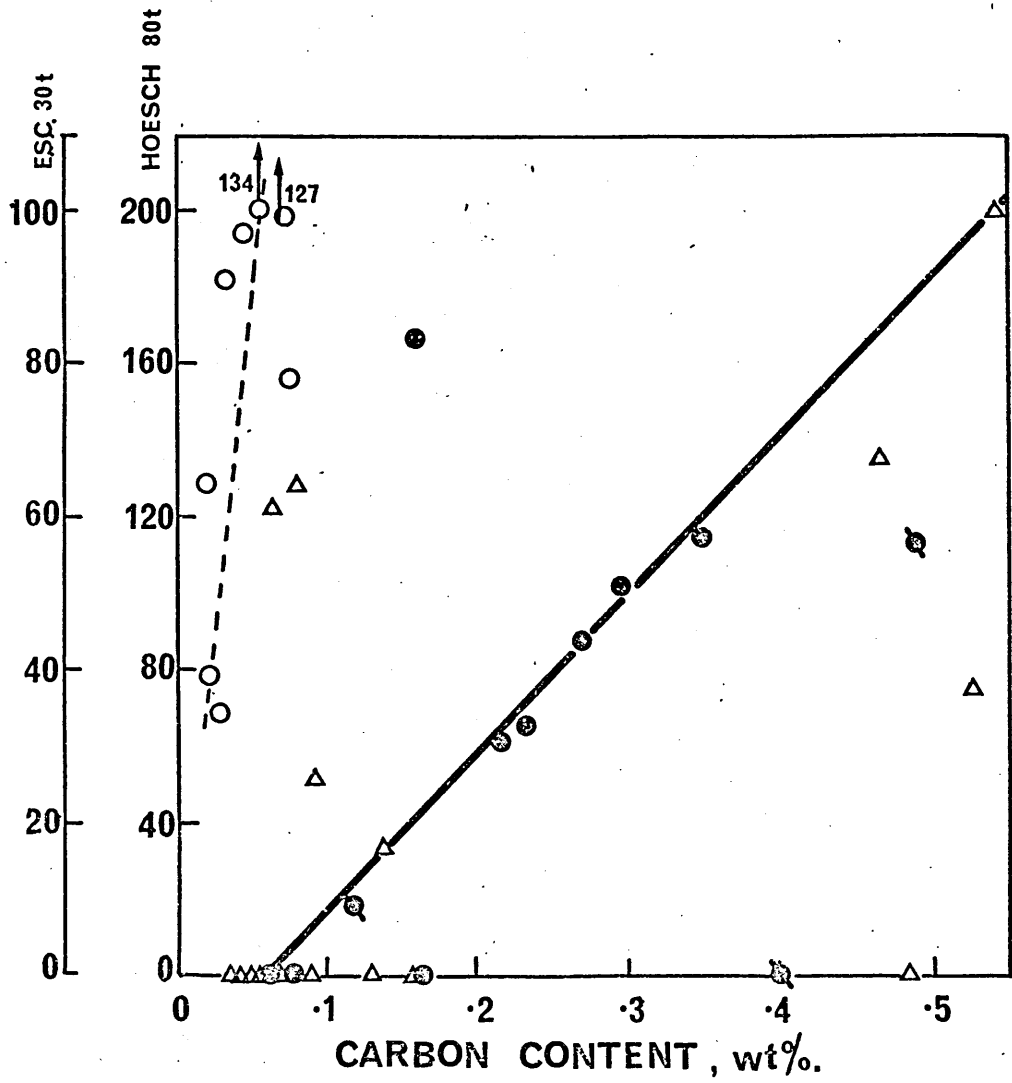


Figure 119.

The influence of carbon content on the donation rate of oxygen from sources other than the silica of the ladle lining. Hoesch heats are included for comparison.

**RATE OF OXYGEN DONATION FROM SOURCES
OTHER THAN SILICA, $\dot{n}_O/s \times 10^{-2}$.**



● ss, blocked in f'ce	} E.S.C. 30t,
○ unkilld	
⊗ double-slag	
△ unkilld, normally no slag -HOESCH 80t.	

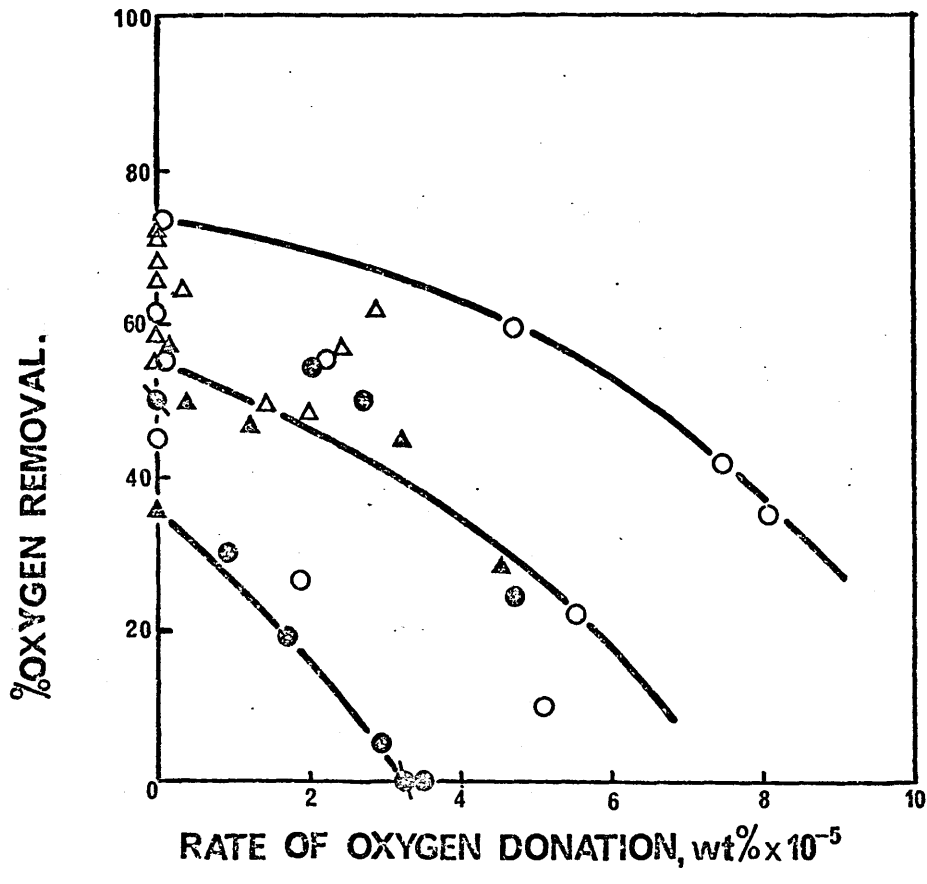
Figure 120.

The influence of the total rate of oxygen donation on the efficiency of oxygen removal during degassing. The efficiency is defined as,

$$\frac{\%O_{\text{initial}} - \%O_{\text{final}}}{\%O_{\text{initial}}} \times 100\%.$$

The amount of oxygen removed can be decreased by 50% at high donation rates.

Δ < 0.1% C, 80T HOESCH
 \circ < 0.1% C, 30T ESC
 \blacktriangle > 0.1% C, 80T HOESCH
 \bullet > 0.1% C, 30T ESC



List of Courses and Special Visits

1. Tutorials with college supervisor 8 hrs.
2. Lectures on "Mathematics of diffusion" 30 hrs
3. Visit to Dortmund Hürder Hüttenunion,
Dortmund, W.Germany (Now Hoesch A.G.)
1965 7 days
4. Visit to Böhler Bros, Kapfenburg, (Austria)
and Hoesch A.G. (Germany), 1967 7 days
5. 4th International D.H. Conference,
Lucerne, Switzerland, 1968 8 days